AWARD NUMBER: **W81XWH-15-1-0415**

TITLE: **NON-INVASIVE URINE MARKETS OF INTERSTITIAL CYSTITIS**

PRINCIPAL INVESTIGATOR: **JAYOUNG KIM, PhD**

CONTRACTING ORGANIZATION: **Cedars-Sinai Medical Center**

REPORT DATE: **October 2019**

TYPE OF REPORT: Annual

PREPARED FOR: U.S. Army Medical Research and Materiel Command
Fort Detrick, Maryland 21702-5012

DISTRIBUTION STATEMENT: Approved for Public Release;
Distribution Unlimited

The views, opinions and/or findings contained in this report are those of the author(s) and should not be construed as an official Department of the Army position, policy or decision unless so designated by other documentation.

REPORT DOCUMENTATION PAGE

Form Approved
OMB No. 0704-0188

Public reporting burden for this collection of information is estimated to average 1 hour per response, including the time for reviewing instructions, searching existing data sources, gathering and maintaining the data needed, and completing and reviewing this collection of information. Send comments regarding this burden estimate or any other aspect of this collection of information, including suggestions for reducing this burden to Department of Defense, Washington Headquarters Services, Directorate for Information Operations and Reports (0704-0188), 1215 Jefferson Davis Highway, Suite 1204, Arlington, VA 22202-4302. Respondents should be aware that notwithstanding any other provision of law, no person shall be subject to any penalty for failing to comply with a collection of information if it does not display a currently valid OMB control number. **PLEASE DO NOT RETURN YOUR FORM TO THE ABOVE ADDRESS.**

1. REPORT DATE	2. REPORT TYPE	3. DATES COVERED
October 2019	Annual	8 Sep 2018 - 7 SEP 2019

4. TITLE AND SUBTITLE

Noninvasive Urine Markers of Interstitial Cystitis

5a. CONTRACT NUMBER

5b. GRANT NUMBER
W81XWH-15-1-0415

5c. PROGRAM ELEMENT NUMBER

6. AUTHOR(S)
Jayoung Kim

Email: Jayoung.Kim@cshs.org

5d. PROJECT NUMBER

5e. TASK NUMBER

5f. WORK UNIT NUMBER

7. PERFORMING ORGANIZATION NAME(S) AND ADDRESS(ES)
CEDARS-SINAI MEDICAL CENTER
Los Angeles, CA 90048

8. PERFORMING ORGANIZATION REPORT NUMBER

9. SPONSORING / MONITORING AGENCY NAME(S) AND ADDRESS(ES)
U.S. Army Medical Research and Materiel Command
Fort Detrick, Maryland 21702-5012

10. SPONSOR/MONITOR'S ACRONYM(S)

11. SPONSOR/MONITOR'S REPORT NUMBER(S)

12. DISTRIBUTION / AVAILABILITY STATEMENT
Approved for Public Release;

13. SUPPLEMENTARY NOTES

14. ABSTRACT

Interstitial cystitis/painful bladder syndrome (IC) is a debilitating condition that presents with a confusing array of symptoms, including bladder pain, urinary urgency, frequency, nocturia, and small voided volumes in the absence of other identifiable symptoms. Currently, the diagnosis of IC is largely dependent on subjective parameters, leading to extreme difficulties in accurately phenotyping patients. There is no gold standard for IC diagnosis. In general, it takes approximately 4-5 years from the first office visit to obtain a definitive diagnosis of IC. Thus, differentiating IC from other conditions is still a diagnostic challenge, and objective diagnostic markers are urgently needed to improve prospects for clinical care. In this study, we will assess whether these promising biomarkers can segregate IC patients from control subjects, and whether they are potentially involved in bladder pain.

15. SUBJECT TERMS

Nothing listed

16. SECURITY CLASSIFICATION OF:			17. LIMITATION OF ABSTRACT	18. NUMBER OF PAGES	19a. NAME OF RESPONSIBLE PERSON
a. REPORT	b. ABSTRACT	c. THIS PAGE			USAMRMC
U	U	U	UU	76	19b. TELEPHONE NUMBER *(include area code)*

Standard Form 298 (Rev. 8-98)
Prescribed by ANSI Std. Z39.18

Table of Contents

	Page
1. Annual Technical Progress Report	**3**
2. Work in Progress 1	**6**
3. Work in Progress 2	**10**
4. Work in Progress 3	**15**
5. Work in Progress 4	**20**
6. Impact	**24**
7. Changes and Problems	**25**
8. Products	**26**
9. Participants and Other Collaborating Organizations	**29**
10. Special Reporting Requirements	**30**
11. Appendices	**30**

1. INTRODUCTION:

Interstitial cystitis (IC)/painful bladder syndrome is a debilitating condition that presents itself as a confusing array of symptoms. These include bladder pain, urinary urgency, frequent urination, nocturia, and small voided volumes. Currently, there are is gold standard for diagnosing IC and it is largely dependent on subjective parameters; thereby, leading to extreme difficulties in accurately phenotyping patients. In general, it takes approximately 4-5 years from the first office visit to obtain a definitive diagnosis of IC. Thus, differentiating IC from other conditions remains to be an important clinical challenge and identifying objective diagnostic markers would improve prospects for all patients. In this study, we will assess whether our promising biomarkers can segregate IC patients from control subjects, and whether they are potentially involved in bladder pain.

2. KEYWORDS:

Interstitial cystitis/painful bladder syndrome
Biomarkers
Diagnosis and prognosis
Chronic bladder pain

3. ACCOMPLISHMENTS:

3.1. What were the major goals of the project?

The overall goal of this study is to improve the methodology of diagnosis for IC and to develop new insight into the underlying mechanisms that trigger this condition. To achieve this goal, this project focuses on identifying urinary species and assessing their clinical significance to IC. Our hypothesis is that DNA methylation of CNR2 and urinary levels of tyramine can segregate IC patients from controls while also risk-stratifying patients with severe clinical symptoms.

This is originally three-year project plan with two times NCE. Original plan included assembly of the Cedars-Sinai Medical Center (CSMC) cohort and the targeted metabolomics analysis to quantify tyramine will be completed in Y2 and Y3 of the funding period, respectively. An enzyme reaction-based tyramine assay will be optimized and performed in Y2. Quantification of CNR2 (or other hypomethylated genes) will start from Y2 and will be completed in Y3. A mechanistic understanding of nuclear occupancy and DNA methylation of CNR2 will be completed by Y3. In the extended funding period, we have the detail plan to complete these aims.

Approved SOW

Subtask 1. CONTINUATION OF CSMC IC COHORT

- CSMC cohort for Aim 1 and 2
  (300 cases in total, patients and controls)

Subtask 2. BIOINFORMATICS ANALYSIS

- Establishing pipeline for computational analysis
- Calculation to test the correlation with clinical symptoms
- Network/pathway analysis

Subtask 3. COMPUTATIONAL ANALYSIS

- Data preprocessing

- Quality control (QC)
- Normalization
- Generation of models
- Calculation of classifier scores
- Biostatistical analysis to determine the correlation of DNA methylation levels with bladder dysfunction and associated pain

Subtask 4. PUBLICATION AND PATENT APPLICATION

- Paper preparation
- Data report and presentation at scientific meetings
- Patent application

In our 3rd funding year, we have focused on (1) identification on baseline of urine collection, (2) expansion of database for better urine biomarker discovery, (3) technology application to further identify metabolites associated with IC, and (4) continuation of CSMC IC cohort construction.

3.2. What was accomplished under these goals?

(1) Major activities

- **Goal:** CSMC cohort for Aim 1 and 2 (300 cases in total, patients and controls)

- We continued recruiting IC patients and collecting specimens through additional urologists at CSMC.
  - Dr. Brian Benway
  - Dr. Timothy Daskivich
  - Dr. Stephen Freedland
  - Dr. Hyung Kim
  - Dr. Howard Kim
  - Dr. Amit Gupta

- We opened our study to the public and amended our IRB to promote recruitment.

- Since initiation of the study to today (October 1, 2019), we have collected 296 urine specimens from healthy controls and IC patients.

(3) Significant results or key outcomes

- We made significant key scientific outcomes since the previous funding period. Several full research papers and review articles were published in this funding period. **Please refer to the APPENDICES.**

- We were able to optimize the DNA methylation and gene expression assays, which were designed for high-throughput screening (HTS). Using this optimized assay system, we found that an IC-specific metabolite marker, alpha-oxoglutarate, regulates DNA methylation and can turn on an epigenetic switch through ARID1A, a chromatin remodeler in normal bladder epithelial cells.

  - To perform a quantitative targeted mass spectrometry-based metabolomics analysis (Dr. Kim, Dr. Fiehn, Dr. Yang, Dr. Van Eyk)
  - To set up and perform the enzyme-reaction based biochemical assay (Dr. Kim)
  - Primer design and protocol set up (Dr. Kim, Dr. Berman, Dr. Weisenberger)
  - Pyrosequencing or MethyLight assay optimization

(Dr. Kim, Dr. Liang)

- We were able to optimize the DNA methylation and gene expression assays, which were designed for high-throughput screening (HTS). Using this optimized assay system, we found that an IC-specific metabolite marker, alpha-oxoglutarate, regulates DNA methylation and can turn on an epigenetic switch through ARID1A, a chromatin remodeler in normal bladder epithelial cells.

- We optimized metabolic profiling of urine samples. Updated state-of-the-art mass spectrometry technology was applied to identify additional previously unknown IC biomarker metabolites. We found several biologically relevant candidates from this new approach and our experimental results were recently published.

- UsingametabolomicsapproachtocaptureodorcompoundsinurinesamplesofICpatientsand healthy controls, we found that urinary menthol levels were significantly lower in IC urine. Further biochemical and functional analyses revealed that urinary menthol may suppress the inflammatory response of immune cells that have infiltrated the bladder epithelium. These findings suggest that the decreased levels of urinary menthol may explain the chronic inflammation in IC bladders.

- In order to identify sex differences in metabolite profiles, we assembled a sub-cohort for a pilot study. This cohort consisted of urine specimens from healthy males and females. Our project was conducted through a close collaboration with Dr. Oliver Fiehn's metabolomics core at UC Davis. This data was published as a full research paper.

- Many lipids and lipid metabolites are still not properly annotated nor functionally characterized, which hinders the diagnostic potential of lipid profiling. Our research team actively worked to address this discrepancy and has since developed numerous software and databases that can aid in the lipid structure elucidation process.

- Recently we establish new collaboration with a big metabolomics group at our own institute for further validation of target candidates. While our preliminary are based on small numbers and require validation in a large dataset, they nonetheless demonstrate the feasibility of the current study and provide strong support to the fact that we are likely to identify many clinically and biological important linkages with IC and the various IC phenotypes within this study. Also, our concentrated efforts focused on subject recruitment and collection of urine samples.

- Our recent review paper summarized the underlying mechanisms that induce the chronic pain associated with IC and vulvodynia and explain why these two conditions often coexist. We also developed a statistical model to determine whether the biosignatures to be enhanced by additional systemic changes, such as widespread pain or associated clinical depression.

- In the following sections, we will update our progress in detail for your reference.

Work in progress 1:

Sexual Pain and IC/BPS in Women

Female sexual dysfunction (FSD) and interstitial cystitis/bladder pain syndrome (IC/BPS) are important factors affecting women's health. A study conducted on the association between sexual and general well-being found that women reported better quality of life (QoL) with higher sexual satisfaction, regardless of age and/or menopausal status.[1] Both FSD and IC/BPS significantly impairs women's abilities to pursue and enjoy sexual relations. Approximately 40-50% of women experience FSD and 0.5-12% experience IC/BPS. Considering these incidence rates in the general population, both these diseases become serious challenges for patients and clinicians.[2-6]

Chronic pain deteriorates not only personal health and wellness, but also quality of life. Chronic pain can induce sexual dysfunction, such as arousal disorder and relationship problems.[7] Furthermore, studies have shown that significantly more women with chronic pelvic pain (CPP) showed FSD compared to those without CPP. Women with CPP and FSD had various types of FSD, such as hypoactive sexual desire disorder, sexual arousal disorder, orgasmic disorder, and sexual pain disorder.[8]

The symptoms of IC/BPS, such as urinary frequency, urgency, and pelvic pain, have a negative impact on sexual activity and life quality.[9] Women with overactive bladder (OAB) frequently have a risk for sexual dysfunction.[10] In the postmenopausal group, women with scores indicating severe OAB had worse sexual function, mainly in the arousal, lubrication, orgasm, pain, and total domains.[11] Despite the known association of sexual dysfunction with bladder diseases, contributing risk factors have yet to be explored. Evaluating the impact of duration, severity, pain localization, sexual trauma history, anxiety, and depression on sexual dysfunction may help elucidate risk factors. Increasing our knowledge about sexual dysfunction as it relates to bladder diseases may aid in clinical diagnoses and play a major role in treatment strategies and overall symptom improvement in this patient population. This review will provide an overview of studies that address FSD in women with IC/BPS.

A. PAIN IN FSD

FSD is classified as hypoactive sexual desire dysfunction, female sexual arousal dysfunction, female orgasmic dysfunction, female-genital-pelvic pain dysfunction, persistent genital arousal disorder, postcoital syndrome, hypohedonic orgasm, or painful orgasm through consensus by the 4th International Consultation on Sexual Medicine (ICSM).[2, 12] Guidelines from the 4th ICSM defines pain-associated FSD as female-genital-pelvic pain dysfunction and includes all conditions that inhibit sexual intercourse and induce negative effects on sexual functions. Female-genital-pelvic pain dysfunction is different from the previous classification noted pain associated with FSD as sexual pain disorder including dyspareunia and vaginismus.[13] In the 4th ICSM, female-genital-pelvic pain dysfunction includes persistent or recurrent difficulties with at least one of the following: (1) vaginal penetration during intercourse, (2) marked vulvovaginal or pelvic pain during genital contact, (3) marked fear or anxiety about vulvovaginal or pelvic pain in anticipation of, during, or as a result of genital contact, or (4) marked hypertonicity or overactivity of pelvic floor muscles with or without genital contact.[14] Painful orgasm is also considered and means the occurrence of genital and/or pelvic pain during or shortly after orgasm.[2] These recent new definitions reflect the evolving concept behind pain-associated FSD as it also now includes pain in the vulvovaginal and pelvic area and pelvic floor hypertonicity. The new categorization of female-genital-pelvic pain dysfunction has broadened the view on pain-associated FSD and has differentiated it from its previous classification that confined symptoms to each organ or single disease. This recent change in classification by the ICSM considers pain-associated FDS as a complex condition influenced by psychological and physical factors and supports the general thought that FSD is multifactorial.

Previously, vulvodynia had been generalized under chronic vulvar pain and there was no precise discrimination for it. However, recent consensus has redefined chronic vulvar pain as vulvar pain associated with specific diseases, such as inflammation, neoplasm, and/or injury. This was conducted at a conference with the International Society for the Study of Vulvovaginal Disease, the International Society for the Study of Women's Sexual Health, and the International Pelvic Pain Society.[15] Vulvodynia is reported with diverse pain

characteristics; therefore, pain-based classification helps in identification, diagnosis, and treatment. Vulvodynia can be characterized as either general (entire vulva) or localized (parts of the vulva) according to the location of pain. Additionally, based on the situation of the pain, vulvodynia can be classified as either provoked (triggered by physical contact) or unprovoked (spontaneous occurrence without specific triggers).[16] Women of all ages can experience vulvodynia and provoked vulvodynia is the most commonly diagnosed.[17,18] Provoked vulvodynia is thought to be more widely diagnosed than unprovoked because its symptoms can be better recognized by doctors. Therefore, there is an important need to better identify these patients.

B. SEXUAL PAIN AND IC/BPS

IC/BPS is a disorder that induces chronic pain or discomfort in the bladder and surrounding pelvic organs.[19,20] At present, IC/BPS is not a disease confined to just the bladder and pelvic area; it is a complex disease that includes outside the genitourinary tract. There is a study that reflects these pain characteristics. Tripp et al.[21] investigated the pain characteristics of IC/BPS using whole-body diagram pain locators. They found that women with IC/BPS reported significantly more pain all over their body, compared to healthy women without. Fifty two of the 193 IC/BPS diagnosed women (27%) presented pain restricted to the bladder and pelvic area. Moreover, various comorbidities are found in IC/BPS patients. Diseases such as irritable bowel syndrome, fibromyalgia, vulvodynia, chronic pelvic pain, endometriosis, OAB, allergies and chronic fatigue syndrome often coexist in IC/BPS patients.[22-28]

In addition, there are several reports that IC/BPS can increase the risk for or worsen other diseases, including FSD. A population based study found higher prevalence of FSD in women with IC/BPS.[29] Moreover, FSD increased depending on the severity of IC/BPS symptoms, suggesting that FSD is a factor worsening IC/BPS. In regards to the pain associated with FSD, vulvodynia may be contributing to flare-ups of IC/BPS symptoms and could be the reason why IC/BPS patients avoid sexual activity.[9,30]

C. FSD AND IC/BPS: BE GENERALIZED AS ONE DISEASE?

Diseases with lower urinary tract symptoms (LUTS) in female such as incontinence and OAB are known to have negative impact on female sexual function over all domains-arousal, orgasm, pain, and satisfaction. Symptoms of IC/BPS also deteriorate patient's sexual activities and life quality. Significant numbers of IC/BPS patients avoid sexual activity because of pain. In addition, FSD and IC/BPS share similar clinical characteristics and comorbidities, making it difficult to discriminate between the two.[31-33] As mentioned previously, there are many clinical reports presenting the association between IC/BPS and vulvodynia, particularly from various conditions of FSD.

Although the mechanisms of these correlations are unclear, visceral nerve cross-talking and the anatomic relationship between genital organs and the bladder offer a simple proximity explanation for the relationship between IC/BPS and vulvodynia. Another possible mechanism to explain the association between IC/BPS and vulvodynia is abnormal pain hypersensitivity induced by peripheral and central sensitization. The abnormal pain response frequently observed in vulvodynia patients is caused by central or peripheral maladaptive pain processing due to local insult, injury, or trauma (Figure 1).

D. Role of Peripheral Sensitization in the Pain Hypersensitivity of Vulvodynia and IC/BPS

Exposure of nociceptors to repetitive pain stimulation reduces the pain threshold and amplifies the responsiveness of nociceptors. Therefore, peripheral transduction of sensitivity can abnormally increase and peripheral pain hypersensitivity can develop.[34-36] The potential underlying mechanism of peripheral pain hypersensitivity noted in both vulvodynia and IC/BPS could be sensory nerve upregulation. Previous studies have shown that sensory nerve density is significantly increased in vulva vestibule and bladder. Compared to the normal population, patients with vulvodynia were found to have increased nociceptors in their vulvar vestibule.[37-40] Consequentially, this increased density of peripheral nociceptors results in increased sensitivity. It was also found that transient receptor potential V1 (TRPV1) exists in these nociceptive nerve endings and enhances pain signaling.[37,41,42] Pukall CF et al.[43] and Giesecke J et al.[44] reported increased peripheral tactile, pressure, and pain sensitivity in the patients with vulvodynia and confirmed histologic and molecular changes of

peripheral nociceptors is associated with clinical manifestations. Similarily with vulvodynia, upregulation of sensory innervation and TRPV1 in the bladder is reported in patients with IC/BPS.[45-47]

E. Role of Central Sensitization in the Pain Hypersensitivity of Vulvodynia and IC/BPS

Central sensitization is an important mechanism underlying various conditions associated with chronic pain and induces pain hypersensitivity through pathologically enhanced pathways that are not normally associated with nociception; for example, the low-threshold Aδ fiber that is mostly used for temperature and pressure signaling. Chronic pain induced by central sensitization is persistent even after the initiating and peripheral cause has gone.[48] Studies have shown that the pain characteristics of central sensitization can be found in patients with vulvodynia. Foster DC et al.[49] observed that vulvar vestibulitis syndrome patients experienced hyperalgesia and allodynia more often than normal controls after intradermal foot and forearm capsaicin injections. In addition, pelvic organ crosstalk has an important role in central sensitization because pelvic organs, such as, the bladder, colon and vulva, are controlled by same neural pathway.[50] Thus, afferent signals from other pelvic organs provoked pain through neural crosstalk even though initiating and peripheral causes of vulvodynia and IC/BPS disappeared. Therefore, central sensitization plays an important role in the chronic pain observed in vulvodynia and IC/BPS. Clinically, similar manifestation of vulvodynia and IC/BPS has also existed. Moreover, recently, there has been an attempt to categorize various pain associated conditions due to central sensitization as central sensitivity syndrome (CSS). Vulvodynia and IC/BPS are considered subgroups of CSS.[51] Previous studies on clinical findings support the notion that the same mechanism associated with central sensitization is involved in the pain behind vulvodynia and IC/BPS.[52-54]

Recently, evidence supporting central sensitization using functional and structural brain imaging were reported in vulvodynia and IC/BPS. Previously, Pukall et al.[55] showed that increased perception and activation of pain-related brain regions were observed in women with vulvar vestivulitis syndrome, compared to normal women, after tacticle stimulation of the vulvar vestibule. Other studies have reported that patients with vulvodynia showed increased grey matter density in pain-modulating and stress-related regions of the brain as well as alterations in the intrinsic connectivity of regions comprising the sensorimotor, salience, and default mode resting state networks.[56,57] Similarly, women with IC/BPS showed alterations of oscillation frequency and functional connectivity of brain regions previously reported in other chronic pain conditions[58] and various white matter (right anterior thalamic radiation, left forceps major, and right longitudinal fasciculus, right superior and bilateral inferior longitudinal fasciculi) abnormalities that correlated with severity of pain, urinary symptoms, and impaired quality of life.[59] Figure 2 shows common therapeutic approaches and points of divergence among the these IC, IC+vulvodynia, and vulvodynia patient groups.

F. APPROACH AND MANAGEMENT FO VULVODYNIA AND IC/BPS PATIENTS

Clinically, vulvodynia and IC/BPS often coexists and differentiation between the two is not easy, especially when the patient reports of LUTS combined with pain. A majority of patients also seek medical care after relatively longer periods of initially feeling pain, leading to central sensitization that has is firmly established. Furthermore, clinical manifestations of chronic pain found in various other comorbidities can mask vulvodynia and IC/BPS, making it confusing and difficult to officially diagnose.

Many previous studies have revealed the close correlation between LUTS and impaired sexual function; IC/BPS is not an exception. Besides, it is not uncommon to have trouble differentiating sexual pain and IC-BPS-related genital pain in women. Unfortunately, there is a lack of comprehensive studies regarding sexual dysfunction and IC/BPS despite the growing population of affected individuals (Table 1). Clinicians should take more concern regarding sexual dysfunction and pain in IC/BPS patients and more randomized controlled studies should be conducted to better understand correlations and diagnostic differentiations.

CONCLUSION

Both vulvodynia and IC/BPS are common and irritable conditions that disrupt normal life and reduce QoL in women. Vulvodynia also manifests itself along with IC/BPS and there are several reports supporting the association between the two diseases. Unfortunately, knowledge concerning vulvodynia and IC/BPS is inadequate when considering the clinical impact and importance of these two conditions. Therefore, there is an essential need for further studies that delve into discovering the features of vulvodynia and IC/BPS.

Work in progress 2:
Complete compound annotation of all mass spectra from untargeted urine metabolomics

To this date, metabolomics is considered to be one of the major "omics" tools, with the great potential for application in personalized medicine and health[1]. Over the last decade, metabolomics has become an integral part of clinical laboratories worldwide for targeted analysis. However, untargeted metabolomics is still widely used as it provides comprehensive insights into complex metabolomes and allows for biomarker discovery. While untargeted metabolomics can be powerful, its main challenge is its low identification rates[2,3]. Since there is no single platform capable of capturing the entire metabolome of urine, we have employed two platforms most suited for untargeted urine analysis: (1) hydrophilic interaction chromatography (HILIC), for polar metabolite profiling, and (2) charged surface hybrid (CSH) technology, for lipidomics profiling. Through this integration of lipidomics and intensive systems biology, our experimental results provided a comprehensive list of lipid species and biogenic amines in human urine. Lipidomics, a lipid-targeting subarea of metabolomics, involves studying the unique structure and functional roles of cellular lipids in biological systems. Recent technological advancements in high-resolution MS have made comprehensive lipid metabolic profiling of clinical specimens and biofluids, including urine, possible. As important structural components of cellular membranes, lipids play key biological roles in various diseases. However, clinical application of lipidomics profiling still remains a challenge due to the limited databases available for data interpretation. Many lipids and lipid metabolites are still not properly annotated nor functionally characterized. Our group is actively working to address this issue by developing software and databases that can aid in lipid identification. The biologically active metabolites in urine can be identified through global metabolomics profiling and can provide an unbiased chemical fingerprint of the metabolism in the human body. The urinary metabolome in particular is associated with urological diseases, including bladder dysfunctions such as IC[4-6]. IC is characterized by chronic bladder and/or pelvic pain, as well as nocturia and an increase in urinary frequency and urgency.[7,8] For our work, we sought to derive urinary metabolomic signatures from IC patients using newly developed comprehensive annotation tools[9] on all five levels of annotation, as defined by the Metabolomics Standards Initiative (MSI). The objective of this work is to provide insight into increasing compound annotation levels in the clinical setting by utilizing a variety of freely available software tools and databases.

EXTRACTION
Subjects, urine specimen collection, and clinical and pathological features of subjects were described in a previous paper from our team. De-identified urine samples were stored at −80°C until further analysis. Urinary lipids were extracted with methanol and methyl tert-butyl ether containing a cocktail of lipid standards. Water was subsequently added for phase separation. This extraction protocol extracts all main lipid classes in urine with high recoveries, specifically phosphatidylcholines (PC), sphingomyelins (SM), phosphatidylethanolamines (PE), lysophosphatidylcholines (LPC), ceramides (Cer), cholesteryl esters (CholE), and triacylglycerols (TG).[10] Lipid standards were purchased from Avanti Polar lipids (Alabaster, USA). Polar metabolite extraction was done by taking the polar phase of the lipid extraction procedure. Samples were dried in a centrivap prior to a clean-up step of 50% acetonitrile and dried again. Samples were then reconstituted in 80:20 acetonitrile and water solution containing internal standards from Sigma and CDN Isotopes.

INSTRUMENTATION
For lipids, all measurements were carried out on a Thermo Q Exactive Hybrid Quadrupole-Orbitrap Mass Spectrometer. Briefly, 1 µL of diluted samples were separated on a Waters Acquity Ultra-Peformance LC (ULPC) CSH C18 column (100 × 2.1 mm; 1.7 µm) coupled to an Acquity UPLC CSH C18 VanGuard Precolumn (5 × 2.1 mm; 1.7 µm). The column was maintained at 65°C with a flow rate of 0.6 mL/min. The positive ionization mobile phases consisted of (A) acetonitrile:water (60:40, v/v) with ammonium formate (10 mM) and formic acid (0.1%) and (B) 2-propanol:acetonitrile (90:10, v/v) with ammonium formate (10 mM) and formic acid (0.1%). The negative ionization mobile phases consisted of (A) acetonitrile:water (60:40, v/v) with ammonium formate (10 mM) and (B) 2-propanol:acetonitrile (90:10, v/v) with ammonium formate (10 mM). The separation was conducted under the following gradient: 0 min 15% B; 0−2 min 30% B; 2−2.5 min 48% B; 2.5−11 min 82% B; 11−11.5 min 99% B; 11.5−12 min 99% B; 12−12.1 min 15% B; 12.1−15 min 15% B. The Thermo Q Exactive Hybrid Quadrupole-Orbitap Mass Spectrometer was operated using electrospray ionization (ESI CSH) in positive mode used the following parameters: mass range, 120-1200 m/z; sheath gas flow rate, 60; aux gas flow rate,

25; sweep gas flow rate, 2; spray voltage (kV) 3.6; capillary temp, 300°C; S-lens radio frequency level, 50; aux gas heater temp, 370°C. The full MS parameters were set as follows: resolution, 60,000; automatic gain control (AGC) target, 1e6; maximum IT, 100ms; spectrum data type, centroid. Data dependent tandem MS parameters: resolution, 15,000; AGC target 1e5; maximum IT, 50 ms; loop count, 4; TopN, 4; isolation window, 1.0 m/z; fixed first mass, 70.0 m/z; (N)CE / stepped (N)CE, 20, 30, 40; spectrum data type, centroid. For HILIC, all measurements were carried out on the same Thermo Q Exactive Mass Spectrometer. Briefly, 1 µL of diluted samples were separated on an Waters Acquity UPLC Ethylene Bridged Hybrid (BEH) Amide Column (150 × 2.1 mm; 1.7 µm) coupled to an Acquity UPLC BEH Amide VanGuard Precolumn (5 × 2.1 mm; 1.7 µm). The column was maintained at 45°C with a flow rate of 0.4 mL/min. The mobile phases consisted of (A) water with ammonium formate (10 mM) and formic acid (0.125%) and (B) acetonitrile:water (95:5, v/v) with ammonium formate (10 mM) and formic acid (0.125%). The separation was conducted under the following gradient: 0 min 100% B; 0−2 min 100% B; 2−7.7 min 70% B; 7.7−9.5 min 40% B; 9.5−10.25 min 30% B; 10.25−12.75 min 100% B; 12.75−17 min 100% B. The Thermo Q Exactive MS instrument was operated using ESI HILIC in positive mode with the following parameters: mass range, 60-900 m/z; sheath gas flow rate, 60; aux gas flow rate, 25; sweep gas flow rate, 2; spray voltage (kV) 3.6; capillary temp, 300°C; S-lens RF level, 50; aux gas heater temp, 370°C. Full MS parameters: microscans, 1; resolution, 60,000; AGC target, 1e6; maximum IT, 100ms; number of scans, 1; spectrum data type, centroid. Data dependent MS2 parameters: microscans, 1; resolution, 15,000; AGC target, 1e5; maximum IT, 50 ms; loop count, 4; multiplexing (MSX) count, 1; TopN, 4; isolation window, 1.0 m/z; isolation offset 0.0 m/z; (N)CE / stepped (N)CE, 20, 30, 40; spectrum data type, centroid.

DATA PROCESSING AND IDENTIFICATION

The LC-MS/MS data was analyzed using MS-DIAL software.[11] Detailed parameter settings are listed in Supplemental Tables 1 and 2 (HILIC and lipidomics data processing settings). Accurate masses, retention times, and peak heights were then exported, and further analysis was performed in R Studio and our in-house developed software for statistical analysis, Metabox.[12] Automated annotation of metabolites was performed separately for polar metabolites and lipids. Table 1 lists libraries, methods, and software used for each platform. Metabolite annotations were done with the help of our in-house developed library containing >600 authentic lipid standards of different classes and >800 standards of polar metabolites. Next, MS/MS database matching was performed with freely available MS/MS spectra obtained from Mass Bank of North America (MoNA), National Institute of Standard and Technology (NIST) 17, LipidBlast, and the NIST Hybrid Library.[13-15] Workflow summarizing all the tools, software and databases are shown in Figure 5.

Figure 5. Workflow summarizing tools, software, and databases used for completing annotation of urine metabolome.

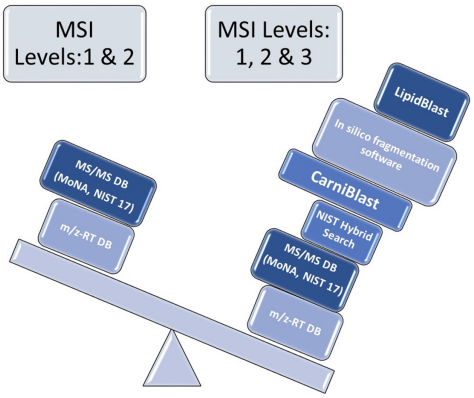

RESULTS AND DISCUSSION

m/z-RT and MS/MS databases

Untargeted lipidomics analysis in the positive ionization mode resulted in 112 identified lipids encompassing several lipid classes. The same sample set was also analyzed using HILIC chromatography. Using the established in-house library, we identified 117 metabolites, which consisted of amino acids, biogenic amines, and derivatives. These annotations are level 1 according to MSI, meaning that the experimental data was compared to authentic standards measured under the same instrumental conditions. Chemical standards (n= 874) were analyzed on two instrument types: quad time-of-flight (QToF) and orbitrap in positive ionization mode. These standards provide several orthogonal parameters: accurate mass (m/z), retention time (RT), and MS/MS. This level of annotation is laboratory/chromatography specific and is clearly a limitation if used exclusively. It takes both time and money to develop and establish such a chromatography. In our own experience, two skilled researchers require two years of work to create and validate a chromatographic run with 1000 metabolites measured on it robustly. It is a common practice in metabolomics research to use MS/MS libraries and perform mass spectral similarity searches in order to increase the annotation rate, as fragmentations are not chromatography specific. Those libraries contain mass spectra of authentic standards from a variety of

instrumentation and chromatography (this metadata is available in .msp/.mgf formats), and this level of compound ID is described as level 2. Users can use freely available databases, such as MoNA, or can opt for commercially available MS/MS databases such as NIST17. We combined two mass spectral databases, MoNA and NIST17, and used the merged .msp within MS-DIAL software for mass spectral similarity matching. Metadata such as dot product, reverse dot product scores, number of matching ions, and MS-DIAL calculated MS2 similarity have been taken into account.

Table 1.

Chromatography and databases	Type of matching	MSI level of annotation	Number of annotations accomplished
HILIC	m/z, RT and MS/MS	1	117
Lipidomics	m/z, RT, MS/MS, in silico MS/MS	1	72
Lipidomics: CarniBlast	m/z , in silico MS/MS	2	18
HILIC: MoNA+NIST14	m/z and MS/MS	2	440
HILIC: CarniBlast	m/z and in silico MS/MS	2	107
Lipidomics: mzRT lookup	m/z	3	96
Hybrid search	MS/MS (hybrid)	3	Sample depending: 4000-8000
In silico fragmentation software: CSI:FingerID	MS1 and in silico MS/MS	3	Sample depending: 4000-8000

M/Z Lookup Table in LipidBlast

This essentially stand-alone tool can be used in addition to LipidBlast. It provides an automated approach for lipid annotations based on their accurate masses and/or chromatographic RT. Additional structure information of the lipids and their side chains (sn1, sn2, sn3) cannot be made using accurate mass alone. For comprehensive structure elucidation, another orthogonal parameter like MS/MS is needed. We extracted m/z precursor information from the MS-DIAL output in positive ionization mode and used the M/Z Lookup Macro to assign additional lipid annotations. Mass tolerance for lipid assignments was calculated based on the mass accuracy of the Thermo Q Exactive instrument and the internal standards, 0.005 Da. This way, an additional 96 lipid annotations were obtained from the lipidomics data set in positive ionization mode.

CarniBlast

The process of lipid degradation (β-oxidation) in human cells occurs in the mitochondria. This allows for the direct coupling of fatty acid degradation to energy generation via the citric acid cycle and respiratory electron transport chain localized in the inner mitochondrial membrane. For the corresponding import process, fatty acids of different chain lengths and saturation are esterified to L-carnitine with the formation of acylcarnitines.[16] L-carnitine can be *de novo* synthesized from *N*-trimethyl-lysine with butyrobetaine as an intermediate in a multi-step pathway. However, most carnitine comes from dietary intake. Fatty acids destined for degradation are first activated via thioesterification into coenzyme A (CoA). Then, three types of carnitine acyltransferases with different chain-length specificities (short, medium, long) transfer fatty acids via transesterification to carnitine with the release of CoA. These are carnitine acyltransferase, carnitine octanoyltransferase, and carnitine palmitoyltransferase. Next, a transport system consisting of carnitine palmitoyltransferase I (outer membrane), carnitine-acylcarnitine translocase, and carnitine palmitoyltransferase II (both inner membrane) transfer the acylcarnitines into the lumen of the mitochondria, where transesterification with CoA regenerates the acyl-CoAs and carnitine.[17,18] Carnitine then leaves the mitochondria via the above outlined transport complex. During β-oxidation, the fatty acids are cleaved between C2 and C3 with the release of a C_2-unit of acetyl-CoA. A *trans*-2 double bond is formed between C2 and C3, hydrated, oxidized, and finally cleaved by the action of four enzymes. Odd chain and unsaturated fatty acids require additional enzymes.[19] The described overall process is an essential part of the lipid homeostasis which covers all fatty acids of different lengths and saturation. Consequently, diseases that disturb this described lipid homeostasis ultimately increase acylcarnitines in the blood and the urine. Therefore, acylcarnitines can be biomarkers for diseases, including heart failure[20], obesity and diabetes[21], chronic kidney disease[22], chronic psychiatric illness[23], migranes[24], and endometrial cancer.[25]

Acylcarnitines in urine serve as biomarkers for bladder cancer[26], diabetic nephropathy[27], obesity[28] and human kidney cancer.[29] It is well documented that carnitine and its esters can be found in almost every bodily fluid, yet the chemical standards are severely limited and/or nonexistent. To overcome this obstacle, we used an in-house developed in silico database of acylcarnitines as they, like many lipid species, fragment in a predictable manner. We exported the .msp files from both polar and lipidomics profiling and matched them against an in silico database of acylcarnitines. Some of the acylcarnitines were already present in our m/z-RT libraries, so using CarniBlast for the lipidomics .msp resulted in only three additional annotations. However, when HILIC .msp was used for the CarniBlast search, it resulted in an additional 793 annotations of acylcarnitines. This number suggests that there are far more carnitines present in urine than previous reports suggest.[30] This increase in annotation rates of acylcarnitines is important due to their role in lipid metabolism and various metabolic diseases. Interestingly, a majority of acylcarnitines couldn't be annotated with any other software or database.

Figure 6. Head-to-tail comparison of an MS/MS spectra of an amino acid shows distinct shift in the spectrum: methylated vs. non-methylated.

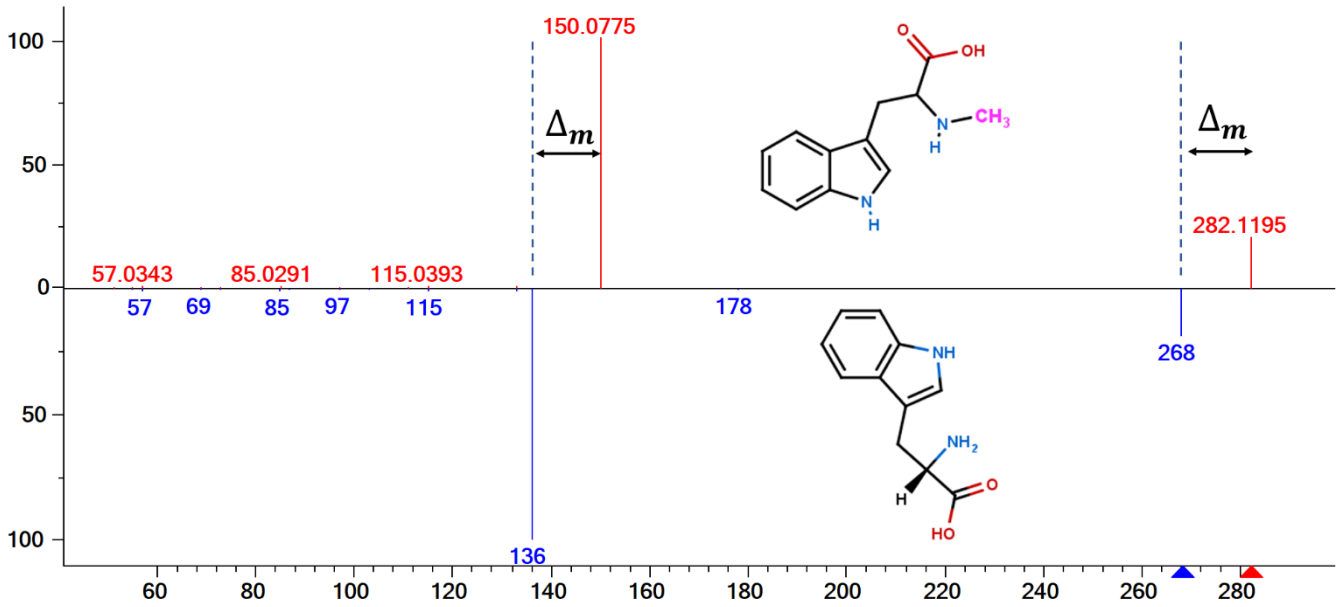

In silico fragmentation software

For the compounds that are not present in our m/z-RT library and have collected MS/MS spectra that cannot be matched in mass spectral libraries, software tools, like MS-FINDER, Sirius, and CFM-ID, are of great value.[31-33] We used the latest Sirius software with CSI:FingerID Interface (Sirius 4.0 built 19) to assign molecular identities to acquired MS/MS spectra.[34] We selected Sirius with CSI:FingerID because it has consistently scored very high during the latest Critical Assessment of Small Molecule Identification (CASMI) challenges. Furthermore, the current version has been improved in accuracy and speed. The MS/MS spectra were exported as a Mascot Generic Format (MGF) file from each raw file using the MSConvert. The MGF file largest in size contained the most MS/MS data and was therefore used for further analysis. A standard MGF file with 6482 MS/MS spectra was imported and 6447 features were available in the software. Formula assignment in positive ionization mode was performed with 10 ppm while retaining the 10 best formula candidates. Processing time was 2 minutes on a 16 CPU machine and the software was capable to assign formulas to a total of 6184 features. Fingerprint matching with CSI:FingerID via a webservice was subsequently performed to annotate isomer structures. Through this, 728 MS/MS peaks could be assigned when searching bio-databases and 1557 features could be assigned when querying the much larger PubChem database. The search time was around 5 minutes. The results, isomer structures, and their scores are presented in the Graphical User Interface (GUI) software. Additionally, results can be exported to CSV files. For the biodatabase search, up to 130 results were obtained per MS/MS scan, while the PubChem fingerprint research resulted in up to 10,000 candidates per MS/MS spectrum searched. Here individual and time-consuming investigations have to be performed to investigate the correctness of the found structures. In order to show the accuracy of CSI:FingerID we also performed a search

on compounds that were annotated by our in-house database. Sirius 4.0 and CSI:FingerID with 5ppm mass accuracy and search in bio-databases correctly identified 41 compounds as a top hit. Approximately 52% of the known compounds were correctly assigned within the top 3. The median rank for all 103 compounds was one and the average rank ten. Considering its excellent search speed and accuracy, CSI:FingerID should be considered a useful annotation tool for the identification of unknown compounds. The associated results can be found in the supplement. In our previous work, we have shown that it is possible to combine the outputs (results) of multiple software to create a new ranking system based on the accuracy of each software and rank the correct structure as the top hit in 93% of the cases.[35] However, this approach is not easily applicable as it requires both compound database boosting as well as thorough software comparison for the defined sample set.

Figure 7. Structural classification of metabolites present in the urine of 12 patients diagnosed with IC

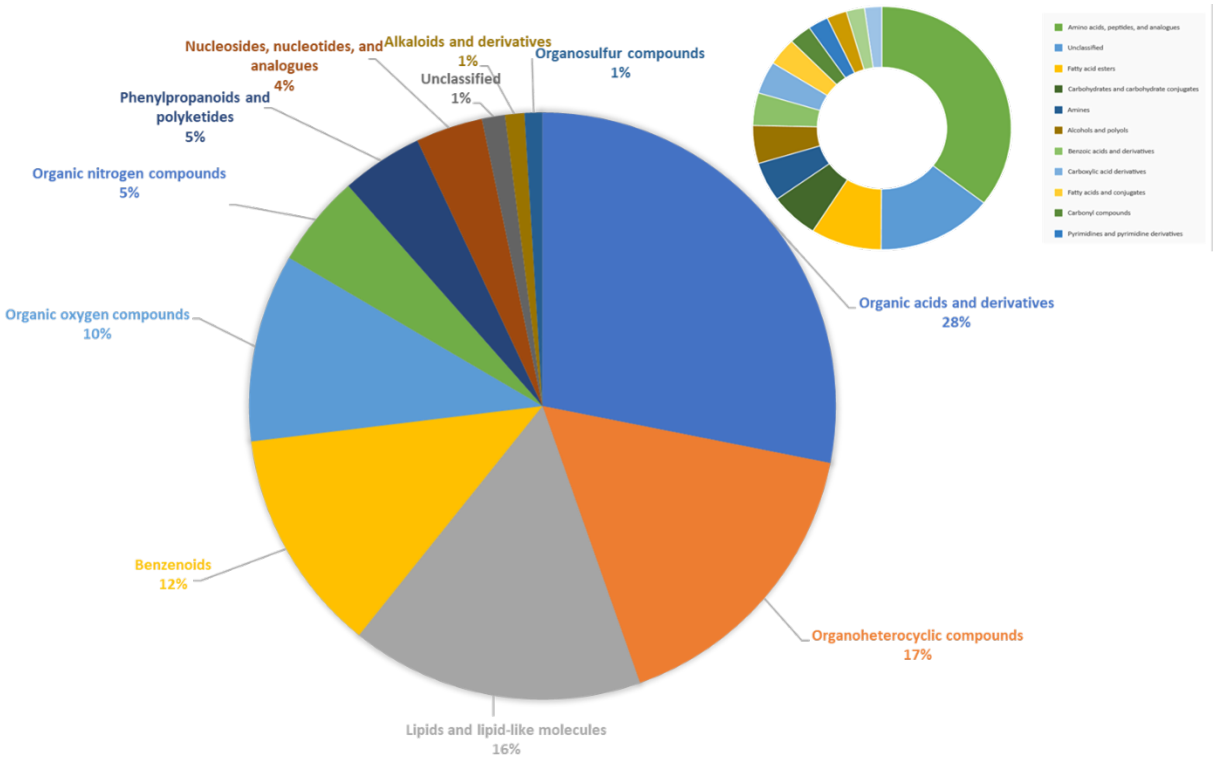

NIST Hybrid search coupled with ClassyFire

Epimetabolites are defined as regulatory metabolites that have been removed from their classical functions by modification (for example, methylation or acetylation) but often remain chemically similar to their canonical counterparts.[36] NIST recently introduced a fantastic mass spectral library-based method to annotate MS/MS spectra that contain the aforementioned modifications. It is described as a "hybrid" method because it combines matching fragments but not the m/z of the precursor (to allow for modification calculations that are then reflected).[37] Such a tool is of great assistance in structure elucidation of unknown metabolites, as it mimics the knowledge and experience of a well-trained chemist.[38] The hybrid search comparison is shown in Figure 2, where the head-to-tail comparison of an amino acid shows a distinct shift in the spectrum, methylated versus non-methylated. We exported the .msp files from MS-DIAL to the NIST pepSearch GUI, activated the hybrid search function, and ran it against the MS/MS hybrid libraries. As a result of the hybrid search, every MS/MS spectra are now associated with an annotation and a variety of scores. Results of the hybrid search for both HILIC and CSH data are presented in Supplemental Table 5. The advantage of using NIST Hybrid search is that it supports batch processing, offers restrictions in terms of which MS/MS spectra should be included or excluded, and allows users to quickly get a snapshot of the metabolome they are measuring. The result list contains a lot of meta-data, such as chemical name, International Chemical Identifier (InChI) key, simplified molecular-input line-entry system (SMILES), probability score, etc. Those annotations should be treated with caution as they do not represent an identification but rather a "nearest known neighbor" to the unknown molecule. Next, the result list

of NIST hybrid search was coupled with a fully automated, comprehensive chemical classification tool that utilizes a well-defined chemical hierarchy system - ClassyFire. ClassyFire successfully annotated and classified thousands of molecules from various libraries, including DrugBank, LIPID MAPS, HMDB, ChEBI, and PubChem.[39] We used ClassyFire Batch by Fiehn Lab (**http://cfb.fiehnlab.ucdavis.edu/**), a user-friendly web application capable of batch classifications directly from InChIKeys.

Figure 7 shows complexity of urine metabolome based on the superclass and subclass classifications as defined by Classyfire. Results of classifications are organized into Kingdom, Superclass, Class, Subclass, and two parent levels. Subsets of those results is shown in Supplemental Table 6. We can imagine that such combinatorial approach becomes of importance in personalized medicine or health research in general, since it is evident from Supplemental Tables that the metabolic profile of urine varies from patient to patient. While biomarker discovery focuses on the shared metabolites between patients, it is also important to recognize and investigate differences due to diet, exposure, genetics, and other factors.

Summary

Metabolomics reports and data should be annotated with confidence levels for clarity and reproducibility purposes. Sharing the MS/MS data with the community will directly improve not only other researchers' work but will also help the development of tools that aid structure elucidation process. Hopefully this work provides a comprehensive overview of some of the best freely available tools and databases for metabolomics research and will be of use to analysts when annotating unknown metabolites.

Work in progress 3: (ready for submission)

Pioglitazone Alters the Proteomes of Normal Bladder Endothelial Cells but Shows No Tumorigenic Effects

Thiazolidinediones (TZDs), such as pioglitazone and rosiglitazone, are currently the only oral drugs with a confirmed antihyperglycemic impact in type 2 diabetes mellitus (T2DM) patients. As agonists of peroxisome proliferator-activated receptor γ (PPARγ), TZDs are known to positively influence insulin sensitivity and β-cell function and potentially alter lipid profiles. Pioglitazone is a synthetic ligand of PPAR*γ* and is used as a therapeutic treatment for patients with T2DM. PPARγ, a ligand-activated transcription factor, is expressed in white and brown adipose tissues as well as in the urinary bladder [40]. Pioglitazone has also been shown to reduce macrophage infiltration through the activation of PPARγ and induction of apoptotic cell death [41], which can lead to decreased numbers of macrophages in adipose tissues [42]. To examine the impact of PPAR*γ* on bladder cell function, several studies analyzed the expression of PPAR*γ* in normal bladder and bladder cancer (BC) mucosal samples. They observed different rates of cell migration and invasion in various BC cell lines that express PPAR*γ*. In addition, prior studies have shown that vascular endothelial growth factor A (VEGF-A), a primary proangiogenic factor, is positively regulated by PPARγ [43]. PPARγ can also exert its functions via the activation of signaling pathways, interaction with Wnt/β-catenin, and induction of signaling pathways involved in proliferation and survival, such as IGF-I/PI3K/AKT/mTOR and MAPK [44]. Furthermore, PPAR*γ* can regulate the inflammatory response of macrophages through TLR4/NF-κB signaling [45].

There have been contradictory reports on the potential association between diabetes mellitus (DM) and elevated risk of BC [46,47]. Studies have demonstrated that pioglitazone can have adverse effects that exaggerate the risk of BC. DM patients, particularly males, on long-term, high doses of pioglitazone, are at a higher risk of developing BC [48,49]. The Kaiser Permanente Northern California (KPNC) study determined that inflated dose and length of pioglitazone treatment correlated to increased rates of BC [43]. Currently, the U.S. Food and Drug Administration (FDA) allows the use of pioglitazone in patients with special caution to those with a prior history or active BC [50]. A potential reason for this observation could be that PPAR*γ* signaling in BC cells may provide a tumor microenvironment that allows for de novo lipogenesis of lipids that can be utilized in increasing tumor mass and energy usage [51]. However, other studies have shown that TZDs posed no risk on survival in BC patients who

underwent radical cystectomy [52]. A recent meta-analysis found no difference in BC incidence among users of pioglitazone and nonusers [53]. These inconsistencies between studies have led to questions in the legitimacy of studies and the actual dangers of continued pioglitazone use. Due to the inherent difficulty of accurately assessing the link between TZDs and BC, the association between the two is still in controversy.[54]

The goal of our study was to determine whether TZDs have any negative or positive effects on the healthy bladder epithelium. Since pathophysiological changes require the actions of a series of key proteins, global proteomic analysis of protein alterations using state-of-the-art mass spectrometry is ideal for acquiring unbiased biological information regarding molecular mechanisms. Using such a method, this study aimed to understand the mechanistic meanings of proteome perturbations in the normal bladder due to TZD treatment. We sought to examine the effects of pioglitazone specifically, being that is the most widely used TZD. Our global quantitative proteomic analyses found that pioglitazone alters the proteome and biological networks in normal human bladder cells without tumorigenic effects.

MATERIALS AND METHODS

Cell culture. Immortalized normal human bladder epithelial cells, TRT-HU1, were established and characterized as described previously [55].·Cell lines that were initially established, frozen, and under a passage number of 10 were used in this study. Culture media was changed after one day of subculturing and cells were passed again when there was 70-80% confluence. All cells were negative for mycoplasma contamination, and this was tested for monthly via PCR. Cells were maintained in Dulbecco's modified Eagle's medium (DMEM) supplemented with 10% fetal bovine serum (FBS) (Invitrogen), 1% penicillin/streptomycin, and 1% L-glutamine (Sigma-Aldrich Corp., St. Louis, MO, USA) under a humidified atmosphere of 5% CO_2 at 37 °C.

Antibodies and reagents. Antibodies against various proteins were obtained from the following sources: ACTG2 (ab189385), MYH3 (ab124205), OXPHOS (ab110413) from Abcam; phospho-NF-κB (3033), phospho-HER2/ErbB2 (2247), phospho-PAK1 (2601), phospho-GSK-3β (9336), Snail (3879), N-cadherin (13116), Slug (9585), β-catenin (8480), E-cadherin (14472), Tight Junction Antibody Kit (8683) from Cell Signaling Technology, and β-actin (A1978) from Sigma. Commercially available horseradish peroxidase (HRP)-conjugated secondary antibodies (7074, 7076) were obtained from Cell Signaling Technologies. All other chemical reagents were procured from Sigma Chemical Corp.

Quantitative proteomics. For quantitative proteomics, the tandem mass tagging (TMT)-based method was performed, as previously described [56,57]. In brief, cellular proteins from 25 μM pioglitazone-treated and control TRT-HU1 cells were extracted using a 4% SDS-containing buffer. The protein concentration was then determined from each sample using the Pierce 660nm Assay Kit (Thermo Fisher Scientific). The kit was carried out using 60 μg of protein from each sample, which was digested with trypsin via filter-aided sample preparation (FASP) and labeled with TMT6plex reagents in parallel.

After TMT-labeling, the peptides were reconstituted and desalted via C18 spin columns (Thermo Scientific) and separated by high-pH reversed-phase liquid chromatography (RPLC) using an Ultimate 3000 XRS System (Thermo Scientific). For high-pH RPLC, 50 μg of TMT-labeled peptides were injected onto a 100-mm Hypersil GOLD C_{18} column (2.1 mm inner diameter, 3 μm particle size, 175 Å pore size) (Thermo Scientific) and eluted for 3 min with a flow rate of solvent A, which consisted of 10 mM ammonium formate at pH10. Peptides were then separated with a 7 min linear gradient of 0-40% solvent B, which consisted of 10 mM ammonium formate and 95% acetonitrile at pH10. The labeled peptides were then separated into 24 fractions, concentrated into 12 fractions, and dried down through a SpeedVac (Thermo Scientific). Peptides in each fraction were rehydrated with 0.2% formic acid, and liquid chromatography-tandem mass spectrometry (LC-MS/MS) analysis was performed using an EASY-nLC 1000 connected to an LTQ Orbitrap Elite Mass Spectrometer (Thermo Scientific). Briefly, peptides were loaded onto a 2-cm trap column (PepMap 100 C18, 75 μm inner diameter, 3 μm particles, 100 Å pore size) and separation was done using a 50-cm EASY-Spray column (PepMap RSLC C_{18}, 75 μm inner diameter, 2 μm particles, 100 Å pore size) heated up to 55°C. To separate low-pH peptides, RPLC was employed using a mobile phase that consisted of either 0.1% formic acid in water (phase A) or acetonitrile (phase B). The

LC gradient was 4-24% B over 200 min, 24-50% B over 20 min, and 50-100% B over 5 min at a flow rate of 150 nL/min, which was then followed by 100% B over 15 min at a flow rate of 300 nL/min.

Mass spectra were acquired in a data-dependent manner, selecting up to the 15 most abundant precursor ions for higher-energy collisional dissociation. No further data processing, such as smoothing, de-isotoping, and/or filtering, was carried out. The mass resolution for precursor and fragment ions were set to 120,000 and 30,000, respectively. The isolation width was set to 1.5 and the normalized collision energy was set to 40. Database searching and protein quantification was performed by Proteome Discoverer (v2.1) using the SEQUEST algorithm. The acquired raw data were searched against the human Uniprot Protein Sequence Database (released on 01/22/2016, containing 20,985 protein sequences). Several parameters were set as follows: trypsin, up to two missed tryptic cleavages were allowed; precursor ion tolerance of 10 ppm, fragment ion tolerance of 0.02 Da; followed by numerous modifications: carbamidomethylation of cysteines and TMT6plex alteration of lysines. The N-terminal of peptides was set as fixed variations; while the acetylation of protein N-term, oxidation of methionine, and deamination of asparagines and glutamines were variable modifications. To identify peptides identifications and proteins, a standard false discovery rate (FDR) of 1% was applied to filter peptide-spectrum matches (PSMs).

To quantify proteins, peptides with >30% precursor ion interference were excluded to minimize inaccurate quantifications caused by precursor ion interference. PSM level information was extracted using Proteome Discoverer [58]. After quantifying each PSM intensity, the peptide intensities were summarized, as previously described [59]. In brief, this was done in 4 steps: 1) the normalized log2 intensity of the PSMs matched to each peptide by the substrate mean PSM from each reporter intensity was centered, 2) outliers were detected using Dixon's Q-test and generalized electrostatic discharge (ESD) test, 3) the mean intensity without outliers was taken, and 4) the grand mean intensities of the three highest abundant PSMs were added before being mean-centered. Bipartite graphs of peptides and protein groups were generated according to the information of the aligned peptides. Among the protein group, we defined the representative protein that had the largest number of peptides or unique peptide [60]. When there was more than one protein with the same number of peptides in the same protein group, we selected the protein that had the highest sequence coverage. We then computed the relative intensity of the protein group using a linear-programming formulation, as previously described [61].

Identification of differentially expressed proteins (DEPs). To identify DEPs, we first selected proteins that have more than two non-redundant peptides in each sample. We then performed a one sample t-test using the $\log_2$ fold-changes to compute the significance. For hypothesis testing, an empirical null distribution, which means that a protein is not differentially expressed, was estimated through the following steps: 1) we applied 100,000 random permutations of the samples, 2) we computed t-values using $\log_2$ fold-changes of randomly permuted samples, and 3) we applied the Gaussian kernel density estimation method to t statistics. FDRs of each protein for the one sample t-test were then calculated using Storey's correction method[62]. Proteins were identified as DEPs if they had FDR<0.05 and absolute $\log_2$ fold-change ≥0.58 (1.5 fold). Functional enrichment analysis of DEPs was performed using DAVID (Ver. 6.8) [63]. Significantly enriched cellular processes were selected for if they had an enrichment p-value<0.05. Functional classification analysis was performed using PANTHER (Ver. 11) [64].

***Master regulator analysis (MRA*)**. To identify master regulators, we discerned each DEP and counted their individual partners. The protein-protein interaction information was obtained from six interactome databases: the Biological General Repository for Interaction Datasets (BioGRID)[65], the Database of Interacting Proteins (DIP)[66], High confidence protein-protein interactions (HitPredict)[67], the IntAct molecular interaction database (IntAct)[68], the Molecular INTeraction database (MINT)[69], and the STRING database [70]. We then computed the enrichment p-values using Fisher's exact test. Finally, we selected proteins with p-values lower than 0.01 and prioritized the DEPs based on the number of interaction partners.

Western blot analysis. Whole-cell lysates were prepared as previously described [71]. Briefly, cells were seeded onto 10 cm plates and exposed to 25 μM concentrations of pioglitazone for 72 h. Control and treated cells were then collected, lysed with RIPA buffer (20 mM Tris, 150 mM NaCl, 1% Nonidet, P-40, 0.1 mM EDTA) (Pierce, ThermoFisher) supplemented with a phosphatase inhibitor cocktail (ThermoFisher), homogenized, and centrifuged at 13,000 g and 4°C for 20 min to obtain whole-cell lysates. Using 25 μg of extracted protein, we

separated the proteins using a 4-15% SDS-PAGE gel and transferred them onto a polyvinylidene fluoride (PVDF) membrane. The membranes were then blocked with either 5% bovine serum albumin (BSA) or 5% nonfat milk in Tris-buffered saline with 0.1% Tween 20 (TBST [2.42 g/L Tris–HCl, 8 g/L NaCl, and 1 mL/L Tween 20 (pH 7.6)]) for 1 h at room temperature. All primary antibodies incubations were done at 4°C overnight followed by 3 X 10 min washes with TBST. HRP-conjugated secondary antibody incubations were done at room temperature for 1 h and followed by 3 X 10 min washes with TBST. β-actin was used as an internal control. All western blot experiments were run in at least triplicates for each antibody and analyzed from different lysates using standard procedures.

Measurement of Reactive Oxygen Species (ROS). Intracellular ROS levels were measured with 2',7'-dichlorofluorescin diacetate (DCF-DA) using fluorescence-activated cell sorting (FACS) analysis as previously described [72]. Cells were loaded with 20 μM of DCF-DA and fluorescence was measured with a flow cytometer (FACSCalibur, Becton-Dickinson, Franklin Lakes, NJ). The mean DCF fluorescence intensity was measured with maximum excitation and emission spectra of 495 nm and 529 nm, respectively.

Cell proliferation assay. To determine cell growth during exposure to pioglitazone, TRT-HU1 cells were seeded at a density of 5 x 10^4 cells/well in six-well plates. Cells were then incubated with standard growth medium and treated with varying doses of pioglitazone (0, 25, 50, or 100 μM) (E6910, Sigma-Aldrich Corp.) or vehicle. Cell numbers were evaluated after 24, 48, and 72 h by removing the medium, incubating cells with trypsin/EDTA for 5 min, adding trypan blue, and counting the suspended live cells using a hemocytometer. The formula averages of each count were used as the total density of the well after each time point. For crystal violet staining, the medium was removed and replaced by 200 μl of a 0.05% solution of crystal violet. After incubation at room temperature for 15 min, the dye was removed, and the wells were washed thoroughly with phosphate buffered saline (PBS). Later, the cells were fixed with 4% paraformaldehyde at room temperature for 5 min. The cells were then washed with tap water and dried out on filter paper. For quantitative analysis, the stained cells were

Figure 1. Overview of global proteomics workflow for data generation and analysis. (A) Western blot analysis shows the effects of pioglitazone treatment on PPARγ expression. **(B)** Proteomics analysis workflow for this study.

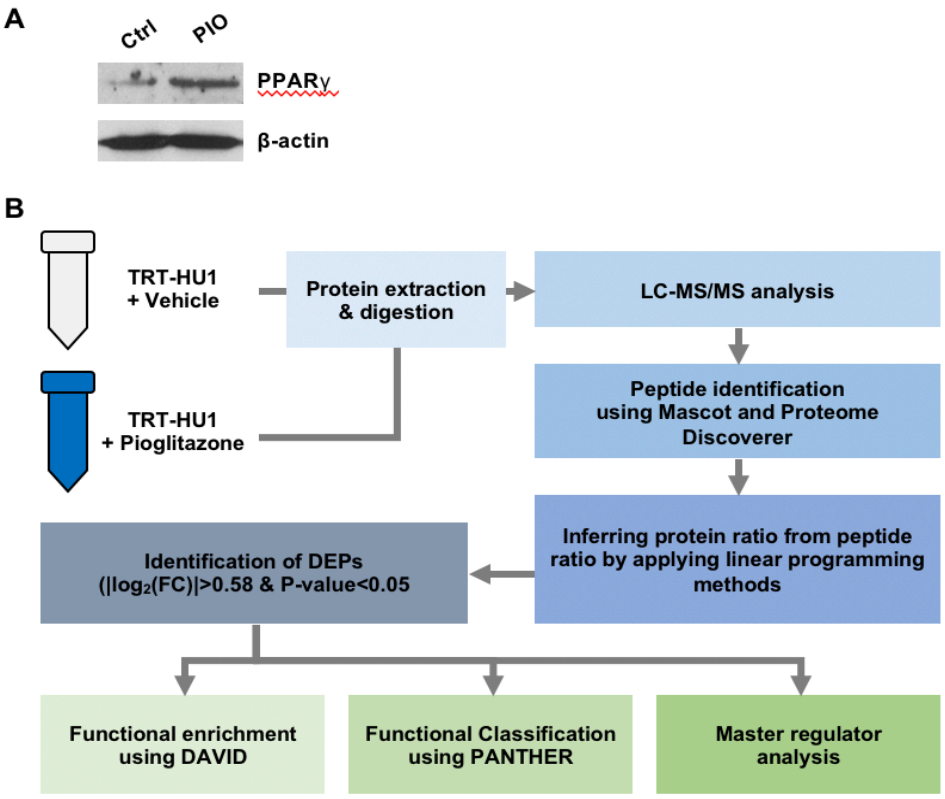

dissolved in 10% acetic acid and subjected to absorbance measurements at 570-590 nm [73]. Each assay condition was run in triplicates, and the data are representative of three independent trials.

Statistical analysis. Student's t-tests were performed to evaluate differential expression of the proteins between two groups. Variables with normal distribution were expressed as mean ± standard deviation (SD). All reported p-values are two-tailed, with p <0.05 being considered as statistically significant.

RESULTS

Pioglitazone perturbs the whole proteome in bladder epithelial cells. Labeled LC-MS/MS proteomic analysis was conducted to identify the global proteomes TRT-HU1 bladder cells treated with or without 25 μM of pioglitazone. We found that pioglitazone treatment increased PPARγ protein expression (**Figure 1A**). Our proteomics analysis workflow is summarized in **Figure 1B**.

We detected 5,769 proteins in total, including proteins from the cell part (n=2,375), organelle (n=1,663), macromolecular complex (n=1,060), membrane (n=643), extracellular region (n=88), cell junction (n=61), synapse (n=43), and extracellular matrix (n=29) (**Figure 2A**). To identify DEPs between the control vs. pioglitazone groups, we performed a statistical hypothesis test using an empirical null model (see Methods). Among the 5,769 proteins, 124 DEPs (including 95 upregulated and 29 downregulated proteins) were found to have absolute log2 fold-changes ≥0.58 and p-values <0.05. Approximately 70% of the DEPs (n=95) showed increased expression due to pioglitazone treatment (**Figure 2B**).

Figure 2. Total proteins and differentially expressed proteins (DEPs) perturbed by pioglitazone treatment. (**A**) Pie chart depicts the cellular location of the detected DEPs. (**B**) Pie chart shows proportion of up- and downregulated DEPs in cells treated with pioglitazone. (**C**) Volcano plot showing the up- or downregulated DEPs in bladder epithelial cells treated with pioglitazone. Up- and downregulated DEPs are marked as red or blue, respectively. Protein symbol of the top 5 up- or downregulated proteins are presented in the volcano plot.

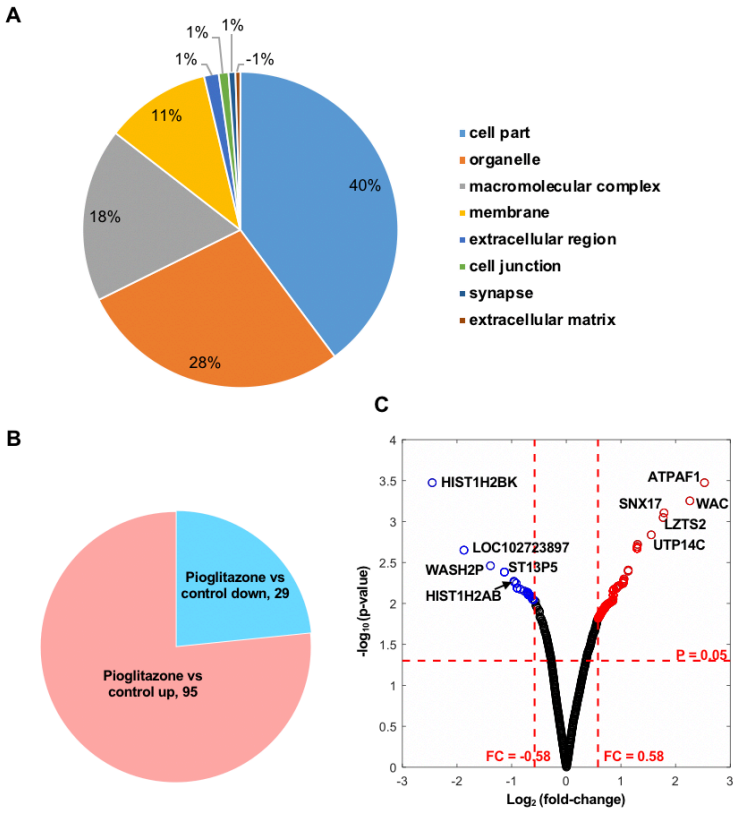

Volcano plot displays DEPs between control and pioglitazone groups. The top 5 most significantly up- or downregulated proteins were highlighted with their official symbol (**Figure 2C**). HIST1H2BK (histone cluster 1 H2B family member K), ST13P5 (ST13, Hsp70 interacting protein pseudogene 5), and WASH2P (WAS Protein Family Homolog 2 Pseudogene) were the most significantly downregulated by pioglitazone treatment. ATPAF1 (ATP Synthase Mitochondrial F1 Complex Assembly Factor 1), SNX17 (Sorting Nexin 17), LZTS2 (Leucine Zipper Tumor Suppressor 2), and UTP14C (UTP14C, Small Subunit Processome Component) were the most upregulated in response to pioglitazone. **Supplementary Table S1** shows the list of DEPs that were altered in response to pioglitazone along with the transcriptional targets of PPARγ and test statistics. This data suggest that pioglitazone may induce transcriptional programming through PPARγ, which contributes to increased protein expression.

Functional enrichment analysis reveals that pioglitazone modulates key biological processes. To check the function of proteins perturbed by pioglitazone, we performed functional enrichment and classification using DAVID and PANTHER, respectively [63,64]. Muscle filament sliding, actin-mediated cell contraction, cellular oxidant detoxification, cell adhesion, purine nucleoside monophosphate metabolic process, ATP metabolic process, and cytoskeleton organization were enriched by upregulated DEPs. However, chromatin silencing, gene silencing, and regulation of gene expression were enriched by downregulated DEPs **(Figure 3A**). We listed the DEPs belonging to actin-mediated cell contraction, cellular oxidant detoxification, cell adhesion, purine nucleoside monophosphate metabolic process, and chromatin silencing **(Table 1).**

Table 1. Enriched biological processes and corresponding proteins in upregulated (A) and downregulated proteins (B).

A.

GO term	Gene	P-value	Z Score
Muscle filament sliding	MYH2, MYH3, MYH4, MYH7, MYH8, MYL1, MYL3	3.84E-08	7.41
Actin-mediated cell contraction	MYH2, MYH3, MYH4, MYH7, MYH8, MYL1, MYL3	1.29E-05	4.89
Cellular oxidant detoxification	SOD1, TXN, CCS, PARK7, TXNDC17, SRXN1	7.75E-05	4.11
Cell adhesion	ARHGDIB, DSG1, S100A11, SOD1, PCDHGB4, PCDHGA8, CCS, PARK7, PCDHGA12, PYCARD, PCDHGC5, PCDHGC4, PCDHGB3, PCDHGA9, PCDHGA6, PCDHGA5, PCDHGA4, PCDHGA3, PCDHGA2, PCDHGA1	0.000906	3.04
Cytoskeleton organization	ARHGDIB, CFL1, KRT5, KRT9, KRT16, MYH3, SOD1, PHPT1, PYCARD, SH3BGRL3, KRT74, MTPN, WASH3P	0.014298	1.84

B.

GO term	Gene	P-value	Z Score
Negative regulation of gene expression	BMI1, HIST1H2AD, HIST1H2AJ, HIST1H2AC, HIST1H2AB, HIST2H2AA3, HIST2H2AC, HIST1H4A, HIST1H2AG, H2AFJ, HIST1H2AH, HIST3H2A	5.9895E-06	5.22
Regulation of gene expression	ACTG2, BMI1, HIST1H2AD, HIST1H2AJ, HIST1H2AC, HIST1H2AB, HIST2H2AA3, HIST2H2AC, HIST1H4A, HIST1H2AG, H2AFJ, HIST1H2AH, HIST3H2A	0.021575	1.66
Chromatin silencing	HIST1H2AD, HIST1H2AJ, HIST1H2AC, HIST1H2AB, HIST2H2AA3, HIST2H2AC, HIST1H4A, HIST1H2AG, H2AFJ, HIST1H2AH, HIST3H2A	1.13049E-15	14.94
Gene silencing	HIST1H2AD, HIST1H2AJ, HIST1H2AC, HIST1H2AB, HIST2H2AA3, HIST2H2AC, HIST1H4A, HIST1H2AG, H2AFJ, HIST1H2AH, HIST3H2A	2.35734E-12	11.63

Interestingly, the classified molecular functions of the DEPs include binding, catalytic activity, structural molecule activity, antioxidant activity, translation regulator activity, transporter activity, receptor activity, and signal transducer activity **(Figure 3B).** Binding function was the largest portion of both the upregulated and downregulated DEPs. Catalytic, antioxidant, translation regulator, and transporter activity were the major molecular functions in the upregulated DEPs. However, receptor and signal transducer activity were the major functions in downregulated DEPs. The classified cellular compartments of the DEPs were cell part, membrane, organelle, cell junction, macromolecular complex, and extracellular region **(Figure 3C).** Membrane, cell junction, and extracellular region were the major cellular compartments in upregulated DEPs. Organelle and macromolecular complex are major cellular compartments in the outer circle.

Identification of protein interaction networks regulated by pioglitazone treatment. Our present study revealed a large set of proteins (n=5,769) with relevant levels of abundance in normal bladder epithelial cells. These proteins actively participate in various cellular processes, including actin regulation and chromatin remodeling (**Figure 3A**). Pioglitazone perturbs and modulates these cellular processes by affecting protein-protein interactions. We therefore performed MRA using all the proteins detected in our global proteomic analysis to identify key proteins that can be major nodes in the protein-protein interaction networks. To select key proteins, we first identified proteins with a large number of interactions from those detected. We then determined the top 5 proteins with the largest number of interactions and the most significant p-values **(Figure 4A and Supplementary Table S2).**

Figure 3. Functional enrichment and classification of the DEPs. (**A**) Bar plot shows biological processes enriched by the up- and downregulated DEPs. (**B**) Top molecular functions of upregulated (inner circle) and downregulated (outer circle) proteins. (**C**) Top cellular compartments of upregulated (inner circle) and downregulated (outer circle) proteins.

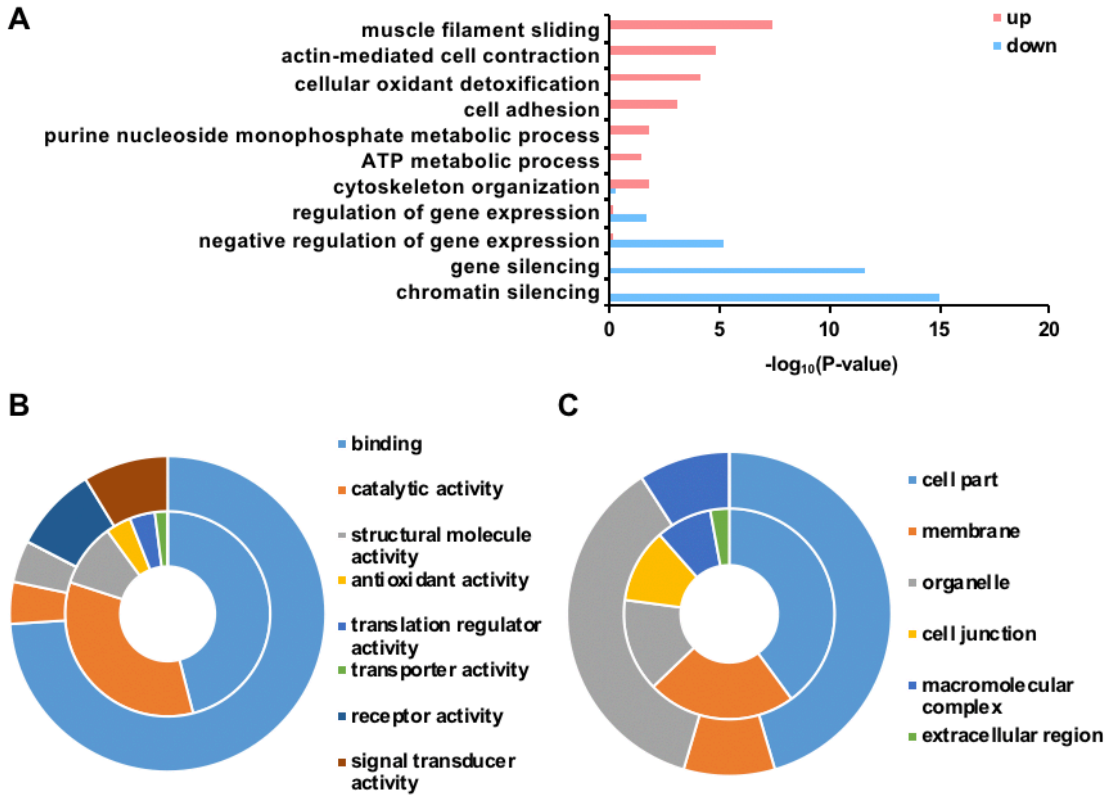

To reconstruct the network model, top 3 proteins were then used. Of note, B lymphoma Mo-MLV insertion region 1 homolog (BMI1), HIST1H4A, and superoxide dismutase 1 (SOD1) were found to be the top 3 regulators, with p-values <0.01 and large target counts. The network model describes the interactions among the top 3 regulators and their interactors with significant differential expression when treated with pioglitazone. Pioglitazone treatment downregulated expression of BMI1, which was found to interact mainly with histone proteins, such as HIST2AH2AA3, HIST2H2AC, HIST1H4A **(Figure 4B).** Expression of SOD1 increased with pioglitazone treatment and it was found to interact with two other upregulated proteins, PARK7 (parkinsonism associated deglycase) and CCS (copper chaperone for superoxide dismutase). Interestingly, downregulation of BMI1 and its interacting histone proteins in the network model suggests potential epigenetic regulation by pioglitazone, which is consistent with functional enrichment data indicating “chromatin silencing” **(Figure 3A)**.

Figure 4. Potential master regulators suggested by master regulator analysis (MRA). (**A**) Scatter plot displays distribution of detected proteins by number of interactions and level of significance driven by MRA. **(B)** Network model describing the interactions of the top 3 master regulators and their interacting DEP partners. Red font denotes the top 3 master regulators.

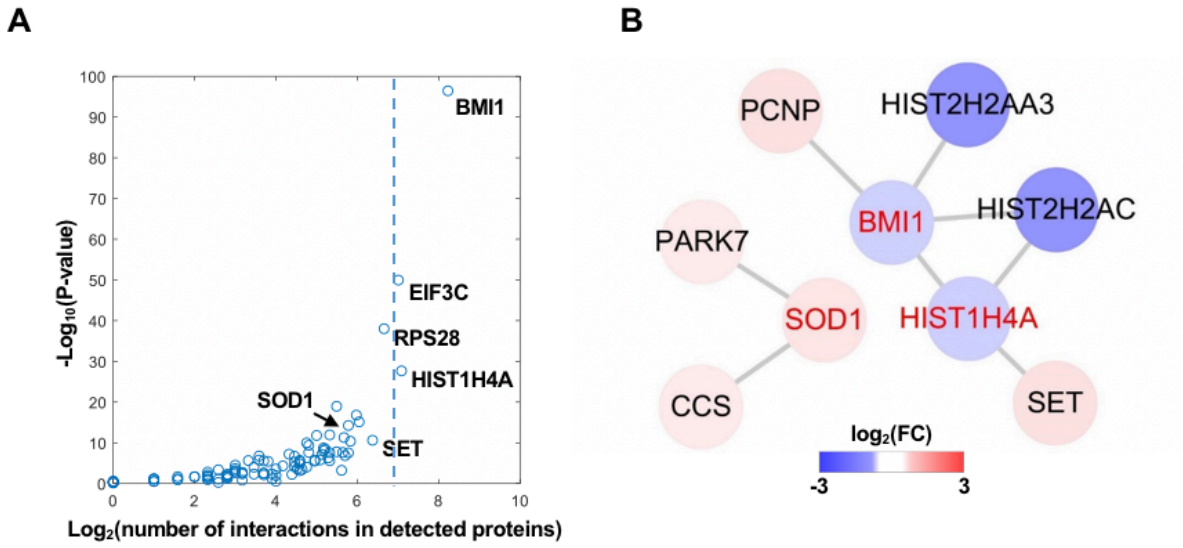

Biological effects of pioglitazone on immortalized normal bladder epithelial cells. To further validate the DEPs between the control vs. pioglitazone groups, proteins were selected for based on functional enrichment analyses. Additional western blot analysis demonstrated that expression of MYH3 (myosin heavy chain 3) was upregulated, while expression of ACTG2 (actin gamma 2) was downregulated in cells treated with 25 μM of pioglitazone **(Figure 5A)**. Consistent with morphological changes in pioglitazone-treated cells, we found that protein expression of mesenchymal cell markers, including N-cadherin, Snail, Slug, and β-catenin, were significantly reduced in pioglitazone-treated cells, compared to control cells (**Figure 5B**). In addition, tight junction proteins, including zonula occludens (ZO) 1 and 2 and CD2AP (CD2-associated protein), that are involved in cell-cell contact regions [74] were greatly reduced in pioglitazone-treated cells **(Figure 5C)**.

To determine whether pioglitazone regulates mitochondrial quantity or metabolic respiration-associated proteins, a series of mitochondrial oxidative phosphorylation (OXPHOS) proteins [75] were measured via western blot analysis. The expression levels of OXPHOS subunits, such as C I subunit (NDUFB8), C II subunit [SDHB (succinate dehydrogenase)], C III core protein 2 [UQCRC2 (ubiquinol- cytochrome C reductase core protein 2)], C IV subunit [MTCO1 (Mitochondrially Encoded Cytochrome C Oxidase I)], and C V alpha subunit [ATP5A (ATP synthase subunit alpha)], did not change by pioglitazone treatment **(Figure 5D)**. To profile the phosphorylation events in normal bladder cells, human TRT-HU1 cells were treated with or without pioglitazone. We performed a series of western blot analyses between the control and pioglitazone-treated groups and found that several phosphorylation events of specific signaling pathways were regulated by pioglitazone. The phosphorylation levels of NF-κB, Erk/MAPK, ERBB2 and p21 activated kinase 1 (PAK1) decreased. On the contrary, only the phosphorylation levels of GSK3β increased. Additionally, studies have shown that the activation of PPARγ through agonists reduces diabetic myocardial fibrosis via regulation of the TGF-β/ERK pathway and EMT [76], which were both found to be upregulated in pioglitazone-treated cells compared to controls **(Figure 5E)**.

To further elucidate on the role of pioglitazone on oxidative stress, cells were treated with pioglitazone for 72 h, and the resulting ROS levels were measured and analyzed. Levels of ROS were unchanged between the control and pioglitazone groups **(Figure 5F)**. In addition to our proteomic analysis, we assessed whether pioglitazone affects cell proliferation. After incubating TRT-HU1 cells in varying concentrations of pioglitazone (25, 50, or 100 μM) for 24 and 48 h, we found that the cell proliferation rates of cells treated for 48 h were significantly suppressed, compared to controls (**Figure 5G-H**).

Figure 5. Effects of pioglitazone treatment on THT-HU1 cells. Cells were incubated in DMEM supplemented with 25 μM of pioglitazone for 72 h before cell lysates were immunoblotted with various antibodies as indicated. **(A)** Immunoblot analyses were performed to validate the expression levels of identified DEPs. The protein expression levels of MYH3 and ACTG2 significantly decreased with pioglitazone treatment (PIO), compared to controls (Ctrl). **(B)** Several EMT markers, including Slug, Snail, N-cadherin, β-catenin, and E-cadherin, were measured by immunoblot analysis. **(C)** Cell junction markers (ZO-1, ZO-2, and CD2AP) were also measured by immunoblot analysis. β-actin was used as the loading control. **(D)** Levels of mitochondrial oxidative phosphorylation (OXPHOS) markers were compared between Ctrl and PIO groups. No significant changes were observed in response to pioglitazone treatment. **(E)** Western blot analysis of key signal transduction proteins, including phospho-NF-κB, phospho-Erk/MAPK, phospho-HER2/ErbB2, phospho-PAK1 and phospho-GSK-3β. β-actin was used as an internal control. **(F)** ROS production levels were compared between Ctrl and PIO groups. NS, nonsignificant. **(G)** Cell proliferation rate was measured by counting with trypan blue staining. *, P < 0.01; **, P < 0.005; NS, nonsignificant. **(H)** Dose- and time-dependent cell growth rates were measured in an independent set of experiments. *, P < 0.01; **, P < 0.005; NS, nonsignificant.

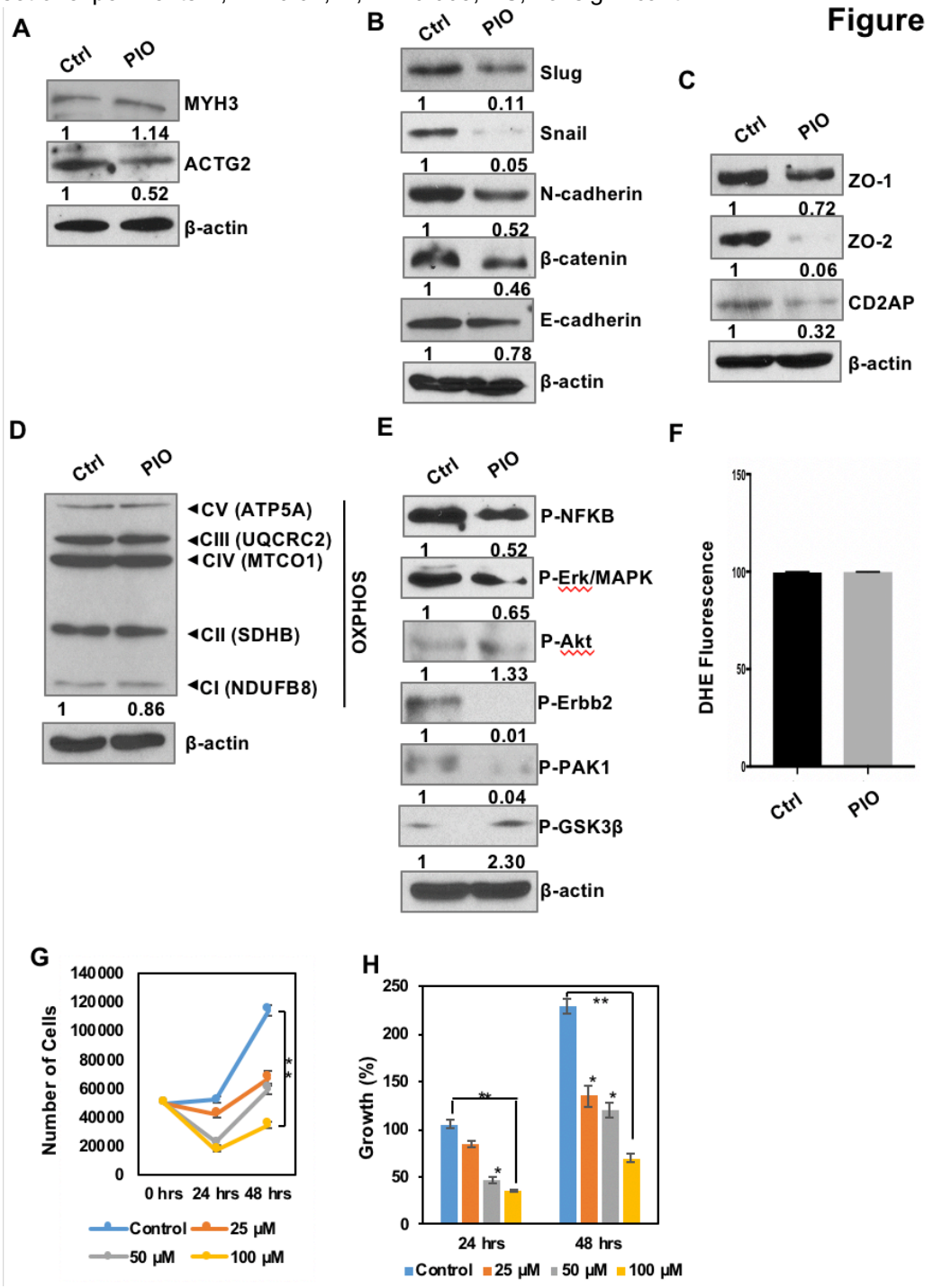

DISCUSSION

There are many discrepancies surrounding the link between TZD usage and side effects on bladder function. Diabetic bladders can have several dysfunctions, ranging from bladder overactivity to impaired contractility, which represent a wide spectrum of clinical symptoms. The widespread pathophysiology of bladder dysfunction in diabetic patients is associated with multiple factors, including neuronal dysfunction, smooth muscle dysfunction, and urothelial impairment [77]. In patients, diabetes has been shown to be a significant predictor of death from cancer, including BC [78]. Evidence from a meta-analysis study has linked the use of pioglitazone to increased BC risk as well [53] .The tumorigenic effect of pioglitazone is thought to be due to signaling modifications in the PPAR pathway [79]. However, it is still unclear whether the long-term use of pioglitazone increases the chances of developing bladder dysfunctions or disease.

PPARγ is part of the PPAR subfamily that consists of two other subunits, alpha and beta/delta. As the most extensively studied subunit, the functions of PPARγ have been linked to several crucial biological processes, including glucose metabolism, lipid biosynthesis, and anti-inflammatory response [80]. The association of PPARγ to diabetes is based on the its role in lipid and glucose metabolism [81]. It has been shown that patients with dominant negative mutations of PPARγ have severe hypoglycemia, insulin resistance, and DM [82]. This means that there is a significant genetic link between both PPARγ and DM. Treatment with TZDs has proven to substantially decrease insulin resistance in diabetes and possibly induces transcription of adipose cell differentiation, which generates smaller insulin-sensitive adipocytes [83]. However, despite their beneficial effects in patients with diabetes, TZDs are known to have adverse effects. This includes weight gain, fluid retention, bone mineral density reduction, and excess myocardial infarction [84]. The fluid retention induced by TZDs has also been proven to significantly increase urine volume and excretion of sodium [85]. Because of this, there is some controversy surrounding the safety of long-term TZD usage to treat diabetes.

In addition to the documented roles of PPARγ in lipid metabolism and DM, there has been growing research on its functions in both BC and interstitial cystitis (IC). Approximately 20-25% of human BC is driven by hyperactive PPAR signaling that is due to either PPARγ gene amplification or RXRA hot-spot mutations [86]. Furthermore, it was found that the PPARγ transcription pathway can be a tumor-intrinsic mechanism for immune evasion in muscle-invasive BC [87]. Along with this immune escape, it has been proposed that PPARγ cooperates with the FOXA1 (forkhead box protein A1) and GATA3 (GATA binding protein 3) networks to drive transdifferentiation of basal BC cells into luminal types [88]. PPARγ has also been identified to be associated with IC. Mahal A et al. found that treating their IC rat model with PPARγ agonists improved bladder function and urinary health [89]. Based on the complex relationship of PPARγ with diabetes and urological malignancies, it would be compelling to better understand how patients who routinely take TZDs are affected.

This study revealed that BMI1 is a master node in pioglitazone-regulated networks. A recent study showed that overexpression of BMI1 repressed transcripts of PPARγ in mesenchymal stem cells (MSCs)[90]. Our proteomic profiling of BMI1 exhibited significant downregulation in normal bladder epithelial cells treated with pioglitazone, suggesting a potential inverse relationship between PPARγ and BMI1. One possible hypothesis for our future study is that PPARγ signaling induced by pioglitazone may cause loss of BMI1 expression in bladder cells. Expression of telomere maintenance proteins including HIST1H4A, HIST2H2AA3 and HIST2H2AC, which interact with BMI1, are downregulated as well. The presence of an upregulated telomere maintenance mechanism is a hallmark of cancer, and it is interesting to note that HIST2H2AA3 and HIST2H2AC were identified as genes upregulated, differentially expressed in BC [91]. This may signify a stage shift, by pioglitazone treatment, from developing cancer. PPARγ agonism has also been shown to increase the antitumor effects of histone deacetylase inhibitors in multiple myeloma cells.[85]

Most notably, in our study, we found a series of contractile and cytoskeleton proteins, such as myosin light polypeptides, myosin heavy polypeptides, keratins, and ACTG2, as being significantly up- or downregulated in TRT-HU1 bladder epithelial cells treated with pioglitazone. Myosin is a particularly important structural component of muscles that interacts with actin filaments and plays a vital role in actin filament contraction, bundling, motor action, and binding. Furthermore, our network modeling revealed that these actin-binding proteins comprise the central hub. These results suggest the potential pathophysiological mechanisms of pioglitazone's effects.

Our data demonstrated that the activation of PPARγ signaling pathways inhibits the proliferation of bladder epithelial cells. Interestingly, these findings are consistent with clinical observations that the IC bladder has thinner epithelial layers [92] and that IC bladder cells exhibit reduced proliferation due to cell cycle arrest [93]. Our epigenetic remodeling study supports this mechanistic link between IC and defective cell proliferation.[94] Furthermore, previous reports suggest that the anti-proliferative role of PPARγ is through the upregulation of PTEN expression in various cancers, which leads to decreased PI-3K activity [95]. It is currently known that PPARγ agonists promote cell cycle arrest by downregulating cyclin D1 in several tumor lines; thereby, inhibiting cyclin D1/CDK-mediated retinoblastoma (pRb) phosphorylation and maintaining its active form to prevent the G1 to S phase transition [96]. Activation of PPARγ via agonists in normal human urothelial cells has been shown to induce expression of gene/protein markers associated with late/terminal urothelial differentiation, including uroplakins, cytokeratins, and tight junction constituents [97,98].

In summary, although pioglitazone is widely used among T2DM patients, its effects on the bladder are still in controversy. While there have been studies examining the effects of pioglitazone on healthy bladder cells, there is no conclusive evidence. Through unbiased quantitative proteomic profiling, our report comprehensively characterized the proteome of normal bladder epithelial cells treated with pioglitazone. We observed suppressed cell proliferation, which may be explained by the decreased expression of tight junction proteins. Taken together, our study provides no experimental evidence to support a tumorigenic effect of pioglitazone on the bladder. This proteomic approach will be useful for examining any potential side effects of the one of the most commonly used drugs.

3.3. What opportunities for training and professional development has the project provided?
This project was not intended to provide training and professional development opportunities.
"Nothing to Report."

3.4. How were the results disseminated to communities of interest?
Although this project was not originally proposed to enhance public awareness for communities of interest, I was able to provide several talks through media and outreach activities that were undertaken to reach members of communities who are not usually aware of these project activities. I have also provided scientific seminars on IC research to the science and medical community, focusing on post-doctoral fellows, medical students, nurses, and urologists. I believe these talks and educational campaigns greatly enhance public understanding, which then increases interest in learning and encourages careers in science, technology, and the humanities.

3.5. What do you plan to do during the next reporting period to accomplish the goals?

- Number of patients completed/ original planned target: 266/300. We will continue with our efforts to build upon the CSMC IC cohort for Specific Aims 1 and 2, as planned.

- The goals include to complete quantification of urinary tyramine and CNR2 DNA methylation status in our samples. The assay optimization was completed under a close collaboration with other professionals, as stated in our study proposal.

- The experimental data is to be published, submitted, or will be submitted for peer-reviewed publications.

- Most of our research results were presented in major scientific conferences and talks. New data will be submitted into the 2019 Annual American Urological Association Meeting, Annual Experimental Biology Conference, and/or Annual Society of Urodynamics, Female Pelvic Medicine, and Urogenital Reconstruction (SUFU) meeting.

4. IMPACT:

4.1. What was the impact on the development of the principal discipline(s) of the project?

This study will have significant ***clinical impact*** because the results may lead to novel clinical methods that can increase diagnostic accuracy and an improved understanding of the molecular origins of IC and its relationship with other urological conditions that share overlapping symptoms. In the long term, we seek to validate viable drug targets for therapeutic strategies using the expertise of our research team (urology, molecular and cell biology, chemical analysts, pathology, and biomarker development). We also believe that these findings can promote the adoption of effective and proven tests for IC diagnosis.

There have been many prior efforts attempting to identify unique and directly quantitative biomarkers associated with IC. However, these studies have overlooked the potential impact of gender on IC biomarkers. The biological basis of gender variability among IC states is not well established and there has been little advancement in investigating gender-related metabolomic differences in urine specimens. This underlies the misconception that risk factors and treatment regimens should be the same for both males and females. Considering that the composition of urine reflects the generation of metabolic by-products in the body, a urine metabolomics approach would be a great scientific tool for better understanding IC metabolism. Urine metabolite profiles provide a window of opportunity to study the global chemical fingerprints associated with physiological and pathological states. However, the discovery of biologically active metabolites in urine has raised questions on the clinical value and biological role of urine in IC.

We previously reported that our urine metabolomics profiling identified α-oxoglutarate (α-OG) as a female-specific IC biomarker. Our preliminary EPIC DNA methylation profiling and mechanistic preliminary studies on human bladder epithelial cells revealed the potential role of α-OG in epigenetic remodeling, through its effects on ARID1A in the bladder. Interestingly, an additional independent preliminary study conducted by our group found ***sex-associated differences in baseline urinary metabolites in healthy adults***. In other preliminary studies, comprehensive metabolomics profiling combined with bioinformatic analyses on urine samples from healthy males and females revealed biologically meaningful and sex-related baseline characteristics. Interestingly, we found that levels of a series of metabolites, including α-OG, were greater in male samples. Recently established chemical similarity enrichment analysis further revealed that differentially expressed metabolites were significantly related to gender. These findings indicate that there are baseline sex-related differences in urinary metabolites, which should be considered for biomarker discovery, diagnosis, development of therapeutic strategies, and treatment options.

4.2. What was the impact on other disciplines?

Nothing to Report

4.3. What was the impact on technology transfer?

Nothing to Report

4.4. What was the impact on society beyond science and technology?

(1) Enhancing public awareness through broadcasting and media:

I moved to Los Angeles from Boston to continue my academic career as an Associate Professor of Surgery at CSMC and University of California Los Angeles. I immediately involved myself in a local Korean community-based radio broadcasting career and developed a rapidly growing base of listeners. Since 1989, I have been a primary interviewer, a reporter, and a scripter for two major media outlets in South Korea. I have covered many of the biggest local stories on business, education, and science, either at the anchor desk or as a frontier reporter. I have also hosted an hour-long educational quiz show on a weekly basis for three years.

Since this Department of Defense (DoD) research project started in 2015, I have worked closely with my Korean radio show and have hosted the daily "*Health and Science Story"* column series.

(2) Enhancing public awareness by community health educational lecture (only selected from very recent events)

I always seek chances to enhance public awareness of IC. Here are some examples of health lectures I have done for the local community. I believe that these outreach activities will improve public knowledge, attitudes of physicians and other health providers, social, economic, and environmental conditions for patients and their family members.

June 5, 2018
CSMC Health Fair, Koreatown Senior Center, Los Angeles, CA

August 15, 2018
Korea Senior Center in Koreatown, Los Angeles, CA

September 9, 2018
Oriental Mission Church, Los Angeles, CA

September 22, 2018
Free Prostate Cancer Screening Day, Cedars-Sinai Medical Center, CA

September 24, 2018
Health Lecture Series
Young Nak Church, Evergreen College, Celebration Chapel, Los Angeles, CA

October 19, 2018
Korean Health Fair (Free Flu Vaccine)
Young Nak Church, Evergreen College, Celebration Chapel, Los Angeles, CA

December 1, 2018
KSEA-KWISE STEM FAIR
Santa Monica College, Los Angeles, CA

May 4, 2019
KWISE Westcoast Annual Conference
Biola University, CA

January 12, 2019
Ygnit 2019 Conference
Renaissance Los Angeles Airport Hotel, CA

April 12, 2019
Health Lecture Series
Young Nak Church, Evergreen College, Celebration Chapel, Los Angeles, CA

April 13, 2019
KSEA-KWISE Math Competition, Chair
Harvey Mudd College, CA

April 27, 2019
KSEA SWRC (South West Regional Conference)
Speaker
Chapman University School of Pharmacy, Irvine, CA

May 10, 2019
Health Lecture Series
Young Nak Church, Evergreen College, Celebration Chapel, Los Angeles, CA

October 1, 2019
Breast Cancer Awareness Initiative
Khier Clinic, Los Angeles, CA

October 1, 2019
Korean American Community Advisory Committee Lauching
Khier Clinic, Los Angeles, CA

5. CHANGES/PROBLEMS:

5.1. Changes in approach and reasons for change
Nothing to Report

5.2. Actual or anticipated problems or delays and actions or plans to resolve them
Nothing to Report

5.3. Changes that had a significant impact on expenditures
Nothing to Report

5.4. Significant changes in use or care of human subjects, vertebrate animals, biohazards, and/or select agents
Nothing to Report

5.5. Significant changes in use or care of human subjects
Nothing to Report

5.6. Significant changes in use or care of vertebrate animals.
Nothing to Report

5.7. Significant changes in use of biohazards and/or select agents
Nothing to Report

6.PRODUCTS:

6.1. Publications, conference papers, and presentations

Papers Published in 2018 (directly relevant to the proposed study)

1. Shahid M, Yeon A, Cho E, Bae J, Park RJ, **Kim J.** (2018) Language and Culture Appropriate Approaches Needed to Improve Health Education to Reduce Disparities among Korean American Immigrants Living in Los Angeles Area. (2018) *International Journal of Innovative Research in Medical Science*, Volume 03 Issue 08.

2. Jung JH, You S, Oh JW, Yeon A, Shahid M, Cho E, Sairam V, Park TD, Kim KP, **Kim J.** (2018) Integrated Analysis of Global Proteome and Phosphoproteome in Cisplatin Resistant Bladder Cancer Cell Revealed the Molecular Signature Predictive to Patient Survival, *Cancer Letters,* 437:1-12. PMID: 30145203

3. Shahid M, Kim M, Yeon A, Andres AM, You S, **Kim J.** Quantitative Proteomic Analysis Reveals Caffeine-Perturbed Proteomic Profiles in Normal Bladder Epithelial Cells, *Proteomics*, e1800190. PMID: 30232827

4. Mansour AM, Abdulreheem M, Laymon M, Elsherbeeny M, Sultan M, Shokeir A, Mosbah A, Abol-Enein H, Cho E, Sairam V, Park TD, Shahid M, **Kim J** (2018) Epidermal Growth Factor Expression as a Predictor of Chemotherapeutic Resistance in Muscle-Invasive Bladder Cancer, *BMC Urology,* 18(1):100. PMID:30413194

5. Blaženović I, Kind T, Vaniya A, Wancewicz B, Roberts BS, Lee T, Song H, Ji J, Roselius L, Biedendieck R, Jahn M, Schauer N, Jahn D, **Kim J*,** Fiehn O*. (2018) Structure annotation of all mass spectra in untargeted metabolomics, *Analytical Chemistry*, in press, ***co-corresponding authors**

6. Shahid M, Andreas A, Li P, Yeon A, Lee M, Yang W, Zhou B, Cho E, Bae J, Wang Y, Kim M, Kim HL, Kim J. (2018) Centromere protein F (CENPF), a microtubule binding protein, modulates cancer metabolism by regulating pyruvate kinase M2 phosphorylation signaling, *Cell Cycle* doi: 10.1080/15384101.2018.1557496. [Epub ahead of print] PMID: 30526248

7. Kim S, Yeon A, Cho E, Shahid M, **Kim J** (2019) Effectiveness of a Tailored Colorectal Cancer Educational Seminar in Enhancing the Awareness, Knowledge, and Behavior of Korean Americans Living in the Los Angeles Koreatown Area, *Diversity & Equality in Health and Care*, *16(1): 1-8,* **Publications with *University of California Students (SRP program, CSMC Research Interns)** PMID: 31019695

8. Shahid M, You S, Lee MY, Yeon A, Bae J, **Kim J.** (2019) Downregulation of CENPF Remodels Prostate Cancer Cells and Alters Cellular Metabolism, *Proteomics,* 2019 Apr 8:e1900038. PMID:30957416

9. Nickel JC, Stephens A, Landis R, Mullins C, Bokhoven A, Anger J, Ackerman L, **Kim J,** Sutcliffe S, Krol J, Sen B, Hammond J, Ehrlich G. (2019) Urinary Fungi Associated with Urinary Symptom Severity among Women with Interstitial Cystitis/Bladder Pain Syndrome (IC/BPS), *World Journal of Urology*, doi: 10.1007/s00345-019-02764-0. [Epub ahead of print] PMID:31028455

10. Ackerman AL, Anger JT, Khalique MU, Ackerman JE, Tang J, **Kim J**, Underhill DM, (2019) Optimization of DNA Extraction from Human Urinary Samples for Mycobiome Community Profiling, *PLoS ONE*, 14(4):e0210306, PMID:31022216

11. Sutcliffe S , Gallop R, Lai HH, Andriole GL, Bradley CS, Chelimsky G, Chelimsky T, Clemens JQ, Colditz GA, Erickson B, Griffith JW, **Kim J,** Krieger JN, Labus J, Bruce D. Naliboff BD, Rodriguez LV, Sutherland SE, Taple BJ, Landis JR. (2019) A Longitudinal Analysis of Urologic Chronic Pelvic Pain Sundrome Flares in the MAPP Research Network, *British Journal of Urology International*, doi: 10.1111/bju.14783, PMID:31012513

12. Skove SL, Howard LE, Senechal J, Hoedt AD, Bresee C, **Kim J,** Freedland SJ, Anger JA. (2019) The Misdiagnosis of Interstitial Cystitis/Painful Bladder Syndrome in a VA Population, *Neurourology and Urodynamics*, doi: 10.1002/nau.24100. [Epub ahead of print] PMID:31302944

13. Kim SJ, **Kim J***, Yoon H*. (2019) Sexual Pain and IC/BPS in Women, *BMC Urology*, 19(1):47, PMID:31170952 ***co-corresponding authors**

14. **Kim J.** (2019) Looking into Clinical Application of CD47-targeted Near-Infrared Photoimmunotherapy for Human Bladder Cancer Treatment, *Translational Andrology and Urology,* 8(Suppl 3): S322-S324, PMID: 31392158

15. Kim W-J, **Kim J.** (2019) Innovative technologies for the smart E-Healthcare system *Investig Clin Urol.* 60(1):1-3. PMID:30637354

16. Myung **NV,** Jung S, **Kim J.** (2019) Application of low-cost, easy-to-use, portable biosensor systems for diagnosing bladder dysfunctions *International Neurourology Journal*. 23(1):86-87, PMID:30943698

Research Papers (Peer-Reviewed, in revision)

1. Shahid M, Kim M, Yeon A, You S, **Kim J.** (2018) The Effects of Pioglitazone on Proteome of Normal Bladder Epithelial Cells, *Proteomics*, in revision

2. Jo YH, Choi TG, Kim J, Nguyen NNY, Chang S-G, **Kim J,** Kim SS. (2018) Molecular Gene Panel-Based Subtyping for Surgical Decision on Bladder Cancer Patients, *Journal of Urology*, in review

3. Regulation of MAOA Palmitoylation by ACSS2 Contributes to Cisplatin Resistance in Bladder Cancer, *Molecular Cancer Research*, in review

4. Laden BF, Bresee C, De Hoedt A, Scharfenberg A, Saxena R, Senechal JF, Barbour KE, **Kim J,** Freedland SJ, Anger JT. Comorbidities in a Nationwide, Heterogenous Population of Veterans with Interstitial Cystitis/Bladder Pain Syndrome, Journal of Urology, in review

Publications Published in 2018 (acknowledged DoD grant support)

6.2. Books or other non-periodical, one-time publications.

1. **Genetic Engineering & Biotechnology News (GEN)**
    i. Metabolomics in Precision Medicine
    ii. http://www.genengnews.com/gen-articles/metabolomics-in-precision-medicine/5502/?kwrd=jayoung%20kim#gsaccess
    iii. Acknowledgement of federal support (no)

2. **UroToday**
    i. UroToday since 2003, has established itself as a global leader in the delivery of quality, clinically relevant content.

3. Metabolomics insights into pathophysiological mechanisms of interstitial cystitis,
    i. http://www.urotoday.com/recent-abstracts/pelvic-health-reconstruction/interstitial-cystitis/79104-metabolomics-insights-into-pathophysiological-mechanisms-of-interstitial-cystitis-beyond-the-abstract-by-jayoung-kim-phd.html
    ii. Acknowledgement of federal support (no)

4. Metabolic Pathway Signatures Associated with Urinary Metabolite Biomarkers Differentiate Bladder Cancer Patients from Healthy Controls.
    i. http://www.urotoday.com/recent-abstracts/urologic-oncology/bladder-cancer/88889-metabolic-pathway-signatures-associated-with-urinary-metabolite-biomarkers-differentiate-bladder-cancer-patients-from-healthy-controls.html
    ii. Acknowledgement of federal support (no)

5. Commentary articles on IC and painful sex
    https://www.urotoday.com/recent-abstracts/pelvic-health-reconstruction/interstitial-cystitis/113380-what-we-know-about-sexual-pain-and-ic-bps-in-women-beyond-the-abstract.html

    This article was well received by science community. There was a lot of requests of talk and phone calls from physicians and patients.

6.3. Other publications, conference papers, and presentations

6.3.1.Conference

1. Shahid M, Lee MY, Yeon A, Cho E, Sairam V, You S, **Kim J.** Urinary Volatile Compound Associated with Chronic Inflammation in Interstitial Cystitis, Immunology LA 2018, California, June 15, 2018

2. Yeon Y, Lee MY, Shahid M, Cho E, Sairam V, Figlin R, Kim K-H, **Kim J**. Reprogrammed Lipid Metabolism in Bladder Cancer with Cisplatin Resistance, Immunology LA 2018, California, June 15, 2018

3. Laden BF, Hoedt AD, Scharfenberg A, Saxena R, Senechal JF, Barbour KE, **Kim J,** Freedland SJ, Anger JT, Comorbid Conditions in a Nationwide, Heterogenous Population of Patients with Interstitial Cystitis/Bladder Pain Syndrome, 2019 American Urological Association (AUA) Annual Conference, 2019

4. The Serum Proteome Correlates with Clinical Phenotypes of UCPPS: A MAPP Study, 2019 Annual Meeting of the American Urological Association, Chicago, Illinois, May 3-6, 2019

5. Rewiring of cisplatin-resistant bladder cancer cells through epigenetic regulation of genes involved in amino acid metabolism, 2019 Keystone Symposia Conference, Cancer Metastasis: The Role of Metabolism, Immunity and the Microenvironment, Firenze Fiera- Fortezza da Basso, Florence, March 15-19, 2019

6. Wen H, Lee S, Zhu W-G, Lee O-J, Yun SJ, Kim J, Park S, Glucose-derived Acetate and ACSS2 as Key Players in Cisplatin Resistance in Bladder Cancer, AACR Annual Meeting 2019, March 30-April 3, 2019

7. Epigenetic remodeling of cancer metabolisms in cisplatin resistant bladder cancer, AACR Bladder Cancer: Transforming the Field Special Conference, taking place May 18–21, 2019, in Denver, Colorado

8. Acetate metabolism mediated by Acetyl-CoA synthetase 2 in cisplatin resistant bladder cancer, AACR Bladder Cancer: Transforming the Field Special Conference, taking place May 18–21, 2019, in Denver, Colorado

9. Characterization of the global proteome and phosphoproteome in cisplatin resistant bladder cancers revealed the CDK2 network as a potential therapeutic target, AACR Bladder Cancer: Transforming the Field Special Conference, taking place May 18–21, 2019, in Denver, Colorado

6.3.2. International presentation (Seminar and invited research talks)

1. Invited Speaker, International US-Korea Conference (UKC) 2018, St. Johns, August 2-5, 2018

2. Invited Speaker, the US-Egypt Science and Technology Development Fund Symposium held in Cairo, Egypt, November 5-7, 2018

3. Keynote Speaker, Ain Shams University, Egypt, November 8-9, 2018

4. Invited Speaker, Korean Women in Science and Engineering (KWiSE) 12nd West Coast Annual Conference

5. Invited panelist, Ygnite Conference 2019, “Future of Research & New Challenges & Emerging Trends”, 2019

6. Speaker, University of Texas Arlington, Department of Electrical Engineering, March 7-9, 2019

7. Invited Speaker, The 29th Annual South West Regional Conference, The Southern California Chapter of Korean-American Scientists and Engineers Association, *'data driven real world problem solving', April 27, 2019*

8. Invited Speaker, University of Texas Arlington, Department of Electrical Engineering, March 7-9, 2019

9. Invited Speaker, University of East Virginia Medical School, March 28, 2019

10. Invited Speaker, UKC 2019, Chicago, August 15-18, 2019

11. Forum panel, UKC 2019, Chicago, August 15-18, 2019

12. Keynote Speaker, Urinomics 2019, Caparica, Portugal, September 2-4, 2019

13. Keynote Speaker, Ewha Urology Symposium, Seoul, Republic of Korea, September 19-21, 2019

14. Invited Speaker, Chapman University School of Pharmacy, Irvine, October 24, 2019

15. Invited Speaker, West Regional Conference (WRC) 2019 “Smart Science, Engineering and Technology”, November 2, 2019

6.3.4. Website(s) or other Internet site(s)
Please refer the above section

6.3.5.Technologies or techniques
Nothing to report

6.3.6.Inventions, patent applications, and/or licenses
Nothing to report

6.3.7. Other Products
Daily radio shows to enhance public awareness through broadcasting and media
(Please refer the above section)

7. PARTICIPANTS & OTHER COLLABORATING ORGANIZATIONS

7.1. What individuals have worked on the project?
No change
Jayoung Kim

7.2. Has there been a change in the active other support of the PD/PI(s) or senior/key personnel

since the last reporting period?
Nothing to Report

7.3. What other organizations were involved as partners?
Nothing to Report

8.SPECIAL REPORTING REQUIREMENTS

8.1.COLLABORATIVE AWARDS: Nothing to Report

8.2.QUAD CHARTS: Nothing to Report

9. APPENDICES:

Original copies of journal articles (published only) with reprints of manuscripts are attached.

References

1 Jacob, M., Lopata, A. L., Dasouki, M. & Abdel Rahman, A. M. Metabolomics toward personalized medicine. *Mass spectrometry reviews*, doi:10.1002/mas.21548 (2017).

2 Bloszies, C. S. & Fiehn, O. Using untargeted metabolomics for detecting exposome compounds. *Current Opinion in Toxicology* **8**, 87-92, doi:https://doi.org/10.1016/j.cotox.2018.03.002 (2018).

3 Blazenovic, I., Kind, T., Ji, J. & Fiehn, O. Software Tools and Approaches for Compound Identification of LC-MS/MS Data in Metabolomics. *Metabolites* **8**, doi:10.3390/metabo8020031 (2018).

4 Antunes-Lopes, T., Cruz, C. D., Cruz, F. & Sievert, K. D. Biomarkers in lower urinary tract symptoms/overactive bladder: a critical overview. *Current opinion in urology* **24**, 352-357, doi:10.1097/MOU.0000000000000064 (2014).

5 Kuo, H. C. Potential urine and serum biomarkers for patients with bladder pain syndrome/interstitial cystitis. *International journal of urology : official journal of the Japanese Urological Association* **21 Suppl 1**, 34-41, doi:10.1111/iju.12311 (2014).

6 Pedroza-Diaz, J. & Rothlisberger, S. Advances in urinary protein biomarkers for urogenital and non-urogenital pathologies. *Biochemia medica* **25**, 22-35, doi:10.11613/BM.2015.003 (2015).

7 Clemens, J. Q. *et al.* Comparison of baseline urological symptoms in men and women in the MAPP research cohort. *The Journal of urology* **193**, 1554-1558, doi:10.1016/j.juro.2014.11.016 (2015).

8 Naliboff, B. D. *et al.* Widespread Psychosocial Difficulties in Men and Women With Urologic Chronic Pelvic Pain Syndromes: Case-control Findings From the Multidisciplinary Approach to the Study of Chronic Pelvic Pain Research Network. *Urology* **85**, 1319-1327, doi:10.1016/j.urology.2015.02.047 (2015).

9 Hanno, P. M. *et al.* AUA guideline for the diagnosis and treatment of interstitial cystitis/bladder pain syndrome. *The Journal of urology* **185**, 2162-2170, doi:10.1016/j.juro.2011.03.064 (2011).

10 Matyash, V., Liebisch, G., Kurzchalia, T. V., Shevchenko, A. & Schwudke, D. Lipid extraction by methyl-tert-butyl ether for high-throughput lipidomics. *Journal of lipid research* **49**, 1137-1146, doi:10.1194/jlr.D700041-JLR200 (2008).

11 Tsugawa, H. *et al.* MS-DIAL: data-independent MS/MS deconvolution for comprehensive metabolome analysis. *Nature methods* **12**, 523-526, doi:10.1038/nmeth.3393 (2015).

12 Wanichthanarak, K., Fan, S., Grapov, D., Barupal, D. K. & Fiehn, O. Metabox: A Toolbox for Metabolomic Data Analysis, Interpretation and Integrative Exploration. *PloS one* **12**, e0171046, doi:10.1371/journal.pone.0171046 (2017).

13 Kind, T. *et al.* LipidBlast in silico tandem mass spectrometry database for lipid identification. *Nature methods* **10**, 755-758, doi:10.1038/nmeth.2551 (2013).

14 Kind, T., Okazaki, Y., Saito, K. & Fiehn, O. LipidBlast templates as flexible tools for creating new in-silico tandem mass spectral libraries. *Analytical chemistry* **86**, 11024-11027, doi:10.1021/ac502511a (2014).

15 Cajka, T., Smilowitz, J. T. & Fiehn, O. Validating Quantitative Untargeted Lipidomics Across Nine Liquid Chromatography-High-Resolution Mass Spectrometry Platforms. *Analytical chemistry* **89**, 12360-12368, doi:10.1021/acs.analchem.7b03404 (2017).

16 Zammit, V. A., Ramsay, R. R., Bonomini, M. & Arduini, A. Carnitine, mitochondrial function and therapy. *Adv Drug Deliv Rev* **61**, 1353-1362, doi:10.1016/j.addr.2009.04.024 (2009).

17 Wang, G. L. *et al.* Expanded molecular features of carnitine acyl-carnitine translocase (CACT) deficiency by comprehensive molecular analysis. *Mol Genet Metab* **103**, 349-357, doi:10.1016/j.ymgme.2011.05.001 (2011).

18 Indiveri, C. *et al.* The mitochondrial carnitine/acylcarnitine carrier: function, structure and physiopathology. *Mol Aspects Med* **32**, 223-233, doi:10.1016/j.mam.2011.10.008 (2011).

19 Adeva-Andany, M. M., Carneiro-Freire, N., Seco-Filgueira, M., Fernandez-Fernandez, C. & Mourino-Bayolo, D. Mitochondrial beta-oxidation of saturated fatty acids in humans. *Mitochondrion*, doi:10.1016/j.mito.2018.02.009 (2018).

20 Albert, C. L. & Tang, W. H. W. Metabolic Biomarkers in Heart Failure. *Heart Fail Clin* **14**, 109-118, doi:10.1016/j.hfc.2017.08.011 (2018).
21 Pallares-Mendez, R., Aguilar-Salinas, C. A., Cruz-Bautista, I. & Del Bosque-Plata, L. Metabolomics in diabetes, a review. *Ann Med* **48**, 89-102, doi:10.3109/07853890.2015.1137630 (2016).
22 Hocher, B. & Adamski, J. Metabolomics for clinical use and research in chronic kidney disease. *Nat Rev Nephrol* **13**, 269-284, doi:10.1038/nrneph.2017.30 (2017).
23 Cuturic, M., Abramson, R. K., Moran, R. R. & Hardin, J. W. Carnitine and metabolic correlates in hospitalized psychiatric patients: a follow-through report. *J Psychiatr Pract* **17**, 35-40, doi:10.1097/01.pra.0000393842.63841.bc (2011).
24 Ren, C. *et al.* Lipidomic analysis of serum samples from migraine patients. *Lipids Health Dis* **17**, 22, doi:10.1186/s12944-018-0665-0 (2018).
25 Knific, T. *et al.* Models including plasma levels of sphingomyelins and phosphatidylcholines as diagnostic and prognostic biomarkers of endometrial cancer. *J Steroid Biochem Mol Biol* **178**, 312-321, doi:10.1016/j.jsbmb.2018.01.012 (2018).
26 Kim, W. T. *et al.* Metabolic Pathway Signatures Associated with Urinary Metabolite Biomarkers Differentiate Bladder Cancer Patients from Healthy Controls. *Yonsei Med J* **57**, 865-871, doi:10.3349/ymj.2016.57.4.865 (2016).
27 Mirzoyan, K. *et al.* Increased urine acylcarnitines in diabetic ApoE-/- mice: Hydroxytetradecadienoylcarnitine (C14:2-OH) reflects diabetic nephropathy in a context of hyperlipidemia. *Biochem Biophys Res Commun* **487**, 109-115, doi:10.1016/j.bbrc.2017.04.026 (2017).
28 Rauschert, S., Uhl, O., Koletzko, B. & Hellmuth, C. Metabolomic biomarkers for obesity in humans: a short review. *Ann Nutr Metab* **64**, 314-324, doi:10.1159/000365040 (2014).
29 Ganti, S. *et al.* Urinary acylcarnitines are altered in human kidney cancer. *Int J Cancer* **130**, 2791-2800, doi:10.1002/ijc.26274 (2012).
30 Zuniga, A. & Li, L. Ultra-high performance liquid chromatography tandem mass spectrometry for comprehensive analysis of urinary acylcarnitines. *Analytica chimica acta* **689**, 77-84, doi:10.1016/j.aca.2011.01.018 (2011).
31 Bocker, S., Letzel, M. C., Liptak, Z. & Pervukhin, A. SIRIUS: decomposing isotope patterns for metabolite identification. *Bioinformatics* **25**, 218-224, doi:10.1093/bioinformatics/btn603 (2009).
32 Tsugawa, H. *et al.* Hydrogen Rearrangement Rules: Computational MS/MS Fragmentation and Structure Elucidation Using MS-FINDER Software. *Analytical chemistry* **88**, 7946-7958, doi:10.1021/acs.analchem.6b00770 (2016).
33 Allen, F., Pon, A., Wilson, M., Greiner, R. & Wishart, D. CFM-ID: a web server for annotation, spectrum prediction and metabolite identification from tandem mass spectra. *Nucleic acids research* **42**, W94-99, doi:10.1093/nar/gku436 (2014).
34 Duhrkop, K., Shen, H., Meusel, M., Rousu, J. & Bocker, S. Searching molecular structure databases with tandem mass spectra using CSI:FingerID. *Proc Natl Acad Sci U S A* **112**, 12580-12585, doi:10.1073/pnas.1509788112 (2015).
35 Blazenovic, I. *et al.* Comprehensive comparison of in silico MS/MS fragmentation tools of the CASMI contest: database boosting is needed to achieve 93% accuracy. *J Cheminform* **9**, 32, doi:10.1186/s13321-017-0219-x (2017).
36 Showalter, M. R., Cajka, T. & Fiehn, O. Epimetabolites: discovering metabolism beyond building and burning. *Current opinion in chemical biology* **36**, 70-76, doi:10.1016/j.cbpa.2017.01.012 (2017).
37 Burke, M. C. *et al.* The Hybrid Search: A Mass Spectral Library Search Method for Discovery of Modifications in Proteomics. *Journal of Proteome Research* **16**, 1924-1935, doi:10.1021/acs.jproteome.6b00988 (2017).
38 Nikolic, D., Macias, C., Lankin, D. C. & van Breemen, R. B. Collision-induced dissociation of phenethylamides: role of ion-neutral complexes. *Rapid communications in mass spectrometry : RCM* **31**, 1385-1395, doi:10.1002/rcm.7915 (2017).

39 Djoumbou Feunang, Y. *et al.* ClassyFire: automated chemical classification with a comprehensive, computable taxonomy. *J Cheminform* **8**, 61, doi:10.1186/s13321-016-0174-y (2016).
40 Guan, Y., Zhang, Y., Davis, L. & Breyer, M. D. Expression of peroxisome proliferator-activated receptors in urinary tract of rabbits and humans. *Am J Physiol* **273**, F1013-1022 (1997).
41 Bodles, A. M. *et al.* Pioglitazone induces apoptosis of macrophages in human adipose tissue. *J Lipid Res* **47**, 2080-2088, doi:10.1194/jlr.M600235-JLR200 (2006).
42 Di Gregorio, G. B. *et al.* Expression of CD68 and macrophage chemoattractant protein-1 genes in human adipose and muscle tissues: association with cytokine expression, insulin resistance, and reduction by pioglitazone. *Diabetes* **54**, 2305-2313 (2005).
43 Lewis, J. D. *et al.* Risk of bladder cancer among diabetic patients treated with pioglitazone: interim report of a longitudinal cohort study. *Diabetes Care* **34**, 916-922, doi:10.2337/dc10-1068 (2011).
44 Belfiore, A., Genua, M. & Malaguarnera, R. PPAR-gamma agonists and their effects on IGF-I receptor signaling: Implications for cancer. *PPAR Res* **2009**, 830501, doi:10.1155/2009/830501 (2009).
45 Necela, B. M., Su, W. & Thompson, E. A. Toll-like receptor 4 mediates cross-talk between peroxisome proliferator-activated receptor gamma and nuclear factor-kappaB in macrophages. *Immunology* **125**, 344-358, doi:10.1111/j.1365-2567.2008.02849.x (2008).
46 Fang, H. *et al.* Diabetes mellitus increases the risk of bladder cancer: an updated meta-analysis of observational studies. *Diabetes Technol Ther* **15**, 914-922, doi:10.1089/dia.2013.0131 (2013).
47 Xu, X. *et al.* Diabetes mellitus and risk of bladder cancer: a meta-analysis of cohort studies. *PLoS One* **8**, e58079, doi:10.1371/journal.pone.0058079 (2013).
48 Lewis, J. D. *et al.* Proteinuria testing among patients with diabetes mellitus is associated with bladder cancer diagnosis: potential for unmeasured confounding in studies of pioglitazone and bladder cancer. *Pharmacoepidemiol Drug Saf* **23**, 636-645, doi:10.1002/pds.3619 (2014).
49 Tuccori, M. *et al.* Pioglitazone use and risk of bladder cancer: population based cohort study. *BMJ* **352**, i1541, doi:10.1136/bmj.i1541 (2016).
50 Hampp, C. & Pippins, J. Pioglitazone and bladder cancer: FDA's assessment. *Pharmacoepidemiol Drug Saf* **26**, 117-118, doi:10.1002/pds.4154 (2017).
51 Chiu, M., McBeth, L., Sindhwani, P. & Hinds, T. D. Deciphering the Roles of Thiazolidinediones and PPARgamma in Bladder Cancer. *PPAR Res* **2017**, 4810672, doi:10.1155/2017/4810672 (2017).
52 Li, R. *et al.* Effects of thiazolidinedione in patients with active bladder cancer. *BJU Int* **121**, 244-251, doi:10.1111/bju.14009 (2018).
53 Filipova, E., Uzunova, K., Kalinov, K. & Vekov, T. Pioglitazone and the Risk of Bladder Cancer: A Meta-Analysis. *Diabetes Ther* **8**, 705-726, doi:10.1007/s13300-017-0273-4 (2017).
54 Garry, E. M., Buse, J. B., Lund, J. L., Pate, V. & Sturmer, T. Comparative safety of pioglitazone versus clinically meaningful treatment alternatives concerning the risk of bladder cancer in older US adults with type 2 diabetes. *Diabetes Obes Metab* **20**, 129-140, doi:10.1111/dom.13049 (2018).
55 Kim, J. *et al.* An hTERT-immortalized human urothelial cell line that responds to anti-proliferative factor. *In vitro cellular & developmental biology. Animal* **47**, 2-9, doi:10.1007/s11626-010-9350-y (2011).
56 Qu, Y. *et al.* Transcriptome and proteome characterization of surface ectoderm cells differentiated from human iPSCs. *Scientific reports* **6**, 32007, doi:10.1038/srep32007 (2016).
57 Shahid, M. *et al.* Quantitative Proteomic Analysis Reveals Caffeine-Perturbed Proteomic Profiles in Normal Bladder Epithelial Cells. *Proteomics* **18**, e1800190, doi:10.1002/pmic.201800190 (2018).
58 Rinas, A., Espino, J. A. & Jones, L. M. An efficient quantitation strategy for hydroxyl radical-mediated protein footprinting using Proteome Discoverer. *Analytical and bioanalytical chemistry* **408**, 3021-3031, doi:10.1007/s00216-016-9369-3 (2016).
59 Niu, M. *et al.* Extensive Peptide Fractionation and y1 Ion-Based Interference Detection Method for Enabling Accurate Quantification by Isobaric Labeling and Mass Spectrometry. *Analytical chemistry* **89**, 2956-2963, doi:10.1021/acs.analchem.6b04415 (2017).
60 Zhang, B., Chambers, M. C. & Tabb, D. L. Proteomic parsimony through bipartite graph analysis

improves accuracy and transparency. *Journal of proteome research* **6**, 3549-3557, doi:10.1021/pr070230d (2007).
61 Lee, H. *et al.* Comprehensive Proteome Profiling of Platelet Identified a Protein Profile Predictive of Responses to An Antiplatelet Agent Sarpogrelate. *Molecular & cellular proteomics : MCP* **15**, 3461-3472, doi:10.1074/mcp.M116.059154 (2016).
62 Storey, J. D. & Tibshirani, R. Statistical significance for genomewide studies. *Proc Natl Acad Sci U S A* **100**, 9440-9445, doi:10.1073/pnas.1530509100 (2003).
63 Huang da, W., Sherman, B. T. & Lempicki, R. A. Systematic and integrative analysis of large gene lists using DAVID bioinformatics resources. *Nat Protoc* **4**, 44-57, doi:10.1038/nprot.2008.211 (2009).
64 Mi, H. *et al.* PANTHER version 11: expanded annotation data from Gene Ontology and Reactome pathways, and data analysis tool enhancements. *Nucleic Acids Res* **45**, D183-D189, doi:10.1093/nar/gkw1138 (2017).
65 Stark, C. *et al.* BioGRID: a general repository for interaction datasets. *Nucleic Acids Res* **34**, D535-539, doi:10.1093/nar/gkj109 (2006).
66 Salwinski, L. *et al.* The Database of Interacting Proteins: 2004 update. *Nucleic Acids Res* **32**, D449-451, doi:10.1093/nar/gkh086 (2004).
67 Patil, A., Nakai, K. & Nakamura, H. HitPredict: a database of quality assessed protein-protein interactions in nine species. *Nucleic Acids Res* **39**, D744-749, doi:10.1093/nar/gkq897 (2011).
68 Orchard, S. *et al.* The MIntAct project--IntAct as a common curation platform for 11 molecular interaction databases. *Nucleic Acids Res* **42**, D358-363, doi:10.1093/nar/gkt1115 (2014).
69 Licata, L. *et al.* MINT, the molecular interaction database: 2012 update. *Nucleic Acids Res* **40**, D857-861, doi:10.1093/nar/gkr930 (2012).
70 Szklarczyk, D. *et al.* The STRING database in 2017: quality-controlled protein-protein association networks, made broadly accessible. *Nucleic Acids Res* **45**, D362-D368, doi:10.1093/nar/gkw937 (2017).
71 Shahid, M. *et al.* Menthol, a unique urinary volatile compound, is associated with chronic inflammation in interstitial cystitis. *Sci Rep* **8**, 10859, doi:10.1038/s41598-018-29085-3 (2018).
72 Jo, A. *et al.* Inhibition of Carbonyl Reductase 1 Safely Improves the Efficacy of Doxorubicin in Breast Cancer Treatment. *Antioxid Redox Signal* **26**, 70-83, doi:10.1089/ars.2015.6457 (2017).
73 Choi, D. Y. *et al.* Extracellular vesicles shed from gefitinib-resistant nonsmall cell lung cancer regulate the tumor microenvironment. *Proteomics* **14**, 1845-1856, doi:10.1002/pmic.201400008 (2014).
74 Zhang, C. O., Wang, J. Y., Koch, K. R. & Keay, S. Regulation of tight junction proteins and bladder epithelial paracellular permeability by an antiproliferative factor from patients with interstitial cystitis. *J Urol* **174**, 2382-2387, doi:10.1097/01.ju.0000180417.11976.99 (2005).
75 Formosa, L. E. & Ryan, M. T. Mitochondrial OXPHOS complex assembly lines. *Nat Cell Biol* **20**, 511-513, doi:10.1038/s41556-018-0098-z (2018).
76 Yan, X. L., Wang, Y. Y., Yu, Z. F., Tian, M. M. & Li, H. Peroxisome proliferator-activated receptor-gamma activation attenuates diabetic cardiomyopathy via regulation of the TGF-beta/ERK pathway and epithelial-to-mesenchymal transition. *Life Sci*, doi:10.1016/j.lfs.2018.09.004 (2018).
77 Gomez, C. S., Kanagarajah, P. & Gousse, A. E. Bladder dysfunction in patients with diabetes. *Curr Urol Rep* **12**, 419-426, doi:10.1007/s11934-011-0214-0 (2011).
78 Coughlin, S. S., Calle, E. E., Teras, L. R., Petrelli, J. & Thun, M. J. Diabetes mellitus as a predictor of cancer mortality in a large cohort of US adults. *Am J Epidemiol* **159**, 1160-1167, doi:10.1093/aje/kwh161 (2004).
79 Peters, J. M., Shah, Y. M. & Gonzalez, F. J. The role of peroxisome proliferator-activated receptors in carcinogenesis and chemoprevention. *Nat Rev Cancer* **12**, 181-195, doi:10.1038/nrc3214 (2012).
80 Mansure, J. J., Nassim, R. & Kassouf, W. Peroxisome proliferator-activated receptor gamma in bladder cancer: a promising therapeutic target. *Cancer Biol Ther* **8**, 6-15 (2009).
81 Kim, H. I. & Ahn, Y. H. Role of peroxisome proliferator-activated receptor-gamma in the glucose-

sensing apparatus of liver and beta-cells. *Diabetes* **53 Suppl 1**, S60-65 (2004).
82 Barroso, I. *et al.* Dominant negative mutations in human PPARgamma associated with severe insulin resistance, diabetes mellitus and hypertension. *Nature* **402**, 880-883, doi:10.1038/47254 (1999).
83 Spiegelman, B. M. PPAR-gamma: adipogenic regulator and thiazolidinedione receptor. *Diabetes* **47**, 507-514 (1998).
84 Wang, S., Dougherty, E. J. & Danner, R. L. PPARgamma signaling and emerging opportunities for improved therapeutics. *Pharmacol Res* **111**, 76-85, doi:10.1016/j.phrs.2016.02.028 (2016).
85 Zhou, L. *et al.* Increased susceptibility of db/db mice to rosiglitazone-induced plasma volume expansion: role of dysregulation of renal water transporters. *Am J Physiol Renal Physiol* **305**, F1491-1497, doi:10.1152/ajprenal.00004.2013 (2013).
86 Halstead, A. M. *et al.* Bladder-cancer-associated mutations in RXRA activate peroxisome proliferator-activated receptors to drive urothelial proliferation. *Elife* **6**, doi:10.7554/eLife.30862 (2017).
87 Korpal, M. *et al.* Evasion of immunosurveillance by genomic alterations of PPARgamma/RXRalpha in bladder cancer. *Nat Commun* **8**, 103, doi:10.1038/s41467-017-00147-w (2017).
88 Warrick, J. I. *et al.* FOXA1, GATA3 and PPAR Cooperate to Drive Luminal Subtype in Bladder Cancer: A Molecular Analysis of Established Human Cell Lines. *Sci Rep* **6**, 38531, doi:10.1038/srep38531 (2016).
89 Mahal, A., Young-Lin, N., Dobberfuhl, A., Estes, J. & Comiter, C. V. Peroxisome proliferator-activated receptor gamma agonist as a novel treatment for interstitial cystitis: A rat model. *Investig Clin Urol* **59**, 257-262, doi:10.4111/icu.2018.59.4.257 (2018).
90 Jung, Y. & Nolta, J. A. BMI1 Regulation of Self-Renewal and Multipotency in Human Mesenchymal Stem Cells. *Curr Stem Cell Res Ther* **11**, 131-140 (2016).
91 Han, Y., Jin, X., Zhou, H. & Liu, B. Identification of key genes associated with bladder cancer using gene expression profiles. *Oncol Lett* **15**, 297-303, doi:10.3892/ol.2017.7310 (2018).
92 Keay, S., Zhang, C. O., Shoenfelt, J. L. & Chai, T. C. Decreased in vitro proliferation of bladder epithelial cells from patients with interstitial cystitis. *Urology* **61**, 1278-1284 (2003).
93 Kim, J., Keay, S. K., Dimitrakov, J. D. & Freeman, M. R. p53 mediates interstitial cystitis antiproliferative factor (APF)-induced growth inhibition of human urothelial cells. *FEBS Lett* **581**, 3795-3799, doi:10.1016/j.febslet.2007.06.058 (2007).
94 Shahid, M. *et al.* Alpha-oxoglutarate inhibits the proliferation of immortalized normal bladder epithelial cells via an epigenetic switch involving ARID1A. *Sci Rep* **8**, 4505, doi:10.1038/s41598-018-22771-2 (2018).
95 Patel, L. *et al.* Tumor suppressor and anti-inflammatory actions of PPARgamma agonists are mediated via upregulation of PTEN. *Curr Biol* **11**, 764-768 (2001).
96 Qin, C. *et al.* Peroxisome proliferator-activated receptor gamma agonists induce proteasome-dependent degradation of cyclin D1 and estrogen receptor alpha in MCF-7 breast cancer cells. *Cancer Res* **63**, 958-964 (2003).
97 Varley, C. L., Stahlschmidt, J., Smith, B., Stower, M. & Southgate, J. Activation of peroxisome proliferator-activated receptor-gamma reverses squamous metaplasia and induces transitional differentiation in normal human urothelial cells. *Am J Pathol* **164**, 1789-1798 (2004).
98 Varley, C. L. *et al.* PPARgamma-regulated tight junction development during human urothelial cytodifferentiation. *J Cell Physiol* **208**, 407-417, doi:10.1002/jcp.20676 (2006).

SCIENTIFIC REPORTS

OPEN

Sex-associated differences in baseline urinary metabolites of healthy adults

Received: 8 January 2018
Accepted: 16 July 2018
Published online: 08 August 2018

Sili Fan[1], Austin Yeon[2], Muhammad Shahid[2], Jennifer T. Anger[3], Karyn S. Eilber[3], Oliver Fiehn[1,4] & Jayoung Kim[5,6,7,8]

The biological basis for gender variability among disease states is not well established. There have been many prior efforts attempting to identify the unique urine metabolomic profiles associated with specific diseases. However, there has been little advancement in investigating the metabolomic differences associated with gender, which underlies the misconception that risk factors and treatment regimens should be the same for both male and female patients. This present study aimed to identify biologically-meaningful baseline sex-related differences using urine samples provided by healthy female and male participants. To elucidate whether urinary metabolic signatures are globally distinct between healthy males and females, we applied metabolomics profiling of primary metabolism with comprehensive bioinformatics analyses on urine samples from 60 healthy males and females. We found that levels of α-ketoglutarate and 4-hydroxybutyric acid increased 2.3-fold and 4.41-fold in males compared to females, respectively. Furthermore, chemical similarity enrichment analysis revealed that differentially expressed metabolites, such as saturated fatty acids, TCA, and butyrates, were significantly related to the gender effect. These findings indicate that there are baseline sex-related differences in urinary metabolism, which should be considered in biomarker discovery, diagnosis, and treatment of bladder diseases, such as interstitial cystitis.

Interstitial cystitis (IC), also known as painful bladder syndrome (PBS), is a chronic pain disorder with no known etiology[1]. Due to the limited amount of objective diagnostic tools for IC[2,3], there is great need to identify sensitive and non-invasive biomarkers that can vastly improve the accuracy of IC diagnoses[4]. Unfortunately, current understanding of the basic mechanisms behind pelvic pain are also fragmented[5,6]. One area of interest that may provide a wealth of information is the impact of gender on IC. Epidemiological studies have consistently demonstrated a sex-based dimorphism in IC prevalence rates[7–11]. It is generally accepted that the female to male ratio is approximately 8:2 or 9:1[7–12]. However, the reasons for this difference are currently not well understood.

One suggestion for the stark discrepancy between male and female IC prevalence rates is sexual dimorphism. Moreover, there are sex-determined differences when diseases start and develop. Although these disparities are well-noted, the biological, cellular, and molecular basis of these gender biases remain elusive. One theory is that sex hormones are possibly associated with noted variations in metabolism. This is evident in other diseases. For example, it has been reported that female cases of autoimmune disease are three to four times higher than that of males[13–15]. Another study suggested that multiple sclerosis (MS) patients showed distinct gene signatures between females and males[16].

In addition to the aforementioned diseases, heart failure and cardiovascular disease (CVD) have been reported to be associated with sex differences[17–21]. In females, hypertension is more common and is often the cause of heart failure. However, females also have a better prognosis than males with heart failure. For CVD, blood pressure and glucose metabolism play more important roles in females, whereas male CVD is affected mostly by cholesterol. The average starting age of CVD incidence in males is around the mid-30s and gradually increases; while

[1]West Coast Metabolomics Center, University of California, Davis, Davis, CA, USA. [2]Departments of Surgery, Cedars-Sinai Medical Center, Los Angeles, CA, USA. [3]Division of Urology, Department of Surgery, Cedars-Sinai Medical Center, Los Angeles, CA, USA. [4]King Abdulaziz University, Jeddah, Saudi Arabia. [5]Departments of Surgery and Biomedical Sciences, Cedars-Sinai Medical Center, Los Angeles, CA, USA. [6]Samuel Oschin Comprehensive Cancer Institute, Cedars-Sinai Medical Center, Los Angeles, CA, USA. [7]University of California Los Angeles, Los Angeles, CA, USA. [8]Department of Urology, Ga Cheon University College of Medicine, Incheon, Republic of Korea. Correspondence and requests for materials should be addressed to J.K. (email: Jayoung.Kim@cshs.org)

in females, CVD usually occurs much later, around 50 years of age. Furthermore, the plasma lipid profiles of younger-aged females are generally better than similarly aged males, which may explain why females have lower risk for CVD. In an effort to examine these sex-biases, mammalian animal models have been used to explore how males and females develop diseases differently and identify potential therapeutic targets. A study in female and male Sprague–Dawley rat models showed that hearts from female rats have better cardioprotection than male rats. Phosphorylation of mitochondrial proteins in female rats were altered, leading to less reactive oxygen species (ROS) generation and oxidative metabolism[22].

Despite the numerous metabolic studies on various types of diseases in animal models[23,24], gender bias in metabolic signatures has not been mechanistically investigated in the healthy human setting. One study used a metabolomics approach to identify specific urinary markers for major depressive disorder (MDD). The authors reported that male and female MDD patients showed very distinct metabonomic signatures[25]. More recently, in the cross-sectional KarMeN (Karlsruhe Metabolomics and Nutrition) study, the metabolite profile of healthy human urine was reported to be capable of predicting age and sex[26]. While research into sex differences in other diseases has progressed, the same cannot be said for lower urinary tract symptoms, such as IC or overactive bladder (OAB). The biological mechanisms underlying sex variation in various bladder dysfunctions are still not fully understood. Further investigation into the relationships among sex-specific risk factors, metabolic rewiring, IC prevalence, and symptom severity are essential for explaining these sex-related differences.

In this study, our first aim was to determine the base levels of urinary metabolites in healthy controls. We additionally attempted to test whether urinary metabolomic profiles were globally different between females and males. To achieve these goals, we performed untargeted global gas chromatography-time-of-flight-mass spectrometry (GC-TOF-MS) profiling of primary metabolism and comprehensive bioinformatics analysis. Our metabolomic profiles showed distinct patterns of differentially expressed metabolites (DEMs) and suggested an interesting list of DEMs specific to healthy females and males. Given that sex influences some of the biomarkers reported, our findings provide evidence showing that baseline gender-related differences should be considered when developing urine-based strategies for metabolomic biomarkers.

Materials and Methods

Ethics statement. The Ethics Committee and the Institutional Review Board of Cedars-Sinai Medical Center (CSMC) approved recruitment, sample collection, curation, and analysis of metabolomics profiling data for this study (IRB# Pro00040261). All subjects who participated in this study provided written informed consent, and all experiments were performed in accordance with relevant guidelines and regulations.

Participants and urine collection. Healthy participants were recruited from an outpatient urology clinic at CSMC. Subjects with a history of any chronic diseases (such as any types of cancer, inflammatory conditions, diabetes, etc.) were excluded. We enrolled 60 females and 60 age-matched males in this study. All participants were >2 months "free of treatment or medication" (2015–2016).

To minimize possible contamination with vaginal or urethral cells, urine was collected using the clean catch method in a sterile environment. The de-identified samples were assigned with new identification numbers by laboratory staff in a double-blinded manner. To remove cell debris, samples were then centrifuged at 2500 rpm for 10 min.

GC-TOF-MS analysis of urine. *Sample pre-processing and preparation.* We investigated the metabolite profiles of the individual urine samples via gas-chromatography/mass-spectrometry (GC-MS) analysis[27,28]. The Gerstel CIS4–with dual MPS Injector and Agilent 6890 GC-Pegasus III TOF MS was used for this analysis.

First, 10 µl of urine was dissolved in a 1 ml −20 °C mixture of acetonitrile, isopropanol, and water (3:3:2 v/v) at a pH of 7.0. The urine volume was adjusted between 2–10 µl to match externally measured creatinine levels based on a linear calibration curve. The solution was then vortexed at 4 °C for 5 min in 1.5 ml centrifuge tubes. Samples were additionally centrifuged for 2 min at 14,000 rcf and 500 µl of the supernatants were aliquoted. Aliquots were evaporated in a Labconco Centrivap cold trap to complete dryness. The methoximation step was done using a 10 µl solution of 40 mg/ml o-methylhydroxylamine hydrochloride (CAS:[593-56-6]; formula $CH_5NO.HCl$) in pyridine (Cas:[11-0-86-1]; formula C_5H_5N) and shaken for 90 min at 30 °C. Then, 90 µl of a n-methyl-n-trimethylsilyltrifluoroacetamide (MSTFA) and fatty acid methyl esters (FAME) retention time markers mixture (100:1 v/v) was added and the entire solution was shaken for 30 min at 37 °C. The mixture was transferred to amber crimp auto-sampler vials with flat bottom micro-inserts. Measurements were performed on a Leco Pegasus IV TOF coupled to an Aglient 6890GC with an Agilent 6890 split/splitless injector. The column used was a Restek RTX-5Sil MS (95% dimethyl/5% diphenyl polysiloxane) with a 30 m length, 0.25 mm i.d., and 0.25 µm film thickness with a 10 m guard column. Each injection had a set volume of 0.5 µl and was done at 50 °C. The GC parameters were set to a 1 ml/min constant flow helium and an oven ramp temperature of 50 °C (1 min hold) that steadily increased to 330 °C at a rate of 20 °C/min, with a 5 min hold before cooling-down. The transfer line temperature was set to 280 °C and the spectra were recorded in the electron ionization mode at 70 eV with a source temperature of 250 °C TOF and scan range of 85–500 u.

Injector conditions. The Agilent 6890 GC was equipped with a Gerstel Automatic Liner Exchange System (ALEX) that included a multipurpose sample (MPS2) dual rail and a Gerstel cold injection system (CIS) (Gerstel, Muehlheim, Germany). The temperature program was set as follows: 50 °C to a final temperature of 275 °C at a rate of 12 °C/sec with a hold for 3 min. Injections were done at a speed of 10 µl/sec on a splitless injector with a purge time of 25 sec. The liner (Gerstel #011711-010-00) was changed after every 10 samples using the Maestro1 Gerstel software (version 1.1.4.18). Before and after each injection, the 10 µl injection syringe was washed 3x with 10 µl of ethyl acetate.

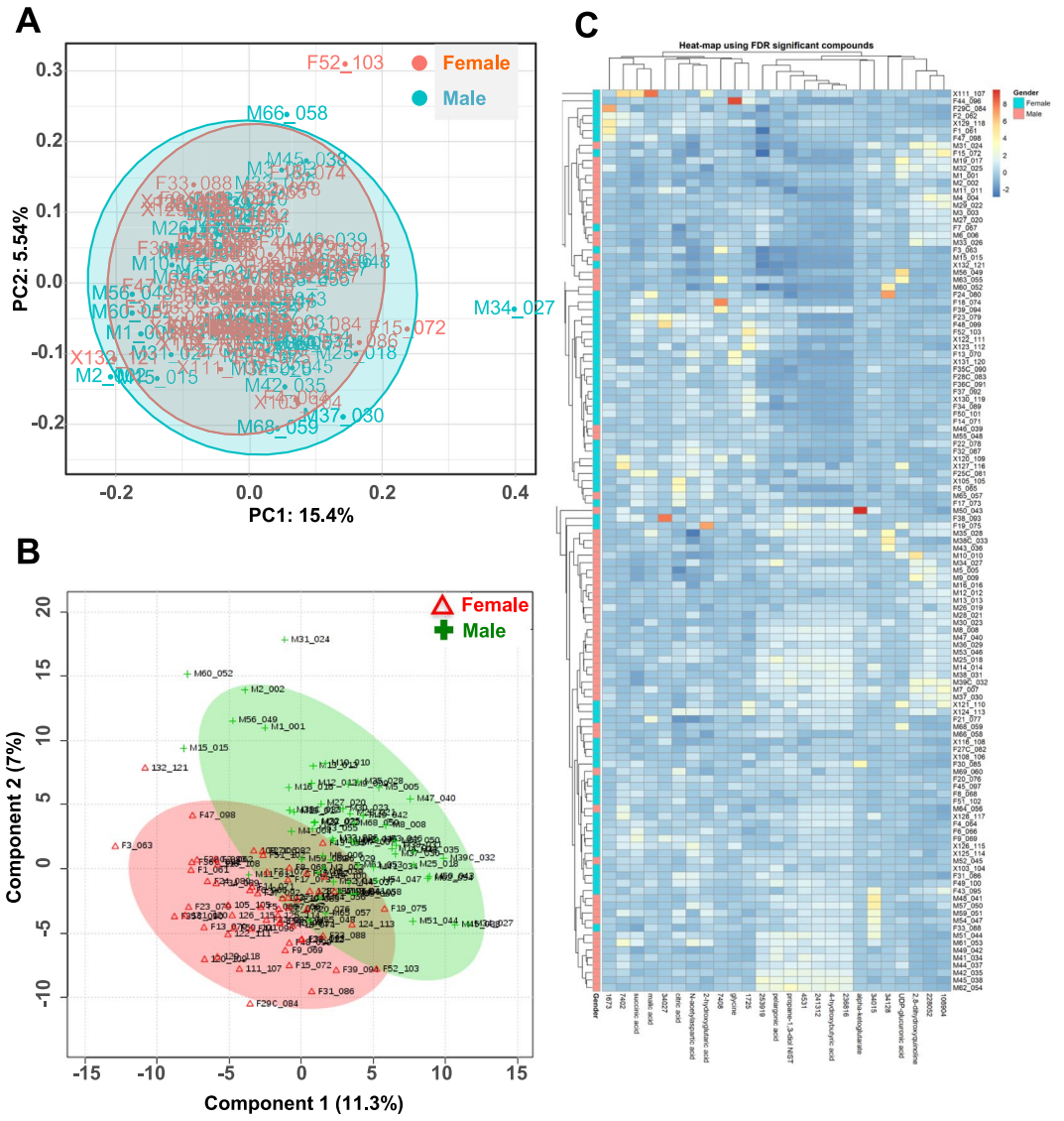

Figure 1. Differentiation of male and female groups using multivariate analysis. (**A**) Score plot of the PCA model distinguishing male and female urine samples. (**B**) PLS-DA scores plot. It depicted obvious differences between male and female urine samples, with PC1 (11.3%) and PC2 (7%). (**C**) Heat map showed the distribution of 25 metabolites, which include 12 annotated ones, that were significantly different (FDR adjusted p-value < 0.05) between male and female urine samples.

Gas chromatography conditions. A 30 m long, 0.25 mm i.d. RTX-5Sil MS column (0.25 µm, 95% dimethyl 5% diphenyl polysiloxane film) with an additional 10 m integrated guard column was used (Restek, Bellefonte, PA). A constant flow of 1 ml/min 99.99% pure helium, with a built-in purifier, was set. The oven temperature was held at 50 °C for 1 min and then ramped up to 330 °C at a rate of 20 °C/min, where it was then maintained constant for 5 min.

Mass spectrometer settings. A Leco Pegasus IV Time-of-Flight Mass Spectrometer was used and controlled using the Leco ChromaTOF software (vers. 4.1) (St. Joseph, MI). The transfer line temperature between the gas chromatograph and mass spectrometer was set to 280 °C. A 70 V electron impact ionization was employed with an ion source temperature of 250 °C. The acquisition rate was set to 17 spectra/sec, with a scan mass range of 85–500 Da.

Annotation and ID of compounds. The peak and compounds detection or deconvolution was performed with the Leco ChromaTOF software. Spectra were matched against the FiehnLib Mass Spectral and Retention Index Library[28]. Post-curation and peak replacements were performed with the in-house developed BinBase software and the sample matrix with all known and unknown compounds was exported to an excel sheet. Missing peak intensity data was automatically replaced with the raw extracted ion intensities at the target retention times for each compound, subtracted by adjacent noise levels. This way, only 2 of the 49,680 values were reported with 'zero' values, compound BB 109708 and creatinine. These two values were replaced with a value of 1.

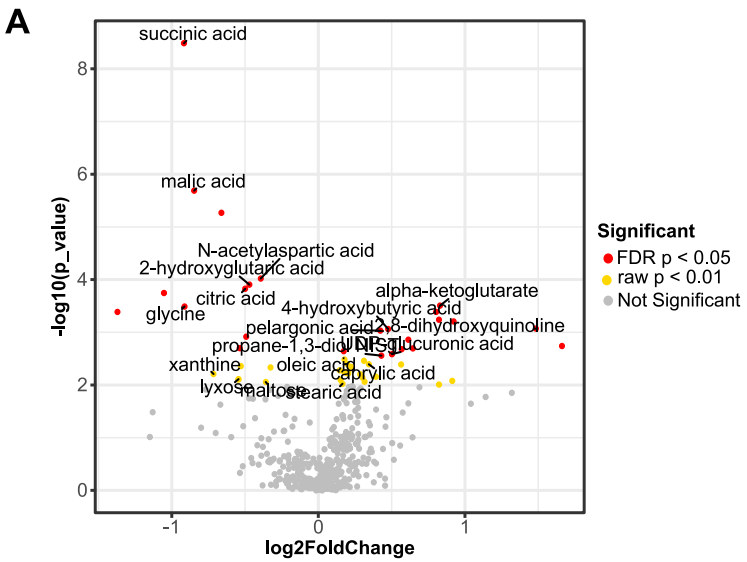

B

compounds	p value	FDR p value	Fold Change (M/F)	PLS-DA VIP
succinic acid	<0.0001	<0.0001	0.40	3.11
malic acid	<0.0001	0.00042	0.43	1.67
N-acetylaspartic acid	<0.0001	0.00991	0.68	2.43
2-hydroxyglutaric acid	0.0001	0.0103	0.62	2.17
citric acid	0.0001	0.0103	0.61	1.98
alpha-ketoglutarate	0.0003	0.0149	2.29	0.92
glycine	0.0003	0.0149	0.40	1.55
2,8-dihydroxyquinoline	0.0009	0.0239	4.41	2.16
4-hydroxybutyric acid	0.0009	0.0239	1.61	1.69
pelargonic acid	0.0009	0.0241	1.53	1.74
UDP-glucuronic acid	0.0026	0.0448	1.65	1.31
propane-1,3-diol NIST	0.0028	0.0460	1.54	1.70
oleic acid	0.0040	0.0563	1.22	1.34
caprylic acid	0.0040	0.0563	1.41	1.38
xanthine	0.0062	0.0646	0.49	0.87
lyxose	0.0078	0.0737	0.58	1.11
maltose	0.0088	0.0757	0.70	0.62
stearic acid	0.0095	0.0800	1.18	1.47
fumaric acid	0.0109	0.0834	0.81	1.21
capric acid	0.0110	0.0834	1.27	1.51
heptadecanoic acid	0.0110	0.0834	1.23	1.32
gluconic acid	0.0124	0.0883	0.72	1.57
isothreonic acid	0.0163	0.1036	1.21	1.13
hydroxylamine	0.0170	0.1049	1.31	1.26
xylose	0.0187	0.1077	0.70	1.28
galactonic acid	0.0369	0.1798	0.80	1.46
palmitic acid	0.0408	0.1890	1.24	1.28
4-hydroxyhippuric acid NIST	0.0427	0.1941	0.65	0.45
ribitol	0.0440	0.1959	0.85	0.59

Figure 2. Volcano plot and significant metabolite table. (**A**) In the volcano plot, a total of 50 peaks were significantly changed (Mann-Whitney U test p-value < 0.01) in urine samples. Red dots represent 25 significant peaks with FDR adjusted p-values < 0.05. The annotated significant metabolites are labeled on the plot. (**B**) List of the 21 potential biomarkers in urine samples. P-values were calculated using two-tailed Mann-Whiney U tests. FDR p-values were p-values corrected for the multiple comparison problem using the Benjamini and Hochberg procedure. Fold changes were defined as the ratio of median of male over female for each compound. The variable importance for projection (VIP) reflects the capability of the compounds to explain Y (gender effect).

Missing value replacement method. BinBase was used for post-curation and peak replacements and the sample matrix was exported to an excel sheet. Any missing peak intensity data was automatically replaced by the raw extract ion intensity subtracted by their adjacent noise levels. For each positively detected metabolite, the average retention time was calculated. For each chromatogram and each missing value, the intensity of the quantification ion at this retention time was extracted by seeking its maximum value in a retention time region of 1 sec and subtracting the minimum (local background) intensity in a retention time region of 5 sec around the peak maximum. The resulting report table therefore did not have any missing values[29].

The two missing values (*ion intensity = 0*), for compound 109708 and creatinine, were replaced with a value of 1. All peak intensities were normalized to the sum of the peak intensities of all identified metabolites to account

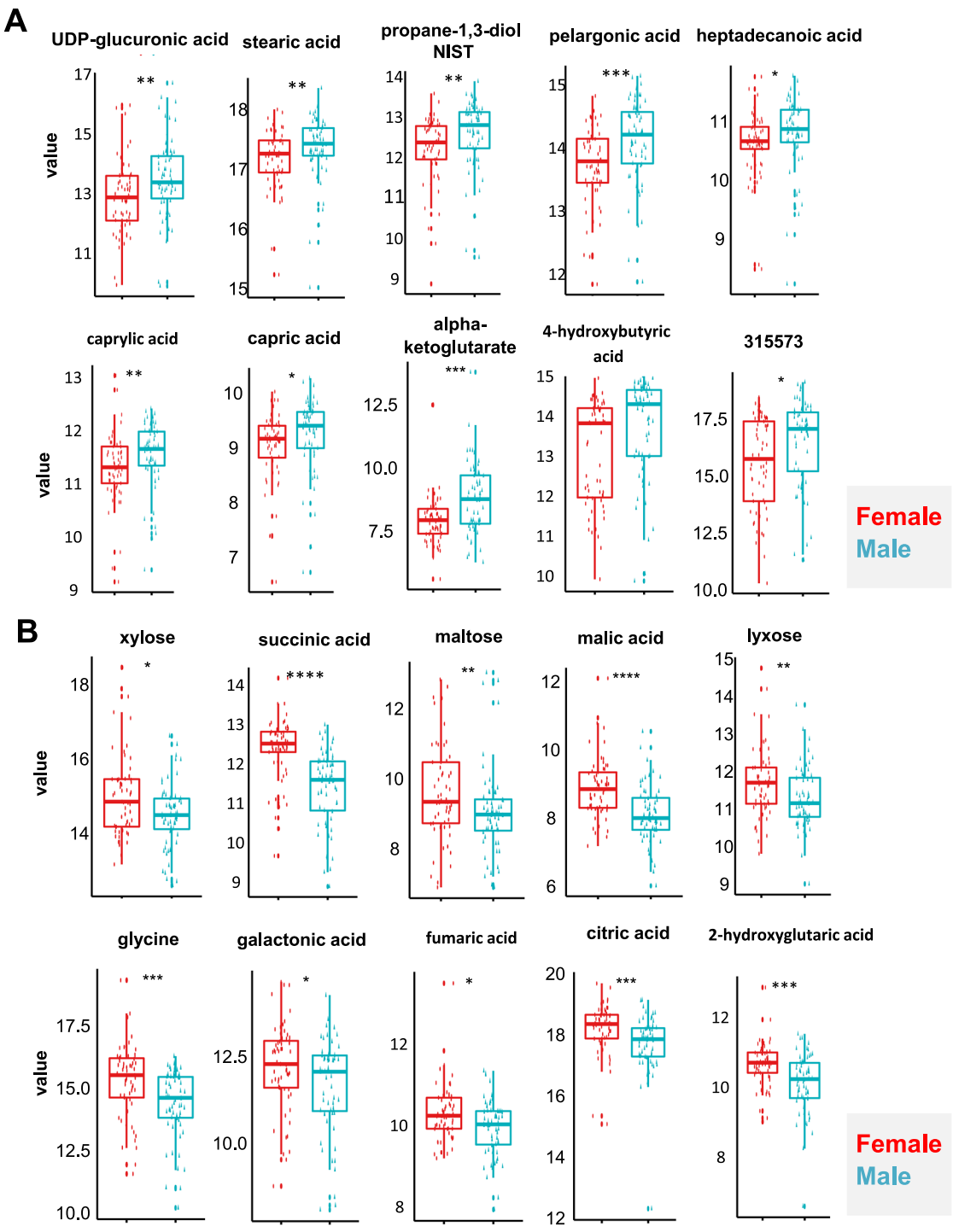

Figure 3. Compound individual boxplots. Boxplots showing upregulated (**A**) and downregulated (**B**) metabolites that could be used to differentiate male and female samples. Significance levels were highlighted using *(p value < 0.05), **($p < 0.01$), ***($p < 0.001$), and ****($p < 0.0001$).

for small errors during extraction or normalization. We found that 77% of all compounds yielded a non-normality distribution. Hence, a nonparametric univariate method, the Mann-Whitney U test, was performed to measure and discover significantly changed metabolites between the male and female urine samples. Additionally, we adopted the Benjamini-Hochberg false discovery rate (FDR) correction procedure to deal with the multiple comparison problem and ensure the reproducibility of our significant metabolites detection. Multivariate statistical analyses, principal component analysis (PCA) and partial least-square discriminant analysis (PLS-DA), were performed to discriminate males and females.

Num	Name	Fold-change	p-value	FDR
1	Unknown BB_31554	2.56	0.000132	0.064576
2	Unknown BB_34163	0.55	0.000514	0.12586
3	oleic acid	0.63	0.001933	0.315675
4	2-deoxytetronic acid	1.26	0.008732	0.571396
5	Unknown BB_17651	0.66	0.009136	0.571396
6	saccharic acid	0.80	0.012642	0.571396
7	Unknown BB_17140	1.44	0.015588	0.571396
8	phosphate	0.70	0.016252	0.571396
9	trehalose	1.79	0.017026	0.571396
10	Unknown BB_5900	0.81	0.017487	0.571396
11	erythronic acid	2.25	0.018393	0.571396
12	Unknown BB_109809	0.56	0.018576	0.571396
13	oxalic acid	0.48	0.018665	0.571396
14	Unknown BB_34027	0.44	0.019904	0.571396
15	Unknown BB_1704	0.63	0.020865	0.571396
16	sulfuric acid	0.31	0.021197	0.571396
17	Unknown BB_23635	0.69	0.02138	0.571396
18	cystine	1.47	0.021607	0.571396
19	Unknown BB_3029	0.70	0.022156	0.571396
20	Unknown BB_12330	2.19	0.02596	0.614149
21	Unknown BB_31549	0.37	0.026702	0.614149
22	lyxitol	1.42	0.028288	0.614149
23	Unknown BB_31756	1.74	0.028827	0.614149
24	lysine	1.49	0.034624	0.706901
25	histidine	1.79	0.040576	0.743323
26	Unknown BB_31359	0.81	0.043988	0.743323
27	Unknown BB_5121	0.64	0.045462	0.743323
28	Unknown BB_100869	1.58	0.046685	0.743323
29	Unknown BB_3294	1.37	0.046907	0.743323
30	Unknown BB_31764	1.33	0.048566	0.743323

Table 1. List of metabolites differentially expressed in IC, compared to controls (p-value = 0.005, FDR (Benjamini Hochberg).

Statistical analysis. The Mann-Whitney U test was performed on each compound to compare males vs. females. The Benjamini-Hochberg false discovery rate (FDR) correction was utilized to deal with the multiple comparison problem.

Results

GC-TOF-MS analysis of urine specimens from healthy females and males. In total, we enrolled 60 females and 60 age-matched males (age range, 45–65) in this study. All participants were >2 months free of treatment and/or medication. In order to compare the metabolite profiles of urine samples from healthy females and males, individual urine samples were analyzed using GC-TOF mass spectrometry. Multivariate statistical analyses, PCA and PLS-DA, were performed to discriminate males and females (Fig. 1A, B).

Metabolites responsible for the differences in multivariate metabolic phenotypes between male and female urine was obtained based on variable importance in the projection (VIP) from a 10-fold cross-validated PLS-DA model. This model achieved a 48.5% rate of discrimination for Q2 and an 89.1% for R2. In addition, the model was further validated with the permutation test on prediction accuracy and had a significant result ($p < 0.05$), indicating that the model was robust and results were not obtained by chance. Significantly altered metabolites distinguishing male and female urine were acquired based on conditions of $p < 0.05$, fold-change < 0.8 or >1.2, and VIP > 1 (Fig. 1B). Hierachical clustering analysis (*Euclidean* distance and *complete* method) and constructed heatmaps, using the significant metabolites (corrected FDR $p < 0.05$), depicted the relatively disturbed and unbalanced metabolism states between male and female samples (Fig. 1C).

Distinct urinary metabolite patterns between healthy females and males. Next, we performed the Mann-Whitney U test and Benjamini-Hochberg false discovery rate (FDR) correction on each compound to compare them between males and females. There were 25 significantly different compounds with FDR correction and 94 without (Supplementary Table 1). The volcano plot shows the fold change and significance of each annotated metabolite. Significant metabolites in the volcano plot had a fold-change threshold >1.20 or <0.83 with a t-test p-value < 0.05 (Fig. 2A). The 25 significantly different compounds are shown with their p-values, FDR p-values, fold-changes of male vs. female, and PLS-DA VIP values (Fig. 2B). These compounds

label	PubChem	PLS-DA VIP Score	p_value	p_value_adj	Fold Change
xylose	135191	1.28	0.0187	0.1077	0.70
UDP-glucuronic acid	17473	1.31	0.0026	0.0448	1.65
succinic acid	1110	3.11	0.0000	0.0000	0.40
propane-1,3-diol NIST	10442	1.70	0.0028	0.0460	1.54
pelargonic acid	8158	1.74	0.0009	0.0241	1.53
palmitic acid	985	1.28	0.0408	0.1890	1.24
oleic acid	445639	1.34	0.0040	0.0563	1.22
N-acetylaspartic acid	65065	2.43	0.0001	0.0099	0.68
malic acid	525	1.67	0.0000	0.0004	0.43
lyxose	439240	1.11	0.0078	0.0737	0.58
isothreonic acid	151152	1.13	0.0163	0.1036	1.21
hydroxylamine	787	1.26	0.0170	0.1049	1.31
heptadecanoic acid	10465	1.32	0.0110	0.0834	1.23
glycine	750	1.55	0.0003	0.0149	0.40
gluconic acid	6857417	1.57	0.0124	0.0883	0.72
galactonic acid	128869	1.46	0.0369	0.1798	0.80
citric acid	311	1.98	0.0001	0.0103	0.61
caprylic acid	379	1.38	0.0040	0.0563	1.41
capric acid	2969	1.51	0.0110	0.0834	1.27
4-hydroxybutyric acid	10413	1.69	0.0009	0.0239	1.61
2-hydroxyglutaric acid	43	2.17	0.0001	0.0103	0.62
2,8-dihydroxyquinoline	97250	2.16	0.0009	0.0239	4.41

Table 2. List of metabolites with a PLS-DA VIP score > 1, Mann-Whitney U test p-value < 0.05, fold-change (male/female) <0.8 or >1.2.

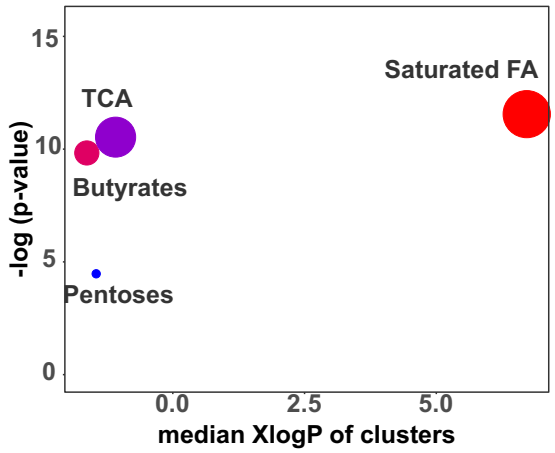

Figure 4. Chemical similarity enrichment analysis results. Y-axis shows the most significantly altered clusters on the top. Cluster color gives the proportion of increased or decreased metabolites (red = increased, blue = decreased, purple = mostly decreased). Chemical enrichment statistics was calculated using Kolmogorov–Smirnov test. Only significantly different enrichment clusters (raw $p < 0.05$) were shown.

include succinic acid, malic acid, N-acetylaspartic acid, 2-hydroxyglutaric acid, citric acid, α-ketoglutarate and others. Among these, α-ketoglutarate (male/female fold-change of 2.29) or 4-hydroxybutyric acid (male/female fold-change 4.41) increased in healthy males compared to females. In contrast, levels of succinic acid (male/female fold-change of 0.40), malic acid (male/female fold-change of 0.43), or glycine (male/female fold-change of 0.40) greatly decreased in males compared to females.

Significantly increased and decreased metabolites in males, compared to females, are shown in Fig. 3A and 3B, respectively. Box-whisker plots were constructed after log2 transformation. The Mann-Whitney U test was used to determine significance ($*p < 0.05$, $**p < 0.01$, or $***p < 0.005$). All metabolites identified in this study are shown in Supplementary Tables 1 and 2. A few example metabolites whose expression was lower or higher in healthy females compared to healthy males are shown in Fig. 3A and 3B. Expression levels of UDP-glucuronic acid, stearic acid, propane-1,3-diol, pelargonic acid, heptadecanoic acid, caprylic acid, capric acid, α-ketoglutarate, hydroxybutyric acid, and unknown compound BB 315573 were all detected to be considerably lower in urine

Cluster name	Cluster size	p-values	FDR	Increased	Decreased	Increased ratio	Altered Ratio
Saturated FA	10	0.0000096	0.00018	6	0	0.6	0.6
TCA	8	0.000027	0.00025	1	5	0.1	0.8
Butyrates	5	0.000054	0.00034	2	0	0.4	0.4
Pentoses	4	0.011	0.054	0	2	0	0.5
Sugar Acids	9	0.26	0.99	0	2	0	0.2
Amino Acids	7	1	1	0	1	0	0.1
Benzoates	3	1	1	0	0	0	0
Cinnamates	3	1	1	0	0	0	0
Dicarboxylic Acids	3	1	1	0	0	0	0
Disaccharides	4	1	1	0	1	0	0.2
Gum Arabic	3	1	1	0	0	0	0
Hexoses	7	1	1	0	0	0	0
Hippurates	3	1	1	0	1	0	0.3
Indoles	4	1	1	0	0	0	0
Phenols	5	1	1	0	0	0	0
Phenylacetates	4	1	1	0	0	0	0
Purinones	3	1	1	0	1	0	0.3
Pyrimidinones	3	1	1	0	0	0	0
Sugar Alcohols	14	1	1	0	1	0	0.07

Table 3. Chemical similarity enrichment analysis. Cluster name is redefined metabolite chemical clusters. Cluster size indicates the size of the cluster. P-values are the result of the Kolmogorov–Smirnov test evaluating how significant difference a metabolite cluster was represented by chance. FDR is the Benjamini-Hochberg corrected p values. The Increase/ratio (Decreased/ratio) shows the numbers/ratio of directions of significant compounds in a cluster.

obtained from healthy females compared to males (Fig. 3A). In contrast, levels of xylose, succinic acid, maltose, malic acid, lyxose, glycine, galactonic acid, fumaric acid, citric acid, and 2-hydroxyglutaric acid were found to be greater in females than in males (Fig. 3B). Table 1 shows a list of metabolites differentially expressed in IC, compared to controls (p-level = 0.005, FDR (Benjamini Hochberg). A list of metabolites with PLS-DA VIP score > 1, Mann-Whitney U test p value < 0.05, and fold change (male/female) <0.8 or >1.2 are shown in Table 2.

We speculated that metabolite enrichment analysis may be able to provide the corresponding gender-specific pathways derived from the specific metabolites on their differential networks. We performed metabolite set enrichment analysis (MSEA) with the 29 significant metabolites (Mann-Whitney U test p-value < 0.05). We found that differentially expressed metabolites in female and male groups were highly related to α-ketoglutarate dehydrogenase complex deficiency, with a FDR of 0.00524 (raw p, 0.0000181; Holm p, 0.00524) (Supplementary Fig. 1).

Recently, we published a paper demonstrating that the hypergeometric test could be flawed for metabolomics analyses and should not be used[30]. We also noted that MSEA may be faulty as well. Thus, in this study, we opted to utilize the newly developed chemical similarity enrichment analysis (ChemRICH)[30] instead (http://chemrich.us). ChemRICH is a chemical similarity-based statistical enrichment tool with better subsequent enrichment statistics than pathway enrichments and is not dependent on biochemical knowledge annotations. However, it does not provide information regarding enzymes or diseases. To better understand the metabolic signature specific to female and male groups, we performed ChemRICH using the Mann-Whitney U test p-values and median fold-changes of our 140 identified metabolites. ChemRICH was implemented using the Kolmogorov–Smirnov test on the identified clusters to evaluate whether a metabolite cluster was represented more than expected by chance. As a result, we found that saturated fatty acids (FA) (raw p, 0.0000096; FDR p, 0.00018), TCA (raw p, 0.000027; FDR p, 0. 0.00025), and butyrates (raw p, 0.000054; FDR p, 0.00034) were significantly related (FDR $p < 0.05$) to the gender effect (Fig. 4, Table 3).

Discussion

Our objective in this study was to systematically examine sex differences in urine samples obtained from healthy participants. The experimental results from this study provided evidence suggesting that gender influences the global metabolome in healthy female and male subjects. It has been generally accepted that pathogenesis in females may be influenced by metabolic perturbations caused by various hormones, such as estrogen, and other reproductive factors. Although further research is needed, levels of sex hormones may be related to the differences in metabolites detected in the urine of healthy adults.

As proposed in our previously published review articles, monitoring the changes in metabolic landscape, cholesterol, and sex hormones through metabolic profiling can be of immense benefit to patients[31,32]. Our urinary metabolomics data clearly suggests that sex differences should be considered in future laboratory and clinical studies. Sex has not been heavily considered as an important factor when it comes to identifying druggable targets in diseases, resulting in few biomarker studies that actively look at sex. Since gender is an influencing factor on

pharmacological responses, which in turn is monitored through biomarker changes, careful should be done when consideration should be given when developing effective treatments for males and females.

Levels of urinary metabolites, including UDP-glucuronic acid, α-ketoglutarate, and 2-hydroxyglutaric acid, were found to be higher or lower in females than in males (Fig. 3). We further hypothesized the biology associated with sex-specific metabolites detected in urine samples is linked with sex hormones. Our data suggested the level of UDP-glucuronic acid is higher in healthy males, compared to females. UDP-glucuronic acid is oxidized from UDP-glucose and NAD^+ by UDP-glucose dehydrogenase (UGDH). Considering that the expression of UGDH is known to be stimulated by androgen, a male sex hormone[33], it would be interesting to see if androgen causes the differential levels of UDP-glucuronic acid found in urine samples of female vs. males. In addition, 2-hydroxyglutaric acid (2HG) was found to be greater in females than in males (Fig. 3B). 2HG is known as an oncometabolite that can accumulate in estrogen receptor-negative breast tumors[34], suggesting a potential association between increased 2HG levels and estrogen, a female sex hormone.

Previous work from our laboratory and others proposed a series of urinary metabolites as potential IC biomarker candidates[35–40]. Compared to healthy controls, these metabolites significantly increased or decreased in IC patient urine samples[36]. One metabolite of interest that we found was α-ketoglutarate, which is an important TCA cycle product and is involved in lipid and acetate metabolism. It is also an epigenetic regulator, controlling transcription and translation of DNA through histone acetylation. Treatment with α-ketoglutarate slowed cell proliferation in normal bladder epithelial cells[39]. This is consistent with prior clinical observations suggesting that there are thinner layers of bladder epithelium in IC[41,42]. It was interesting that our current study found higher levels of α-ketoglutarate in healthy males, compared to females. Furthermore, a recent finding from our laboratory suggested the molecular mechanism through which α-ketoglutarate epigenetically regulates bladder epithelial cells[43].

Unfortunately, in this current study, we could not provide solid experimental evidence explaining why healthy male urine samples contained these higher levels of α-ketoglutarate. Furthermore, considering that previous results from our group were based only on female participants, expansion of our earlier findings in both sexes would be warranted in the near future.

In summary, our findings suggested that baseline sex-determined differences would be helpful in identifying sex specific biomarkers. Currently, gender differences have not been carefully considered as important confounding factors for biomarker development. Our results provide evidence demonstrating otherwise; drug development and therapies may need more precise and detailed experimental designs that recognize the effects of sex differences on therapeutic efficacy.

References

1. Hanno, P., Keay, S., Moldwin, R. & Van Ophoven, A. International Consultation on IC - Rome, September 2004/Forging an International Consensus: progress in painful bladder syndrome/interstitial cystitis. Report and abstracts. *International urogynecology journal and pelvic floor dysfunction* **16**(Suppl 1), S2–S34, https://doi.org/10.1007/s00192-005-1301-x (2005).
2. Hanno, P. M. *et al*. AUA guideline for the diagnosis and treatment of interstitial cystitis/bladder pain syndrome. *The Journal of urology* **185**, 2162–2170, https://doi.org/10.1016/j.juro.2011.03.064 (2011).
3. Hanno, P. *et al*. Diagnosis of interstitial cystitis. *The Journal of urology* **143**, 278–281 (1990).
4. Erickson, D. R. *et al*. A comparison of multiple urine markers for interstitial cystitis. *The Journal of urology* **167**, 2461–2469 (2002).
5. Nordling, J. *et al*. Primary evaluation of patients suspected of having interstitial cystitis (IC). *European urology* **45**, 662–669, https://doi.org/10.1016/j.eururo.2003.11.021 (2004).
6. Warren, J. W. & Keay, S. K. Interstitial cystitis. *Current opinion in urology* **12**, 69–74 (2002).
7. Berry, S. H. *et al*. Prevalence of symptoms of bladder pain syndrome/interstitial cystitis among adult females in the United States. *The Journal of urology* **186**, 540–544, https://doi.org/10.1016/j.juro.2011.03.132 (2011).
8. Clemens, J. Q., Meenan, R. T., Rosetti, M. C., Gao, S. Y. & Calhoun, E. A. Prevalence and incidence of interstitial cystitis in a managed care population. *The Journal of urology* **173**(discussion 102), 98–102, https://doi.org/10.1097/01.ju.0000146114.53828.82 (2005).
9. Forrest, J. B. & Schmidt, S. Interstitial cystitis, chronic nonbacterial prostatitis and chronic pelvic pain syndrome in men: a common and frequently identical clinical entity. *The Journal of urology* **172**, 2561–2562 (2004).
10. Link, C. L. *et al*. Prevalence and psychosocial correlates of symptoms suggestive of painful bladder syndrome: results from the Boston area community health survey. *The Journal of urology* **180**, 599–606, https://doi.org/10.1016/j.juro.2008.04.009 (2008).
11. Parsons, J. K., Kurth, K. & Sant, G. R. Epidemiologic issues in interstitial cystitis. *Urology* **69**, 5–8, https://doi.org/10.1016/j.urology.2006.05.050 (2007).
12. Barry, M. J., Link, C. L., McNaughton-Collins, M. F. & McKinlay, J. B., Boston Area Community Health, I.. Overlap of different urological symptom complexes in a racially and ethnically diverse, community-based population of men and women. *BJU international* **101**, 45–51, https://doi.org/10.1111/j.1464-410X.2007.07191.x (2008).
13. Oertelt-Prigione, S. The influence of sex and gender on the immune response. *Autoimmunity reviews* **11**, A479–485, https://doi.org/10.1016/j.autrev.2011.11.022 (2012).
14. Scotland, R. S., Stables, M. J., Madalli, S., Watson, P. & Gilroy, D. W. Sex differences in resident immune cell phenotype underlie more efficient acute inflammatory responses in female mice. *Blood* **118**, 5918–5927, https://doi.org/10.1182/blood-2011-03-340281 (2011).
15. Weyand, C. M., Schmidt, D., Wagner, U. & Goronzy, J. J. The influence of sex on the phenotype of rheumatoid arthritis. *Arthritis and rheumatism* **41**, 817–822, doi:10.1002/1529-0131(199805)41:5<817::AID-ART7>3.0.CO;2-S (1998).
16. Menon, R. *et al*. Gender-based blood transcriptomes and interactomes in multiple sclerosis: involvement of SP1 dependent gene transcription. *Journal of autoimmunity* **38**, J144–155, https://doi.org/10.1016/j.jaut.2011.11.004 (2012).
17. Blenck, C. L., Harvey, P. A., Reckelhoff, J. F. & Leinwand, L. A. The Importance of Biological Sex and Estrogen in Rodent Models of Cardiovascular Health and Disease. *Circulation research* **118**, 1294–1312, https://doi.org/10.1161/CIRCRESAHA.116.307509 (2016).
18. Buoncervello, M. *et al*. Preclinical models in the study of sex differences. *Clinical science* **131**, 449–469, https://doi.org/10.1042/CS20160847 (2017).
19. Santilli, F., D'Ardes, D., Guagnano, M. T. & Davi, G. Metabolic Syndrome: Sex-Related Cardiovascular Risk and Therapeutic Approach. *Current medicinal chemistry* **24**, 2602–2627, https://doi.org/10.2174/0929867324666170710121145 (2017).
20. Mihailidou, A. S. & Ashton, A. W. Cardiac effects of aldosterone: does gender matter? *Steroids* **91**, 32–37, https://doi.org/10.1016/j.steroids.2014.08.013 (2014).

21. Rosen, S. E., Henry, S., Bond, R., Pearte, C. & Mieres, J. H. Sex-Specific Disparities in Risk Factors for Coronary Heart Disease. *Current atherosclerosis reports* **17**, 49, https://doi.org/10.1007/s11883-015-0523-8 (2015).
22. Lagranha, C. J., Deschamps, A., Aponte, A., Steenbergen, C. & Murphy, E. Sex differences in the phosphorylation of mitochondrial proteins result in reduced production of reactive oxygen species and cardioprotection in females. *Circulation research* **106**, 1681–1691, https://doi.org/10.1161/CIRCRESAHA.109.213645 (2010).
23. Garcia-Perez, I. *et al*. Urinary metabolic phenotyping the slc26a6 (chloride-oxalate exchanger) null mouse model. *Journal of proteome research* **11**, 4425–4435, https://doi.org/10.1021/pr2012544 (2012).
24. Won, E. Y. *et al*. Gender-specific metabolomic profiling of obesity in leptin-deficient ob/ob mice by 1H NMR spectroscopy. *PloS one* **8**, e75998, https://doi.org/10.1371/journal.pone.0075998 (2013).
25. Zheng, P. *et al*. Identification of sex-specific urinary biomarkers for major depressive disorder by combined application of NMR- and GC-MS-based metabonomics. *Translational psychiatry* **6**, e955, https://doi.org/10.1038/tp.2016.188 (2016).
26. Rist, M. J. *et al*. Metabolite patterns predicting sex and age in participants of the Karlsruhe Metabolomics and Nutrition (KarMeN) study. *PloS one* **12**, e0183228, https://doi.org/10.1371/journal.pone.0183228 (2017).
27. Kind, T., Tolstikov, V., Fiehn, O. & Weiss, R. H. A comprehensive urinary metabolomic approach for identifying kidney cancerr. *Analytical biochemistry* **363**, 185–195, https://doi.org/10.1016/j.ab.2007.01.028 (2007).
28. Kind, T. *et al*. FiehnLib: mass spectral and retention index libraries for metabolomics based on quadrupole and time-of-flight gas chromatography/mass spectrometry. *Analytical chemistry* **81**, 10038–10048, https://doi.org/10.1021/ac9019522 (2009).
29. Fiehn, O. *et al*. Quality control for plant metabolomics: reporting MSI-compliant studies. *The Plant journal: for cell and molecular biology* **53**, 691–704, https://doi.org/10.1111/j.1365-313X.2007.03387.x (2008).
30. Barupal, D. K. & Fiehn, O. Chemical Similarity EnrichmentAnalysis (ChemRICH) as alternative to biochemical pathway mapping for metabolomic datasets. *Scientific reports* **7**, 14567, https://doi.org/10.1038/s41598-017-15231-w (2017).
31. Kim, W. J. & Kim, J. Looking to the metabolic landscapes for prostate health monitoring. *Prostate international* **5**, 85–88, https://doi.org/10.1016/j.prnil.2017.03.004 (2017).
32. Moon, J. Y., Choi, M. H. & Kim, J. Metabolic profiling of cholesterol and sex steroid hormones to monitor urological diseases. *Endocrine-related cancer* **23**, R455–467, https://doi.org/10.1530/ERC-16-0285 (2016).
33. Wei, Q., Galbenus, R., Raza, A., Cerny, R. L. & Simpson, M. A. Androgen-stimulated UDP-glucose dehydrogenase expression limits prostate androgen availability without impacting hyaluronan levels. *Cancer research* **69**, 2332–2339, https://doi.org/10.1158/0008-5472.CAN-08-3083 (2009).
34. Terunuma, A. *et al*. MYC-driven accumulation of 2-hydroxyglutarate is associated with breast cancer prognosis. *The Journal of clinical investigation* **124**, 398–412, https://doi.org/10.1172/JCI71180 (2014).
35. Kind, T. *et al*. Interstitial Cystitis-Associated Urinary Metabolites Identified by Mass-Spectrometry Based MetabolomicsAnalysis. *Scientific reports* **6**, 39227, https://doi.org/10.1038/srep39227 (2016).
36. Wen, H. *et al*. Urinary metabolite profiling combined with computational analysis predicts interstitial cystitis-associated candidate biomarkers. *Journal of proteome research* **14**, 541–548, https://doi.org/10.1021/pr5007729 (2015).
37. Blalock, E. M., Korrect, G. S., Stromberg, A. J. & Erickson, D. R. Gene expression analysis of urine sediment: evaluation for potential noninvasive markers of interstitial cystitis/bladder pain syndrome. *The Journal of urology* **187**, 725–732, https://doi.org/10.1016/j.juro.2011.09.142 (2012).
38. Keay, S. *et al*. Antiproliferative factor, heparin-binding epidermal growth factor-like growth factor, and epidermal growth factor in men with interstitial cystitis versus chronic pelvic pain syndrome. *Urology* **63**, 22–26 (2004).
39. Kuo, H. C. Potential urine and serum biomarkers for patients with bladder pain syndrome/interstitial cystitis. *International journal of urology: official journal of the Japanese Urological Association* **21**(Suppl 1), 34–41, https://doi.org/10.1111/iju.12311 (2014).
40. Tyagi, P. *et al*. Urinary chemokines as noninvasive predictors of ulcerative interstitial cystitis. *The Journal of urology* **187**, 2243–2248, https://doi.org/10.1016/j.juro.2012.01.034 (2012).
41. Ratliff, T. L., Klutke, C. G. & McDougall, E. M. The etiology of interstitial cystitis. *The Urologic clinics of North America* **21**, 21–30 (1994).
42. Tomaszewski, J. E. *et al*. Biopsy features are associated with primary symptoms in interstitial cystitis: results from the interstitial cystitis database study. *Urology* **57**, 67–81 (2001).
43. Shahid, M. *et al*. Alpha-oxoglutarate inhibits the proliferation of immortalized normal bladder epithelial cells via an epigenetic switch involving ARID1A. *Scientific reports* **8**, 4505, https://doi.org/10.1038/s41598-018-22771-2 (2018).

Acknowledgements

The authors acknowledge support from National Institutes of Health (1U01DK103260, 1R01DK100974, U24 DK097154, NIH NCATS UCLA CTSI UL1TR000124), Department of Defense (W81XWH-15-1-0415), Centers for Disease Controls and Prevention (1U01DP006079), IMAGINE NO IC Research Grant, the Steven Spielberg Discovery Fund in Prostate Cancer Research Career Development Award, the U.S.-Egypt Science and Technology Development Fund by the National Academies of Sciences, Engineering, and Medicine (to J.K.). J.K. is former recipient of Interstitial Cystitis Association Pilot Grant, a Fishbein Family IC Research Grant, New York Academy of Medicine, and Boston Children's Hospital Faculty Development. The funders had no role in the design, data collection and analysis, decision to publish or preparation of the manuscript.

Author Contributions

J.K. designed the study, led obtaining funding, and overviewed the literature analysis and drafting the manuscript. S.F., A.Y. and M.S. performed metabolomics analysis and sample preparation. S.F. and O.F. performed data analysis and visualize the data. O.F., S.F., J.A. and K.E. helped writing the manuscript. All authors read and approved the final manuscript.

Additional Information

Supplementary information accompanies this paper at https://doi.org/10.1038/s41598-018-29592-3.

Competing Interests: The authors declare no competing interests.

Publisher's note: Springer Nature remains neutral with regard to jurisdictional claims in published maps and institutional affiliations.

Open Access This article is licensed under a Creative Commons Attribution 4.0 International License, which permits use, sharing, adaptation, distribution and reproduction in any medium or format, as long as you give appropriate credit to the original author(s) and the source, provide a link to the Creative Commons license, and indicate if changes were made. The images or other third party material in this article are included in the article's Creative Commons license, unless indicated otherwise in a credit line to the material. If material is not included in the article's Creative Commons license and your intended use is not permitted by statutory regulation or exceeds the permitted use, you will need to obtain permission directly from the copyright holder. To view a copy of this license, visit http://creativecommons.org/licenses/by/4.0/.

© The Author(s) 2018

Cancer Letters 437 (2018) 1–12

Contents lists available at ScienceDirect

Cancer Letters

journal homepage: www.elsevier.com/locate/canlet

Original Articles

Integrated proteomic and phosphoproteomic analyses of cisplatin-sensitive and resistant bladder cancer cells reveal CDK2 network as a key therapeutic target

Jae Hun Jung[a,1], Sungyong You[b,e,1], Jae Won Oh[a], Junhee Yoon[b], Austin Yeon[b], Muhammad Shahid[b], Eunho Cho[b,c], Vikram Sairam[b,c], Taeeun D. Park[b,d], Kwang Pyo Kim[a,**], Jayoung Kim[b,c,e,*]

[a] Department of Applied Chemistry, College of Applied Science, Kyung Hee University, Yongin, Republic of Korea
[b] Department of Surgery and Biomedical Sciences, Cedars-Sinai Medical Center, Los Angeles, CA, USA
[c] University of California, Los Angeles, CA, USA
[d] University of California, Berkeley, CA, USA
[e] Samuel Oschin Comprehensive Cancer Institute, Cedars-Sinai Medical Center, Los Angeles, CA, USA

ARTICLE INFO

Keywords:
Global proteome
Phosphoproteomics
Cisplatin resistance
Bladder cancer
Biological network
Competing interests

ABSTRACT

Background: Cisplatin-based chemotherapy is currently part of the standard of care for bladder cancer (BC). Unfortunately, some patients respond poorly to chemotherapy and have acquired or developed resistance. The molecular mechanisms underlying this resistance remain unclear. Here, we introduce a multidimensional proteomic analysis of a cisplatin-resistant BC model that provides different levels of protein information, including that of the global proteome and phosphoproteome.

Methods: To characterize the global proteome and phosphoproteome in cisplatin-resistant BC cells, liquid chromatography-mass spectrometry/mass spectrometry experiments combined with comprehensive bioinformatics analysis were performed. Perturbed expression and phosphorylation levels of key kinases associated with cisplatin resistance were further studied using various cell biology assays, including western blot analysis.

Results: Analyses of protein expression and phosphorylation identified significantly altered proteins, which were also EGF-dependent and independent. This suggests that protein phosphorylation plays a significant role in cisplatin-resistant BC. Additional network analysis of significantly altered proteins revealed CDK2, CHEK1, and ERBB2 as central regulators mediating cisplatin resistance. In addition to this, we identified the CDK2 network, which consists of CDK2 and its 5 substrates, as being significantly associated with poor survival after cisplatin chemotherapy.

Conclusions: Collectively, these findings potentially provide a novel way of classifying higher-risk patients and may guide future research in developing therapeutic targets.

1. Introduction

Bladder cancer (BC) is a common malignancy of the urinary tract. Resection of the tumor (when possible) and cisplatin-based chemotherapy is the present standard of care. However, resistance to chemotherapy has been a clinical challenge for long-term remission [11]. Chemo-resistance can rapidly develop and a majority of patients ultimately experience disease progression and a poor prognosis [4]. The failure of conventional treatment following remission typically results in a < 15% chance of 5-year survival [10,18,39]. Therefore, therapeutic strategies that can re-sensitize tumors to chemotherapy would significantly benefit BC patient care. Additionally, a molecular signature panel capable of predicting cisplatin resistance in BC would greatly improve prognostic and clinical outcomes for high-risk patients. Unfortunately, despite multiple independent studies aimed at identifying the subset of patients who will develop chemo-resistance, research on predictive biomarker(s) is still in its infancy [3,36,38].

Overexpression, amplification, or mutations of EGFR family

* Corresponding author. Department of Surgery and Biomedical Sciences, Cedars-Sinai Medical Center, 8700 Beverly Blvd., Los Angeles, CA, 90048, USA.
** Corresponding author. Department of Applied Chemistry, Kyung Hee University, Yongin, Gyeonggi-do, 463-707, Republic of Korea.
E-mail addresses: kimkp@khu.ac.kr (K.P. Kim), Jayoung.Kim@cshs.org (J. Kim).
[1] These authors equally contributed to this manuscript.

https://doi.org/10.1016/j.canlet.2018.08.014
Received 20 April 2018; Received in revised form 30 July 2018; Accepted 10 August 2018
0304-3835/ © 2018 Elsevier B.V. All rights reserved.

members are often observed in BC. This suggests that the proteins involved in the epidermal growth factor receptor (EGFR) signaling pathways may play important roles in the carcinogenesis and maintenance of BC, making them relevant therapeutic targets. Our group had previously established cisplatin-sensitive (T24S) and resistant (T24R) T24 human BC cell lines [21]. The viability of the resistant cells was reduced by inhibition of EGFR kinase activity [21]. Either expression or phosphorylation of the proteins involved in signaling pathways can contribute to alterations of pathway activations. Thus, analyses of the global proteome and phosphoproteome would allow for direct interrogation of the altered activation of signaling pathways and provide comprehensive profiles regarding protein quantification and phosphorylation [6,8,41]. A network model describing such protein alterations in cancer cells could provide novel insights into the molecular mechanisms of resistance and contribute to identifying new biomarkers or therapeutic targets.

To obtain such a systems-level insight into cisplatin-resistance, we used high-resolution mass spectrometry and investigated the temporal changes in protein abundance and phosphorylation in T24S and T24R cells after EGF stimulation. Our comprehensive proteomic analysis identified proteins involved in EGFR signaling that were perturbed in cisplatin-resistant cells. This included substrates of EGF receptors and downstream kinases. Further network analysis of our proteomic and phosphoproteomic data identified downstream kinases of EGFR signaling pathways.

2. Materials and methods

2.1. Reagents

Antibodies against CDK2 (1:1000, Novus Biologicals; Littleton, CO), and β-actin (1:5000, Sigma) were used for this study. The following antibodies: P-CDK2 (Thr160) (2561, 1:1000), P-ERBB2 (Tyr1196) (6942, 1:1500), P-CHEK1 (Ser345) (2348, 1:750), phospho-mTOR (Ser2448) (5536; 1:1000), p-Rb (Ser807/811) (8516, 1:1000), p-tyrosine (P-Tyr-100) (9411, 1:2000), and HRP-conjugated secondary antibodies (7074, 1:1000; 7076, 1:1000) were obtained from Cell Signaling Technologies.

2.2. Cell culture

T24, J82, and RT4 BC cells were obtained and cultured, according to instructions provided by the American Type Culture Collection (ATCC) (Manassas, VA). Media was supplemented with 10% fetal bovine serum, 2% glutamine, and 1% antibiotics (Invitrogen, Carlsbad, CA). Cells were maintained in a humidified incubator with 5% CO_2 at 37 °C [21].

2.3. Protein extraction and quantification

The cell pellets were kept at −80 °C for 30 min. Afterwards, the cells were lysed with RIPA buffer [50 mM Tris-HCl, 150 mM NaCl, 0.1% (w/v) sodium dodecyl sulfate (SDS), 1% (v/v) NP-40, 1 mM PMSF, 1X protease inhibitor cocktail, 1X phosphatase inhibitor cocktail, PhoSTOP] and left on ice for 15 min while undergoing sonication. The cellular lysates were centrifuged at 14,000 g for 15 min at 4 °C. The supernatant was collected and 500 μg of protein for each cell line was digested using the filter aided sample preparation (FASP) method [43].

2.4. Filter aided sample preparation (FASP)

Proteins were reduced in a sodium dodecyl sulfate (SDS)-lysis buffer (4% (w/v) SDS; 0.1 M Tris/HCl pH 7.6; 0.1 M DTT) at 37 °C for 45 min. The proteins were then boiled at 95 °C for 10 min and then sonicated for 10 min. The solution was transferred to a 30 k membrane filter (Microcon devices, YM-30, Millipore, MA) and centrifuged at 14,000 g and 20 °C for 60 min. The concentrates were diluted in their filters with 0.2 ml of UA solution (8 M urea in 0.1 M Tris/HCl, pH 8.5) and centrifuged at 14,000 g for 30 min to remove the remaining SDS (×3). After that, the concentrates were mixed with 0.1 ml of 50 mM indole-3-acetic acid (IAA) in UA solution and incubated in darkness at room temperature for 25 min. Following centrifugation, the resulting product was diluted with 0.2 ml of UA solution and concentrated again. This step was repeated 3 times. Next, the concentrates were washed with 0.2 ml of 100 mM triethyl ammonium bicarbonate (TEAB) and centrifuged at 14,000 g for 30 min (×3). Subsequently, 10 μg of trypsin prepared in 0.1 ml of 100 mM TEAB (with the enzyme to protein ratio of 1:50) was added to the filter and the samples were incubated at 37 °C overnight. The second digestion was done using trypsin with an enzyme to protein ratio of 1:100 for 6 h. Peptides were collected by centrifuging the filter units at 14,000 g for 30 min. TEAB (75 μL, 100 mM) was added to the filter and centrifuged at 14,000 g for 20 min (×3). Finally, the peptide solutions were dried in a speed vacuum concentrator and stored at −80 °C.

2.5. TMT labeling of peptide

Peptides were labeled with TMT™ Isobaric Mass Tagging Reagent, according to the manufacturer's instructions (ThermoScientific, Foster City, CA). For each sample of 500 μg peptides, 250 μl of 200 mM TEAB were added. TMT reagents were resuspended in anhydrous acetonitrile and then added to each sample (126: Cisplatin sensitive/EGF 0 min, 127: Cisplatin sensitive/EGF 10 min, 128: Cisplatin sensitive/EGF 30 min, 129: Cisplatin resistant/EGF 0 min, 130: Cisplatin resistant/EGF 10 min, 131: Cisplatin resistant/EGF 30 min). After 1 h, the reaction was quenched with 5% hydroxylamine. The chemically tagged samples were pooled into one tube and concentrated via speed vacuum centrifugation. The labeled samples were then mid-pH fractionated.

2.6. Mid-pH reversed phase liquid chromatography (RPLC) fractionation

Mid-pH RPLC fractionation was performed to separate peptides based on their hydrophobicity. An Accucore™ 150 C18 LC column (150 × 2.1 mm, 4 μm) was used for fractionation with mid-pH buffers A and B; (A) the mobile phase was 10 mM TEAB in water (pH 7.5) and (B) the mobile phase was 10 mM TEAB in 90% CAN (pH 7.5). The samples were then divided into 15 smaller samples using the Agilent 1260 Series HPLC System (Agilent Technologies, Santa Clara, CA). The resultant gradient was 0–10 min, 5% B; 10–70 min, 5–35% B; 70–80 min, 70% B; 80–105 min, 5% B. The separated peptides were collected and dried in a speed vacuum. Each fraction was vacuum dried and stored at −80 °C until liquid chromatography-mass spectrometry/mass spectrometry (LC-MS/MS) experiments.

2.7. Phosphopeptide enrichment using immobilized metal affinity chromatography (IMAC)

IMAC beads were prepared from Ni-NTA magnetic agarose beads. Ni-NTA beads (500 ml) were washed (3×) with deionized water (DIW). The beads were then reacted with 100 mM of EDTA (pH 8.0) for 30 min with end-over-end rotation to remove nickel ions. The reacted EDTA solution was eliminated and the beads were washed 3× with DIW. The NTA beads were treated with 10 mM of aqueous $FeCl_3$ solution for 30 min with end-over-end rotation. Iron-chelated IMAC beads were washed (×3) with DIW. IMAC beads were aliquoted into 10 microcentrifuge tubes and each bead was washed with 400 μl of 80% acetonitrile (CAN)/0.1% trifluoroacetic acid (TFA). In total, 10 fractions, which were obtained by combining some fractions from 15 (#1 and #11, #2 and #12, #3 and #13, #4 and #14, #5 and #15, #6, #7, #8, #9, #10), were used to enrich for phosphopeptides. The 10 fractionated peptide samples were suspended in 500 μl of 80% ACN/0.1% TFA and were reacted with IMAC beads again for 30 min with end-over-end

rotation. Phosphopeptides were eluted using 125 µl of 1:1 ACN/2.5% ammonia in 2 mM phosphate buffer (pH 10) after incubating for 1.5 min. All phosphopeptides were acidified immediately with 10% TFA. The collected phosphopeptides were dried in a speed vacuum and purified in C18 spin columns for LC-MS/MS analysis.

2.8. LC-MS/MS analysis

All peptide samples were separated on an ultra performance liquid chromatography (UPLC) system that was equipped with analytical columns (75 µm × 50 cm, C18, 3 µm, 100 Å) and trap columns (75 µm × 2 cm, C18, 3 µm, 100 Å). The temperature of the analytical columns was set to 60 °C. The solvents A and B were 0.1% formic acid in water and 0.1% formic acid in acetonitrile, respectively. A gradient made after 180 min (1–40% solvent B for 160 min, 40–80% solvent B for 5 min, 80% solvent B for 10 min, and 1% solvent B for 5 min) was used for global proteome profiling analysis. A gradient made after 134 min (5–40% solvent B for 120 min, 40–80% solvent B for 2 min, 80% solvent B for 10 min, and 1% solvent B for 2 min) was used for phosphoproteome analysis. The flow rate of all experiments was set to 250 nl/min. The eluted peptides from LC were mass-analyzed on a Q Exactive Orbitrap Mass Spectrometer (ThermoScientific, Bremen, Germany). The electric potential of electrospray ionization was kept at 2.0 kV and the temperature of desolvation capillary was set to 250 °C. Full MS scans were acquired for a mass range of 400–2000 Th at a resolution of 70,000. The 10 most abundant ions, with charges of 2, 3, 4, and 5, were dynamically selected with an isolation width of 2.0 Th and fragmented with an exclusion duration of 30 s with a normalized collision energy (NCE) of 30 for higher energy collisional dissociation (HCD). The LC-MS/MS scans were acquired at a resolution of 17,500 with a fixed initial m/z of 100 Th. Maximum ion injection times were 120 ms for both the full MS and LC-MS/MS scans. The automated gain control (AGC) target value was set to 1.0×10^6 for both the MS and LC-MS/MS scans.

2.9. Identification of peptides and proteins

MS and MS/MS spectra were converted from Thermo.RAW files into the mzML format using Msconvert (ProteoWizard) and searched with MSGF + against the Universal Protein Resource Human Database (Uniprot released 2016_02, 20,198 entries, http://www.uniprot.org/). Search parameters were as follows: 20 ppm tolerance for precursor ion mass error and fixed modification for carbamidomethylation (+57.0214 Da) to cysteine, variable modification for methionine oxidation (+15.994915 Da), phosphorylation (+79.966330 Da) to serine, threonine, tyrosine, TMT (+229.162932) to N-termini and lysine and acetylation (+42.010564) to N-terminal of protein. The peptide identification stringency was set to a maximum of 1% peptide-to-spectrum matches (PSMs) FDR in the target-decoy way. The intensities of all TMT-6 plex reporter ions were extracted using the MAGIC software [27]. When multiple phosphopeptides were assigned to a phosphoprotein, the phosphopeptide that had the largest comparative fold change [44] was used as the representative fold change of the phosphoprotein. The mass spectrometry proteomics data has been deposited to the PRIDE [17] repository with the dataset identifier, PXD005308.

2.10. Identification of proteins with altered expression or phosphorylation

TMT intensities of the peptides were normalized using the quantile normalization method [5]. Protein abundance was estimated by summing all TMT reporter ion intensities of different fully tryptic peptides belonging to the same protein groups. Of these qualified proteins, those with more than 2 non-redundant peptides were chosen for the next analyses. We then identified differentially expressed proteins (DEPs) using an integrative statistical method, as reported previously [14]. Briefly, for each protein, the t-test and $\log_2$-median-ratio test were applied to its abundances for all 3 replicates. An empirical null distribution was estimated by applying the Gaussian Kernel Density Estimation method to $\log_2$ fold-changes that were obtained after performing all possible permutations on all the TMT labels [1]. Using the distributions for each protein, we computed the adjusted p-values for the two tests. We then combined the p-values to compute the overall p-value using Stouffer's method. Finally, we computed the false discovery rate (FDR) for the overall p-values using Storey's method. We selected DEPs that had a combined FDR < 0.05, fold change ≥ 1.5, and were detected as proteins in at least 2 of the 3 replicates.

For the phosphoproteome, we applied differential phosphorylation analysis at the peptide level to identify significantly altered phosphopeptides between cell types or time points. For this, the same normalization and statistical testing methods described above were used. Phosphopeptides were selected and considered as significantly altered if they had a FDR < 0.05 and fold-change ≥ 1.5. Finally, differentially phosphorylated proteins (DPPs) were identified as proteins that contained significantly altered phosphopeptides that were uniquely assigned to the protein. The Phospho-UMC filter was used to localize the site of phosphorylation. This simple method uses unique mass class (UMC) information to differentiate phosphopeptides with different phosphorylation sites [28]. Briefly, MS features within 10 ppm, but emerging over a period of time during their LC elution, were identified and grouped into an UMC. Then, the links between the LC-MS/MS data and the UMCs were made. The resultant LC-MS/MS data were subjected to a database search using the MSGF + engine and peptide identifications within 1% FDR were used.

To explore the cellular processes and subcellular localizations represented by the DEPs and DPPs, functional enrichment analyses of gene ontology biological processes (GOBPs), gene ontology cellular components (GOCCs), and Kyoto Encyclopedia of Genes and Genomes (KEGG) pathways [19] were performed using the DAVID software [13]. The GOBPs, GOCCs, and KEGG pathways represented by DEPs and DPPs were identified as those with $p < 0.05$.

2.11. Reconstruction of cellular network models and identification of key kinases

To identify key kinases regulating DPPs, data for more than 12,000 kinase-substrate interactions (KSI) was collected from the SIGNOR database [34]. For each kinase, the number of targets in the DEPs was calculated using the KSI data. The p-value for the number of substrates was then computed based on a hypergeometric distribution from Fisher's exact test. Of the kinases with $p < 0.05$, those belonging to DEPs or DPPs were selected as key kinases. We estimated an empirical distribution of network density by randomly sampling the same number of proteins in each kinase group with KSIs 100,000 times. Significance levels of the kinases were computed using the right-sided test.

2.12. Western blot analysis

After EGF treatment (10 ng/ml), cells were quickly harvested, flash frozen in liquid nitrogen, and stored at −80 °C. Total protein was extracted using a lysis buffer [1% Nonidet P-40, 50 mM Tris (pH 7.4), 10 mM NaCl, 1 mM NaF, 5 mM $MgCl_2$, 0.1 mM EDTA, 1 mM phenylmethylsulfonyl fluoride] with a complete protease inhibitor cocktail (Roche Diagnostics GmbH, Mannheim, Germany). The solution was centrifuged at 12,500 × g for 15 min. After measuring for protein concentration, 25 µg of protein per line were subjected to SDS-PAGE gel running and then transferred onto nitrocellulose membranes for western blot analysis. After blocking for 1 h with 10% bovine serum albumin (BSA) in phosphate buffered saline with Tween 20 (PBST), the membranes were incubated with specific antibodies in PBST, overnight. β-actin was used as the loading control. The blots were visualized using enhanced chemiluminescence.

2.13. Gene silencing and cell viability assay

For transient cell transfections of siRNA oligonucleotides, T24R cells were grown to 80% confluence in 6-well culture plates and transfected with siRNAs targeting CDK2, CHEK1, ERBB2, and control (ThermoScientific) using Lipofectamine 2000 (Invitrogen), according to the manufacturer's instructions. Cisplatin-resistant BC cells (T24R, J82R, and RT4R) were incubated with cisplatin and/or CDK2 inhibitor for 72 h. Post-treatment cell survival was determined by measuring cell viability using MTS reagents (Promega Corporation, Madison, WI), according to the provided protocols.

2.14. Tissue micro-array (TMA) construction

Patient consent and IRB approval was given prior to tissue collection, and TMA slides were constructed from a cohort of 42 BC patients at Cedars-Sinai Medical Center (IRB #: Pro00044997). Detailed information was not available except that a majority of the patients were male and over 60 years old. Although tumors were pathologically graded prior to tissue collection, the annotations and image analysis were blindly conducted by two trained scientists, including one certified pathologist. Tumor and normal bladder tissue samples were received from all patients. Circular TMA cores 1 mm in diameter were constructed for all tissue samples onto glass slides. In total, there were 82 TMA cores per slide.

2.15. Immunohistochemistry (IHC) analysis

Antibodies against CDK2 (Novus Biologicals; Littleton, CO) were incubated on their respective slides for 32 min. Following antibody incubation, antigen retrieval was done at a high pH for 64 min. Ultraview DAB Detection (Ventana Medical Systems; Tucson, AZ) was used for nuclear and cytoplasmic counterstaining. These slides were scanned and uploaded onto the Leica Biosystems cloud drive.

2.16. Digitalized image analysis

Following staining with both the antibodies of interest and pan-CK, the slides were scanned using the Aperio Turbo Scanscope AT (Leica Biosystems; Buffalo Grove, IL). High resolution images of each slide were uploaded onto the Leica Biosystems cloud drive for annotations and analysis.

Annotation and analysis of slides were done using the Leica Tissue Image Analysis (IA) 2.0 software program (Copyright, 2012 by SlidePath Ltd.). Stromal and structural tissues were not included in the annotations. Although these structures may provide additional insight, the focus of the experiment was based on tumor epithelium only. Each annotated core had a minimum threshold of 100,000 cells to be analyzed. Following annotations, the “Measure Stained Cells Algorithm” option in the Leica Tissue IA software was used. For each antibody slide, color definition preferences were defined and algorithm input parameters were optimized based on several cores. These individualized parameters were used to analyze the annotated regions on each slide.

For the color definition, haematoxylin was set as the nuclear counter stain, and DAB was set as the nuclear, cytoplasmic, and membrane marker. Parameters in the program were based on a numbered greyscale between 0 and 255, with 0 being the minimum intensity (black) and 255 being the maximum (white). The max threshold in our analysis was set to 220, with 180 being the threshold for positive or negative staining. The max nuclear window size radius was set to 37 (default) and the nuclear area threshold was set to be 0–1500 mm^2; any nuclei or cells out of these parameters were eliminated from analysis. The minimum percent of stained area in the nucleus to be considered as positive was set to 20%. The threshold for positive identification of cytoplasmic staining was set at a higher threshold for some of the antibodies due to differences in background and staining. The maximum threshold range was set for cytoplasmic staining detection between 220 and 240, with a minimum percent of stained area set to 70%.

After analysis, data regarding the nuclear h-score, % of positive nuclei, % of positive nuclear area in tissue, cytoplasmic h-score, and % positive cytoplasm of cells was collected and used for comparative graphing. These scores were chosen to represent the level and intensity of nuclear and cytoplasmic staining in the epithelial cells. Test runs of the analysis were conducted with a pathologist to assure that the program correctly identified and graded the nuclear and cytoplasmic components of epithelial cells.

2.17. Comparative graphing and statistical analysis

R Studio was used for analyzing and graphing the data. Using the ggplot2 package, violin plots were constructed to demonstrate the differences in nuclear h-score, % of positive nuclei, % of positive nuclear area in tissue, cytoplasmic h-score, and % of cells with positive cytoplasmic staining between tumor and normal adjacent to tumor (NAT) cores. Statistical analysis was done via a two-sided Wilcoxon rank-sum test. Statistical significance was defined as $p < 0.05$.

3. Results

3.1. Global proteome and phosphoproteome in cisplatin-resistant BC cells

We sought to understand the molecular mechanisms of cisplatin resistance using a paired cell culture system consisting of T24S and T24R cells. Alterations of EGFR signaling pathways have been frequently observed and reported in various cancer types. It has also been considered a critical module associated with resistance mechanisms against several kinase inhibitors and other drugs, including cisplatin [9,12,15,29]. Based on this knowledge, we applied a multiplexed TMT and LC/LC-MS/MS approach to samples and replicates harvested after 0 min, 10 min, and 30 min of EGF stimulation (10 ng/ml) (Fig. 1A). After a FASP peptide digestion, each conditioned peptide was respectively labeled with 6-plex TMT reagents. For mid-pH fractionation, we used TEAB as a buffer solvent. Several benefits of using TEAB include compatibility with TMT labeling, high volatility (allowing us to skip the desalting step), and low harmful impact on separation columns. After fractionation, 5% of the peptides from each of the 15 fractions were used for global proteome analysis. The remaining 95% of the peptides were subjected to an IMAC enrichment experiment and analyzed using an orbitrap-based high resolution/accurate-mass mass spectrometer (Fig. 1B). This serial enrichment strategy was done to simultaneously observe changes in either global or phosphopeptides from the same peptide pool [32]. We then searched for acquired mass spectra using MS/MS automated selected ion chromatography (MASIC) in the Uniprot Human Protein Database (2016) with MSGF + TMT reporter ion extraction [20] (see methods). From the 3 biological replicates of the global proteome, we identified an average of 48,044 non-redundant peptides (9405 protein groups) (Supplementary Table 1 and Fig. 1C). We also identified an average of 13,980 phosphopeptides and 16,700 phosphosites (Supplementary Table 2) belonging to 3939 protein groups (Supplementary Table 3 and Fig. 1D).

3.2. Altered proteins in cisplatin-resistant BC cells

To identify proteins with altered expression and phosphorylation between T24R and T24S cells before any EGF stimulation, we performed separate statistical hypothesis testing for the global proteome and phosphoproteome. From the global proteome, we identified 223 DEPs between T24R and T24S cells (Fig. 2A). When analyzing the phosphoproteome, we identified 899 differentially phosphorylated peptides belonging to 501 DPPs (Fig. 2B). Comparing the list of DEPs and DPPs (Supplementary Table 4), we observed that 33 proteins

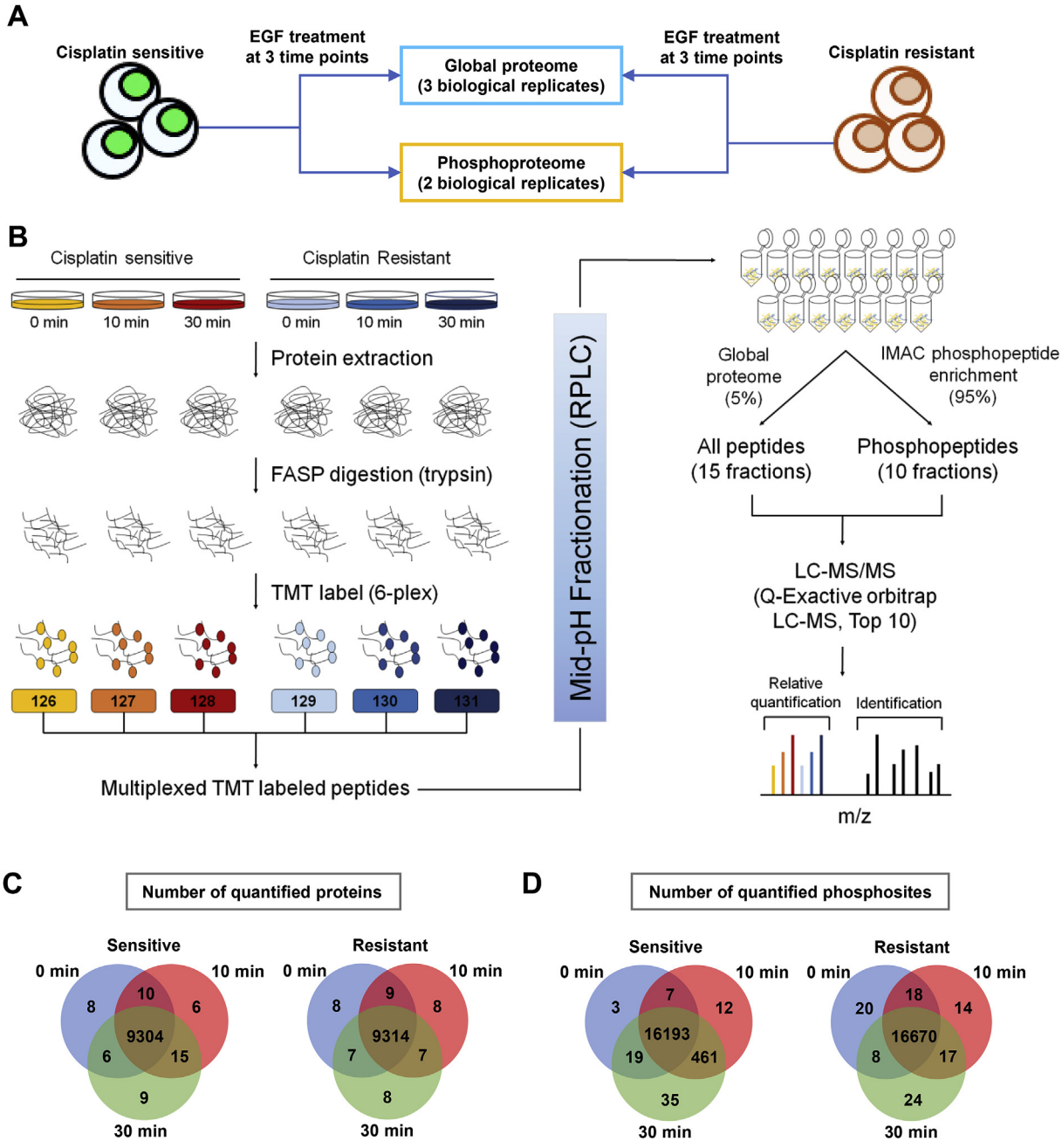

Fig. 1. Quantitative measuring of the proteome and phosphoproteome using TMT labeling. A. Experimental design to study the effects of EGF stimulation across 3 time points. A total of 3 and 2 biological replicates from T24S and T24R cells were analyzed for their global proteome and phosphoproteome, respectively. **B.** Overall experimental workflow for multiplex TMT labeling and comprehensive profiling of the global proteome and phosphoproteome. Both T24S and T24R cells were treated with EGF (0, 10, or 30 min). Proteins were extracted using RIPA buffer and peptides were FASP digested with trypsin. Peptide samples were derived at 6 different time points, labeled using TMT reagents, mixed, and separated using mid-pH reverse phase chromatography. Fractions were combined in a non-contiguous way into 15 fractions for proteome analysis (5% of total proteins) and 10 fractions for phosphoproteome analysis (95% of total proteins). All peptides and phosphopeptides were analyzed on a Q Exactive Mass Spectrometer. Protein identification and quantification was achieved using the MSGF + search engine and MASIC (reporter ion intensity extractor). **C** and **D**. Numbers of identified (**C**) proteins or (**D**) phosphopeptides from T24S and T24R cells. Venn diagrams depict the number of common and uniquely identified proteins or phosphopeptides in T24S and T24R cells after 0, 10 and 30 min of EGF stimulation.

exhibited a positive correlation (Spearman's rho = 0.50; $P < 0.001$), with significant changes at both the phosphorylation and expression levels (Fig. 2C). Functional enrichment analysis, using DAVID [13], showed that DEPs and DPPs were enriched for common and distinct cellular processes (Fig. 2D). DEPs exhibited predominant enrichment for cell adhesion and migration-related processes, including extracellular matrix organization and leukocyte migration. DPPs, on the other hand, displayed direct association with the EGFR signaling pathway and downstream processes, such as small GTPase signal transduction, mitotic cell cycle, and chromatin organization. Both DEPs and DPPs were enriched for cell survival and proliferation-related processes. These results suggest that DPPs in cisplatin-resistant BC cells represent the activation of EGFR signaling pathways or EGF-driven resistance mechanisms.

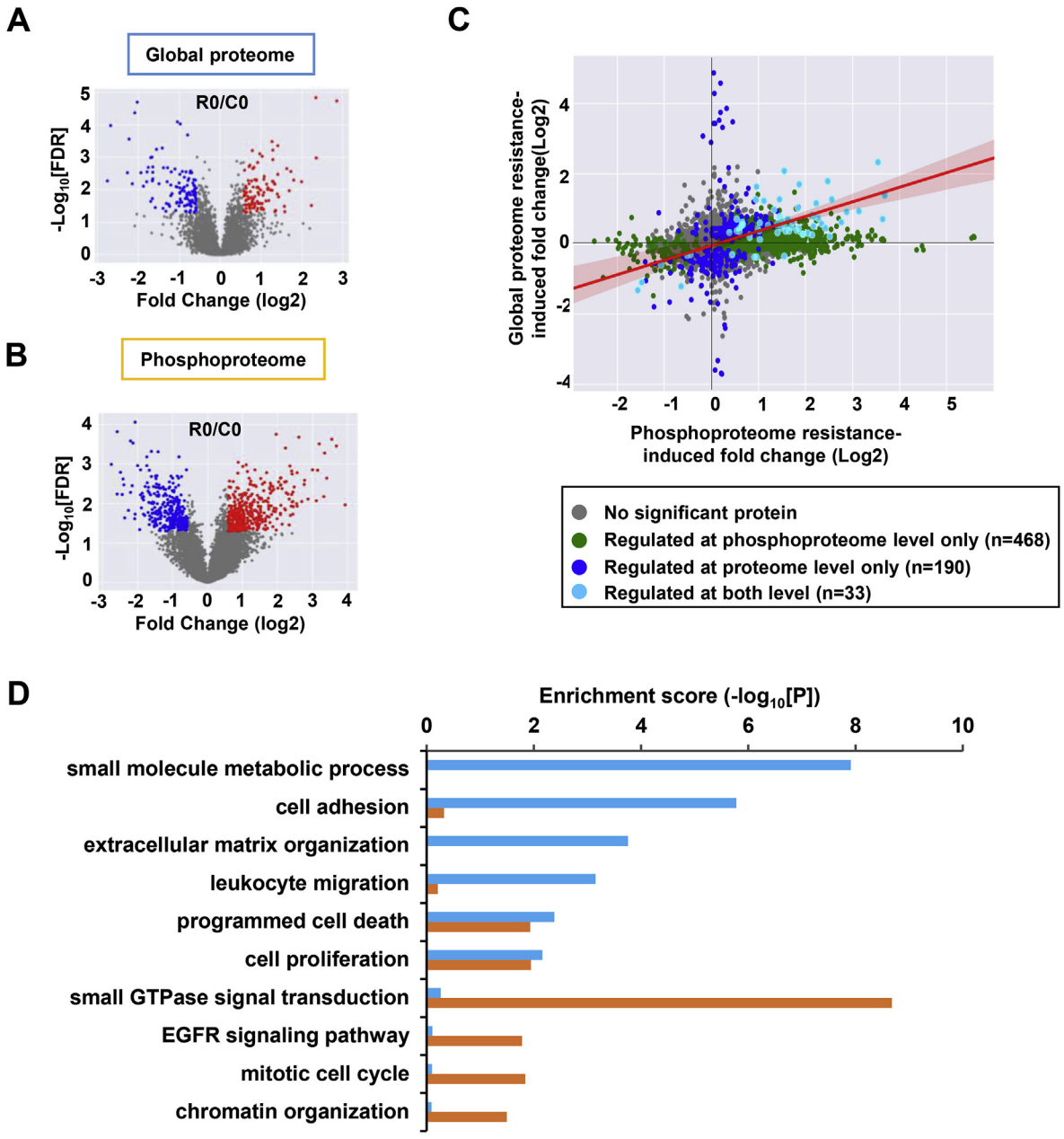

Fig. 2. Altered proteins in the global proteome and phosphoproteome between T24R and T24S cells. A and **B**. Volcano plots display differentially expressed (**A**) proteins or (**B**) differentially phosphorylated peptides. Red and blue dots represent upregulated and downregulated proteins or peptides, respectively. **C**. Protein expression and phosphorylation levels were compared and represented in the scatterplot. Proteins and phosphorylation sites were considered to be perturbed by cisplatin resistance based on the integrative hypothesis testing method (FDR $<$ 0.05). Comparison between biological replicates of MS-based quantitative proteomic and phosphoproteomic experiments of T24R and T24S cells. Each dot represents one protein. **D**. Enrichment analysis using DAVID software showed that differentially expressed proteins (cyan) and differentially phosphorylated peptides (purple) were enriched for various cellular functions. (For interpretation of the references to color in this figure legend, the reader is referred to the Web version of this article.)

3.3. Altered proteins belonging to the EGFR signaling pathway are involved in cisplatin resistance

Using our global proteome and phosphoproteome data, we next performed differential analyses of EGF stimulation in T24R and T24S cells. For the global proteome in both T24R and T24S cells, only the tails of the density distribution in the $\log_2$ fold change increased with EGF stimulation (Fig. 3A and Supplementary Fig. 1A). In contrast, the global median of the phosphoproteome in T24S cells increased in abundance when stimulated with EGF (Fig. 3B). The largest changes in EGF-induced phosphorylation were observed in T24S cells, which exhibited phosphosite changes of 4% (656) and 5.3% (887) after 10 min and 30 min of EGF stimulation, respectively. T24R cells were altered less, with the percentage of altered phosphorylation sites being 1.1% and 0.7% after 10 min and 30 min, respectively (Supplementary Fig. 1B). This suggested that the effects of EGF stimulation impacts T24S cells more. Volcano plots for differentially phosphorylated proteins were consistent with the density plots shown in Fig. 3B (Fig. 3C).

We next sought to select altered proteins (APs) that were associated with cisplatin resistance and were part of the EGFR signaling pathway. Both DEPs and DPPs were considered as APs because either protein expression or phosphorylation can reflect alterations in signaling pathways. A total of 749 APs (454 APs at 10 min and 547 APs at 30 min) were identified in T24S cells (Supplementary Table 5). Of these

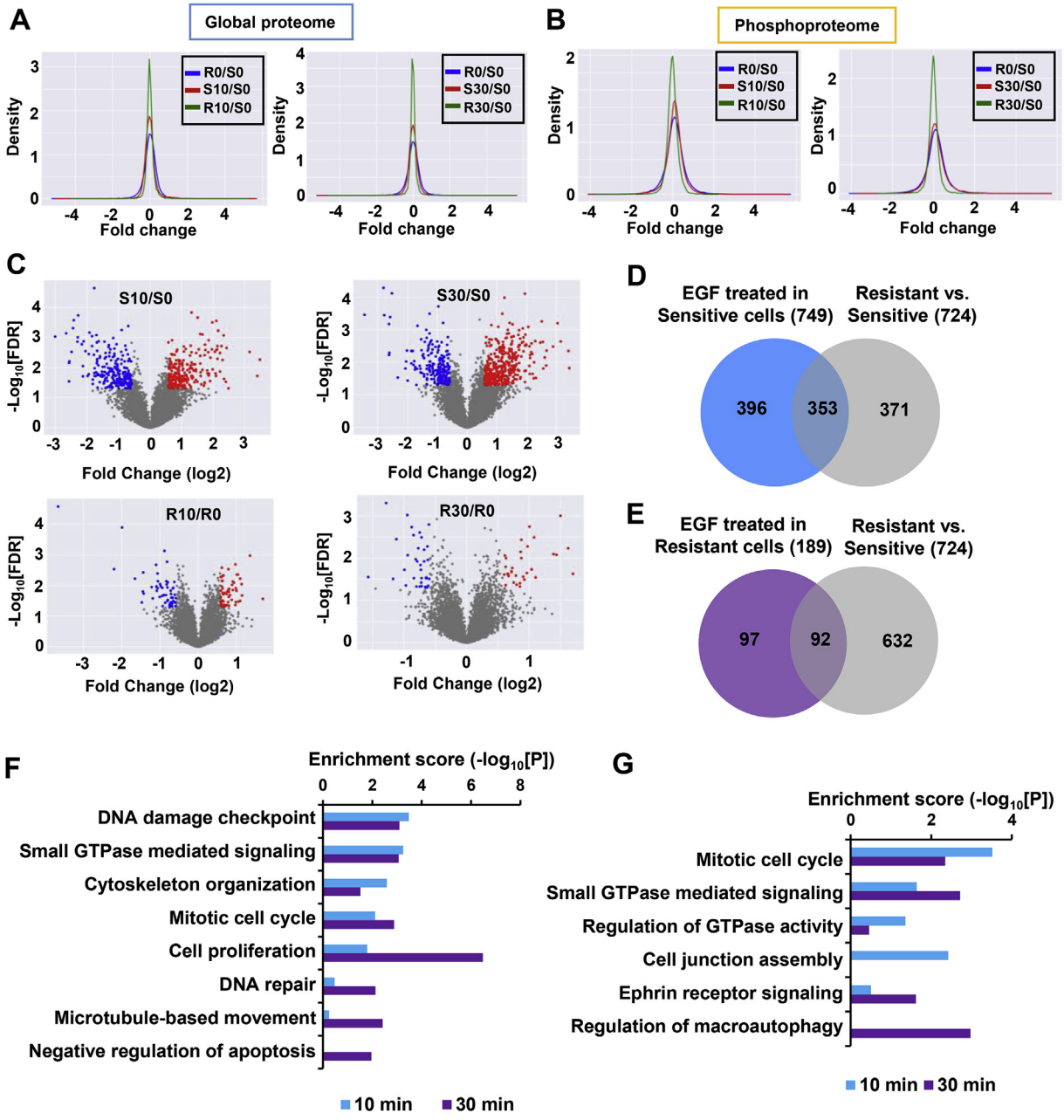

Fig. 3. Distinct protein alteration patterns in T24R and T24S cells after EGF stimulation. A and B. Density plots are shown for the $\log_2$fold changes of the (**A**) global proteome and (**B**) phosphoproteome for T24R and T24S cells after 10 min and 30 min of EGF treatment. Only phosphopeptides or proteins quantified in at least two samples were plotted. Log_2 fold changes in T24S cells at 10 min (S10) vs. 0 min (S0) of EGF treatment, T24S cells at 30 min (S30) vs. 0 min (S0) of EGF treatment, T24R cells at 10 min (R10) vs. 0 min (R0) of EGF treatment, T24R cells at 30 min (R30) vs. 0 min (R0) of EGF treatment, and R0 vs. S0 are displayed. **C**. Volcano plots display differentially expressed phosphopeptides in T24R and T24S cells after 10 min and 30 min of EGF treatment. Red and blue dots indicate up- and down-regulated phosphopeptides, respectively. Only those quantified in at least two samples were plotted. **D and E**. Number of phosphoproteins associated with cisplatin resistance mechanisms that are involved in EGFR signaling in (**D**) T24S and (**E**) T24R cells. Venn diagram depicts the overlapping altered phosphoproteins in (**D**) T24S or (**E**) T24R cells with or without EGF treatment. **F and G.** Enriched cellular functions of the overlapping proteins after 10 min and 30 min of EGF treatment in (**F**) T24S and (**G**) T24R cells. (For interpretation of the references to color in this figure legend, the reader is referred to the Web version of this article.)

749 APs, 353 overlapped with the 724 APs identified from T24S vs. T24R cells with no EGF treatment. Interestingly, 49% (353 out of 724) of the APs responsible for cisplatin resistance were regulated by EGF stimulation (Fig. 3D). This suggested that a large proportion of APs are involved in downstream EGFR signaling and are likely to also be associated with cisplatin resistance. In contrast, T24R cells exhibited a relatively smaller number of APs (n = 92) that overlapped with those found between T24R and T24S cells (Fig. 3E). Functional enrichment analysis of the 353 APs (Supplementary Table 6) in T24S cells revealed known associations of cisplatin resistance with DNA damage, repair, and cell cycle regulation (Fig. 3F). This was replicated with the 92 APs (Supplementary Table 7) found in T24R cells (Fig. 3G). The results were consistent with previous reports demonstrating inherent and persistent downstream EGFR signaling in resistant cells [21].

3.4. Several key kinases involved in cisplatin resistance were identified

Given this total list of 374 APs, 353 from T24S and 92 from T24R (with overlap), we next aimed to identify the key regulators of the observed phosphorylation profiles linked to cisplatin resistance. To this

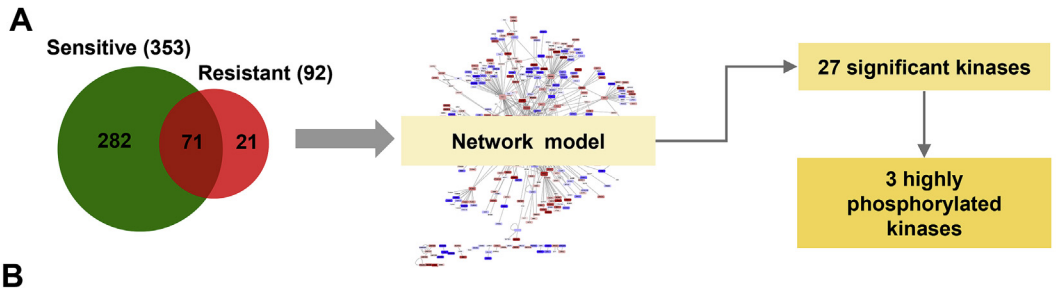

B

Protein Symbol	# of targets in Up-regulated DPP	P value
CDK2	49	< 0.00001
CHEK1	21	< 0.00001
ERBB2	7	0.00040

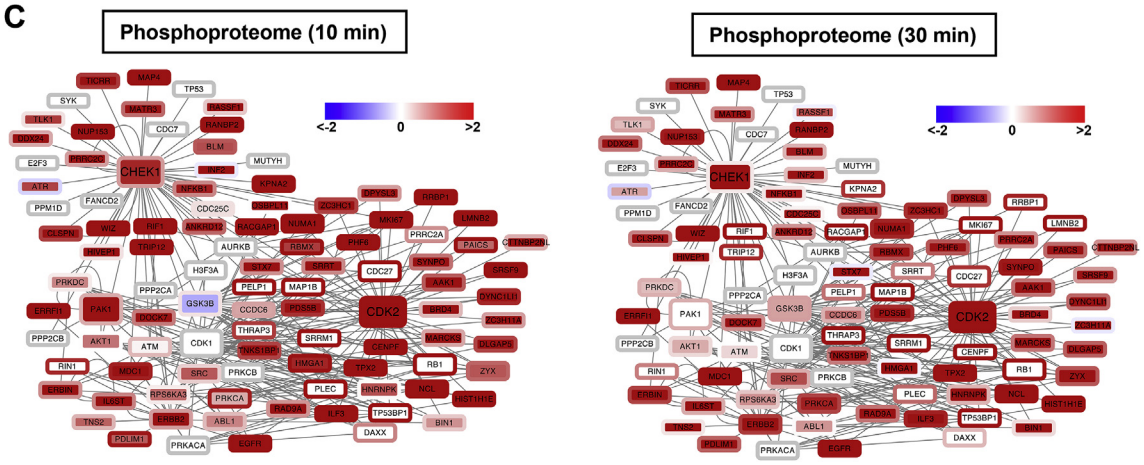

Fig. 4. Identification of key kinases linked to cisplatin resistance through the activation of EGFR signaling. A. Schematic diagram describing the process of reconstructing the networks of proteins significantly altered by EGF stimulation in T24R and T24S cells. Venn diagram depicts number of altered proteins involved in cisplatin resistance in downstream EGFR signaling. Using kinase-substrate interaction information of the significantly altered proteins and their upstream kinases, 27 kinases were initially selected. Of those, 3 kinases were found to be significant altered in either protein expression or phosphorylation after EGF treatment. **B**. List of the 3 key kinases with the number of significantly altered substrates and number of interactions. **C**. Network model describing the interactions of the 3 kinases and their substrates. Node and border color represent proteins phosphorylation ratios in T24R vs. T24S cells after 10 min or 30 min of EGF treatment, respectively. Red and green indicate up- and downregulated phosphorylation following EGF treatment, respectively. (For interpretation of the references to color in this figure legend, the reader is referred to the Web version of this article.)

end, we focused on the kinases that can regulate the phosphorylation levels of these differential sites by performing a kinase enrichment analysis. Using kinase-substrate interactions obtained from the SIGNOR database [34], we constructed a network model consisting of 121 kinases and 329 substrates with 893 interactions (Supplementary Fig. 2). Kinase enrichment analysis of the network model identified 3 out of the 27 kinases (Supplementary Table 8), checkpoint kinase 1 (CHEK1), cyclin-dependent kinase 2 (CDK2), and Erb-B2 receptor tyrosine kinase 2 (ERBB2), as having a significant number of interactions with APs when stimulated by EGF (Fig. 4A and B). Based on these 3 key kinases and their substrates, we reconstructed a subnetwork consisting of 101 nodes connected by 265 edges (Fig. 4A). The subnetwork was visualized using Cytoscape [37]. Notably, most of the substrates were highly phosphorylated in T24R, rather than T24S cells (Fig. 4C).

Validation with western blot analysis confirmed that phosphorylation of CDK2, CHEK1, ERBB2, mTOR, AKT, and RB significantly increased in T24R cells after treatment with 10 ng/ml of EGF (Fig. 5A). These results provide potential molecular mechanisms through which these 3 major kinases mediate cisplatin resistance. To further identify genes that have a critical effect on cisplatin resistance, we knocked-down the 3 kinases, CDK2, CHEK1, and ERBB2, in T24R cells using siRNAs. Western blot analysis was conducted to confirm knockdown of these kinases (Fig. 5B, right). T24R cells were significantly sensitized to cisplatin when CDK2 was knocked-down, suggesting that CDK2 may be important in maintaining resistance (Fig. 5B). We next tested whether a potent and selective inhibitor of CDK2, dinaciclib (SCH 727965) [33], could overcome resistance in three independent cisplatin-resistant human BC cell lines, T24R, J82R, and RT4R (Fig. 5C). Consistent to the data shown in Fig. 5B, inhibition of CDK2 sensitized resistant cells when they were incubated in combination with cisplatin (Fig. 5C).

To further investigate the correlation of high CDK2 expression in BC, IHC analysis was done on BC TMAs. There were statistically significant differences in comparative scores for CDK2 expression between tumor and normal adjacent to tumor (NAT) cores (Fig. 5D). We applied a digital annotation algorithm to the core images in an effort to quantitatively assess this observation. Our image algorithm was set so that nuclear and cytoplasmic staining could be detected as positive at a color spectrum darker than that for typical DAB staining. Using the scores from our digital image analysis, we observed significantly upregulated expression of CDK2 in tumor cores. Comparative images of the tumor to NAT tissue show increased nuclear and cytoplasmic staining in the tumor epithelium (Fig. 5D). Collectively, these results demonstrate that

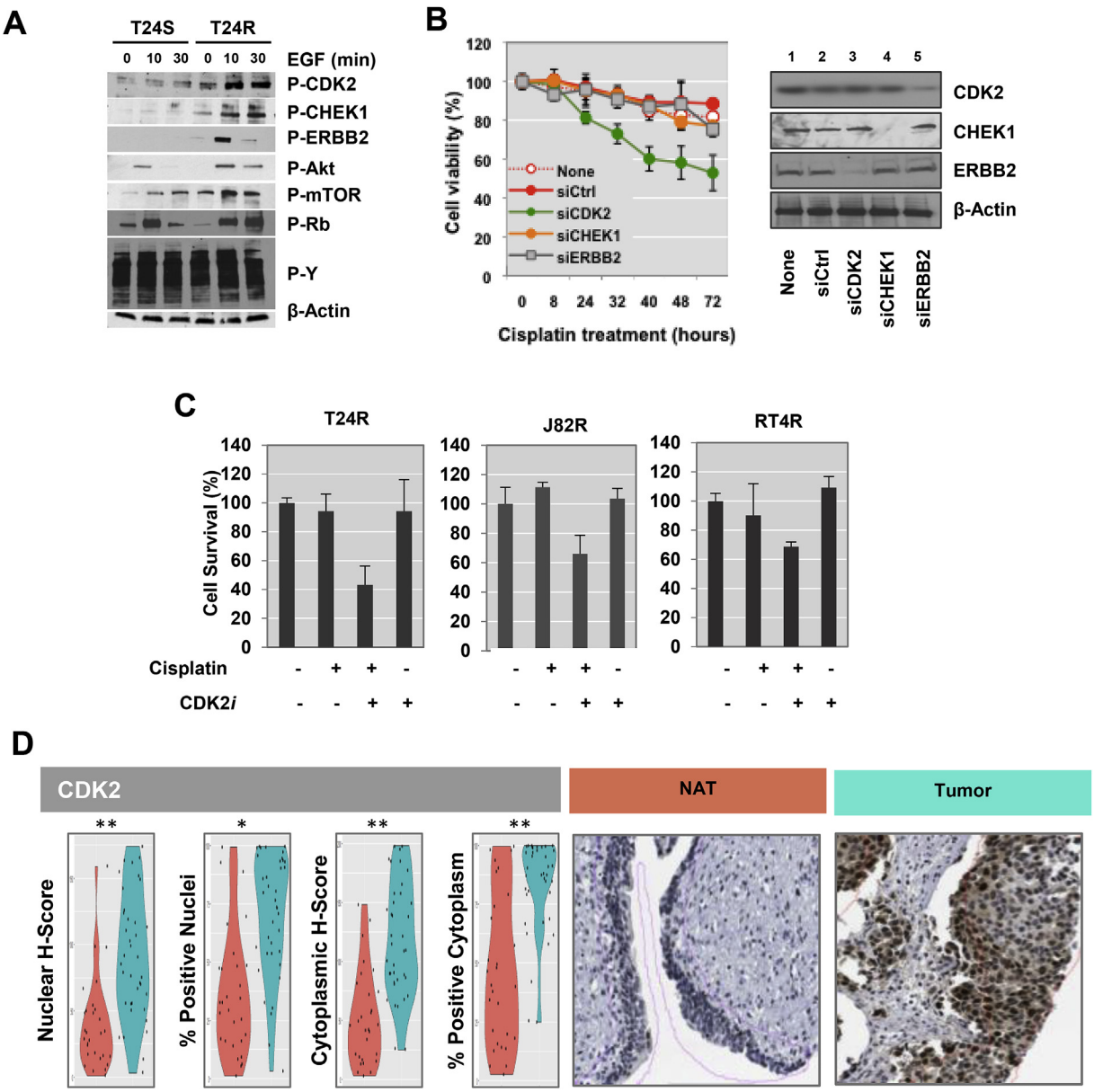

Fig. 5. Functional role of CDK2 associated with cisplatin resistance. A. Western blot analysis of the key protein kinases. After stimulation with 10 ng/ml of EGF treatment for 0, 10, or 30 min, cells were harvested for protein extraction and western blot analysis. Representative western blot images were selected after experiments were repeated at least 3 times. **B.** Gene silencing of CDK2 enhanced cisplatin sensitivity in T24R cells. T24R cells transiently transfected with siRNAs targeting CDK2, CHEK1, or ERBB2 were incubated in culture medium with 10 μM cisplatin. T24R cells transfected with control siRNAs (siCtrl) were used as controls. The cell viability rate was measured at various time points (0, 8, 24, 32, 40, 48, and 72 h). Experiments were done in triplicate. *p < 0.05 (Student's t-test). Representative western blot analysis data demonstrated that the levels expression of CDK2, CHEK1, or ERBB2 in these experiments were downregulated by targeting siRNAs. **C.** Cisplatin resistant BC cell lines (R24R, J82R, or RT4R) were treated with cisplatin alone, CDK2 inhibitor (CDKi), or a combination of both for 72 h. Cell survival rates were quantified as describe in Methods. **D.** Increased expression levels of CDK2 in BC. IHC analysis was performed to measure the protein expression of CDK2 in bladder tissues from BC patients. Violin plots showing expression of CDK2 in NAT and tumor tissue. Representative images of NAT and tumor cores are shown.

our proteome-driven signature may be a useful predictor of survival for patients who have already undergone cisplatin chemotherapy.

3.5. Clinical implications of the key kinases and their substrates

Based on the significance of CDK2 and its substrates to cisplatin resistance, we examined the association of gene expression of CDK2 and its substrates to clinical outcomes. For this, we utilized the transcriptome dataset (GSE5287) from Als et al. [2], which contains the gene expression profiles of 30 BC patients along with their survival information after cisplatin chemotherapy. We first assessed the correlation of APs in the global network model in terms of gene expression versus protein expression or phosphorylation levels (Fig. 6A). Significant positive correlations between gene expression versus protein expression (P = 1.09e-16) and gene expression versus protein phosphorylation (P = 0.003) were observed (Fig. 6A). This suggests that gene expression profiling can reflect protein expression and phosphorylation, supporting the possibility that the gene expression profiles of APs in BC patients can be indicators of dysregulated networks. We then searched for CDK2 substrates from the network model, which resulted in 48 proteins that were selected based on kinase-substrate interaction information from the SIGNOR database (Fig. 6B). For further selection,

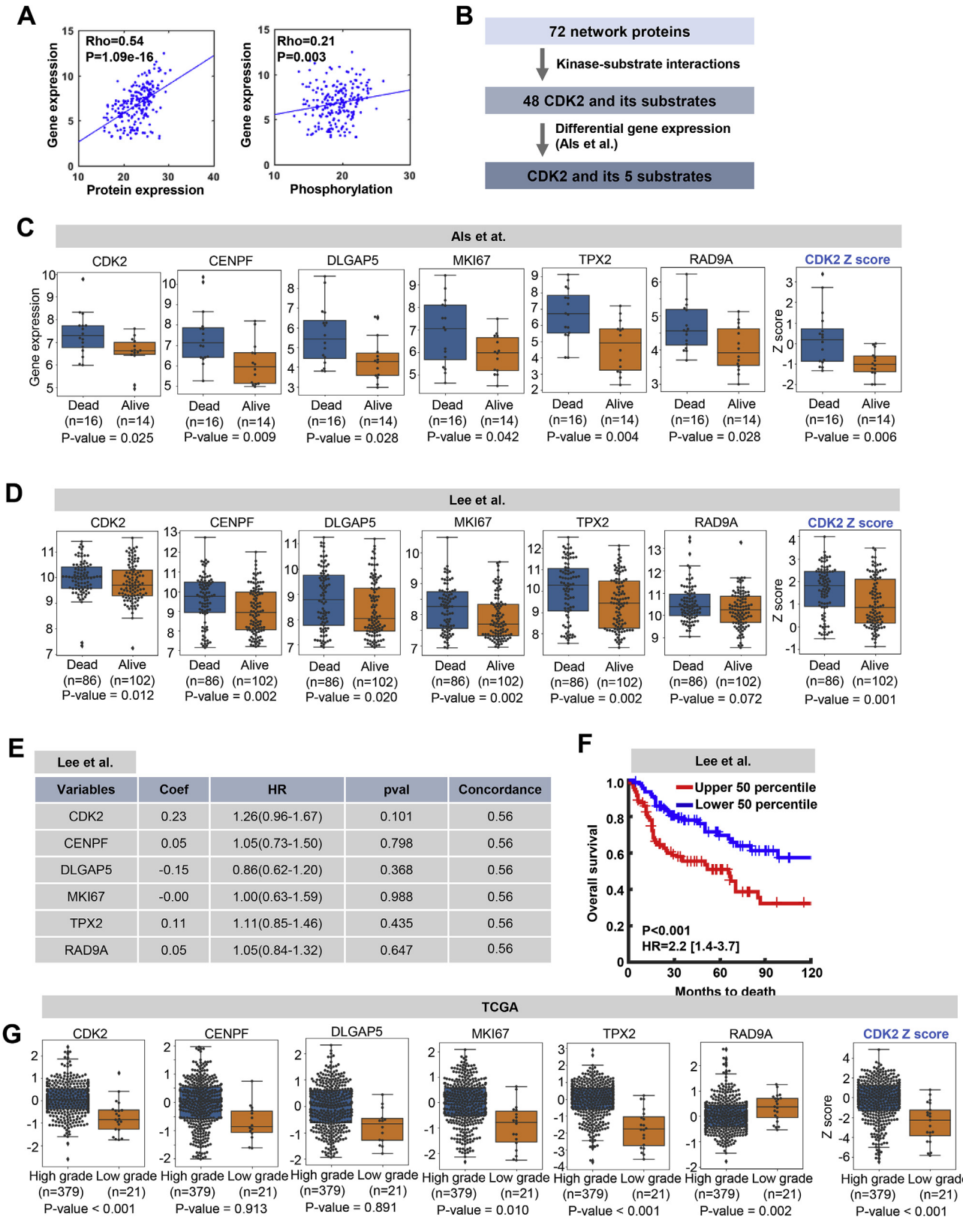

Lee et al.				
Variables	**Coef**	**HR**	**pval**	**Concordance**
CDK2	0.23	1.26(0.96-1.67)	0.101	0.56
CENPF	0.05	1.05(0.73-1.50)	0.798	0.56
DLGAP5	-0.15	0.86(0.62-1.20)	0.368	0.56
MKI67	-0.00	1.00(0.63-1.59)	0.988	0.56
TPX2	0.11	1.11(0.85-1.46)	0.435	0.56
RAD9A	0.05	1.05(0.84-1.32)	0.647	0.56

(caption on next page)

we examined differential gene expression of the 48 proteins, including CDK2 and its substrates, using the BC dataset from Als et al. (GSE5287) [2]. For this we stratified the samples into those who survived 5 or more years (alive) and those who deceased within 5 years after chemotherapy (dead). This allowed us to identify genes in the CDK2 network that were significantly associated with poor survival after cisplatin chemotherapy (Fig. 6C). As a result, 6 genes out of 72 were found to have higher expression in the dead group. These were CDK2, CENPF, DLGAP5, MKI67, TPX2, and RAD9A.

We further investigated the clinical association of the 6 genes to the

Fig. 6. CDK2 network may have clinical implications in BC. A. Correlation of 72 network proteins in levels of gene expression vs. protein expression (left) or phosphorylation (right). Dots on the scatter plot represent proteins and lines represent regression lines. Correlation was measured using the Spearman's rank correlation method. **B**. Selection criteria used to identify the 6 proteins from the 72 network proteins. **C and D**. Box plots display differential gene expression of the selected 6 proteins from the network model using the gene expression datasets from (**C**) Als et al. and (**D**) Lee et al. Box plots at the far right display differential representation of CDK2 network scores computed by the Z-score method. Significance levels of differential gene expression between BC patients who were alive and deceased after cisplatin treatment were computed via the Wilcoxon rank-sum test. **E**. Regression coefficient and significance of the 6 genes based on multivariate Cox regression analysis using Lee at al. dataset. **F**. Kaplan-Meier curves for overall survival based on the expression of the CDK2 network genes are shown for the high (upper 50^{th} percentile; n = 97) and low (lower 50^{th} percentile; n = 91) z-score groups from the Lee et al. patient dataset. P-values and hazard ratios (HRs) were taken from a Cox regression analysis. **G**. Box plots display differential expression of the 6 genes in the TCGA BC cohort. Wilcoxon rank-sum test was performed to compute significance of differential expression between high and low grade samples.

CDK2 network using two gene expression datasets from Als et al. (GSE5287) [2] and Lee et al. (GSE13507) [24]. The Als et al. dataset showed significantly higher expression of the 6 genes in the CDK2 network and its summarized score (Z-score) in the dead group (Fig. 6C). The same was true in the Lee et al. dataset (Fig. 6D). Using the Lee et al. dataset, we then examined the association of these 6 CDK2 network genes to recurrence-free survival (RFS) by performing multivariate Cox regression analysis (Fig. 6E). Although individual genes showed no significant correlation with RFS, the summarized score of the 6 genes presented significant association with RFS (Fig. 6F). We further confirmed that expression of the 6 gene and its summarized score in the CKD2 network were significantly segregated high vs low grade BC samples from The Cancer Genome Atlas (TCGA) [35] (Fig. 6G). Collectively, these results suggest that our AP-derived CDK2 network genes may be helpful in predicting prognosis and treatment options for BC patients.

4. Discussion

Our present work characterized the enriched global proteome and phosphoproteome in cisplatin-resistant BC. By characterizing the signaling network alterations associated with cisplatin resistance, we also demonstrated the utility of quantitative phosphoproteomics in highlighting perturbed networks between cisplatin-resistant and sensitive BC cells. This approach revealed a vastly different cellular context between T24R and T24S cells, suggesting that there are potential key regulators modulating the perturbation of signaling networks. Measuring the abundance of proteins and mapping the phosphorylated kinase-substrate interactions facilitated a comprehensive biological interpretation of the complex network context behind cisplatin resistance. Expanded analysis of transcriptome data from BC patients further provided strong evidence that concurrent molecular alterations in gene expression to protein modification can be the core basis of disease.

Our experimental results illustrated that the global phosphoproteomics profile in cisplatin-resistant cells is significantly altered and that several key kinases may be mediating this. These kinases could potentially be used as therapeutic targets for blocking chemo-resilience. We also observed an increase in the phosphorylation of CDK2, CHEK1, and ERBB2 in cisplatin-resistant cells. Our comprehensive proteomics approach revealed many novel phosphorylation sites of CDK2, CHEK1, ERBB2, and their substrates, suggesting new intervention points in cisplatin resistance-specific signaling networks. The experimental results from this study implicate the active involvement of CDK2, CHEK1, and ERBB2 in contributing to resistance against cisplatin-based chemotherapies.

CHEK1 is a serine/threonine kinase that is involved in the checkpoint-mediated control of the cell cycle and the activation of DNA repair in response to DNA damage or the presence of unreplicated DNA. The ATR-CHEK2 signaling pathway was recently proposed to play an important role in regulating the response to cisplatin in BC [16]. Inhibition of the ATR-CHEK2 pathway with selective inhibitors can sensitize cells to cisplatin [7,26]. ERBB2 (HER2), a member of the EGF receptor family of receptor tyrosine kinases, has been known to be associated with aggressive variants of BC. Mutated ERBB2 is well documented as a cancer driver gene and is primarily found in high-risk tumors. Mutations in ERBB2 have also been found to be independent risk factors associated with death in BC patients [22]. Thus, ERBB2-targeting treatment has been an attractive option in improving clinical outcomes for BC patients.

Our kinase activity-based network modeling suggested that one of the most significantly increased sites of phosphorylation in resistant cells is CDK2. The CDK2 network consists of several putative substrates, including CDC27, DAXX, and CENPF (Fig. 4A). CDK2, a Ser/Thr protein kinase, phosphorylates substrates at the S/TPx(x)R/K consensus motif. CDK2 is originally known to function in cell cycle regulation; increased CDK2 kinase activity is essential for the G1 to S stage transition as well as the phosphorylation of the Rb protein. During the S phase, active CDK2 and cyclin A complexes predominate and phosphorylate E2F [30]. CDK2 inhibitors (e.g., ribociclib, dinociclib, seliciclib et al.), which deregulate E2F, have been suggested as promising pharmacological strategies against various cancer types. However, a comprehensive overview of CDK2 and its substrates has not yet been established and the biological effects or regulatory mechanisms of CDK2 remain elusive.

Our findings suggest that inhibition of CDK2, a key player of cisplatin resistance, could induce cisplatin sensitivity. Therefore, CDK2 may be a potential target in the modulation of cisplatin resistance modulating human BC. This is consistent with previous reports. Alterations of CDK2 that are associated with cisplatin resistance in vitro have been reported in other cancer types, such as ovarian [31,40], oral [25], testicular [23] and cervical [42]. While our results are promising, we are aware of the limitations in our study, mainly owing to a lack in quantity of clinical specimens for phosphoproteomic analysis. Our study was also restricted to cell line-derived signatures; although, it was further validated in the clinical setting. Since this finding was based on a retrospective study from a single institution, the efficacy of the signature could be impaired. Future prospective validation studies using high-throughput assays should be followed up in multiple centers to consolidate our signature's analytical validity and reproducibility in the routine clinical practice setting.

Acknowledgements

The authors acknowledge support from the Bio and Medical Technology Development Program (project no. 2012M3A9B6055305) though the National Research Foundation of Korea funded by the Korean Ministry of Education, Science and Technology. We also appreciate support from the Multiomics Research Program (NRF-2012M3AB9036675), which is funded by the Korean Ministry of Science, ICT, and Future Planning. This work was also supported by the National Institutes of Health grants (1U01DK103260, 1R01DK100974, U24 DK097154, NIH NCATS UCLA CTSI UL1TR000124), Department of Defense (W81XWH-15-1-0415), Centers for Disease Controls and Prevention (1U01DP006079), IMAGINE NO IC Research Grant, Steven Spielberg Discovery Fund in Prostate Cancer Research Career Development Awards, and the U.S.-Egypt Science and Technology Joint Fund (to J.K.). J.K. is a former recipient of the Interstitial Cystitis Association Pilot Grant, Fishbein Family IC Research Grant, New York Academy of Medicine, and Boston Children's Hospital Faculty Development. Any opinions, findings, conclusions, or recommendations expressed in this article are those of the authors alone and do not

necessarily reflect the views of any of the previously mentioned sponsors. In addition, this article is derived from the Subject Data funded in whole or part by National Academy of Sciences, Engineering, and Medicine (NAS) and The United States Agency for International Development. Any opinions, findings, conclusions, or recommendations expressed in this article are those of the authors alone, and do not necessarily reflect the views of USAID or NAS.

Appendix A. Supplementary data

Supplementary data related to this article can be found at https://doi.org/10.1016/j.canlet.2018.08.014.

References

[1] A.W. Bowman, A. Azzalini, Applied Smoothing Techniques for Data Analysis: the Kernel Approach with S-plus Illustrations, Clarendon Press; Oxford University Press, Oxford New York, 1997.
[2] A.B. Als, L. Dyrskjot, H. von der Maase, K. Koed, F. Mansilla, H.E. Toldbod, J.L. Jensen, B.P. Ulhoi, L. Sengelov, K.M. Jensen, T.F. Orntoft, Emmprin and survivin predict response and survival following cisplatin-containing chemotherapy in patients with advanced bladder cancer, Clin. Canc. Res. 13 (2007) 4407–4414.
[3] A.B. Apolo, H.B. Grossman, D. Bajorin, G. Steinberg, A.M. Kamat, Practical use of perioperative chemotherapy for muscle-invasive bladder cancer: summary of session at the Society of Urologic Oncology annual meeting, Urol. Oncol. 30 (2012) 772–780.
[4] P.C. Black, C.P. Dinney, Growth factors and receptors as prognostic markers in urothelial carcinoma, Curr. Urol. Rep. 9 (2008) 55–61.
[5] B.M. Bolstad, R.A. Irizarry, M. Astrand, T.P. Speed, A comparison of normalization methods for high density oligonucleotide array data based on variance and bias, Bioinformatics 19 (2003) 185–193.
[6] P. Casado, M. Hijazi, D. Britton, P.R. Cutillas, Impact of phosphoproteomics in the translation of kinase-targeted therapies, Proteomics 17 (2017).
[7] S. Chen, X. Chen, G. Xie, Y. He, D. Yan, D. Zheng, S. Li, X. Fu, Y. Li, X. Pang, Z. Hu, H. Li, W. Tan, J. Li, Cdc6 contributes to cisplatin-resistance by activation of ATR-Chk1 pathway in bladder cancer cells, Oncotarget 7 (2016) 40362–40376.
[8] P.R. Cutillas, Role of phosphoproteomics in the development of personalized cancer therapies, Proteonomics Clin. Appl. 9 (2015) 383–395.
[9] N. Eckstein, K. Servan, L. Girard, D. Cai, G. von Jonquieres, U. Jaehde, M.U. Kassack, A.F. Gazdar, J.D. Minna, H.D. Royer, Epidermal growth factor receptor pathway analysis identifies amphiregulin as a key factor for cisplatin resistance of human breast cancer cells, J. Biol. Chem. 283 (2008) 739–750.
[10] G. Gakis, J. Efstathiou, S.P. Lerner, M.S. Cookson, K.A. Keegan, K.A. Guru, W.U. Shipley, A. Heidenreich, M.P. Schoenberg, A.I. Sagaloswky, M.S. Soloway, A. Stenzl, ICUD-EAU International Consultation on Bladder Cancer 2012: radical cystectomy and bladder preservation for muscle-invasive urothelial carcinoma of the bladder, Eur. Urol. 63 (2013) 45–57.
[11] O.N. Gofrit, Re: long-term outcomes in patients with muscle-invasive bladder cancer after selective bladder-preserving combined-modality therapy: a pooled analysis of radiation therapy oncology group protocols 8802, 8903, 9506, 9706, 9906, and 0233, Eur. Urol. 68 (2015) 165–166.
[12] M.L. Granados, L.G. Hudson, S.L. Samudio-Ruiz, Contributions of the epidermal growth factor receptor to acquisition of platinum resistance in ovarian cancer cells, PLoS One 10 (2015) e0136893.
[13] W. Huang da, B.T. Sherman, R.A. Lempicki, Systematic and integrative analysis of large gene lists using DAVID bioinformatics resources, Nat. Protoc. 4 (2009) 44–57.
[14] D. Hwang, A.G. Rust, S. Ramsey, J.J. Smith, D.M. Leslie, A.D. Weston, P. de Atauri, J.D. Aitchison, L. Hood, A.F. Siegel, H. Bolouri, A data integration methodology for systems biology, Proc. Natl. Acad. Sci. U. S. A. 102 (2005) 17296–17301.
[15] M. Inoue, F. Koga, S. Yoshida, T. Tamura, Y. Fujii, E. Ito, K. Kihara, Significance of ERBB2 overexpression in therapeutic resistance and cancer-specific survival in muscle-invasive bladder cancer patients treated with chemoradiation-based selective bladder-sparing approach, Int. J. Radiat. Oncol. Biol. Phys. 90 (2014) 303–311.
[16] M. Isono, M.J. Hoffmann, M. Pinkerneil, A. Sato, M. Michaelis, J. Cinatl Jr., G. Niegisch, W.A. Schulz, Checkpoint kinase inhibitor AZD7762 strongly sensitises urothelial carcinoma cells to gemcitabine, J. Exp. Clin. Canc. Res. CR (Clim. Res.) 36 (2017) 1.
[17] P. Jones, R.G. Cote, L. Martens, A.F. Quinn, C.F. Taylor, W. Derache, H. Hermjakob, R. Apweiler, PRIDE: a public repository of protein and peptide identifications for the proteomics community, Nucleic Acids Res. 34 (2006) D659–D663.
[18] A.M. Kamat, P.K. Hegarty, J.R. Gee, P.E. Clark, R.S. Svatek, N. Hegarty, S.F. Shariat, E. Xylinas, B.J. Schmitz-Drager, Y. Lotan, L.C. Jenkins, M. Droller, B.W. van Rhijn, P.I. Karakiewicz, ICUD-EAU international consultation on bladder cancer 2012: screening, diagnosis, and molecular markers, Eur. Urol. 63 (2013) 4–15.
[19] M. Kanehisa, S. Goto, Y. Sato, M. Furumichi, M. Tanabe, KEGG for integration and interpretation of large-scale molecular data sets, Nucleic Acids Res. 40 (2012) D109–D114.
[20] S. Kim, P.A. Pevzner, MS-GF + makes progress towards a universal database search tool for proteomics, Nat. Commun. 5 (2014) 5277.
[21] W.T. Kim, J. Kim, C. Yan, P. Jeong, S.Y. Choi, O.J. Lee, Y.B. Chae, S.J. Yun, S.C. Lee, W.J. Kim, S100A9 and EGFR gene signatures predict disease progression in muscle invasive bladder cancer patients after chemotherapy, Ann. Oncol. 25 (2014) 974–979.
[22] F. Koga, S. Yoshida, M. Tatokoro, S. Kawakami, Y. Fujii, J. Kumagai, L. Neckers, K. Kihara, ErbB2 and NFkappaB overexpression as predictors of chemoradiation resistance and putative targets to overcome resistance in muscle-invasive bladder cancer, PLoS One 6 (2011) e27616.
[23] R. Koster, A. di Pietro, H. Timmer-Bosscha, J.H. Gibcus, A. van den Berg, A.J. Suurmeijer, R. Bischoff, J.A. Gietema, S. de Jong, Cytoplasmic p21 expression levels determine cisplatin resistance in human testicular cancer, JCI (J. Clin. Investig.) 120 (2010) 3594–3605.
[24] J.S. Lee, S.H. Leem, S.Y. Lee, S.C. Kim, E.S. Park, S.B. Kim, S.K. Kim, Y.J. Kim, W.J. Kim, I.S. Chu, Expression signature of E2F1 and its associated genes predict superficial to invasive progression of bladder tumors, J. Clin. Oncol. 28 (2010) 2660–2667.
[25] M.R. Lee, C. Lin, C.C. Lu, S.C. Kuo, J.W. Tsao, Y.N. Juan, H.Y. Chiu, F.Y. Lee, J.S. Yang, F.J. Tsai, YC-1 induces G0/G1 phase arrest and mitochondria-dependent apoptosis in cisplatin-resistant human oral cancer CAR cells, Biomedicine 7 (2017) 12.
[26] C.C. Li, J.C. Yang, M.C. Lu, C.L. Lee, C.Y. Peng, W.Y. Hsu, Y.H. Dai, F.R. Chang, D.Y. Zhang, W.J. Wu, Y.C. Wu, ATR-Chk1 signaling inhibition as a therapeutic strategy to enhance cisplatin chemosensitivity in urothelial bladder cancer, Oncotarget 7 (2016) 1947–1959.
[27] K.S. Lynn, C.C. Chen, T.M. Lih, C.W. Cheng, W.C. Su, C.H. Chang, C.Y. Cheng, W.L. Hsu, Y.J. Chen, T.Y. Sung, MAGIC: an automated N-linked glycoprotein identification tool using a Y1-ion pattern matching algorithm and in silico MS(2) approach, Anal. Chem. 87 (2015) 2466–2473.
[28] Madar, Reduction of ambiguity in phosphorylation-site localization in large-scale phosphopeptide profiling by data filter using unique mass class information, Bull. Kor. Chem. Soc. 35 (2014) 845.
[29] R. Mandic, C.J. Rodgarkia-Dara, V. Krohn, S. Wiegand, R. Grenman, J.A. Werner, Cisplatin resistance of the HNSCC cell line UT-SCC-26A can be overcome by stimulation of the EGF-receptor, Anticancer Res. 29 (2009) 1181–1187.
[30] D.O. Morgan, Cyclin-dependent kinases: engines, clocks, and microprocessors, Annu. Rev. Cell Dev. Biol. 13 (1997) 261–291.
[31] H. Pan, F. Wang, G.O. Rankin, Y. Rojanasakul, Y. Tu, Y.C. Chen, Inhibitory effect of black tea pigments, theaflavin3/3'-gallate against cisplatin-resistant ovarian cancer cells by inducing apoptosis and G1 cell cycle arrest, Int. J. Oncol. 51 (2017) 1508–1520.
[32] J.M. Park, J.H. Park, D.G. Mun, J. Bae, J.H. Jung, S. Back, H. Lee, H. Kim, H.J. Jung, H.K. Kim, H. Lee, K.P. Kim, D. Hwang, S.W. Lee, Integrated analysis of global proteome, phosphoproteome, and glycoproteome enables complementary interpretation of disease-related protein networks, Sci. Rep. 5 (2015) 18189.
[33] K. Paruch, M.P. Dwyer, C. Alvarez, C. Brown, T.Y. Chan, R.J. Doll, K. Keertikar, C. Knutson, B. McKittrick, J. Rivera, R. Rossman, G. Tucker, T. Fischmann, A. Hruza, V. Madison, A.A. Nomeir, Y. Wang, P. Kirschmeier, E. Lees, D. Parry, N. Sgambellone, W. Seghezzi, L. Schultz, F. Shanahan, D. Wiswell, X. Xu, Q. Zhou, R.A. James, V.M. Paradkar, H. Park, L.R. Rokosz, T.M. Stauffer, T.J. Guzi, Discovery of dinaciclib (SCH 727965): a potent and selective inhibitor of cyclin-dependent kinases, ACS Med. Chem. Lett. 1 (2010) 204–208.
[34] L. Perfetto, L. Briganti, A. Calderone, A. Cerquone Perpetuini, M. Iannuccelli, F. Langone, L. Licata, M. Marinkovic, A. Mattioni, T. Pavlidou, D. Peluso, L.L. Petrilli, S. Pirro, D. Posca, E. Santonico, A. Silvestri, F. Spada, L. Castagnoli, G. Cesareni, SIGNOR: a database of causal relationships between biological entities, Nucleic Acids Res. 44 (2016) D548–D554.
[35] A.G. Robertson, J. Kim, H. Al-Ahmadie, J. Bellmunt, G. Guo, A.D. Cherniack, T. Hinoue, P.W. Laird, K.A. Hoadley, R. Akbani, M.A.A. Castro, E.A. Gibb, R.S. Kanchi, D.A. Gordenin, S.A. Shukla, F. Sanchez-Vega, D.E. Hansel, B.A. Czerniak, V.E. Reuter, X. Su, B. de Sa Carvalho, V.S. Chagas, K.L. Mungall, S. Sadeghi, C.S. Pedamallu, Y. Lu, L.J. Klimczak, J. Zhang, C. Choo, A.I. Ojesina, S. Bullman, K.M. Leraas, T.M. Lichtenberg, C.J. Wu, N. Schultz, G. Getz, M. Meyerson, G.B. Mills, D.J. McConkey, T.R. Network, J.N. Weinstein, D.J. Kwiatkowski, S.P. Lerner, Comprehensive molecular characterization of muscle-invasive bladder cancer, Cell 171 (2017) 540–556 e525.
[36] C. Schwentner, A. Stenzl, G. Gakis, Monitoring high-risk bladder cancer, Curr. Opin. Urol. 22 (2012) 421–426.
[37] P. Shannon, A. Markiel, O. Ozier, N.S. Baliga, J.T. Wang, D. Ramage, N. Amin, B. Schwikowski, T. Ideker, Cytoscape: a software environment for integrated models of biomolecular interaction networks, Genome Res. 13 (2003) 2498–2504.
[38] G. Sonpavde, C.N. Sternberg, Neoadjuvant chemotherapy for invasive bladder cancer, Curr. Urol. Rep. 13 (2012) 136–146.
[39] C.N. Sternberg, J. Bellmunt, G. Sonpavde, A.O. Siefker-Radtke, W.M. Stadler, D.F. Bajorin, R. Dreicer, D.J. George, M.I. Milowsky, D. Theodorescu, D.J. Vaughn, M.D. Galsky, M.S. Soloway, D.I. Quinn, ICUD-EAU international consultation on bladder cancer 2012: chemotherapy for urothelial carcinoma-neoadjuvant and adjuvant settings, Eur. Urol. 63 (2013) 58–66.
[40] Y. Sun, L. Jin, J.H. Liu, Y.X. Sui, L.L. Han, X.L. Shen, Interfering EZH2 expression reverses the cisplatin resistance in human ovarian cancer by inhibiting autophagy, Cancer Biother. Radiopharm. 31 (2016) 246–252.
[41] V.M. Tan, L.C. Cheng, J.M. Drake, Complementing genomics and transcriptomics: phosphoproteomics illuminates systems biology in prostate cancer, Mol. Cell Oncol. 3 (2016) e1246075.
[42] B. Wang, Z. Huang, R. Gao, Z. Zeng, W. Yang, Y. Sun, W. Wei, Z. Wu, L. Yu, Q. Li, S. Zhang, F. Li, G. Liu, B. Liu, L. Leng, W. Zhan, Y. Yu, G. Yang, S. Zhou, Expression of long noncoding RNA urothelial cancer associated 1 promotes cisplatin resistance in cervical cancer, Cancer Biother. Radiopharm. 32 (2017) 101–110.
[43] J.R. Wisniewski, A. Zougman, N. Nagaraj, M. Mann, Universal sample preparation method for proteome analysis, Nat. Methods 6 (2009) 359–362.
[44] B. Zhang, M.C. Chambers, D.L. Tabb, Proteomic parsimony through bipartite graph analysis improves accuracy and transparency, J. Proteome Res. 6 (2007) 3549–3557.

IVYSPRING INTERNATIONAL PUBLISHER

Theranostics

2018; 8(16): 4520-4534. doi: 10.7150/thno.25130

Research Paper

Rewiring of cisplatin-resistant bladder cancer cells through epigenetic regulation of genes involved in amino acid metabolism

Austin Yeon[1], Sungyong You[1,6], Minhyung Kim[1], Amit Gupta[1], Myung Hee Park[2], Daniel J. Weisenberger[3], Gangning Liang[4], Jayoung Kim[1,5,6,7,8]✉

1. Departments of Surgery, Cedars-Sinai Medical Center, Los Angeles, CA, USA
2. National Institute of Dental and Craniofacial Research, National Institutes of Health Bethesda, MD, USA
3. Department of Biochemistry and Molecular Medicine, USC Norris Comprehensive Cancer Center, University of Southern California
4. Department of Urology, Keck School of Medicine, University of Southern California, Los Angeles, CA, USA
5. Departments of Biomedical Sciences, Cedars-Sinai Medical Center, Los Angeles, CA, USA
6. Samuel Oschin Comprehensive Cancer Institute, Cedars-Sinai Medical Center, Los Angeles, CA, USA
7. Department of Medicine, University of California Los Angeles, CA, USA
8. Department of Urology, Ga Cheon University College of Medicine, Incheon, Republic of Korea

✉ Corresponding author: Jayoung Kim, PhD., Departments of Surgery and Biomedical Sciences, Cedars-Sinai Medical Center, 8700 Beverly Blvd., Los Angeles, CA 90048. Tel: +1-310-423-7168; Fax: +1-310-967-3809; E-mail: Jayoung.Kim@cshs.org

© Ivyspring International Publisher. This is an open access article distributed under the terms of the Creative Commons Attribution (CC BY-NC) license (https://creativecommons.org/licenses/by-nc/4.0/). See http://ivyspring.com/terms for full terms and conditions.

Received: 2018.01.24; Accepted: 2018.07.23; Published: 2018.08.10

Abstract

Alterations in DNA methylation are important epigenetic markers in bladder cancer (BC). These epigenome modifications may drive the mechanisms of aggressive chemo-resistant BC. Clinicopathological biomarkers that indicate chemotherapeutic resistance are critical for better assessing treatment strategies for individual patients. Thus, in this study, we aimed to determine whether DNA methylation of certain metabolic enzymes is significantly altered in cisplatin-resistant BC cells.

Methods: To characterize CpG methylation and nucleosome accessibility in cisplatin-resistant BC cells, the Illumina Infinium HM450 DNA methylation assay was performed. Perturbed gene expression was found to be associated with cisplatin resistance, and the biological roles of spermidine/spermine N^1-acetyltransferase (SAT1) and argininosuccinate synthase 1 (ASS1) were further studied using qRT-PCR analysis and various cell biology assays, including western blot.

Results: *ASS1* and *SAT1*, genes for amino acid and polyamine metabolism catalysts, respectively, were found to be vastly hypermethylated, resulting in greatly downregulated expression. ASS1 expression is of particular interest because prior studies have demonstrated its potential association with BC stage and recurrence. In regard to chemoresistance, we found that aberrant expression or induced stimulation of SAT1 restored cisplatin sensitivity in the cell culture system. We also found that the addition of exogenous arginine deiminase through administration of ADI-PEG 20 (pegylated arginine deiminase) increased ASS1 expression and enhanced cisplatin's apoptotic effects.

Conclusions: Our study demonstrates a novel mechanistic link between the epigenetic perturbation of SAT1 and ASS1 and cancer metabolism in cisplatin-resistant bladder cancer cells. These findings suggest potential utility of *SAT1* and *ASS1* as predictive biomarkers in re-sensitizing bladder cancer to chemotherapy and personalizing therapy.

Key words: *SAT1*, *ASS1*, cancer metabolism, metabolomics, DNA methylation, chromatin accessibility, cisplatin resistance

Introduction

Bladder cancer (BC) is the second most common genitourinary malignancy worldwide and the fourth most common cancer in the U.S. [1-3]. Most patients are diagnosed with treatable cell carcinoma or non-muscle invasive bladder cancer (NMIBC) [4, 5]. However, approximately 20-30% of all NMIBC cases

eventually progress to become muscle-invasive bladder cancer (MIBC). From there, about 50% of these patients develop metastases within two years, even after radical cystectomy [6, 7]. In addition, MIBC patients who do not respond to adjuvant chemotherapy have a worse prognosis [8]. Unfortunately, there are currently no well-defined and available prognostic marker(s) that can identify these higher-risk patients [9-11]. Therefore, in order to develop new diagnostic technologies, a comprehensive molecular understanding of the patient subsets who will acquire chemoresistance is required. The identification of markers capable of predicting the response in patients treated with platinum-based drugs is urgently needed in order to improve the outcomes for those BC patients who are at higher risk of developing resistance.

Epigenetic regulation has been demonstrated to play an important role in bladder tumorigenesis [12-14]. Recently, three separate subtypes of BC patients have been identified through analysis of DNA methylation profiles [14]. Epigenetic dysregulation occurs via cytosine methylation-dependent gene silencing, which is also considered a characteristic of therapeutic-resistance [15]. Cancer-specific DNA methylation mostly occurs on the CpG islands located in the promoter regions of genes and causes silencing of downstream genes [16, 17]. Currently, two DNA methyltransferase (DNMT) inhibitors (5-azacytidine and its variant, 5-aza-CdR) have been approved by the FDA for the treatment of high-risk myelodysplastic syndrome [18] and are also in clinical trials for solid forms of human cancers [19]. In addition to DNA methylation, there are other relevant epigenetic mechanisms that affect gene expression levels, including histone modification and nucleosome positioning. These processes work together to create the epigenetic landscape that directs the process of gene expression. Chromatin structure, which is based on DNA methylation and nucleosome accessibility (occupancy), plays a critical role in the regulation of gene expression at the transcriptional start sites of genes. Recent computational modeling using molecular dynamics simulations revealed the potential effects of epigenetic DNA methylation on nucleosome stability [20] and demonstrated that CpG methylation that contributes to nucleosome positioning can also be DNMT1 independent [21]. These findings suggest that monitoring chromatin accessibility, DNA methylation, and histone modification is crucial for better understanding therapeutic responses in BC [22-24].

Since first observed 90 years ago by Dr. Otto Warburg, metabolic reprogramming has been accepted as a hallmark of cancer [25-28]. Considering this, targeting cancer-associated amino acid metabolism has been tested as a potential treatment option [29, 30]. Amino acids, such as arginine, proline, and glutamine, play a variety of functional roles in the cell. However, most importantly, they act as essential precursors for the biosynthesis of proteins. Therefore, depletion therapies, such as arginine deiminase (ADI) treatment, are being extensively tested against several cancer types, including ovarian cancer, mesothelioma, and hepatocellular carcinoma [31-35].

In this study, we sought to understand the epigenetic alterations underlying the metabolic reprogramming in cisplatin-resistant BC cells. Our experimental results suggest that cancer-specific epigenetic silencing of two genes encoding for metabolic enzymes, spermidine/spermine N^1-acetyl-transferase (*SAT1*) and argininosuccinate synthase 1 (*ASS1*), is closely associated with cisplatin resistance and is epigenetically regulated in T24 BC cells. Both enzymes are related to arginine metabolism: ASS1 catalyzes the final step in arginine biosynthesis. SAT1, on the other hand, catabolizes spermidine and spermine that are derived from arginine in sequential enzymatic steps that involve the conversion of arginine to ornithine, ornithine to putrescine, putrescine to spermidine, and spermidine to spermine [36, 37].

Results

Characterization of CpG methylation and nucleosome accessibility in cisplatin-resistant BC cells

In order to investigate the epigenetic modulation linked to cisplatin resistance in BC, we used two isogenic T24 BC cell lines—one that is cisplatin sensitive (T24S) and one cisplatin resistant (T24R). T24 cells were utilized because the characteristics of these cells have been previously reported by our group [38]. The T24R cell line exhibited much less responsiveness to cisplatin-induced apoptosis compared to T24S cells (**Figure 1A**). In order to understand the epigenetic reprogramming associated with cisplatin resistance, three independent sets of data profiles, namely (1) DNA methylation, (2) nucleosome accessibility, and (3) gene expression, were generated in T24R and T24S cells (**Figure 1B**).

We first performed DNA methylation analysis using the Illumina HumanMethylation450 BeadChip, in which >482,421 CpG sites are queried across the human genome. We identified 118,465 CpG sites as being differentially methylated in T24R cells compared to T24S cells, with a fold change of M-value ≥ 1.0. Of these 118,465 differentially methylated CpG sites, we identified decreased methylation of 9,014

sites in 4,052 genes and increased methylation of 109,451 sites in 93,068 genes in T24R cells compared to T24S. (**Figure S1** and **Table S1**). These findings suggest that DNA methylation profiles are radically altered in T24R cells and that hypermethylation may be correlated to cisplatin resistance in T24 BC cells.

Given the predominant global DNA hypermethylation pattern in T24R cells, we speculated that T24R cells also have distinctive chromatin modifications and accessibility alterations that affect gene expression. Chromatin structure, which is organized through DNA methylation and nucleosome accessibility (or occupancy), plays a critical role in regulating gene expression at the transcription start site [39]. Thus, monitoring of chromatin accessibility, DNA methylation, and

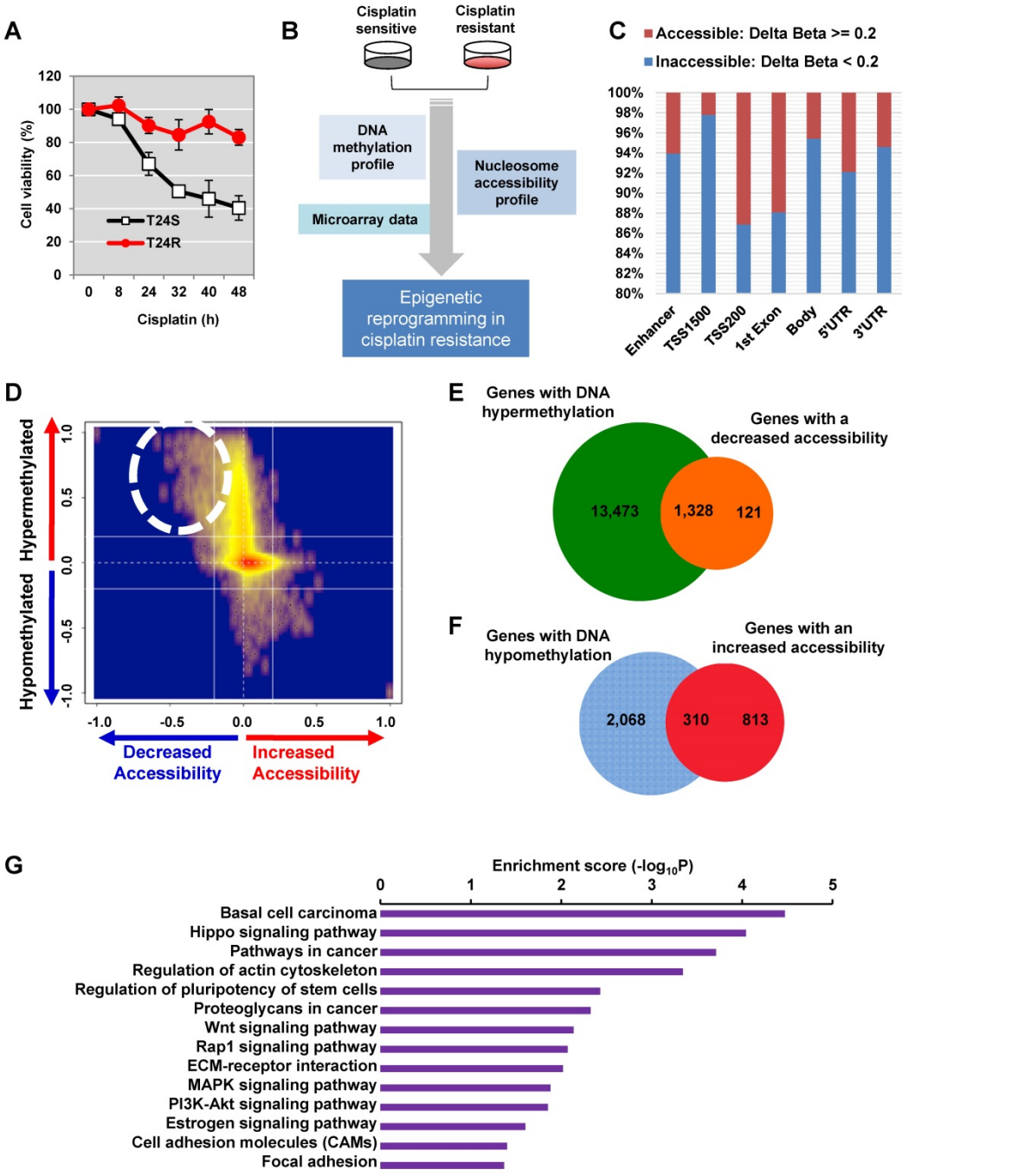

Figure 1. Determination of the epigenetic rewiring in cisplatin-resistant bladder cancer. (A) Cell viability was measured at the indicated times after 10 μM cisplatin treatment. **(B)** Overall experimental workflow of the investigation of epigenetic regulation associated with cisplatin resistance in this study. **(C)** Bar graph showing increased and decreased chromatin accessibility in T24R and T24S cells. Selection of the accessible CpG sites was based on delta beta at a threshold value 0.2. The percentage indicates the changes in accessible chromatin upon cisplatin resistance for individual genome features. **(D)** Chromatin accessibility visualized by Kernel density scatter plot of delta-methylation versus delta-accessibility. Circle depicts the region showing a loss of chromatin accessibility accompanied by DNA hyper-methylation. **(E)** Venn diagram depicting 14,801 genes with DNA hypermethylation and 1,449 genes with decreased accessibility. **(F)** Venn diagram showing 2,378 genes with DNA hypomethylation and 1,123 genes with increased accessibility. **(G)** Bar graph depicting enriched KEGG pathways of 1,328 hypermethylated genes with reduced chromatin accessibility.

histone modification is crucial for understanding disease progression and responses to therapy. Due to its importance in chromatin structuring, we hypothesized that nucleosome accessibility is altered in cisplatin-resistant BC cells, leading to altered DNA methylation.

To test this hypothesis, we used the Acce*Sss*Ible assay [39] to determine nucleosome occupancy and positioning in T24R and T24S cells by probing CpGs using the Illumina HM450 BeadChip [39]. We identified a digital footprint of nucleosome occupancy and positioning in both the CpG-rich islands and CpG-poor regions of T24R and T24S cells. Methylation of nuclei treated with or without M.SssI, a CpG methyltransferase enzyme that methylates CpG sites on nucleosome-depleted unbound DNA, was compared using the Illumina HM450 BeadChip. We then stratified CpG sites with altered nucleosome accessibility (**Figure 1C**). Many genomic regions displayed decreased accessibility, except TSS 200 and the first exon.

Differential DNA methylation plotted against differential chromatin accessibility is shown in the Kernel density scatter plot (**Figure 1D**) with the circle depicting genes with decreased chromatin accessibility and DNA hypermethylation. Interestingly, we observed that nucleosome occupancy was greatly altered in T24R cells compared to the control T24S cells (**Figure S1**). In particular, we identified 1,328 genes with DNA hypermethylation and decreased chromatin accessibility in T24R cells compared to T24S cells (**Figure 1D-E** and **Table S2**). We also identified 310 genes with DNA hypomethylation and increased chromatin accessibility in T24R versus T24S cells (**Figure 1D, F** and **Table S3**). The top 10 genes with hypermethylation and decreased chromatin accessibility and the top 10 genes with hypomethylation and increased accessibility are listed in **Table S4** and **Table S5**. To understand the biological function of these genes, we performed functional enrichment analysis on the 1,328 hypermethylated genes, which revealed significant advancement of cancer-related pathways in T24R cells (**Figure 1G**). These findings provide a finer resolution on the nature of epigenetic mechanisms and broaden our understanding of nucleosome occupancy and DNA methylation changes in cisplatin-resistant BC cells.

Perturbed epigenetic signatures in cisplatin-resistant BC cells may lead to changes in gene expression

The DNA methylation data was integrated with our previously reported gene expression data [40]. According to the gene expression and DNA methylation pattern, we grouped the genes into 6 clusters (**Figure 2A**). Among these, clusters 1 (up-hypo) and 2 (down-hyper) showed opposite patterns of gene expression and DNA methylation between T24R and T24S cells (**Figure 2A**). Cluster 1 contained genes in T24R cells whose expression was upregulated and DNA methylation was decreased. Cluster 2 consisted of genes in T24R cells whose expression was downregulated and DNA methylation was increased (**Figure 2A**). Follow-up gene ontology bioinformatic analyses of the experimental data further suggested that there is significant epigenetic silencing of genes that regulate arginine and proline metabolism, as well as extracellular matrix receptor interaction, PPAR signaling, adherens junction and focal adhesion**,** in cisplatin-resistant BC cells [40] (**Figure 2B**). In contrast, genes related to DNA replication were found to be epigenetically upregulated (hypomethylated) (**Figure 2B**).

As a result of this hypomethylation, transcription of genes associated with DNA replication, repair, and pyrimidine metabolism was upregulated. This suggests that there may possibly be a metabolic relationship between amino acid metabolism and DNA repair mechanisms. In an independent effort to explore metabolic perturbation of cisplatin resistance, a Kyoto Encyclopedia of Genes and Genomes (KEGG) metabolic map was constructed that displayed the differential regulation of metabolic pathways between cisplatin-resistant BC cells and controls. This also supported the idea that transcripts for the metabolism of amino acids, such as arginine and proline (down-hyper), and of purine and pyrimidine (up-hypo), are significantly altered in T24R cells (**Figure 2C**). In particular, promoters of genes associated with amino acid metabolism, such as arginine and proline metabolism, were hypermethylated, leading to decreased gene expression levels, as shown in the dotted box in **Figure 2C and Figure S2**.

Cisplatin-resistant T24 cells displayed epigenetic silencing (hypermethylation and decreased mRNA expression) of genes associated with arginine and proline metabolism, such as *GLUD2* (glutamate dehydrogenase 2), *ARG2* (arginase 2), *ALDH2* (aldehyde dehydrogenase 2), *P4HA1* (prolyl 4-hydroxylase subunit alpha 1), *ALDH7A1*, (aldehyde dehydrogenase 7 family member A1), *GLUD1* (glutamate dehydrogenase 1), *PYCR1* (pyrroline-5-carboxylate reductase 1), *ASS1* (argininosuccinate synthase 1), *ALDH18A1* (aldehyde dehydrogenase 18 family member A1), *P4HA2* (prolyl 4-hydroxylase subunit alpha 2), *NAGS* (N-acetylglutamate synthase), as well as *SAT1* (spermidine/spermine N1-acetyl-transferase), and *CKB* (creatine kinase B) (fold

change≥2 and FDR<0.05; **Table 1**). We identified *SAT1* and *ASS1* as the two most prominently hypermethylated and downregulated genes in T24R cells. The fold change of *SAT1* expression was -6.09 (FDR<0.001), while that of *ASS1* was -5.27 (FDR=0.017). Given that *SAT1* and *ASS1* have not yet been studied in the context of cisplatin resistance in BC, our results suggest new gene targets.

Expression levels of epigenetically regulated genes are associated with clinical outcomes in BC patients

We next speculated if the differentially methylated genes (DMGs) identified in T24R cells could be clinically predictive indicators for recurrence, tumor grade, overall survival, and/or

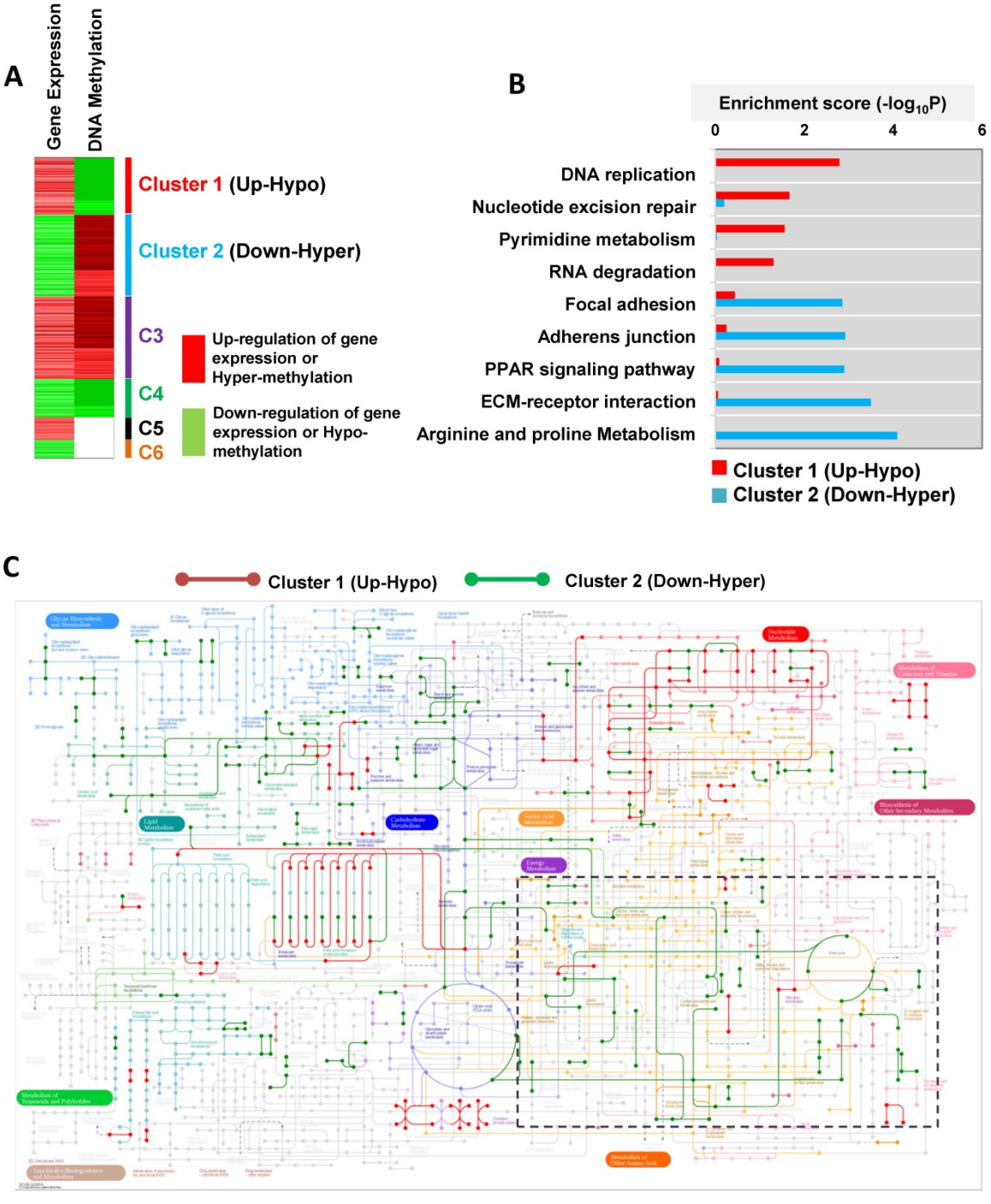

Figure 2. Metabolic pathways directed by differentially expressed and methylated genes. (A) Heatmap depicting differential gene expression and DNA methylation patterns of T24R cells compared to T24S cells. **(B)** The enriched biological processes associated with the upregulated genes with DNA hypomethylation vs. the downregulated genes with DNA hypermethylation. **(C)** Metabolic pathway map displaying the changes seen in cisplatin-resistant BC. The KEGG metabolic map was overlaid with gene expression data. The nodes represent metabolic compounds and edges represent genes involved in the reactions (red lines: upregulated and hypomethylated genes; green lines: downregulated and hypermethylated-genes). The boxes with dotted lines indicate significantly altered pathways, including those for arginine and proline metabolism.

stage. To test this, we performed a series of analyses on the association of the DMGs with clinical outcomes using publicly available gene expression microarray data derived from 103 BC patients [41]. *GLUD1*, *ASS1*, and *ALDH2* were found to be associated with recurrence in BC patients who had already undergone chemotherapy (**Figure 3A**). *ASS1* was downregulated in BC patients who had recurrence (n=36) compared to those without (n=67) (**Figure 3A**). BC tumor grades were positively or negatively associated with gene expression levels of our protein panel, which included *GLUD1*, *ARG2*, *TYMS* (thymidylate synthase), and *TK1* (thymidine kinase 1) (**Figure 3B**). *TYMS* and *TK1* are proteins associated with pyrimidine metabolism and their gene levels were more upregulated and hypomethylated in T24R cells (**Figure 2B**). Furthermore, gene expression patterns of *GLUD1*, *GLS*, *ALDH2*, *SAT1*, *ASS1*, and *TYMS* distinguished patients who had worse overall survival from those with recurrence-free survival (**Figure 3C**). Of note, *ASS1* expression was also negatively correlated with BC stage: lower *ASS1* expression was a feature of higher tumor stage (**Figure 3D**). Collectively, these results suggest that *SAT1* and *ASS1* are hypermethylated in cisplatin-resistant BC cells, thereby resulting in aberrant loss of expression. These defects may be what causes the decrease in recovery efficiency after DNA damage.

Epigenetic landscapes of SAT1 and ASS1 in cisplatin-resistant BC cells

We next sought to determine the DNA methylation landscape of *ASS1*, which is located on chromosome 9 and has several CpG islands. The difference in DNA methylation of *ASS1* between T24R and T24S cells was 4.35-fold (log2) and the gene expression difference was -5.27-fold (log2) (**Figure 4A**). *SAT1* and *TYMS* are localized on chromosomes X and 18, respectively. *SAT1* showed 1.33-fold (log2) increased DNA methylation and 6.09-fold (log2) decreased gene expression in T24R cells. Individual DNA methylation levels at specific CpG sites in *ASS1*, *SAT1*, and *TYMS* are shown in **Figure 4B**.

To further assess the causative relationship of *ASS1* and *SAT1* to cisplatin resistance, protein expression levels were compared between T24R and T24S cells (**Figure 4C**). We also found that *in vitro* addition of decitabin, a DNMT inhibitor, increased protein expression of both *SAT1* and ASS1 in T24R cells (**Figure 4D**). Furthermore, two additional cisplatin-resistant BC cells lines, J82R and RT4R, were used to test whether decitabine treatment increases SAT1 and ASS1 expression. Experimental results showed that protein expression of both SAT1 and ASS1 were significantly enhanced in the presence of decitabine, which was consistent with data from T24R cells (**Figure 5E**). Collectively, these findings indicate that downregulation of *SAT1* and *ASS1* may most likely be due to changes in epigenetic regulation (DNA hypermethylation of CpG promoter regions).

Table 1. Comparison of genes in cisplatin-resistant (T24R) and cisplatin-sensitive (T24S) cells. The genes are listed in two categories, DNA replication (pink) or arginine, proline, and polyamine metabolism (blue). The most downregulated (and hypermethylated) genes in cisplatin-resistant cells are those regulating arginine and proline metabolism, which include *ASS1* and *SAT1*.

Pathways	Symbol	Full name	mRNA Fold change	Accessibility
DNA replication	MCM7	minichromosome maintenance complex component 7	2.35	No change
	POLD1	polymerase (DNA directed), delta 1, catalytic subunit	1.54	No change
	POLE4	polymerase (DNA-directed), epsilon 4, accessory subunit	1.52	No change
	POLE	polymerase (DNA directed), epsilon, catalytic subunit	1.48	No change
	RFC3	replication factor C (activator 1) 3, 38kDa	1.36	No change
	RNASEH2C	Ribonuclease H2, subunit C	1.28	No change
Arginine and proline metabolism	GLUD2	glutamate dehydrogenase 2	-1.12	No change
	ARG2	arginase 2	-3.15	No change
	ALDH2	aldehyde dehydrogenase 2 family (mitochondrial)	-5.09	Decreased
	P4HA1	prolyl 4-hydroxylase, alpha polypeptide I	-1.67	No change
	ALDH7A1	aldehyde dehydrogenase 7 family, member A1	-1.27	Decreased
	GLUD1	glutamate dehydrogenase 1	-1.09	No change
	GLS	glutaminase	-1.88	No change
	PYCR1	pyrroline-5-carboxylate reductase 1	-1.14	No change
	ASS1	argininosuccinate synthase 1	-5.27	Decreased
	ALDH18A1	aldehyde dehydrogenase 18 family, member A1	-1.21	No change
	SAT1	spermidine/spermine N1-acetyltransferase 1	-6.09	Increased
	P4HA2	prolyl 4-hydroxylase, alpha polypeptide II	-1.31	Decreased
	NAGS	N-acetylglutamate synthase	-1.91	No change
	CKB	creatine kinase, brain	-1.22	No change

SAT1 and ASS1 play critical roles in cisplatin resistance

Western blot analysis data demonstrated that cisplatin-resistant BC cells express little SAT1, while cisplatin-sensitive cells exhibit clearly detectable expression. Based on this, we hypothesized that activation or induced expression of SAT1 could re-sensitize T24R cells. T24R cells were transfected with a FLAG-SAT1 vector (**Figure 5A**). We found that induced SAT1 expression in T24R cells enhanced apoptosis in both the absence and presence of cisplatin (**Figure 5B**). Upon cisplatin treatment, SAT1-overexpressing T24R cells displayed a significant increase in apoptosis, an approximate 3.5-fold of untreated basal levels (**Figure 5B**). SAT1 overexpression also led to an estimated 2.3-fold

increase in the production of reactive oxygen species (ROS), which may contribute to the re-sensitization of T24R cells to cisplatin (**Figure 5C**).

Next, to evaluate the potential interdependence of SAT1 activation and drug sensitivity, we treated T24R cells with a combination of cisplatin and BENSpm (a SAT1 inducing reagent) (**Figure 5D**). This resulted in a significant synergistic reduction of cell survival that was greater than treatment with cisplatin or BENSpm alone. Consistent with the findings in T24R cells, additional experiments conducted on J82R (**Figure 5E**) and RT4R (**Figure 5F**) cells showed that BENSpm sensitized cisplatin-resistant BC cells.

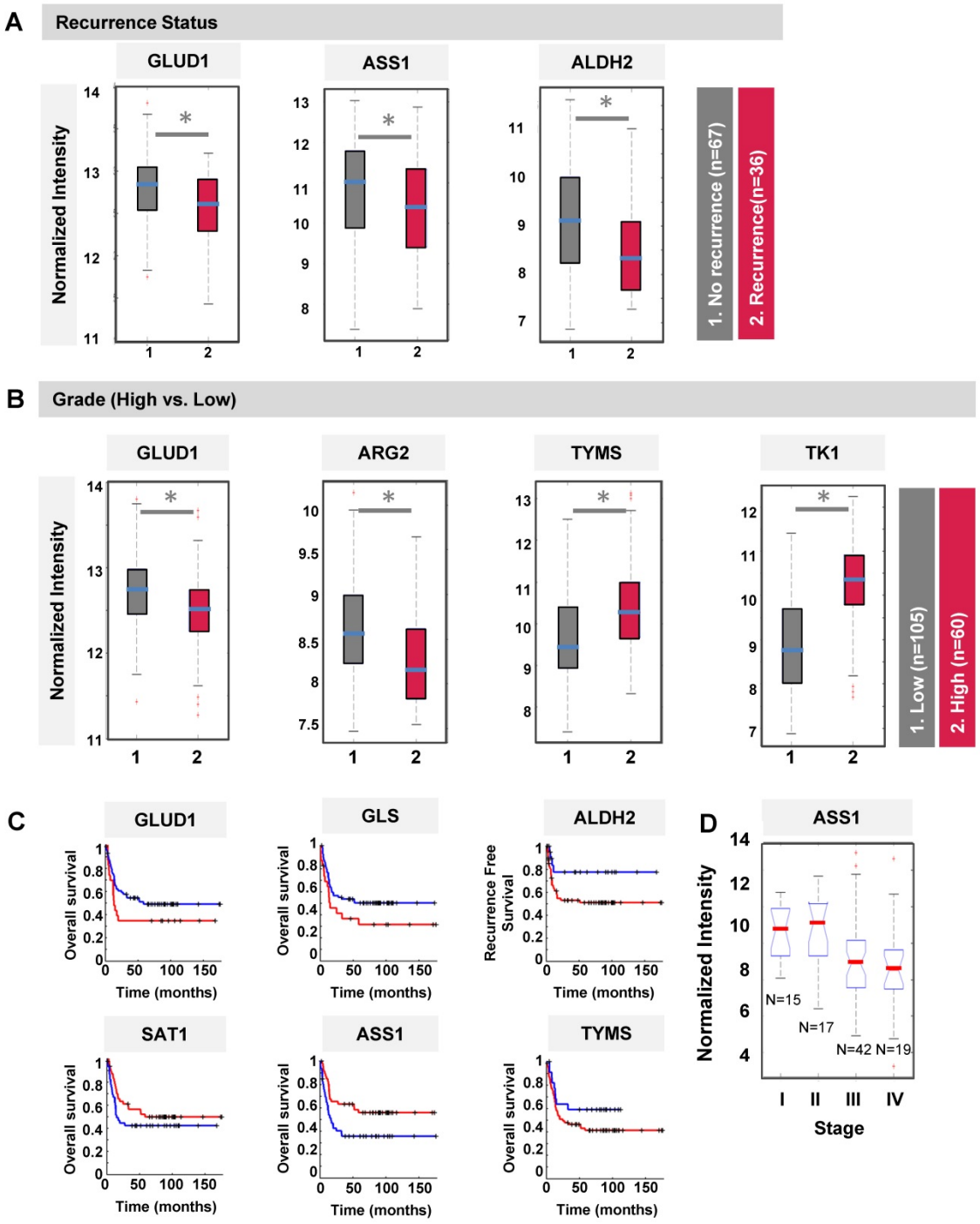

Figure 3. Clinical association of DMGs with differential expression in T24R and T24S cells. (A) Box plot showing recurrence predictability of *GLUD1*, *ASS1*, and *ALDH2*. **(B)** Box plot showing grade predictability of *GLUD1*, *ARG2*, *TYMS*, and *TK1*. **(C)** Overall survival rate graph showing survival predictability of GLID1, GLS, and ALDH2. **(D)** Box plot showing tumor stage predictability of *ASS1*.

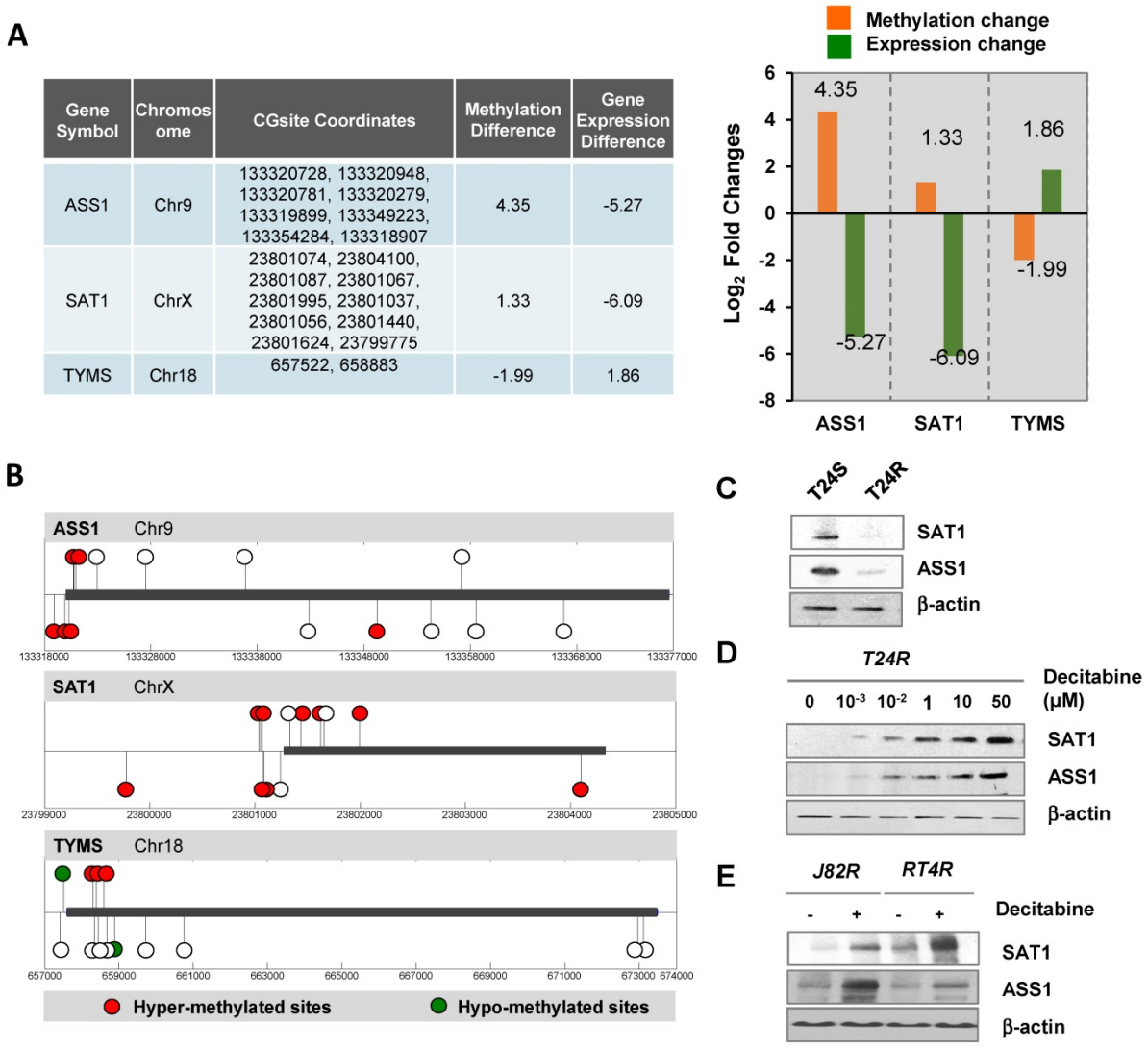

Figure 4. Alteration of DNA methylation landscapes in cisplatin-resistant BC cells. (A) Table showing promoter CpG methylation sites identified by HM450 array, and fold changes in DNA methylation and gene expression of *ASS1*, *SAT1*, and *TYMS*. Fold changes of DNA methylation (orange bars) and gene expression (green bars) of *ASS1*, *SAT1*, and *TYMS* in T24R compared to T24S, are shown. **(B)** Methylation sites on *ASS1*, *SAT1*, and *TYMS* (red circle, hypermethylated sites; green circle, hypomethylated sites; white circle, no changes). **(C)** Downregulation of SAT1 and ASS1 protein expression levels in T24R cells compared to T24S. **(D)** Increased protein expression of SAT1 and ASS1 in T24R cells upon treatment with decitabine, an inhibitor of DNA methylation. **(E)** Increased protein expression of SAT1 and ASS1 in J82R or RT4R cells upon treatment with decitabine.

Our experimental data provided evidence that DNA methylation of *ASS1* is increased and gene expression is decreased in T24R cells (**Figure 4A**). In addition, arginine metabolism is also shown to be defective in T24R cells. This opens the possibility that this may also hold true for other cisplatin-resistant cancers. During analysis of publicly available human BC data collections, we found that ASS1 expression is negatively correlated with BC recurrence and grade. Currently, pegylated arginine deiminase (ADI-PEG 20), an arginine-depleting therapy, is under evaluation in clinical trials for many types of cancers, including BC. We found that similar treatment with ADI-PEG 20 increased ASS1 expression in T24S cells (**Figure 5G**). In T24R cells, ASS1 was not expressed up to 72 h following treatment with ADI-PEG 20 (**Figure 5G**). We also found that ASS1 was not re-expressed when T24R cells were treated for 96 h. Given that T24S cells exhibit *ASS1* expression, *ASS1* deficiency will likely be a key factor in selecting patients for clinical trials involving ADI-PEG 20 therapy, which is consistent with previous observations in other cancer types [42].

Next, we determined whether arginine depletion via ADI-PEG 20 could induce apoptosis in T24R cells that do not express *ASS1*. T24R cells were treated under various conditions: (1) cisplatin alone, or (2) combination of cisplatin and ADI-PEG 20 in a dose-dependent manner (1, 10, 100, and 750 ng/mL). Cell survival rates were measured using two independent assays, the MTS (**Figure 5H**) and crystal violet assay (**Figure 5I**). The following time-dependent experiments showed consistent results (**Figures 5J** (crystal violet assay) and **Figure 5K**

(MTS assay)). In addition, J82R and RT4R cells were tested with ADI-PEG 20 treatment as well. The results suggested that a combination of cisplatin and ADI-PEG 20 greatly enhances responsiveness to cisplatin in resistant BC cell lines and resulted in approximately 50% and 40% reduction in cell survival rates in J82R and RT4R cells, respectively (**Figures 5L-M**).

To further supplement evidence for the association of ASS1 and SAT1 with BC, immunohistochemistry (IHC) analysis was performed using commercial BC tumor microarrays (TMAs). We found that 80% of the tumors (32/40 cores) were negative for SAT1 and ASS1 protein expression (data not shown). These results imply that *SAT1* and/or *ASS1* silencing are potential indicators of disease. In this regard, patients with little to no expression of *SAT1* and *ASS1* may be good candidates for combination treatments with ADI-PEG 20 and cisplatin. This is because SAT1 and ASS1 expression may be indicators of clinical benefit from cisplatin chemotherapy and/or arginine deprivation therapy.

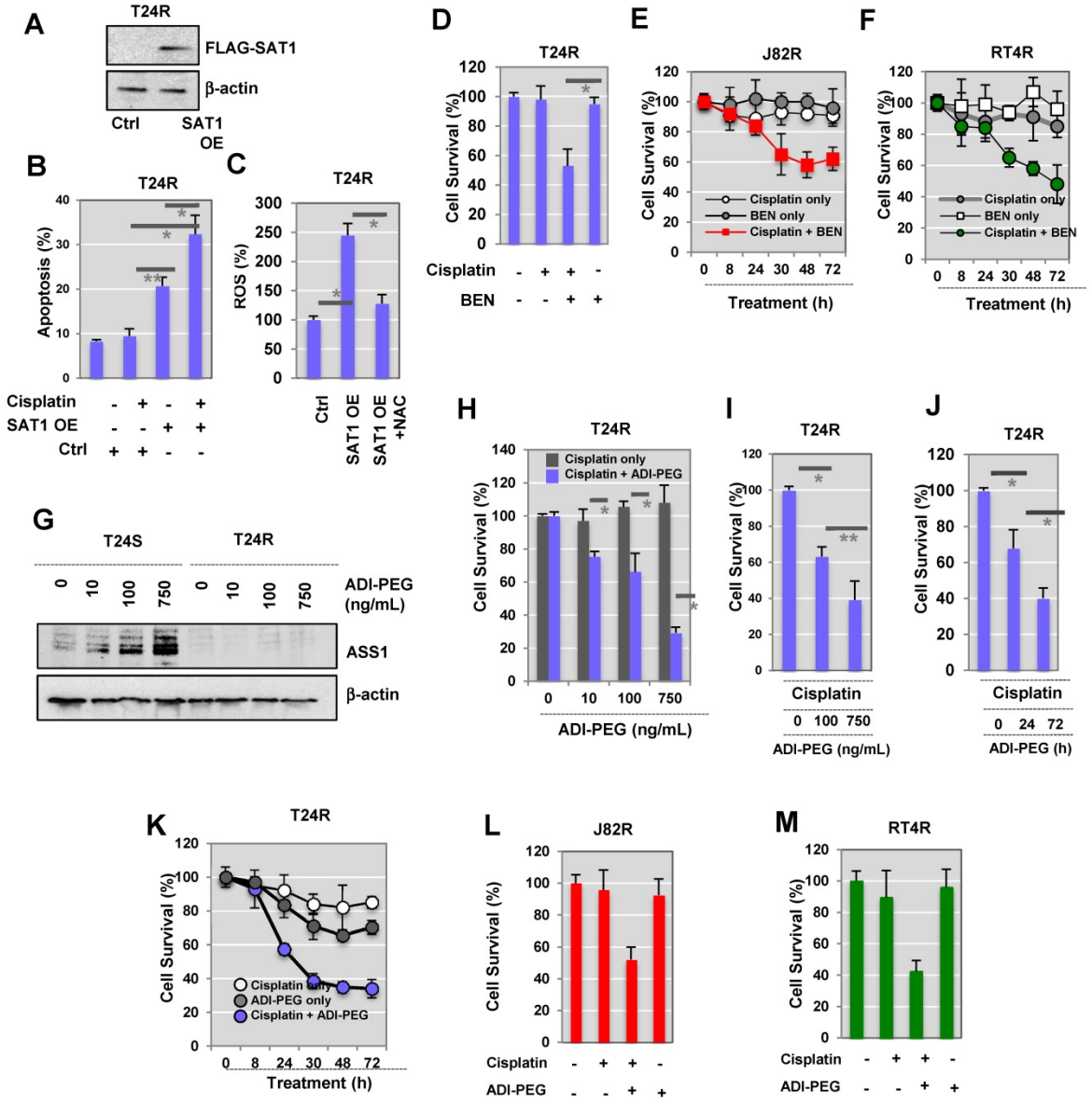

Figure 5. Sensitization of T24R cells to cisplatin-induced apoptosis by overexpression of SAT1 or BENSpm treatment. (A) Overexpression of SAT1 protein in T24R cells transfected with pCMV7.1 3XFLAG-hSAT1 was confirmed by western blot analysis using an anti-flag antibody. **(B)** Sensitization of T24R cells to cisplatin-induced cell apoptosis upon overexpression of SAT1. **(C)** Increase in ROS production through overexpression of SAT1 in T24R cells and reduction of ROS by N-acetylcysteine (NAC). The levels of ROS produced in control cells are set at 100%. Each bar represents the mean ± SD of three independent experiments (*, P<0.05). **(D)** Suppression of survival of cisplatin-treated T24R cells by BENSpm treatment. **(E-F)** Treatment with BENSpm sensitized cisplatin-resistant BC cells, J82R (E) and RT4R (F). **(G)** Restoration of ASS1 expression in T24S cells by API-PEG 20 in a dose-dependent manner. Cells were harvested 72 h after treatment. **(H-J)** Enhancement of apoptosis through the combination of cisplatin and ADI-PEG 20 in cisplatin-resistant T24R, but not T24S, cells. Cell survival was determined used **(H)** MTS assay and **(I)** crystal violet assay 72 h after treatment with cisplatin with or without ADI-PEG 20. **(J)** T24R cells were treated with cisplatin alone, ADI-PEG 20 alone, or with cisplatin plus ADI-PEG 20 for 0, 24, or 72 h. Crystal violet assay was performed. **(K)** T24R cells were treated with cisplatin alone, ADI-PEG 20 alone, or with cisplatin plus ADI-PEG 20 for 0, 8, 24, 30, 48, or 72 h. (Blue circle: ADI-PEG 20 plus cisplatin; white circle: cisplatin alone; gray circle: ADI-PEG 20 alone). Cell survival rates were measured using MTS assay. **(L-M)** Cell survival rates increased in J82R or RT4R cells upon treatment with cisplatin and ADI-PEG 20.

Discussion

In this study, we sought to determine if epigenetically regulated metabolic reprogramming is associated with cisplatin resistance in BC, and if *SAT1* and *ASS1* are potential predictive biomarkers for cisplatin resistance. Generally, treatment for recurrent BC involves systemic cisplatin chemotherapy [43]. Although this current standard has decreased morbidity and mortality, failure of treatment frequently occurs due to acquired chemoresistance. This has resulted in a 5-year survival rate of only 5-15% following recurrence [44-46]. Therefore, concerted efforts are necessary to identify markers associated with cisplatin resistance in BC patients. Moreover, identification of markers is key to comprehending the mechanisms of cisplatin resistance that is critically needed in order to develop novel treatment strategies.

In our study, decitabine reestablished cisplatin susceptibility in resistant BC cells by increasing ASS1 expression. Our experimental results demonstrate the epigenetic regulatory mechanisms of *ASS1* and *SAT1* and their potential contributions to metabolic perturbations that are apparent in the context of drug resistance. This study also provides evidence that therapeutic targeting of metabolic pathways through the use of BENSpm or ADI-PEG 20 may help overcome cisplatin resistance. Furthermore, analysis of tumor tissue samples from BC patients showed that approximately 80% had little to no expression of *ASS1* and *SAT1*, an indication that these genes have profound roles in BC tumorigenesis and development. Although this is out of the scope of this current study, it would be of great interest to evaluate if *ASS1* and/or *SAT1* are predictive indicators of response to adjuvant chemotherapy among assembled BC patient populations.

Global reprogramming of DNA methylation has been linked to the onset and progression of cancer [23, 47]. DNA hypermethylation at promoter regions of tumor suppressor genes often leads to silencing of expression. In contrast, DNA hypomethylation has been reported to induce genome instability and can activate proto-oncogenes [48, 49]. DNA-demethylating agents, such as 2′-deoxy-5-azacitidine/decitabine (DAC) and 5-azacitidine/azacitine (AZA), can induce global DNA demethylation in tumor cells when they are transiently given at low doses [50, 51]. DAC and AZA can also reverse epigenetic silencing and reactivate tumor suppressor gene expression, which might contribute to antitumor effects. In non-cancer diseases, such as myelodysplastic syndrome (MDS), the FDA has approved AZA and DAC as treatment options. Next-generation DNMT inhibitors and oral formulations are also currently under development. However, epigenetic therapies alone may not be effective in treating human cancers. They are likely best when combined with other modalities, such as chemotherapies or immunotherapies. Thus, there are a series of ongoing clinical trials using DNMT inhibitors in combination with conventional regimens for many cancer types [52].

Our current study further investigated the epigenetic landscape of cisplatin-resistant BC and found that resistance may be associated with modifications in the arginine metabolome via ASS1, the rate-limiting enzyme in arginine synthesis. Loss of ASS1 drives cancer cells to become dependent on extracellular arginine, effectively converting these cells into arginine auxotrophs. ASS1 deficiency has been observed in various other cancer types, including hepatocellular carcinoma, melanoma, myxofibrosarcoma, mesothelioma, prostate cancer, and renal cancer [53-57]. In terms of BC, ASS1 deficiency is particularly common in urothelial carcinoma, small cell, and squamous cell carcinoma subtypes [57, 58]. Based on this, ADI-PEG 20 is currently being tested in clinical trials for many cancer types (https://clinicaltrials.gov, identifiers NCT01497925, NCT02029690, and NCT02101593, etc.). Given previous findings demonstrating that ASS1 expression is negatively correlated with the anti-cancer effects of ADI-PEG 20 treatment, loss off or reduced ASS1 may be a predictive factor that can determine which patients will benefit from treatment.

Our results also showed that SAT1 overexpression promotes the sensitivity of T24R cells to cisplatin-induced apoptosis. This is consistent with a previous report showing that SAT1 overexpression can lead to the depletion of spermidine and spermine, while simultaneously increasing polyamine oxidation [59]. This depletion of spermidine and spermine causes apoptosis through a mitochondria-mediated pathway [59]. Since mitochondrial dysfunction and redox imbalance are known to contribute to cancer, it would be interesting to investigate the connection between polyamine metabolism and cisplatin resistance in the context of mitochondrial function, metabolic pathways, and cell signaling. Although we did not delve into this area in our study, we believe that a better understanding of the potential link between nitrogen metabolism and cisplatin resistance in BC may provide supplemental information on epigenetic regulation of metabolism.

In summary, our present study suggests that the epigenetic regulation of certain amino acids and polyamine metabolic enzymes is significantly altered in BC and that this change may play a critical role in BC chemoresistance. The main results from our study are expected to lead to a novel molecular signature

that could potentially be applied in clinical tests for guiding treatment decisions. Thereby, these results could pave a path towards identification of novel drugs that can decrease chemoresistance. Our data also suggests the involvement of polyamine and arginine pathways in BC chemoresistance. The experimental results from this study contribute to a better understanding of the dependence of BC on exogenous polyamine or arginine, which may potentially lead to the capability of accurately distinguishing MIBC patients who will not develop cisplatin resistance. The status of SAT1 or ASS1 expression may be a reliable method of identifying which MIBC patients will or will not develop cisplatin resistance after chemotherapy. Furthermore, this study has significant clinical relevance to public health; it provides pre-clinical evidence that enhancing polyamine catabolism or arginine biosynthesis may overcome cisplatin resistance in aggressive BC.

Methods

Reagents

ADI-PEG 20 was generously provided by Polaris Pharmaceuticals (San Diego, CA). A vector construct encoding FLAG-tagged human SAT1 (pCMV7.1 3XFLAG-hSAT1) was provided by Dr. MH Park [60]. BENSpm, a SAT1 agonist, was a gift from Dr. David Oupicky at the University of Nebraska Medical Center. Decitabine, a DNMT inhibitor, was obtained from Selleckchem (Cat. No. S1200). The following antibodies were purchased, as indicated: β-actin (Sigma, USA), SAT1 (Thermo Fisher Scientific, USA), ASS1 (Cell Signaling Technology, USA), PARP, and cleaved-PARP (Cell Signaling Technology, USA).

Tissue culture

Three human BC cell lines (T24, J82, and RT4) were procured from the American Type Culture Collection (Manassas, VA). Cisplatin-sensitive (T24S, J82S, and RT4S) or resistant (T24R, J82R, and RT4R) cells were constructed and characterized in our laboratory [38]. Experiments were carried out in accordance with approved protocols and all methods adhered to institutional guidelines.

Accessibility assay

The principle of this assay has been described and published prior [39, 61]. Cell pellets were washed twice with ice-cold PBS buffer then resuspended in 1 mL PBS. Lysis buffer (10 mM Tris (pH 7.4), 10 mM NaCl, 3 mM $MgCl_2$, 0.1 mM EDTA, 0.5% NP-40) was then added and the lysates were centrifuged at 1006 rcf for 5 min at 4 °C. The supernatant was removed and the pellets were suspended in 2 mL of wash buffer (10 mM Tris (pH 7.4), 10 mM NaCl, 3 mM $MgCl_2$, 0.1 mM EDTA). This suspension was then divided into two microcentrifuge tubes (no enzyme and M.SssI reactions) and centrifuged again at 1006 rcf for 5 min at 4 °C. The supernatant was removed and the following was added to each tube: 84.25 µL 1X NEBuffer 2, 7.5 µL 10X NEBuffer 2, 45 µL 1 M sucrose, 1.5 µL 32 mM S-adenosylmethionine (SAM), and 12.5 µL 4 U/µL M.SssI (or H_2O for the no enzyme tube). The reaction mixtures were incubated at 37 °C for 15 min. Pre-warmed (37 °C) 300 µL stop solution (10 mM Tris-HCl (pH 7.9), 600 mM NaCl, 1% SDS, 0.1 mM EDTA) and 6 µL of Proteinase K were added to each tube, and the reaction mixtures were incubated at 55 °C for 16 h. DNA was then purified via phenol/chloroform extraction and ethanol precipitation, and then redissolved in 20 µL of ddH_2O for subsequent analyses.

Quality control M.SssI treatment

In total, 1 µg of no enzyme or M.SssI-treated DNA was subjected to bisulfite conversion using the Zymo EZ DNA Methylation Kit (using the Illumina Infinium® Methylation Assay alternative incubation conditions). Bisulfite (BS)-converted DNA was then analyzed by the high-resolution melt (HRM) method using the Bio-Rad Precision Melt Supermix (Catalog #172-5110) (reaction mix: 10 µL Precision Melt Supermix, 0.8 µL of 5 µM primer mix, 1 µL BS-converted DNA, 8.2 µL ddH_2O) (PCR protocol: 95 °C for 00:02:00, [95 °C for 00:00:10, 58 °C for 00:00:30, plate read, 72 °C for 00:00:30] × 60 cycles, 95 °C for 00:00:30, 60 °C for 00:01:00, melt curve 65 °C to 90 °C [00:00:10 and plate read at each degree]). Primer sequences: ACTB: 5'-AGAGGGGGTAAAAAAATGTTGTAT-3', 5'-TCGAACCATAAAAAACAACTTTC-3'; GADPH: 5'-TTTTAAGATTTTGGGTTGGGT-3', 5'-CTATCGAACAAAAAAAACAAAAAAC-3'; C1D: 5'-TTTTTGGAGAAGAGTTAAGGAGTAGG-3'; 5'-ACTCCAATCTCCCGAAAAAC-3'; RPLP0: 5'-AGGTGGTAGTAGTTTAGAGTAAGTTTT-3', 5'-CGAATACAAACAACCATTAAATA-3'. Proper M.SssI treatment was verified by a shift in melting curves upon methylation. For HM450 analysis, >0.5 µg of BS-treated DNA samples with verified M.SssI treatment were submitted.

Infinium® HumanMethylation450 BeadChip assay and data processing

The amount of bisulfite-converted DNA and the completion of bisulfite conversion were determined using a panel of MethyLight-based quality control (QC) tests, as described previously [62]. All the samples that passed the QC tests were subjected to the HM450 assay data production [49].

The HM450 probes interrogate the methylation statuses of ~485,000 CpG sites, which covers 99% of RefSeq genes, 96% of CpG islands, and spans promoters 5′ UTRs, first exons, gene bodies, and 3′ UTRs. The probe list was then filtered to remove probes with a detection p-value > 0.05 and those located within 15 base pairs of a single-nucleotide polymorphism, mapped to multiple locations, or are on sex chromosomes. The end result is a dataset of corrected beta-values for 385,826 probes that cover ~19,500 genes. The intensities of methylation-specific probes over the signals of unmethylated-specific probes were computed as M values [63]. The M values from the arrays were normalized using the quantile method [64].

Chromatin accessibility analysis

The beta value method with methylation data was used to analyze bisulfite-treated DNA as described in a previous study [39]. Briefly, The accessibility scale was defined as the beta value of M.SssI-treated cells minus the beta value of the no-enzyme control (delta-beta), defined on a 0–1 scale, after removing the probes with delta-beta <0. Accessible probes were defined as delta-beta >0.2.

Identification of differentially expressed genes

To identify differentially expressed genes (DEGs) between T24S and T24R cells, we performed the integrated hypothesis testing method [65, 66]. Briefly, the *T* value, $\log_2$-median ratios, and *Z* values for rank-sum differences were computed for each gene. Empirical distributions of the null hypothesis were estimates for the *T* values, $\log_2$-median ratios, and *Z* values of the genes after permuting the samples. For each gene, adjusted P-values of its observed *T*-values, $\log_2$-median ratios, and rank-sum ratios were computed using their corresponding empirical distributions in a two-tailed test. The individual P-values from the two tests were then combined and the false discovery rate (FDR) was computed using the Stouffer's method [65, 66]. The DEGs were chosen based on their FDR and fold change (FDR<0.05 and $\log_2$-fold-change≥1.0).

Functional enrichment analysis

Enrichment analysis of gene ontology biological processes (GOBPs) and KEGG pathways for the genes listed as DMGs and DEGs was performed using the DAVID software [67].

Construction of a network model

To construct a network model describing cisplatin resistance in BC cells, we first selected the subsets of genes from Clusters 1 and 2 that were involved in metabolic processes. We then collected the interaction data regarding these genes from the STRING database (Ver. 10.5) and used this information to reconstruct a network model [68]. Finally, the network model was visualized using Cytoscape [69]. The nodes in the network model represent the genes distributed according to the metabolic pathway in which they are involved.

Quantitative RT-PCR analysis

Total RNA was purified using the MagNA Pure Compact RNA Isolation Kit (Roche), according to the manufacturer's instructions. The cDNA was then synthesized using the iScript cDNA Synthesis Kit (Bio-Rad), which was followed by qPCR using iTaq Universal SYBR Green Supermix (Bio-Rad) on an ABI 7500 Fast Real-Time PCR System (Life Technologies). The annealing temperature for qPCR was set to 60 °C and actin-beta (ACTB) was used as an internal control for normalization of gene expression.

Western blot analysis

The collected cells were washed twice with ice-cold PBS and lysed with a whole-cell extract lysis buffer (Bio-Rad) with a protease inhibitor cocktail (Thermo Fisher). Protein levels were measured and cell lysates containing 25 μg of proteins were used for SDS-PAGE. Proteins were then electrophorectically transferred onto nitrocellulose membranes for further processing. After blocking for 30 min with 5% milk in tris-buffered saline with tween 20 (TBST), the membranes were incubated with a specific primary antibody overnight at 4 °C. Following this step, the membranes were washed and incubated with secondary, species-specific horseradish peroxidase-conjugated antibodies. Immunoreactive proteins were detected via chemiluminescence (Pierce Laboratories) and band intensities were quantified using ImageJ.

Cell survival assay

T24 cell lines were incubated with cisplatin, BENSpm, and/or ADI-PEG 20, as indicated. Cell survival after treatment was determined by measuring cell viability using MTS reagents (Promega Corporation, Madison, WI), according to the company's protocols.

Reactive oxygen species (ROS) measurement

To determine intracellular ROS levels, cells were stained using dischlorofluorescein diacetate (DCF-DA) (Sigma-Aldrich). Cells were seeded into 6-well plates at a density of 2×10^5 cells/well. At 24 h post seeding, DCF-DA was added to the wells under low-light conditions and the plates were incubated in the dark at room temperature for 20 min. The cells were then washed twice with PBS and fluorescence intensities were determined using the FACS Calibur

Flow Cytometer. Data was analyzed using FlowJo software.

Statistical analysis

Statistical analyses were conducted using MATLAB (Ver. 9.2). Data was expressed as mean ± standard deviation (SD). For most of the biochemical data analyses, Student's *t*-test was used. Differences were considered statistically significant when $*p < 0.05$, or $**p < 0.01$.

Abbreviations

ADI: arginine deiminase; *ALDH18A1*: aldehyde dehydrogenase 18 family member A1; *ALDH2*: aldehyde dehydrogenase 2; *ALDH7A1*: aldehyde dehydrogenase 7 family member A1; *ARG2*: arginase 2; *ASS1*: argininosuccinate synthase 1; AZA: 5-azacitidine/azacitine; BC: bladder cancer; *CKB*: creatine kinase B; DAC: 2'-deoxy-5-azacitidine/ decitabine DCF-DA: dichlorofluorescein diacetate; DEGs: differentially expressed genes; DMGs: differentially methylated genes; DNMT: DNA methyltransferase; FD: fold-change; FDR: false discovery rate; *GLUD1*: glutamate dehydrogenase 1; *GLUD2*: glutamate dehydrogenase 2; GOBPs: gene ontology biological processes; MDS: myelodysplastic syndrome; MIBC: muscle invasive bladder cancer; *NAGS*: N-acetylglutamate synthase; NMIBC: non-muscle invasive bladder cancer; PARP: poly-(ADP-ribose)-polymerase; PBS: phosphate-buffered saline; *P4HA1*: prolyl-4-hydroxylase subunit alpha 1; *P4HA2*: prolyl-4-hydroxylase subunit alpha 2; *PYCR1*: pyrroline-5-carboxylate reductase 1; ROS: reactive oxygen species; SD: standard deviation; *SAT1*: spermidine/spermine N^1-acetyltransferase; T24R: cisplatin-resistant T24R cells; T24S: cisplatin-sensitive T24R cells.

Supplementary Material

Supplementary figure and table legends,
supplementary figures, supplementary tables 4-5.
http://www.thno.org/v08p4520s1.pdf
Supplementary table 1.
http://www.thno.org/v08p4520s2.xlsx
Supplementary table 2.
http://www.thno.org/v08p4520s3.xlsx
Supplementary table 3.
http://www.thno.org/v08p4520s4.xlsx

Acknowledgements

The authors acknowledge support from National Institutes of Health (1U01DK103260, 1R01DK100974, U24 DK097154, NIH NCATS UCLA CTSI UL1TR000124), Department of Defense (W81XWH-15-1-0415), Centers for Disease Controls and Prevention (1U01DP006079), IMAGINE NO IC Research Grant, the Steven Spielberg Discovery Fund in Prostate Cancer Research Career Development Award, the U.S.-Egypt Science and Technology Development Fund by the National Academies of Sciences, Engineering, and Medicine (to J.K.), the Vicky Joseph Cancer Research Foundation, and Kure it for Cancer Research (to G.L.). J.K. is former recipient of Interstitial Cystitis Association Pilot Grant, a Fishbein Family IC Research Grant, New York Academy of Medicine, and Boston Children's Hospital Faculty Development. The funders had no role in the design, data collection and analysis, decision to publish or preparation of the manuscript.

Authors' Contributions

JK conceptualized and designed the study, led the fund acquisition process, and overviewed the literature analysis and drafting of the manuscript. AY and DJW performed HM450 analysis and nucleosome accessibility analysis. AY contributed to pre-processing of samples. MP, DJW, and GL provided scientific insights to data analyses. SY and MK performed full data analysis and visualization of the data. AG, DJW, and MP assisted in the preparation of the manuscript. All authors read and approved the final manuscript.

Competing Interests

The authors have declared that no competing interest exists.

References

1. Kiemeney LA, Witjes JA, Verbeek AL, Heijbroek RP, Debruyne FM. The clinical epidemiology of superficial bladder cancer. Dutch South-East Cooperative Urological Group. British journal of cancer. 1993; 67: 806-12.
2. Borden LS, Jr., Clark PE, Hall MC. Bladder cancer. Current opinion in oncology. 2003; 15: 227-33.
3. Hall MC, Chang SS, Dalbagni G, Pruthi RS, Seigne JD, Skinner EC, et al. Guideline for the management of nonmuscle invasive bladder cancer (stages Ta, T1, and Tis): 2007 update. The Journal of urology. 2007; 178: 2314-30.
4. Kamat AM. Commentary on "Surveillance guidelines based on recurrence patterns after radical cystectomy for bladder cancer: the Canadian Bladder Cancer Network experience." Yafi FA, Aprikian AG, Fradet Y, Chin JL, Izawa J, Rendon R, Estey E, Fairey A, Cagiannos I, Lacombe L, Lattouf JB, Bell D, Saad F, Drachenberg D, Kassouf W. Department of Surgery (Urology), McGill University, Quebec, Canada: BJU Int 2012;110(9):1317-23 [Epub 2012 Apr 13]. Urologic oncology. 2013; 31: 717-8.
5. Large MC, Cohn JA, Steinberg GD. Optimal risk-adapted surveillance strategies for NMIBC, including upper tract imaging. The Urologic clinics of North America. 2013; 40: 305-15.
6. Babjuk M, Oosterlinck W, Sylvester R, Kaasinen E, Bohle A, Palou-Redorta J. EAU guidelines on non-muscle-invasive urothelial carcinoma of the bladder. European urology. 2008; 54: 303-14.
7. Stenzl A, Cowan NC, De Santis M, Kuczyk MA, Merseburger AS, Ribal MJ, et al. Treatment of muscle-invasive and metastatic bladder cancer: update of the EAU guidelines. European urology. 2011; 59: 1009-18.
8. Black PC, Dinney CP. Growth factors and receptors as prognostic markers in urothelial carcinoma. Current urology reports. 2008; 9: 55-61.
9. Apolo AB, Grossman HB, Bajorin D, Steinberg G, Kamat AM. Practical use of perioperative chemotherapy for muscle-invasive bladder cancer: summary of session at the Society of Urologic Oncology annual meeting. Urologic oncology. 2012; 30: 772-80.
10. Schwentner C, Stenzl A, Gakis G. Monitoring high-risk bladder cancer. Current opinion in urology. 2012; 22: 421-6.
11. Sonpavde G, Sternberg CN. Neoadjuvant chemotherapy for invasive bladder cancer. Current urology reports. 2012; 13: 136-46.

12. Feber A, Dhami P, Dong L, de Winter P, Tan WS, Martinez-Fernandez M, et al. UroMark-a urinary biomarker assay for the detection of bladder cancer. Clinical epigenetics. 2017; 9: 8.
13. Li HT, Duymich CE, Weisenberger DJ, Liang G. Genetic and Epigenetic Alterations in Bladder Cancer. International neurourology journal. 2016; 20: S84-94.
14. Lopez JI, Angulo JC, Martin A, Sanchez-Chapado M, Gonzalez-Corpas A, Colas B, et al. A DNA hypermethylation profile reveals new potential biomarkers for the evaluation of prognosis in urothelial bladder cancer. APMIS : acta pathologica, microbiologica, et immunologica Scandinavica. 2017; 125: 787-96.
15. Hesson LB, Patil V, Sloane MA, Nunez AC, Liu J, Pimanda JE, et al. Reassembly of nucleosomes at the MLH1 promoter initiates resilencing following decitabine exposure. PLoS genetics. 2013; 9: e1003636.
16. Jimenez-Useche I, Ke J, Tian Y, Shim D, Howell SC, Qiu X, et al. DNA methylation regulated nucleosome dynamics. Scientific reports. 2013; 3: 2121.
17. You JS, Jones PA. Cancer genetics and epigenetics: two sides of the same coin? Cancer cell. 2012; 22: 9-20.
18. Silverman LR, Greenberg P, Raza A, Olnes MJ, Holland JF, Reddy P, et al. Clinical activity and safety of the dual pathway inhibitor rigosertib for higher risk myelodysplastic syndromes following DNA methyltransferase inhibitor therapy. Hematological oncology. 2015; 33: 57-66.
19. Treppendahl MB, Kristensen LS, Gronbaek K. Predicting response to epigenetic therapy. The Journal of clinical investigation. 2014; 124: 47-55.
20. Portella G, Battistini F, Orozco M. Understanding the connection between epigenetic DNA methylation and nucleosome positioning from computer simulations. PLoS computational biology. 2013; 9: e1003354.
21. Huff JT, Zilberman D. Dnmt1-independent CG methylation contributes to nucleosome positioning in diverse eukaryotes. Cell. 2014; 156: 1286-97.
22. Yoo CB, Jones PA. Epigenetic therapy of cancer: past, present and future. Nature reviews Drug discovery. 2006; 5: 37-50.
23. Jones PA. Functions of DNA methylation: islands, start sites, gene bodies and beyond. Nature reviews Genetics. 2012; 13: 484-92.
24. Kelly TK, Liu Y, Lay FD, Liang G, Berman BP, Jones PA. Genome-wide mapping of nucleosome positioning and DNA methylation within individual DNA molecules. Genome research. 2012; 22: 2497-506.
25. Masui K, Cavenee WK, Mischel PS. mTORC2 in the center of cancer metabolic reprogramming. Trends in endocrinology and metabolism: TEM. 2014; 25: 364-73.
26. Masui K, Cavenee WK, Mischel PS. mTORC2 dictates Warburg effect and drug resistance. Cell Cycle. 2014; 13: 1053-4.
27. Phan LM, Yeung SC, Lee MH. Cancer metabolic reprogramming: importance, main features, and potentials for precise targeted anti-cancer therapies. Cancer biology & medicine. 2014; 11: 1-19.
28. Kroemer G, Pouyssegur J. Tumor cell metabolism: cancer's Achilles' heel. Cancer cell. 2008; 13: 472-82.
29. Soga T. Cancer metabolism: key players in metabolic reprogramming. Cancer science. 2013; 104: 275-81.
30. Ferreira LM, Hebrant A, Dumont JE. Metabolic reprogramming of the tumor. Oncogene. 2012; 31: 3999-4011.
31. Phillips MM, Sheaff MT, Szlosarek PW. Targeting Arginine-Dependent Cancers with Arginine-Degrading Enzymes: Opportunities and Challenges. Cancer research and treatment : official journal of Korean Cancer Association. 2013; 45: 251-62.
32. Maze I, Noh KM, Soshnev AA, Allis CD. Every amino acid matters: essential contributions of histone variants to mammalian development and disease. Nature reviews Genetics. 2014; 15: 259-71.
33. Cheon DJ, Walts AE, Beach JA, Lester J, Bomalaski JS, Walsh CS, et al. Differential expression of argininosuccinate synthetase in serous and non-serous ovarian carcinomas. The journal of pathology Clinical research. 2015; 1: 41-53.
34. McAlpine JA, Lu HT, Wu KC, Knowles SK, Thomson JA. Down-regulation of argininosuccinate synthetase is associated with cisplatin resistance in hepatocellular carcinoma cell lines: implications for PEGylated arginine deiminase combination therapy. BMC cancer. 2014; 14: 621.
35. Szlosarek PW, Luong P, Phillips MM, Baccarini M, Stephen E, Szyszko T, et al. Metabolic response to pegylated arginine deiminase in mesothelioma with promoter methylation of argininosuccinate synthetase. Journal of clinical oncology : official journal of the American Society of Clinical Oncology. 2013; 31: e111-3.
36. Chang X, Monitto CL, Demokan S, Kim MS, Chang SS, Zhong X, et al. Identification of hypermethylated genes associated with cisplatin resistance in human cancers. Cancer research. 2010; 70: 2870-9.
37. Pegg AE, Casero RA, Jr. Current status of the polyamine research field. Methods in molecular biology. 2011; 720: 3-35.
38. Kim WT, Kim J, Yan C, Jeong P, Choi SY, Lee OJ, et al. S100A9 and EGFR gene signatures predict disease progression in muscle invasive bladder cancer patients after chemotherapy. Annals of oncology : official journal of the European Society for Medical Oncology. 2014; 25: 974-9.
39. Pandiyan K, You JS, Yang X, Dai C, Zhou XJ, Baylin SB, et al. Functional DNA demethylation is accompanied by chromatin accessibility. Nucleic acids research. 2013; 41: 3973-85.
40. Lee S, Yoon CY, Byun SS, Lee E, Lee SE. The role of c-FLIP in cisplatin resistance of human bladder cancer cells. The Journal of urology. 2013; 189: 2327-34.
41. Kim WJ, Kim EJ, Kim SK, Kim YJ, Ha YS, Jeong P, et al. Predictive value of progression-related gene classifier in primary non-muscle invasive bladder cancer. Molecular cancer. 2010; 9: 3.
42. Synakiewicz A, Stachowicz-Stencel T, Adamkiewicz-Drozynska E. The role of arginine and the modified arginine deiminase enzyme ADI-PEG 20 in cancer therapy with special emphasis on Phase I/II clinical trials. Expert opinion on investigational drugs. 2014; 23: 1517-29.
43. Noon AP, Catto JW. Bladder cancer in 2012: Challenging current paradigms. Nature reviews Urology. 2013; 10: 67-8.
44. Kamat AM, Hegarty PK, Gee JR, Clark PE, Svatek RS, Hegarty N, et al. ICUD-EAU International Consultation on Bladder Cancer 2012: Screening, diagnosis, and molecular markers. European urology. 2013; 63: 4-15.
45. Gakis G, Efstathiou J, Lerner SP, Cookson MS, Keegan KA, Guru KA, et al. ICUD-EAU International Consultation on Bladder Cancer 2012: Radical cystectomy and bladder preservation for muscle-invasive urothelial carcinoma of the bladder. European urology. 2013; 63: 45-57.
46. Sternberg CN, Bellmunt J, Sonpavde G, Siefker-Radtke AO, Stadler WM, Bajorin DF, et al. ICUD-EAU International Consultation on Bladder Cancer 2012: Chemotherapy for urothelial carcinoma-neoadjuvant and adjuvant settings. European urology. 2013; 63: 58-66.
47. Baylin SB, Jones PA. A decade of exploring the cancer epigenome - biological and translational implications. Nature reviews Cancer. 2011; 11: 726-34.
48. Jones PA, Baylin SB. The epigenomics of cancer. Cell. 2007; 128: 683-92.
49. Yang X, Han H, De Carvalho DD, Lay FD, Jones PA, Liang G. Gene body methylation can alter gene expression and is a therapeutic target in cancer. Cancer cell. 2014; 26: 577-90.
50. Shen H, Laird PW. In epigenetic therapy, less is more. Cell stem cell. 2012; 10: 353-4.
51. Tsai HC, Li H, Van Neste L, Cai Y, Robert C, Rassool FV, et al. Transient low doses of DNA-demethylating agents exert durable antitumor effects on hematological and epithelial tumor cells. Cancer cell. 2012; 21: 430-46.
52. Juergens RA, Wrangle J, Vendetti FP, Murphy SC, Zhao M, Coleman B, et al. Combination epigenetic therapy has efficacy in patients with refractory advanced non-small cell lung cancer. Cancer discovery. 2011; 1: 598-607.
53. Khadeir R, Szyszko T, Szlosarek PW. Optimizing arginine deprivation for hard-to-treat cancers. Oncotarget. 2017; 8: 96468-9.
54. Kremer JC, Prudner BC, Lange SES, Bean GR, Schultze MB, Brashears CB, et al. Arginine deprivation inhibits the Warburg effect and upregulates glutamine anaplerosis and serine biosynthesis in ASS1-deficient cancers. Cell reports. 2017; 18: 991-1004.
55. Ohshima K, Nojima S, Tahara S, Kurashige M, Hori Y, Hagiwara K, et al. Argininosuccinate synthase 1-deficiency enhances the cell sensitivity to arginine through decreased DEPTOR expression in endometrial cancer. Scientific reports. 2017; 7: 45504.
56. Panosyan EH, Lin HJ, Koster J, Lasky JL, 3rd. In search of druggable targets for GBM amino acid metabolism. BMC cancer. 2017; 17: 162.
57. Sahu D, Gupta S, Hau AM, Nakashima K, Leivo MZ, Searles SC, et al. Argininosuccinate synthetase 1 loss in invasive bladder cancer regulates survival through general control nonderepressible 2 kinase-mediated eukaryotic initiation factor 2 alpha activity and is targetable by pegylated arginine deiminase. The American journal of pathology. 2016.
58. Allen MD, Luong P, Hudson C, Leyton J, Delage B, Ghazaly E, et al. Prognostic and therapeutic impact of argininosuccinate synthetase 1 control in bladder cancer as monitored longitudinally by PET imaging. Cancer research. 2014; 74: 896-907.
59. Mandal S, Mandal A, Park MH. Depletion of the polyamines spermidine and spermine by overexpression of spermidine/spermine N(1)-acetyltransferase 1 (SAT1) leads to mitochondria-mediated apoptosis in mammalian cells. The Biochemical journal. 2015; 468: 435-47.
60. Lee SB, Park JH, Woster PM, Casero RA, Jr., Park MH. Suppression of exogenous gene expression by spermidine/spermine N1-acetyltransferase 1 (SSAT1) cotransfection. The Journal of biological chemistry. 2010; 285: 15548-56.
61. Becket E, Chopra S, Duymich CE, Lin JJ, You JS, Pandiyan K, et al. Identification of DNA methylation-independent epigenetic events underlying clear cell renal cell carcinoma. Cancer research. 2016; 76: 1954-64.
62. Campan M, Weisenberger DJ, Trinh B, Laird PW. MethyLight. Methods in molecular biology. 2009; 507: 325-37.
63. Irizarry RA, Ladd-Acosta C, Carvalho B, Wu H, Brandenburg SA, Jeddeloh JA, et al. Comprehensive high-throughput arrays for relative methylation (CHARM). Genome research. 2008; 18: 780-90.
64. Bolstad BM, Irizarry RA, Astrand M, Speed TP. A comparison of normalization methods for high density oligonucleotide array data based on variance and bias. Bioinformatics. 2003; 19: 185-93.
65. Hwang D, Rust AG, Ramsey S, Smith JJ, Leslie DM, Weston AD, et al. A data integration methodology for systems biology. Proceedings of the National Academy of Sciences of the United States of America. 2005; 102: 17296-301.
66. Hwang D, Smith JJ, Leslie DM, Weston AD, Rust AG, Ramsey S, et al. A data integration methodology for systems biology: experimental verification. Proceedings of the National Academy of Sciences of the United States of America. 2005; 102: 17302-7.
67. Huang da W, Sherman BT, Lempicki RA. Systematic and integrative analysis of large gene lists using DAVID bioinformatics resources. Nature protocols. 2009; 4: 44-57.

68. Szklarczyk D, Morris JH, Cook H, Kuhn M, Wyder S, Simonovic M, et al. The STRING database in 2017: quality-controlled protein-protein association networks, made broadly accessible. Nucleic acids research. 2017; 45: D362-D8.
69. Shannon P, Markiel A, Ozier O, Baliga NS, Wang JT, Ramage D, et al. Cytoscape: a software environment for integrated models of biomolecular interaction networks. Genome research. 2003; 13: 2498-504.

Proteomics
www.proteomics-journal.com

Quantitative Proteomic Analysis Reveals Caffeine-Perturbed Proteomic Profiles in Normal Bladder Epithelial Cells

*Muhammad Shahid, Minhyung Kim, Austin Yeon, Allen M. Andres, Sungyong You, and Jayoung Kim**

Lower urinary tract symptoms (LUTSs) are highly prevalent among the elderly and negatively impact quality of life. Since caffeinated beverages are enjoyed worldwide and the relationship between LUTS and caffeine is still not fully understood, it would be of particular interest to examine the underlying mechanisms that drive caffeine's influence on LUTS development and progression. The aim of this study is to characterize the effects of caffeine on hTert-immortalized normal bladder epithelial cells by investigating whether exposure to caffeine can cause potential changes in the bladder proteome and/or biological pathways. In labeled LC–MS/MS proteomic analysis, 57 proteins are found as being differentially expressed in caffeine-treated bladder epithelial cells, compared to controls; this included 32 upregulated and 25 downregulated proteins. Further functional gene enrichment analysis reveals that caffeine affects major biological pathways, including those for "muscle contraction" and "chromatin assembly." These findings provide new scientific insights that may be useful in future studies investigating the role of caffeine in bladder dysfunctions.

1. Introduction

It is estimated that by the end of 2018, 2.3 billion individuals will be affected by at least one lower urinary tract symptom (LUTS).[1] These symptoms include urinary storage problems, such as urgency, frequency, nocturia, or voiding problems. LUTS also weighs heavily on overall quality of life; patients report significantly higher mental health issues, lower work productivity, and diminished general health status.[2] The current standard treatment for LUTS involves α-blockers, 5α-reductase inhibitors, and antimuscarinics.[3] However, these are mainly palliative and require consistent maintenance. Consequently, there is a substantial economic burden associated with LUTS.[4] Previous reports have demonstrated that diet and stress play important roles in the development and progression of LUTS.[5] In particular, caffeine, a naturally occurring compound, has been reported to be a potential dietary risk factor in developing LUTS.[6] Caffeine is ubiquitously found in many plants, including cocoa beans, tea leaves, and coffee beans. It is a stimulatory drug that is widely used to prevent sleepiness and can be found in over-the-counter medications, such as some pain remedies. It has also been observed that caffeine may aggravate or worsen urinary symptoms in patients who already have some form of LUTS.[7] In recent years, caffeinated drinks have become a staple of the average diet; more than 85% of adults in the United States regularly consume caffeine.[8] A longitudinal study of caffeine intake in young healthy volunteers found that subjects who regularly drank coffee had significant increases in urinary urgency and frequency.[9] Additionally, a separate study observed that greater coffee intake raised the odds of

Dr. M. Shahid, Dr. M. Kim, A. Yeon, Dr. S. You, Dr. J Kim
Departments of Surgery and Biomedical Sciences
Cedars-Sinai Medical Center
Los Angeles, CA, USA
E-mail: Jayoung.Kim@cshs.org
Dr. A. M. Andres
Department of Medicine
Cedars Sinai Medical Center
Los Angeles, CA, USA
Dr. A. M. Andres
Cedars-Sinai Heart Institute
Los Angeles, CA, USA
Dr. S. You, Dr. J. Kim
Samuel Oschin Comprehensive Cancer Institute
Cedars-Sinai Medical Center
Los Angeles, CA, USA
Dr. J. Kim
University of California Los Angeles
CA, USA
Dr. J. Kim
Department of Urology
Ga Cheon University College of Medicine
Incheon, South Korea

The ORCID identification number(s) for the author(s) of this article can be found under https://doi.org/10.1002/pmic.201800190

DOI: 10.1002/pmic.201800190

 © 2018 WILEY-VCH Verlag GmbH & Co. KGaA, Weinheim

LUTS progression in men and women more than carbonated or citrus beverages.[10] The effects of caffeine have also been studied in the context of bladder cancer (BC); however, rather than finding a negative risk, there have been reported benefits. A case-control study of BC patients in Italy found no causal relationship between caffeine and BC.[11] A separate study found that caffeine may actually benefit BC patients by making cells more susceptible to chemotherapy and apoptosis.[12] Mechanistically, this has been reported to be mediated through caffeine's effects on the tumor suppressor protein, p53.[13]

Despite the potential link between caffeine and LUTS, research into causative mechanisms and functions is lacking. One prior study suggested that caffeine may be facilitating bladder instability and frequent urination by enhancing the activation of neuronal micturition centers through increased expression of transcription factor c-Fos and nerve growth factor.[14] While informative, this study focused primarily on the bladder muscles with little attention on the bladder epithelium, which is more anatomically exposed to urine and its biological/chemical contents. A separate study using a mouse model found that oral caffeine administration resulted in detrusor overactivity and increased bladder sensory signaling.[15] Further studies found similar effects on the detrusor muscle in humans.[16] However, the direct effects of caffeine, its delivery into cells, and its mechanisms remain unestablished.

Our present study sought to examine the cellular effects of caffeine on the bladder epithelium without any pathological conditions. Quantitative and global proteomics analysis found that caffeine can perturb the whole proteome, possibly through the regulation of chromatin assembly in normal bladder epithelial cells.

Significance Statement

Caffeine, a methylxantine that is derived from coffee intake, has been reported to be a potential dietary risk factor in developing lower urinary tract symptoms (LUTS). Despite this known potential link, research into causative mechanisms and functions is lacking. Our unbiased proteomics study revealed that caffeine alters the global proteome in human-immortalized normal bladder epithelial cells and enriches biological pathways related to muscle contraction and chromatin assembly. Our study is clinically significant because it provides the potential mechanisms through which caffeine can provoke LUTS and suggests that the restriction of caffeine intake may be benefit muscle contraction and functional gene expression.

2. Experimental Section

2.1. Cell Culture and Cell Proliferation Assay

Immortalized normal human bladder epithelial cells, TRT-HU1, were maintained as described previously.[17] The TRT-HU1 cell line was constructed and extensively characterized in previously published papers. The passage number of each cell line was below ten, and mycoplasma contamination was tested for monthly via PCR analysis. Cells were cultured in Dulbecco's modified Eagle's medium, containing 10% fetal bovine serum (Invitrogen), 1% penicillin/streptomycin, and 1% L-glutamine (Sigma–Aldrich Corp., St. Louis, MO, USA) in a 37 °C humidified incubator with 5% CO_2. To test cell growth during exposure to caffeine, TRT-HU1 cells were seeded onto six-well plates with a density of 5×10^4 cells per well. Cells were then incubated with standard growth medium with varying doses of caffeine at 0, 0.005, 0.05, or 0.1 mM (C6035, Sigma–Aldrich Corp.) or vehicle for 24, 48, or 72 h. Cell proliferation was measured by manually counting cells using a hemocytometer. The averages of each count were used as the total density of the well after each time point. For crystal violet staining, the culture medium was removed, the cells were fixed with 4% paraformaldehyde at room temperature for 5 min and then stained with 0.05% crystal violet for 15 min. The cells were then washed with tap water, after which the water was removed and the cells were dried out on filter paper. The cell plates were scanned and quantified using 10% acetic acid and measured at an absorbance of 570–590 nm.[18] All experiments were run in triplicate for each cell line, and the data are representative of three independent trials.

2.2. Antibodies and Reagents

Antibodies against various proteins were obtained from the following sources: ACTG2 (ab189385, Abcam), ACTA2 (ab5694, Abcam), MYH2 (ab124937, Abcam), MYH7B (ab172967, Abcam), HISTH2B (ab52599, Abcam), HIST1H2BM (SAB1301739, Sigma), and β-actin (A1978, Sigma). Commercially available horseradish peroxidase (HRP)-conjugated secondary antibodies (7074 and 7076) were obtained from Cell Signaling Technology. All other chemical reagents were procured from Sigma Chemical Corp.

2.3. Quantitative Proteomics

Tandem mass tagging (TMT)-based quantitative proteomics was performed as previously described.[19] Briefly, cellular protein was extracted from caffeine-treated and control cells using 4% SDS-containing buffer. The protein concentration was measured using the Pierce 660 nm Assay Kit. From each sample, 60 μg of protein was digested with trypsin using filter-aided sample preparation and labeled with TMT6plex reagents in parallel.

After TMT labeling, the peptides were merged, desalted with C18 spin columns (Thermo Scientific), and fractionated via high-pH reversed phase liquid chromatography (RPLC) using an Ultimate 3000 XRS System (Thermo Scientific). For high-pH RPLC, about 50 μg TMT-labeled peptides were loaded onto a 100-mm Hypersil GOLD C_{18} column (2.1 mm id, 3 μm particle size, 175 Å pore size; Thermo Scientific), flushed for 3 min with solvent A (10 mM ammonium formate, pH 10), and then separated with a 7-min linear gradient of 0–40% solvent B (10 mM ammonium formate, 95% acetonitrile, pH 10.0). A total of 24 fractions were collected, concentrated into 12 fractions, and dried down in a SpeedVac (Thermo Scientific). Peptides in each fraction were redissolved with 0.2% formic acid and analyzed by LC–MS/MS using an EASY-nLC 1000 connected to an LTQ Orbitrap Elite Mass Spectrometer (Thermo Scientific). Briefly, peptides were loaded

© 2018 WILEY-VCH Verlag GmbH & Co. KGaA, Weinheim

onto a 2-cm trap column (PepMap 100 C18, 75 μm id, 3 μm particles, 100 Å pore size) and separated by a 50-cm EASY-Spray column (PepMap RSLC C_{18}, 75 μm id, 2 μm particles, 100 Å pore size) heated to 55 °C. For low-pH RPLC separation, the mobile phase consisted of 0.1% formic acid in water (phase A) or acetonitrile (phase B). The LC gradient was 4–24% B over 200 min, 24–50% B over 20 min, and 50–100% B over 5 min at a flow rate of 150 nL min^{-1}, followed by 100% B over 15 min at a flow rate of 300 nL min^{-1}.

Mass spectra were acquired in a data-dependent manner, selecting up to the 15 most abundant precursor ions for higher-energy collisional dissociation. The mass resolution for precursor and fragment ions was set to 120 000 and 30 000, respectively. The isolation width was set as 1.5 and the normalized collision energy was set as 40. Database searching and protein quantification was performed by Proteome Discoverer (v2.1), using the SEQUEST algorithm. The acquired raw data were searched against the human Uniprot Protein Sequence Database (released on January 22, 2016, containing 20 985 protein sequences). Searching parameters were set as follows: trypsin, up to two missed cleavage; precursor ion tolerance of 10 ppm and fragment ion tolerance of 0.02 Da; carbamidomethylation of cysteins and TMT6plex modification of lysines and peptide N-term as fixed modifications; and acetylation of protein N-term, oxidation of methionine, and deamidation of asparagines and glutamines as variable modifications. A standard false discovery rate (FDR) of 1% was applied to filter peptide-spectrum matches (PSMs), peptide identifications, and protein identifications.

For protein quantification, peptides with >30% precursor ion interference were excluded to minimize erroneous quantification caused by precursor ion interference. PSM level information was extracted using the Proteome Discoverer.[20] After quantifying each PSM intensity, the peptide intensities were summarized, as described by Niu et al.[21] In brief, this was done in four steps: 1) the normalized $\log_2$ intensity of the PSMs matched to each peptide by the substrate mean PSM from each reporter intensity was centered, 2) outliers were detected using Dixon's *Q*-test and generalized electrostatic discharge test, 3) the mean intensity without outliers was taken, and 4) the grand-mean intensities of the three highest abundant PSMs were added before being mean-centered. Bipartite graphs of peptides and protein groups were generated according to the information of the aligned peptides. Among the proteins in the protein group, we defined the representative protein that had the largest number of peptides or unique peptide.[22] When there were more than proteins with the same number of peptides in the same protein group, we selected the protein that had the higher sequence coverage. We then computed the relative intensity of the protein group using a linear-programming formulation, as previously described.[23]

2.4. Identification of Differentially Expressed Proteins

To identify the differentially expressed proteins (DEPs), we selected proteins that have more than two nonredundant peptides. For the selected proteins, we then performed an one sample *t*-test using $\log_2$-fold changes to compute the significance of *t*-values. For this statistical test, an empirical distribution of the null hypothesis, a protein is not differentially expressed, was estimated by following steps: 1) 100 000 random permutations were applied to the samples, 2) *t*-values were computed using the $\log_2$-fold changes of the randomly permutated samples, and 3) the Gaussian kernel density estimation method was applied to *t*-values. The FDRs of each protein from the one sample *t*-tests were then calculated using Storey's method.[24] The DEPs were identified as those with a FDR < 0.05 and absolute $\log_2$-fold change > 0.58 (1.5 fold). Functional enrichment analysis of DEPs was performed using DAVID software (Ver. 6.8).[25] Significantly enriched cellular processes were selected for if they had a *p*-value < 0.05.

2.5. Western Blot Analysis

Cells were seeded onto 10-cm plates and exposed to 0.05 mM concentrations of caffeine for 72 h. Cells were lysed with RIPA buffer (20 mM Tris, 150 mM NaCl, 1% Nonidet, P-40, 0.1 mM EDTA; Pierce, ThermoFisher) supplemented with a phosphatase inhibitor cocktail (ThermoFisher). The protein concentration of each sample was measured with the Bradford Protein Kit Assay, according to the manufacturer's instructions (Pierce, ThermoFisher). Equal amounts of protein extract were separated by SDS–PAGE and transferred onto a PVDF membrane. The membranes were then blocked with 5% bovine serum albumin or 5% nonfat milk in Tris-buffered saline with 0.1% Tween 20 (TBST [2.42 g L^{-1} Tris–HCl, 8 g L^{-1} NaCl, and 1 mL L^{-1} Tween 20 (pH 7.6)]) and incubated overnight at 4 °C with specific primary antibodies in TBST. The membranes were then incubated with secondary antibodies conjugated with HRP, as described previously. β-actin was used as an internal control. All western blot experiments were run in at least triplicates for each antibody.

2.6. Seahorse Respirometry Assay

TRT-HU1 cells were seeded onto a 24-well Seahorse culture plate at a density of 50 000 cells per well 24 h before the Seahorse assay. Media was then changed to XF Base Medium (pH 7.4) supplemented with 10 mM glucose, 1 mM sodium pyruvate, and 1 mM sodium glutamine. Cells were equilibrated for 1 h in a non-CO_2 incubator at 37 °C before the assay began. Cells were treated with caffeine at 0.05 mM, or 0.5 mM for experiments. Chemical reagents (Sigma) were used at final concentrations, as follows: 1 μM oligomycin—an ATP synthase inhibitor, 1 μM (FCCP) carbonyl cyanide 4-(trifluoromethoxy) phenylhydrazone—an uncoupling agent, and a mixture of 0.5 μM antimycin A—a cytochrome C reductase inhibitor and 0.5 μM rotenone—a complex I inhibitor. Oxygen consumption rate (OCR) and extracellular acidification rate (ECAR) was monitored during the duration of the assay run. OCR and ECAR were monitored before and after addition of caffeine. Results were normalized to protein concentrations determined by BCA assay (Thermo Scientific).

2.7. Statistical Analysis

Student's *t*-test was performed to confirm differential expression of the proteins between two groups. Variables with normal distribution were presented as mean ± SD. All reported *p*-values are two-tailed, with *p*-values < 0.05 indicating statistical significance.

© 2018 WILEY-VCH Verlag GmbH & Co. KGaA, Weinheim

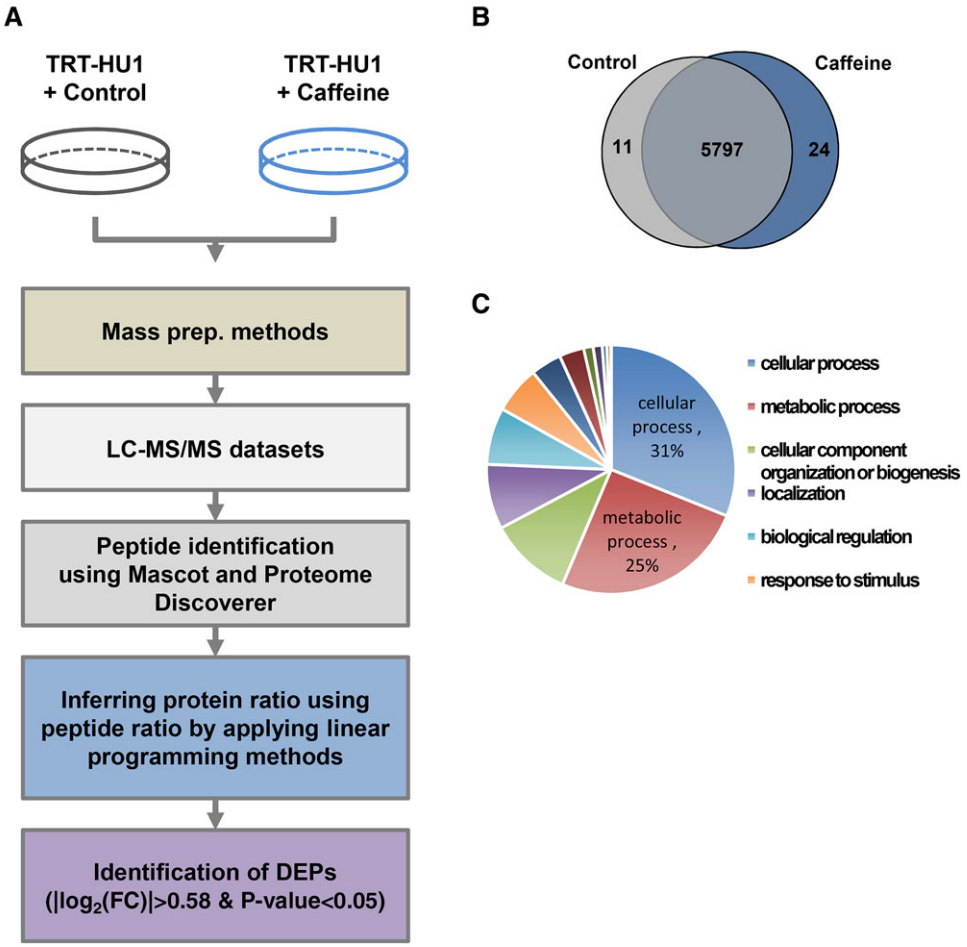

Figure 1. Unbiased proteomics analysis identified proteins in TRT-HU1 cells. A) Experimental scheme describing unbiased global proteomics profiling and bioinformatics analysis. B) Venn diagram depicts number of unique proteins detected in caffeine treated and nontreated normal bladder epithelial cells. C) Pie chart displays functional categories of all the identified proteins.

3. Results

3.1. Quantitative Proteomic Analysis of Normal Bladder Epithelial Cells

Due to the lack of knowledge regarding the effects of caffeine on biological and proteomic perturbations in the normal bladder epithelium, this study aimed to examine the whole proteome alterations caused by caffeine consumption. To gain insight on the underlying mechanism of caffeine on the bladder epithelium, we treated normal bladder epithelial cells with caffeine and performed TMT-based quantitative proteomic analysis, as outlined in **Figure 1**A. Based on previous literature, we opted to use caffeine concentrations within normal physiological consumption.[12,26] Whole-cell lysates in biological duplicates were digested with trypsin. Using LC–MS/MS and followed by bioinformatic analyses, we identified 44 597 peptides corresponding 5832 proteins with more than two peptides in more than two sets of pooled lysates from at least three biological samples per condition. The caffeine-treated group had 5821 identified proteins with high expression, while the control group had 5808 (Figure 1B). We then performed functional categorization of the proteins to check whether our quantitative proteomic analysis was biased by any cellular compartments or biological process-related proteins using Panther software.[27] All the identified proteins can be categorized into 14 cellular processes, including cellular process, metabolic process, cellular component organization of biogenesis, localization, biological regulation, response to stimulus, developmental process, multicellular organismal process, biological adhesion, immune system process, locomotion, reproduction, growth, and cell killing, indicating that this proteome reveals major biological functions of bladder epithelial cells in normal physiology (Figure 1C). In addition to this, we examined the cellular localization of the detected proteins, which showed significant enrichment of eight cellular compartments, including cell part, organelle, macromolecular complex, membrane, extracellular region, cell junction, synapse, and extracellular matrix. (Figure S1, Supporting Information). Collectively, our quantitative proteomic analysis identified a comprehensive list of proteins in all cellular components and illustrated the cellular functions of highly expressed proteins in normal bladder epithelial cells.

© 2018 WILEY-VCH Verlag GmbH & Co. KGaA, Weinheim

3.2. Whole Proteome in Bladder Epithelial Cells Perturbed by Caffeine Treatment

We determined which proteins were differentially expressed after caffeine treatment. DEPs were selected for if they had an absolute $\log_2$-fold change greater than 0.58 and *p*-value less than 0.05. In total, we identified 32 upregulated and 25 downregulated proteins between the control versus caffeine groups (**Table 1** and **2**; **Figure 2**A). As shown in the volcano plot, some DEPs, including PSMC6 (proteasome 26S subunit ATPase 6), RUFY1 (RUN and FYVE domain containing 1), IARS (isoleucyl-tRNA synthetase), MCU (mitochondrial calcium uniporter), NAV1 (neuron navigator 1), RARG (retinoic acid receptor, gamma), etc., were significantly increased with caffeine treatment, while ST13P4 (ST13, Hsp70 interacting protein pseudogene 4), EIF5AL1 (eukaryotic translation initiation factor 5A-like 1), WASH2P (WAS protein family homolog 2 pseudogene), RBMS3 (RNA binding motif single stranded interacting protein 3), etc. decreased (Figure 2B).

Next, to understand the function of the perturbed proteins, we performed gene set enrichment analysis (GSEA) using the hallmark gene sets from the Molecular Signature Database.[28] As a result, we found that the "glycolysis" and "PI3K/AKT/MTOR signaling" gene sets were significantly enriched for by the differentially expressed proteins (Figure 2C). We also checked the enrichment of Kyoto Encyclopedia of Genes and Genomes (KEGG) pathways in the same context and found that the "neurotrophin signaling pathway" and "purine metabolism" were significantly enriched for in caffeine-treated cells (Figure 2D). These results suggest that caffeine may be stimulating the bladder epithelium by altering the activation of the PI3K/AKT/MTOR pathway, neurotrophin signaling, and purine metabolism.

In addition, we conducted separate functional enrichment analyses on each of the 32 up- and 25 downregulated proteins using DAVID.[25] The results suggest that upregulated DEPs were significantly enriched for "actin-myosin filament sliding," "muscle contraction," "purine nucleotide metabolic process," "ATP metabolic process," "autophagy," "response to external biotic stimulus," and "response to other organism." Downregulated DEPs were significantly enriched for "chromatin assembly," "DNA packaging," and "cellular macromolecular complex assembly" (**Figure 3**A). From this, we extracted the list of most significantly upregulated DEPs belonging to "purine nucleotide metabolic process", "autophagy", "muscle contraction", and "response to external biotic stimulus". Additionally, significantly downregulated DEPs for "chromatin assembly" are also listed (Figure 3B and C).

3.3. Biological Effects of Caffeine Treatment on Immortalized Normal Bladder Epithelial Cells

To evaluate the direct effects of caffeine on bladder epithelial cells in vitro, we used TRT-HU1 cells in our study as described in Section 2. After incubating the TRT-HU1 cells in varying concentrations of caffeine (0.005, 0.05, and 0.1 mM) for 24, 48, or 72 h, we sought to determine if caffeine affects or controls cell proliferation and metabolism. We found that the cell proliferation rate of caffeine-treated TRT-HU1 cells was not significantly altered, compared to controls (**Figure 4**A and B).

Table 1. List of upregulated proteins in bladder epithelial cells perturbed by caffeine treatment.

Symbol	Full name	Fold change ($\log_2$)	*p*-value
S100A8	S100 calcium binding protein A8	4.17759	0.000112
ST13	ST13, Hsp70 interacting protein	3.918705	0.000224
SERPINB3	Serpin family B member 3	3.553147	0.000559
SERPINB4	Serpin family B member 4	3.553147	0.000559
WASH3P	WAS protein family homolog 3 pseudogene	2.327444	0.001342
POTEKP	POTE ankyrin domain family member K, pseudogene	2.210099	0.001565
RBMS1	RNA binding motif single stranded interacting protein 1	2.032904	0.001789
KPRP	Keratinocyte proline rich protein	1.526693	0.002124
S100A7	S100 calcium binding protein A7	1.4274	0.002236
TGM1	Transglutaminase 1	1.214751	0.002572
MYH7B	Myosin heavy chain 7B	0.970592	0.003131
MYH3	Myosin heavy chain 3	0.970592	0.003131
MYH1	Myosin heavy chain 1	0.970592	0.003131
MYH7	Myosin heavy chain 7	0.970592	0.003131
MYH8	Myosin heavy chain 8	0.970592	0.003131
MYH2	Myosin heavy chain 2	0.970592	0.003131
MYH13	Myosin heavy chain 13	0.970592	0.003131
MYH4	Myosin heavy chain 4	0.970592	0.003131
MYH7B	Myosin heavy chain 7B	0.970537	0.004025
MYH3	Myosin heavy chain 3	0.970537	0.004025
MYH1	Myosin heavy chain 1	0.970537	0.004025
MYH7	Myosin heavy chain 7	0.970537	0.004025
MYH8	Myosin heavy chain 8	0.970537	0.004025
MYH2	Myosin heavy chain 2	0.970537	0.004025
MYH13	Myosin heavy chain 13	0.970537	0.004025
MYH4	Myosin heavy chain 4	0.970537	0.004025
H2BFS	H2B histone family member S	0.895712	0.005255
S100A9	S100 calcium binding protein A9	0.871394	0.005367
UVRAG	UV radiation resistance associated	0.738812	0.00559
SULT1A4	Sulfotransferase family 1A member 4	0.665067	0.005814
SULT1A1	Sulfotransferase family 1A member 1	0.665067	0.005814
UCHL1	Ubiquitin C-terminal hydrolase L1	0.622981	0.006261
MAGI3	Membrane-associated guanylate kinase, WW and PDZ domain containing 3	0.615023	0.006373
KRT74	Keratin 74	0.598941	0.006485
KRT73	Keratin 73	0.598941	0.006485
ACTA2	Actin, alpha 2, smooth muscle, aorta	0.598824	0.006708
LRRC8E	Leucine rich repeat containing 8 VRAC subunit E	0.594574	0.00682
KRT74	Keratin 74	0.594473	0.006932
KRT73	Keratin 73	0.594473	0.006932
KRT74	Keratin 74	0.594472	0.007156

(*Continued*)

© 2018 WILEY-VCH Verlag GmbH & Co. KGaA, Weinheim

Table 1. Continued.

Symbol	Full name	Fold change (log_2)	*p*-value
KRT73	Keratin 73	0.594472	0.007156
FLCN	Folliculin	0.592834	0.007379
KRT74	Keratin 74	0.589943	0.007491
KRT73	Keratin 73	0.589943	0.007491
CPNE6	Copine 6	0.587267	0.007715
CPNE4	Copine 4	0.587267	0.007715

To examine the effects of caffeine on cell metabolism, we performed Seahorse respirometry analysis. Caffeine treatment over a 12-h period did not alter the OCR (mitochondrial respiration) or ECAR (glycolysis) in TRT-HU1 cells (Figure 4C). Briefly, basal OCR and ECAR measurements (first three time points) were monitored before caffeine (0.05 mM) or vehicle (methanol) was administered. OCR and ECAR continued to be monitored up to 12 h post treatment. Nontreated cells (media administration only) were included to control for any effects of the cells being in the analyzer for an extended period (Figure 4C). We could not detect any changes in both the OCR and ECAR, even after a 12-h treatment with 0.05 mM caffeine. Additional western blot analysis demonstrated that expression of ACTG2 and HIST1H2BM was reduced in the 0.05 mM caffeine-treated cells, while expression of ACTA2, MYH2, and MYH7B was upregulated. The expression of histone H2B and ACTB remained unchanged (Figure 4D).

4. Discussion

Approximately 60% of adults in the United States consume coffee or some other caffeinated beverage. Caffeine, a methylxanthine derived from coffee, is known to affect biological and physiological responses. Low to moderate levels of caffeine intake have been shown to benefit liver function, diabetes, neurological diseases, such as Alzheimer's and Parkinson's, and certain types of cancers. Caffeine is also known to increase urine calcium excretion via translocation of annexin A1 from the apical surface of cells into the cytoplasm. Therefore, caffeine intake is considered to be associated with lower risk of kidney stones.[29] A previous prospective study on the effects of caffeine in coffee suggested that coffee reduction can be a strategy in preventing urinary symptoms, such as frequency, urgency, and bladder pain syndrome.[9]

The aim of this study was to evaluate if caffeine consumption is associated with changes to protein expression in the normal bladder using semiquantitative proteomic analysis. While there are reports about antilipid accumulation via gene expression suppression of proliferator-activated receptor ɣ and CCAAT/enhancer binding protein α in 3T3-L1 adipocytes,[30] or apoptosis induction in various cell lines, the direct effects of caffeine on the bladder remains elusive. Although the amount of caffeine in a cup of coffee varies, it is typically 300–600 mg. Using caffeine concentrations equivalent to typical coffee consumption (one to two cups), we performed unbiased proteomic analysis using LC–MS/MS on bladder epithelial cells treated with caffeine and identified 32 upregulated and 25 downregulated DEPs (log_2-fold change > 0.58; *p*-value < 0.05; Figure 1B; Table 1 and 2). These DEPs were enriched for functions such as actin–myosin filament sliding, muscle contraction,

Table 2. List of downregulated proteins in bladder epithelial cells perturbed by caffeine treatment.

Symbol	Full name	Fold change (log_2)	*p*-value
ST13P4	ST13, Hsp70 interacting protein pseudogene 4	−4.06184	0.000224
EIF5AL1	Eukaryotic translation initiation factor 5A-like 1	−3.14456	0.000559
LOC102723897	–	−2.27955	0.001453
WASH2P	WAS protein family homolog 2 pseudogene	−2.27955	0.001453
RBMS3	RNA binding motif single-stranded interacting protein 3	−2.22487	0.001565
POTEI	POTE ankyrin domain family member I	−1.25276	0.004137
POTEJ	POTE ankyrin domain family member J	−1.25276	0.004137
HIST1H2BM	Histone cluster 1 H2B family member m	−1.07852	0.00436
DES	Desmin	−0.97497	0.004584
TENM1	Teneurin transmembrane protein 1	−0.87939	0.004919
ACTG2	Actin, gamma 2, smooth muscle, enteric	−0.82627	0.005255
HIST1H2BD	Histone cluster 1 H2B family member d	−0.78302	0.006708
HIST1H2BC	Histone cluster 1 H2B family member c	−0.78302	0.006708
HIST2H2BF	Histone cluster 2 H2B family member f	−0.78302	0.006708
HIST1H2BH	Histone cluster 1 H2B family member h	−0.78302	0.006708
HIST1H2BN	Histone cluster 1 H2B family member n	−0.78302	0.006708
RPL29	Ribosomal protein L29	−0.73583	0.007044
RNF175	Ring finger protein 175	−0.71108	0.007267
TFAP2B	Transcription factor AP-2 beta	−0.65122	0.007715
DLG2	Discs large MAGUK scaffold protein 2	−0.64864	0.007826
RAB3A	RAB3A, member RAS oncogene family	−0.62645	0.00805
ZDHHC13	Zinc finger DHHC-type containing 13	−0.60304	0.009951
EPHA6	EPH receptor A6	−0.60218	0.010063
PRC1	Protein regulator of cytokinesis 1	−0.59503	0.010174
MRPL34	Mitochondrial ribosomal protein L34	−0.5944	0.010286

© 2018 WILEY-VCH Verlag GmbH & Co. KGaA, Weinheim

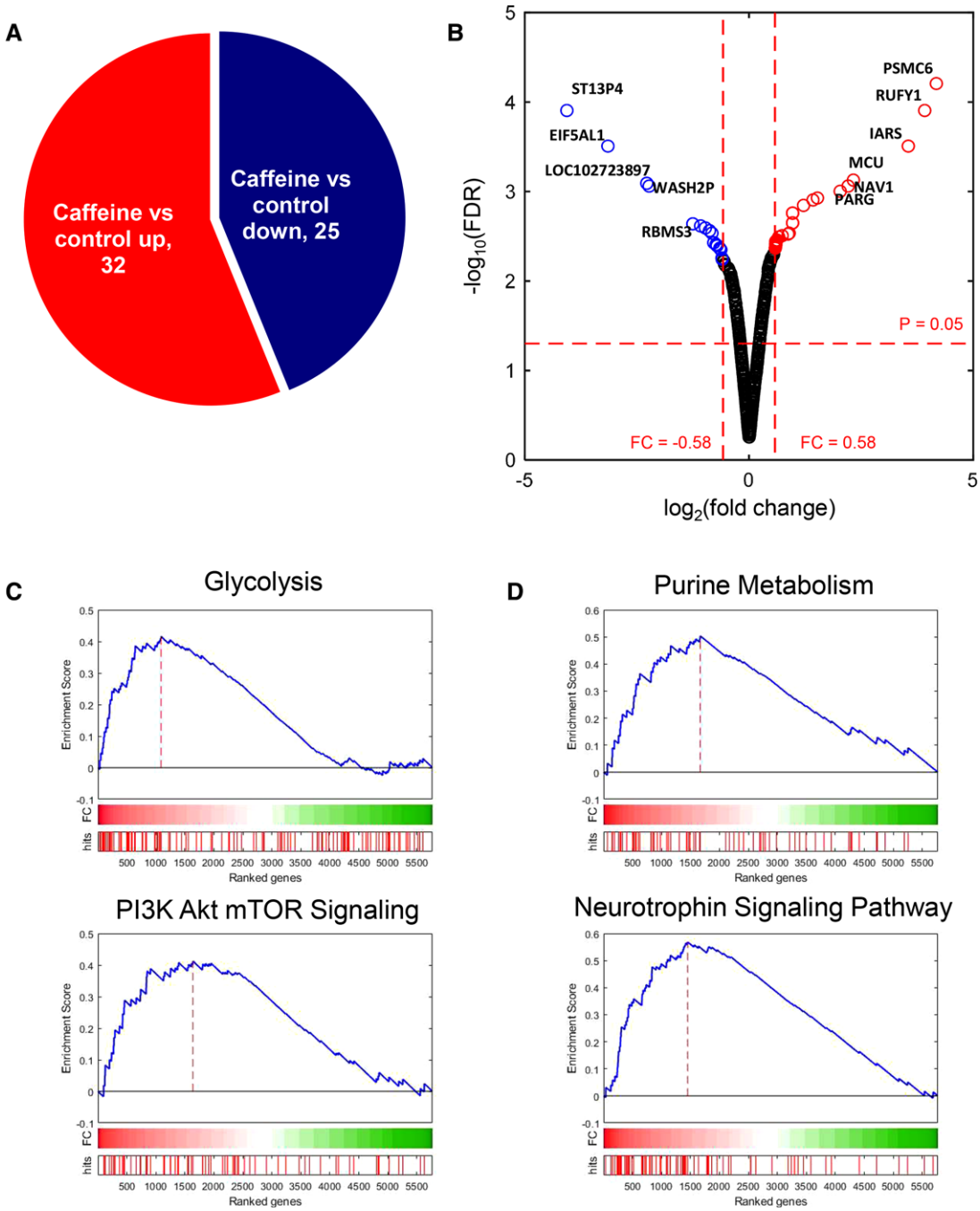

Figure 2. Differentially expressed proteins (DEPs) perturbed by caffeine treatment. A) Pie chart showing the DEPs in presence of caffeine. B) A volcano plot showing the up- or downregulated DEPs due to caffeine in bladder epithelial cells. Up- or downregulated DEPs are marked as red or blue dot. C) GSEA plot of Hallmark gene set MsigDB (Glycolysis and PI3K/AKT/mTOR signaling). D) GSEA plot of KEGG pathway gene sets (Purine Metabolism and Neurotrophin signaling pathway).

and chromatin assembly proteins (Figure 3A). Alterations to the cytoskeleton and the proteins that interact with it have been linked to a wide range of diseases.[31] Caffeine has similar actions with 5′ adenosine monophosphate-activated protein kinase (AMPK), an enzyme whose roles include contraction during energy deprivation in skeletal muscles.[32] Among the proteins involved in the enriched cellular functions, ACTG2, also known as alpha smooth muscle actin, is associated with multiple functions in cell motility, structure, integrity, and intercellular signaling.[33] However, caffeine did not change any of the muscle-associated stabilizing proteins, which regulate the number, or the length, of microtubules.[34] This suggests that increased expression of ACTG2 by caffeine in the bladder may enhance the contractility of bladder and may also be associated with urinary symptoms.

© 2018 WILEY-VCH Verlag GmbH & Co. KGaA, Weinheim

A

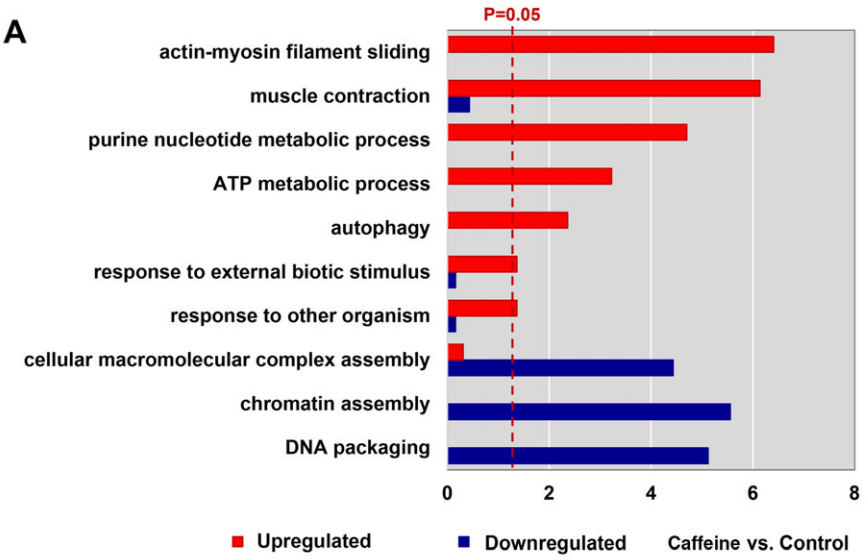

B

Biological process	Upregulated proteins in caffeine treated sample
Purine nucleotide metabolic process	MYH3, MYH4, MYH7, MYH8, SULT1A1, FLCN, MAGI3, SULT1A4
Autophagy	S100A8, S100A9, UCHL1, UVRAG, FLCN
Muscle contraction	ACTA2, MYH1, MYH2, MYH3, MYH4, MYH7, MYH8, MYH13
Response to external biotic stimulus	ACTA2, S100A7, S100A8, S100A9, H2BFS

C

Biological process	Downregulated proteins in caffeine treated sample
Chromatin assembly	HIST1H2BD, HIST1H2BN, HIST1H2BM, HIST1H2BH, HIST1H2BC, HIST2H2BF

Figure 3. Differential enrichment of cellular processes by up- and downregulated proteins perturbed by caffeine. A) Bar plot showing enriched cellular processes in up- or downregulated DEPs. B) List of proteins involved in the enriched cellular processed by upregulated DEPs. C) List of proteins involved in the enriched cellular processed by downregulated DEPs. Proteins reported with cancer are in bold.

Our experimental data suggested that these proteins, such as ACTG2 and HIST1H2BM, become more redundant in bladder epithelial cells upon exposure to caffeine. Although the function of HIST1H2BM as a regulator of caffeine and its effects has not been studied well, it is originally known to be associated with epigenetic regulation in response to DNA methylation.[35]

In this study, we also found that the protein expression level of membrane-associated guanylate kinase inverted 3 (MAGI3) was upregulated in presence of caffeine in normal bladder cells. This was further validated using western blot experiments. MAGI3 localizes to the tight junction in epithelial cells and has originally been identified as a scaffolding protein and tumor suppressor in gliomas and breast cancers. The previous investigations on the role and molecular mechanism revealed that MAGI3 plays a role in phospholipid signaling pathways and suppresses cancer cell proliferation via upregulation of phosphatase and tensin homolog (PTEN), a well-known tumor suppressor.[36] MAGI3 has been found to interact with PTEN, via the PDZ domain of MAGI3, and together contribute to regulation of the kinase activity of AKT/PKB and tumor cell survival. Interestingly, MAGI3 has been reported to be involved in the reduced cell proliferation, arrests of the cell cycle, and inhibition of the migration of glioma cells. Overexpression of MAGI3 resulted in a suppression of β-catenin's transcriptional activity and inhibition the expression of target genes such as Cyclin D1 in glioma cells.[36] More interestingly, mysregulated or modified MAGI3 demonstrated its different roles in cell proliferation and cancer. For example, when MAGI3 is found fused with AKT3, MAGI3-AKT3 contributes to a constitutive phosphorylation and activation of AKT kinase and its downstream targets, such as GSK3b, in breast cancer.[37] Premature cleavage and polyadenylation of MAGI3, MAGI3pPA, was identified to result in an oncogenic protein in breast cancer.[38] Given that overexpressed MAGI3 has a functional link to the suppressed oncogenic characteristics, our data support the hypothesis that caffeine might benefit in the prevention of cancer, which is consistent with previous reports showing that coffee consumption is inversely associated with risk for various cancers, including prostate.[39]

© 2018 WILEY-VCH Verlag GmbH & Co. KGaA, Weinheim

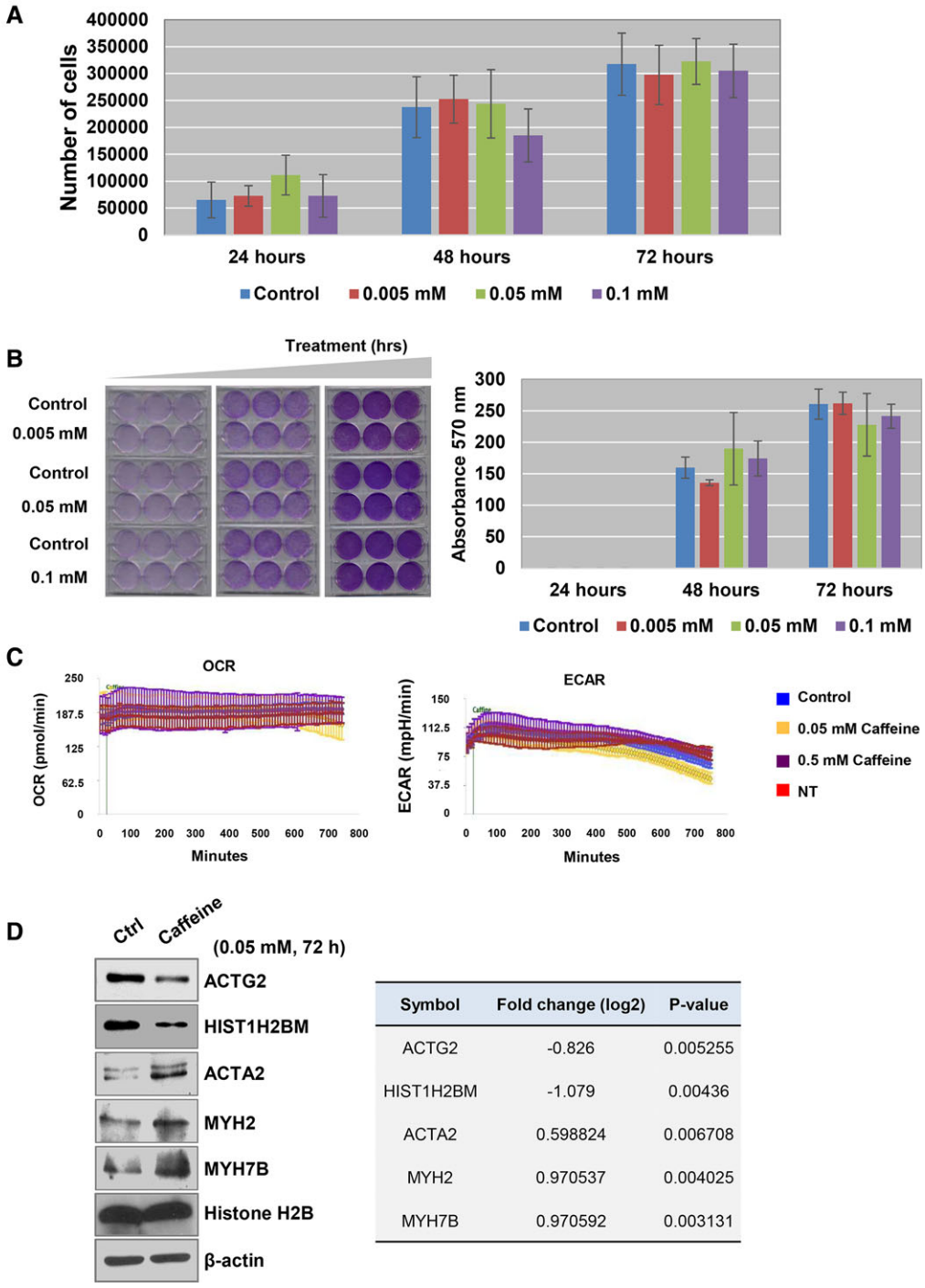

Symbol	Fold change (log2)	P-value
ACTG2	-0.826	0.005255
HIST1H2BM	-1.079	0.00436
ACTA2	0.598824	0.006708
MYH2	0.970537	0.004025
MYH7B	0.970592	0.003131

Figure 4. Cell proliferation was suppressed in response to caffeine treatment. (A and B) TRT-HU1, immortalized normal bladder epithelial cells, were treated with 0.005, 0.05, and 0.1 mM caffeine for 24, 48, or 72 h. A) Cell counting and B) crystal violet proliferation assay were conducted as described in Methods. *$p < 0.05$ (two-sided Student's *t*-test) compared with the control group. Representative images of TRT-HU1 cells treated with caffeine (lower panels). C) Seahorse data showed that caffeine treatment did not alter metabolism of normal bladder epithelial cells. Top, oxygen consumption rate (OCR) chart *$p < 0.05$. Bottom, extracellular acidification rate (ECAR) chart ** $p < 0.05$. D) Quantification results from western blot analysis to measure the expression levels of ACTG2, HIST1H2BM, ACTA2, MYH2, MYH7B, and histone H2B proteins in the presence or absence of caffeine. β-actin was used loading control. The differentially expressed protein levels obtained from proteomics analysis were shown in table (right).

© 2018 WILEY-VCH Verlag GmbH & Co. KGaA, Weinheim

There are several limitations in this study. We are aware that a single proteomic study conducted on one cell line and MS platform is not enough for conclusive statements on whether in vitro protein perturbation due to caffeine can represent the same perturbation in vivo. Urinary caffeine levels can be quantified by ultra high performance LC–MS/MS, and those levels are positively associated with consumption frequency of coffee (area under the curve = 0.849, 95% confidence interval [0.808;0.891]).[40] Also, we conducted two biological replicates under each condition. In general, a small number of replicates has low statistical power. However, we identified DEPs using an empirical null distribution estimated by randomly permuted samples, which should reflect distribution of detected proteins. Furthermore, expression of some DEPs was confirmed using western blot analysis (Figure 4C). Despite these limitations, our experimental findings provide evidence for the potential mechanisms through which caffeine intake is associated with LUTS, suggesting that the restriction of caffeine may benefit muscle contraction and functional gene expression through impaired epigenetic regulation.

Supporting Information

Supporting Information is available from the Wiley Online Library or from the author.

Acknowledgements

M.S. and A.Y. were involved in and performed most of the experiments. S.Y. and M.K. performed proteomics analysis and helped to draft paper. A.A. performed metabolic and biochemical analyses in vitro. J.K. designed and conceived the study and wrote the paper. All authors discussed the results and commented on the manuscript at all stages, and read and approved the manuscript. The authors acknowledge support from National Institutes of Health grants (1U01DK103260, 1R01DK100974, U24 DK097154, NIH NCATS UCLA CTSI UL1TR000124), Department of Defense grants (W81XWH-15-1-0415), Centers for Disease Controls and Prevention (1U01DP006079), IMAGINE NO IC Research Grant, the Steven Spielberg Discovery Fund in Prostate Cancer Research Career Development Award, and the U.S.-Egypt Science and Technology Joint Fund (to J.K.). J.K. is former recipient of Interstitial Cystitis Association Pilot Grant, a Fishbein Family IC Research Grant, New York Academy of Medicine, and Boston Children's Hospital Faculty Development. The funders had no role in the experimental design, data collection, analysis, preparation of the manuscript, or decision to publish. In addition, this article is derived from the Subject Data funded in whole or part by National Academies of Sciences, Engineering, and Medicine (NAS) and The United States Agency for International Development (USAID). Any opinions, findings, conclusions, or recommendations expressed in this article are those of the authors alone, and do not necessarily reflect the views of USAID or NAS.

Conflict of Interest

The authors declare no conflict of interest.

Keywords

biological network, bladder epithelial cells, caffeine, global proteome, lower urinary tract symptoms

Received: May 3, 2018
Revised: August 6, 2018
Published online: October 11, 2018

[1] D. E. Irwin, Z. S. Kopp, B. Agatep, I. Milsom, P. Abrams, *BJU Int.* **2011**, *108*, 1132.
[2] K. S. Coyne, A. J. Wein, A. Tubaro, C. C. Sexton, C. L. Thompson, Z. S. Kopp, L. P. Aiyer, *BJU Int.* **2009**, *103*, 4.
[3] J. Silva, C. M. Silva, F. Cruz, *Curr. Opin. Urol.* **2014**, *24*, 21.
[4] K. S. Coyne, A. Wein, S. Nicholson, M. Kvasz, C. I. Chen, I. Milsom, *J. Manag. Care Pharm.* **2014**, *20*, 130.
[5] D. Robinson, I. Giarenis, L. Cardozo, *Maturitas* **2014**, *79*, 8.
[6] Q. He, Y. Yang, M. Xia, N. Zhang, S. Wu, Y. Xiao, G. Li, S. Zhan, L. Liu, H. Xiao, J. Zhao, *Zhonghua Yi Xue Za Zhi* **2014**, *94*, 428.
[7] M. J. Wells, K. Jamieson, T. C. Markham, S. M. Green, M. J. Fader, *J. Wound Ostomy Continence Nurs.* **2014**, *41*, 371.
[8] B. L. Anderson, L. M. Juliano, J. Schulkin, *J. Women's Health* **2009**, *18*, 1457.
[9] A. Staack, B. Distelberg, A. Schlaifer, J. Sabate, *Neurourol. Urodyn.* **2017**, *36*, 432.
[10] N. N. Maserejian, C. G. Wager, E. L. Giovannucci, T. M. Curto, K. T. McVary, J. B. McKinlay, *Am. J. Epidemiol.* **2013**, *177*, 1399.
[11] F. Turati, C. Bosetti, J. Polesel, A. Zucchetto, D. Serraino, M. Montella, M. Libra, A. Galfano, C. La Vecchia, A. Tavani, *Urology* **2015**, *86*, 1179.
[12] A. M. Bode, Z. Dong, *Cancer Lett.* **2007**, *247*, 26.
[13] Z. He, W. Y. Ma, T. Hashimoto, A. M. Bode, C. S. Yang, Z. Dong, *Cancer Res.* **2003**, *63*, 4396.
[14] Y. S. Cho, I. G. Ko, S. E. Kim, L. Hwan, M. S. Shin, C. J. Kim, S. H. Kim, J. J. Jin, J. Y. Chung, K. H. Kim, *Mol. Med. Rep.* **2014**, *10*, 2931.
[15] R. Kershen, T. Mann-Gow, J. Yared, I. Stromberg, P. Zvara, *J. Urol.* **2012**, *188*, 1986.
[16] J. S. Hockey, C. Wu, C. H. Fry, *BJU Int.* **2000**, *86*, 531.
[17] J. Kim, M. Ji, J. A. DiDonato, R. R. Rackley, M. Kuang, P. C. Sadhukhan, J. R. Mauney, S. K. Keay, M. R. Freeman, L. S. Liou, R. M. Adam, *In Vitro Cell. Dev. Biol. Anim.* **2011**, *47*, 2.
[18] D. Y. Choi, S. You, J. H. Jung, J. C. Lee, J. K. Rho, K. Y. Lee, M. R. Freeman, K. P. Kim, J. Kim, *Proteomics* **2014**, *14*, 1845.
[19] Y. Qu, B. Zhou, W. Yang, B. Han, Y. Yu-Rice, B. Gao, J. Johnson, C. N. Svendsen, M. R. Freeman, A. E. Giuliano, D. Sareen, X. Cui, *Sci. Rep.* **2016**, *6*, 32007.
[20] A. Rinas, J. A. Espino, L. M. Jones, *Anal. Bioanal. Chem.* **2016**, *408*, 3021.
[21] M. Niu, J. H. Cho, K. Kodali, V. Pagala, A. A. High, H. Wang, Z. Wu, Y. Li, W. Bi, H. Zhang, X. Wang, W. Zou, J. Peng, *Anal. Chem.* **2017**, *89*, 2956.
[22] B. Zhang, M. C. Chambers, D. L. Tabb, *J. Proteome Res.* **2007**, *6*, 3549.
[23] H. Lee, S. Chae, J. Park, J. Bae, E. B. Go, S. J. Kim, H. Kim, D. Hwang, S. W. Lee, S. Y. Lee, *Mol. Cell. Proteomics* **2016**, *15*, 3461.
[24] J. D. Storey, R. Tibshirani, *Proc. Natl. Acad. Sci. U. S. A.* **2003**, *100*, 9440.
[25] W. Huang da, B. T. Sherman, R. A. Lempicki, *Nat. Protoc.* **2009**, *4*, 44.
[26] T. Hashimoto, Z. He, W. Y. Ma, P. C. Schmid, A. M. Bode, C. S. Yang, Z. Dong, *Cancer Res.* **2004**, *64*, 3344.
[27] H. Mi, X. Huang, A. Muruganujan, H. Tang, C. Mills, D. Kang, P. D. Thomas, *Nucleic Acids Res.* **2017**, *45*, D183.
[28] A. Liberzon, C. Birger, H. Thorvaldsdottir, M. Ghandi, J. P. Mesirov, P. Tamayo, *Cell Syst.* **2015**, *1*, 417.
[29] a) P. Peerapen, V. Thongboonkerd, *Sci. Rep.* **2016**, *6*, 38536; b) P. M. Ferraro, E. N. Taylor, G. Gambaro, G. C. Curhan, *Am. J. Clin. Nutr.* **2014**, *100*, 1596.
[30] T. Mitani, T. Nagano, K. Harada, Y. Yamashita, H. Ashida, *J. Nutr. Sci. Vitaminol.* **2017**, *63*, 331.

 © 2018 WILEY-VCH Verlag GmbH & Co. KGaA, Weinheim

[31] L. Cicchillitti, R. Penci, M. Di Michele, F. Filippetti, D. Rotilio, M. B. Donati, G. Scambia, C. Ferlini, *Mol. Cancer Ther.* **2008**, *7*, 2070.
[32] T. Egawa, T. Hamada, N. Kameda, K. Karaike, X. Ma, S. Masuda, N. Iwanaka, T. Hayashi, *Metab. Clin. Exp.* **2009**, *58*, 1609.
[33] B. Hinz, G. Celetta, J. J. Tomasek, G. Gabbiani, C. Chaponnier, *Mol. Biol. Cell* **2001**, *12*, 2730.
[34] J. L. Franklin, M. Mirzaei, T. A. Wearne, J. Homewood, A. K. Goodchild, P. A. Haynes, J. L. Cornish, *J. Proteome Res.* **2016**, *15*, 1455.
[35] W. E. Ek, E. W. Tobi, M. Ahsan, E. Lampa, E. Ponzi, S. A. Kyrtopoulos, P. Georgiadis, L. H. Lumey, B. T. Heijmans, M. Botsivali, I. A. Bergdahl, T. Karlsson, M. Rask-Andersen, D. Palli, E. Ingelsson, A. K. Hedman, L. M. Nilsson, P. Vineis, L. Lind, J. M. Flanagan, A. Johansson, C. Epigenome-Wide Association Study, *Hum. Mol. Genet.* **2017**, *26*, 3221.
[36] Q. Ma, Y. Zhang, R. Meng, K. M. Xie, Y. Xiong, S. Lin, Z. L. He, T. Tao, Y. Yang, J. Z. Zhao, J. Q. He, *Biomed. Environ. Sci.* **2015**, *28*, 502.
[37] S. Banerji, K. Cibulskis, C. Rangel-Escareno, K. K. Brown, S. L. Carter, A. M. Frederick, M. S. Lawrence, A. Y. Sivachenko, C. Sougnez, L. Zou, M. L. Cortes, J. C. Fernandez-Lopez, S. Peng, K. G. Ardlie, D. Auclair, V. Bautista-Pina, F. Duke, J. Francis, J. Jung, A. Maffuz-Aziz, R. C. Onofrio, M. Parkin, N. H. Pho, V. Quintanar-Jurado, A. H. Ramos, R. Rebollar-Vega, S. Rodriguez-Cuevas, S. L. Romero-Cordoba, S. E. Schumacher, N. Stransky, K. M. Thompson, L. Uribe-Figueroa, J. Baselga, R. Beroukhim, K. Polyak, D. C. Sgroi, A. L. Richardson, G. Jimenez-Sanchez, E. S. Lander, S. B. Gabriel, L. A. Garraway, T. R. Golub, J. Melendez-Zajgla, A. Toker, G. Getz, A. Hidalgo-Miranda, M. Meyerson, *Nature* **2012**, *486*, 405.
[38] T. K. Ni, C. Kuperwasser, *eLife* **2016**, *5*, e14730.
[39] a) G. Pounis, C. Tabolacci, S. Costanzo, M. Cordella, M. Bonaccio, L. Rago, D. D'Arcangelo, A. Filippo Di Castelnuovo, G. de Gaetano, M. B. Donati, L. Iacoviello, F. Facchiano, i. Moli-sani study, *Int. J. Cancer* **2017**, *141*, 72; b) J. Sado, T. Kitamura, Y. Kitamura, T. Sobue, Y. Nishino, H. Tanaka, T. Nakayama, I. Tsuji, H. Ito, T. Suzuki, K. Katanoda, S. Tominaga; Three-Prefecture Cohort Study Group, *Cancer Sci.* **2017**, *108*, 2079.
[40] D. Petrovic, S. Estoppey Younes, M. Pruijm, B. Ponte, D. Ackermann, G. Ehret, N. Ansermot, M. Mohaupt, F. Paccaud, B. Vogt, A. Pechere-Bertschi, P. Y. Martin, M. Burnier, C. B. Eap, M. Bochud, I. Guessous, *Nutr. Metab.* **2016**, *13*, 81.

 © 2018 WILEY-VCH Verlag GmbH & Co. KGaA, Weinheim

Mansour et al. BMC Urology (2018) 18:100
https://doi.org/10.1186/s12894-018-0413-9

BMC Urology

RESEARCH ARTICLE Open Access

Epidermal growth factor expression as a predictor of chemotherapeutic resistance in muscle-invasive bladder cancer

Ahmed M. Mansour[1,2], Mona Abdelrahim[1], Mahmoud Laymon[1], Mamdouh Elsherbeeny[1], Mohammed Sultan[1], Ahmed Shokeir[1], Ahmed Mosbah[1], Hassan Abol-Enein[1], Amira Awadalla[1], Eunho Cho[3], Vikram Sairam[3], Taeeun D. Park[4], Muhammad Shahid[5] and Jayoung Kim[3,5*]

Abstract

Background: Epidermal growth factor receptor (EGFR) overexpression is believed to be associated with bladder cancer (BC) progression and poor clinical outcomes. In vivo studies have linked EGFR subcellular trafficking and chemo-resistance to cisplatin-based chemotherapies. This has not been studied in the clinical adjuvant setting. We aimed to investigate the prognostic significance of EGFR expression in patients receiving cisplatin-based adjuvant chemotherapy following radical cystectomy for advanced BC.

Methods: The database from the Urology and Nephrology Center at Mansoura University was reviewed. BC patients who were treated with radical cystectomy and adjuvant chemotherapy for adverse pathological features or node positive disease were identified. Patients who underwent palliative cystectomy, had histological diagnoses other than pure urothelial carcinoma, or received adjuvant radiotherapy were excluded from the study. Immunohistochemical staining for EGFR expression was performed on archived bladder specimens. The following in vitro functional analyses were performed to study the relationship of EGFR expression and chemoresponse.

Results: The study included 58 patients, among which the mean age was 57 years old. Majority of patients had node positive disease ($n = 53$, 91%). Mean follow up was 26.61 months. EGFR was overexpressed in 25 cystectomy specimens (43%). Kaplan-Meier analysis revealed that EGFR over-expression significantly correlated with disease recurrence ($p = 0.021$). Cox proportional hazard modeling identified EGFR overexpression as an independent predictor for disease recurrence ($p = 0.04$). Furthermore, in vitro experiments demonstrated that inhibition of EGFR may sensitize cellular responses to cisplatin.

Conclusions: Our findings suggest that EGFR overexpression is associated with disease recurrence following adjuvant chemotherapy for advanced BC. This may aid in patient prognostication and selection prior to chemotherapeutic treatment for BC.

Keywords: EGFR, Bladder cancer, Survival, Adjuvant chemotherapy

* Correspondence: Jayoung.kim@csmc.edu
[3]University of California Los Angeles, Los Angeles, CA, USA
[5]Departments of Surgery and Biomedical Sciences, Samuel Oschin Comprehensive Cancer Institute, Cedars Sinai Medical Center, 8700 Beverly Blvd, Los Angeles, CA 90048, USA
Full list of author information is available at the end of the article

© The Author(s). 2018 **Open Access** This article is distributed under the terms of the Creative Commons Attribution 4.0 International License (http://creativecommons.org/licenses/by/4.0/), which permits unrestricted use, distribution, and reproduction in any medium, provided you give appropriate credit to the original author(s) and the source, provide a link to the Creative Commons license, and indicate if changes were made. The Creative Commons Public Domain Dedication waiver (http://creativecommons.org/publicdomain/zero/1.0/) applies to the data made available in this article, unless otherwise stated.

Background

Bladder cancer (BC) is the second most common genito-urinary malignancy and the fourth most common cancer in the United States (U.S.). Over an estimated $4 billion/year is spent on BC treatment annually in the U.S., making BC one of the most expensive cancer treatments to date [1–3]. Currently, BC is also the most common cancer in Egyptian males, representing about 30% of all cancer types [4]. Thus, BC is a major burden on the health services and economic resources at an international level [5]. Despite the drastic decrease in the prevalence of schistosomiasis in Egypt due to nationwide anti-bilharzial campaigns, there has been an increase in incidences of bladder urothelial carcinoma. This could possibly be due to smoking and carcinogenic chemical exposure [6, 7].

The gold standard therapy for patients with muscle-invasive bladder cancer (MIBC) is radical cystectomy with regional lymphadenectomy. Despite local aggressive therapy, nearly half of patients eventually develop metastasized tumors and, ultimately, die from the disease [8]. In an attempt to improve survival, integration of systemic chemotherapy with surgical management has been suggested to control micrometastasis [9]. However, around 40% of patients receiving neoadjuvant chemotherapy are termed “non-responders”, with a complete pathological down-staging rate of only 14–38% [10, 11]. MIBC patients who do not respond to adjuvant chemotherapy generally have a poor prognosis [12]. The incidence of BC recurrence following chemotherapy remains high with a modest survival advantage of 5–15%. Thus, there is an important and urgent need to identify prognostic marker(s) that will identify patients who are at risk and to better understand the functional contribution of potential predictive markers in aggressive BC.

Prior research has shown that epidermal growth factor receptor (EGFR) overexpression has been associated with BC progression and poor clinical outcomes [13, 14]. In vivo studies have linked EGFR subcellular trafficking and chemo-resistance in many tumor types [15, 16]. However, this has not yet been studied in the clinical adjuvant setting.

In this study, we aimed to investigate the prognostic significance of EGFR expression in patients receiving adjuvant chemotherapy. Our study was conducted on an Egyptian cohort. Our findings suggest that EGFR protein expression may be indicative of aggressive BC and these expression patterns possibly involve direct action on signaling pathways in BC cells.

Methods

Patients and tissue samples

All of the enrolled patients had been treated with similar or identical regimens with at least four cycles of cisplatin-based chemotherapy. Patients previously treated with radical cystectomy and had completed adjuvant chemotherapy for adverse pathological features or node positive diseases were selected. Exclusion criteria were applied to patients who underwent palliative cystectomy, those with histological diagnosis other than pure transitional cell carcinoma, and patients who received adjuvant radiotherapy. Bladder tumors were staged according to the 2002 TNM classification. Disease progression was defined as newly diagnosed distant metastases with a ≥ 20% increment increase in tumor mass following radical cystectomy. Surgical tumor tissues were macro-dissected, typically within 15 min of surgical resection. Each BC specimen was confirmed as representative by analysis of adjacent tissue in fresh frozen sections from radical cystectomy specimens.

Reagents

Cisplatin was purchased from Sigma. Antibodies against EGFR and β-actin were obtained from Cell Signaling Technology (for Western blot analysis), Abcam (for IHC analysis) and Santa Cruz Biotechnology. The ECL detection kit was from BioRad and New England Nuclear. All other biochemical reagents were purchased from Sigma or BD Biosciences.

Immunohistochemical staining

Immunohistochemical (IHC) analysis for EGFR expression was performed on archived bladder specimens. The relationship of EGFR expression and clinical outcomes was assessed. In vitro studies were performed to determine whether EGFR expression was associated with resistance to chemotherapeutic reagents. Paraffin blocks from 58 BC cases were used for immunohistochemical analysis. Tissue sections were cut and placed on Superfrost Plus microscope slides. Using the Benchmark XT automated immunohistochemistry stainer (Ventana Medical Systems, Inc., Tucson, AZ, USA), slides were stained following typical procedure. Detection was done using the Ventana Ultraview DAB Kit (Ventana Medical Systems).

Sections were deparaffinized using EZ Prep solution. CC1 standard (pH 8.4 buffer contained Tris/Borate/EDTA) was used for antigen retrieval. DAB inhibitor (3% H_2O_2, Endogenous peroxidase) was blocked for 4 min at 37 °C temperature. Sections were incubated with an anti-EGFR (Cat # ab32077, Abcam Inc., San Diego, CA, dilution 1/100) primary antibody for 40 min at 37 °C, and then incubated with a secondary antibody of Universal HRP Multimer for 8 min at 37 °C. Slides were then incubated with DAB + H_2O_2 substrate for 8 min, followed by hematoxylin and bluing reagent counterstain at 37 °C. Reaction buffer (pH 7.6 Tris buffer) was used as the washing solution. Staining intensity and proportion of positively-stained cells were evaluated. Staining intensity

Table 1 Baseline characteristics of the patients in this study

Variables		Incidence (SD or %)
Age mean (SD)		57 (6.6)
No. gender (%)	Male	53(91.4)
	Female	5 (8.6)
No. clinical T stage (%)	T2	7 (12.1)
	T3	30 (51.7)
	T4a	18 (31.1)
	T4b	3 (5.2)
No. pathologic T stage (%)	TIS	1 (1.7)
	T1	1 (1.7)
	T2a	7 (12.1)
	T2b	7 (12.1)
	T3a	22 (37.9)
	T3b	15 (25.9)
	T4a	5 (8.6)
No. pathologic N status (%)	N0	5 (8.6)
	N1	14 (24.1)
	N2	37 (63.8)
	N3	2 (3.4)
No. lymphovascular invasion (%)	Yes	45 (77)
	No	13 (23)
No. strong EGFR expression (%)	Yes	10 (17.2)
	No	48 (82.8)

was classified as follows: none (score 0), weak (score 1), moderate (score 2) and strong (score 3). Each specimen was examined and scored separately by two pathologists, and discrepancies were discussed until agreements were reached.

Cell culture and transfection

TCCSUP or T24 human BC cells were purchased from American Type Culture Collection (ATCC, Manassas, VA) and maintained in DMEM or RPMI1640 (Invitrogen, Carlsbad, CA) with 10% FBS and 1% Penicillin/Streptomycin at 37 °C under 5% CO_2. The day before transfection, TCCSUP or T24 cells were trypsinized and counted. Cells were plated in 6-well plate with approximately 6.25×10^5 cells per well in 2 ml of complete growth medium. When cell density reached 80–90% confluence, TCCSUP or T24 BC cells were transiently transfected with 25-50 nM of small interfering RNAs (siRNAs) targeting EGFR (SignalSilence® EGF Receptor siRNA, Cell Signaling #6482) using Lipofactamine 2000. For transfection controls, empty (Ctrl) or non-target siRNAs (siCtrl) were used.

Cell viability assay

Experiments were performed in 6-well plates after cell density reached to about 90% (2×10^3/well). TCCSUP or T24 cells were transfected with various constructs or siRNAs and cisplatin simultaneously for 48 h (siRNA added 2 h before cisplatin). Cells were then incubated with cisplatin containing serum-free medium (RPMI1640

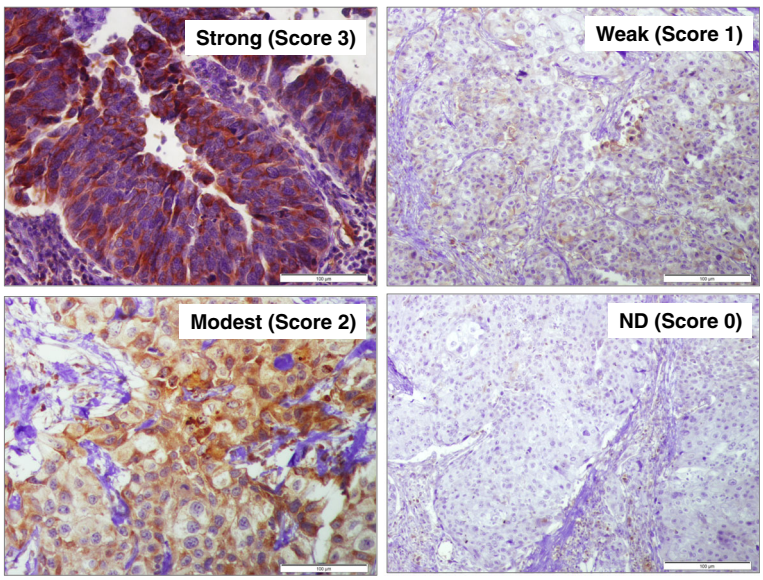

Fig. 1 Representative figures showing IHC slides with different scores. Immunohistochemical staining for EGFR in BC tissue samples. Four representative fields are shown after IHC staining with anti-EGFR (1:1000 dilution). Negative (Score 0), weak (Score 1), intermediate (Score 2), and strong (Score 3). EGFR expression was observed in the cytoplasm, membrane, and/or nucleus in our BC specimens. The intensity of EGFR staining was often heterogeneous within the same cancer tissue.

Table 2 Cox proportional hazard model of overall survival predictors

Covariate	Univariate		Multivariate	
	HR (95% CI)	*P* value	HR (95% CI)	*P* value
Age	1.41 (1.02–2.45)	0.029	1.34 (0.94–1.77)	0.056
Sex (M vs F)	1.88 (1.06–3.34)	0.048	1.48 (0.26–1.80)	0.479
EGFR expression (strong vs negative/weak/moderate)	1.55 (1.30.-2.33)	0.002	1.38 (1.201–2.744)	0.004
Chemotherapy Regimen (MVAC vs GemCis)	1.72 (0.84–3.75)	0.159		
pT stage (T2 or less vs greater than T2)	2.88 (1.92–3.99)	0.003	3.28 (1.54–4.62)	< 0.001
pN stage (N0 vs greater than N0)	2.31 (1.88–2.93)	< 0.001	1.81 (1.23–2.74)	< 0.001

or DMEM) for the indicated time. Cell viability was determined using MTS reagents, as instructed by the company's protocol (Promega Corporation, Madison, WI).

Statistical analysis

Univariate analysis with the Pearson chi-square was performed to analyze associations between strong EGFR expression and pT stage, pN stage, (N0 and greater than N0) and lymphovascular invasion. A Kaplan-Meier estimator curve with the log rank test and a Cox proportional hazard model were used to test whether observed response to chemotherapy predicted disease specific survival.

Results

Baseline characteristics

The study included 58 patients. The mean age of the 57 patients who received adjuvant therapy was 57 ± 6.6 years, and the mean follow-up period was 26.61 months. A majority of patients had node positive disease ($n = 53$, 91%). Forty-five patients (77%) had lymphovascular invasion. Other baseline characteristics of the patients are presented in Table 1.

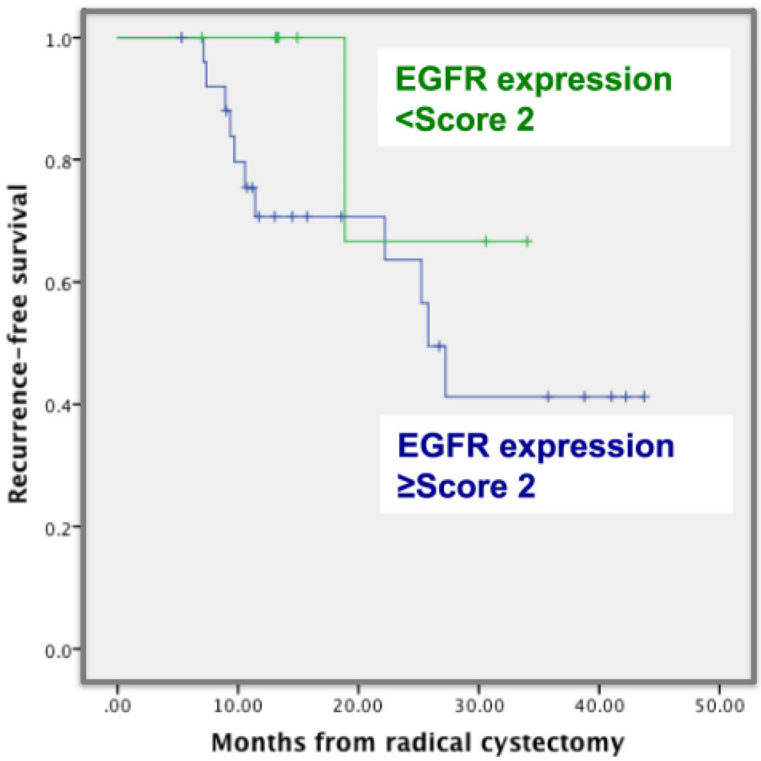

Fig. 2 Cancer-specific survival in BC patients stratified by EGFR staining

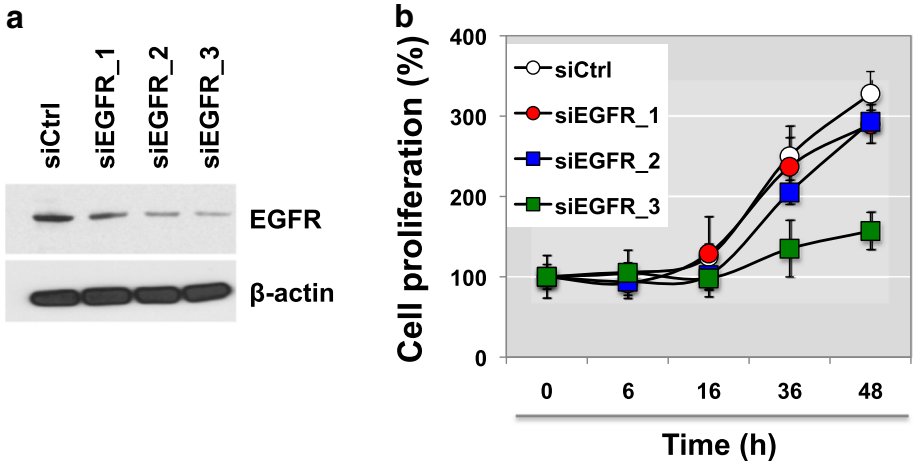

Fig. 3 EGFR expression is associated with drug sensitivity to cisplatin treatment. **a**, **b** TCCSUP cells were transiently transfected with varying doses of siRNA against EGFR. Knockdown of EGFR with control and EGFR-targeted siRNAs shows that proliferation in TCCSUP BC cells decreases in a dose-dependent manner (siEGFR_1, siEGFR_2, siEGFR_3). Cell proliferation assay was performed at the indicated time points (0, 6, 16, 36, or 48 h after transient transfection with siRNAs) using MTT assay at the varying time points. *$p < 0.05$ (Student's t-test)

EGFR expression is negatively correlated with survival

To measure EGFR expression in our cohort, IHC analysis was performed. IHC images were scored from 0 (negative staining) to 3 (highest staining intensity). Representative images are shown in Fig. 1. Cox proportional hazard modeling identified EGFR overexpression as an independent predictor for disease recurrence (OR, 1.38 (1.201–2.744), $p = 0.004$) in the Egyptian cohort (Table 2). Kaplan-Meier analysis revealed that EGFR overexpression (score ≥ 2) significantly correlated with disease recurrence ($p = 0.021$) (Fig. 2).

EGFR silencing alters cell proliferation, viability and response to cisplatin-induced apoptosis

We further performed loss-of-function studies on TCCSUP human BC cells to assess the biological role of EGFR. EGFR was knocked-down using iRNAs and this was subsequently confirmed via western blot analysis (Fig. 3a). Silencing of EGFR did not induce a

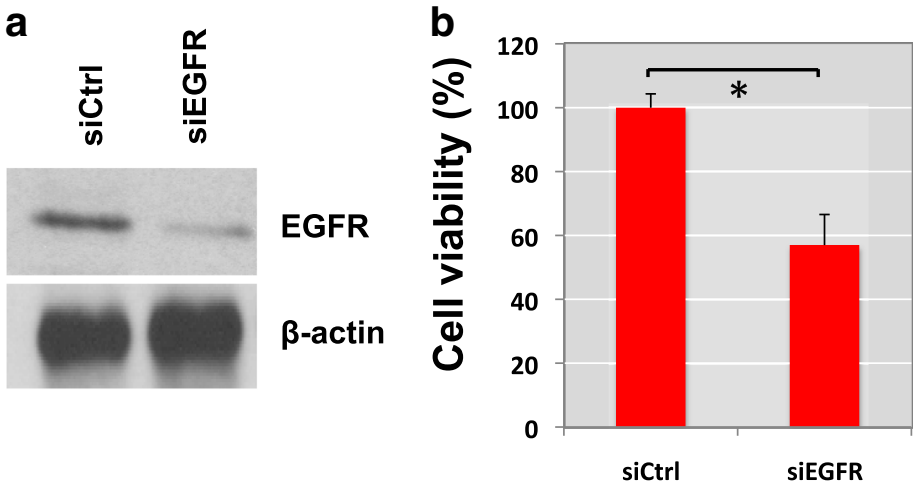

Fig. 4 Knockdown of EGFR suppresses recovery from cisplatin treatment. **a** EGFR silenced TCCSUP cells (siEFGR) or control TCCSUP cells (siCtrl) were challenged with cisplatin treatment. TCCSUP cells were incubated with cisplatin (10 μM) and siRNAs for 48 h and then re-treated with cisplatin alone for an additional 6 h. After, the cisplatin was removed from the culture media and cells were incubated in normal growth medium for 24 h. **b** Cell viability was measured using MTT assay. Cell viability levels of three wells of transfected cells were determined. The graph was plotted as %, compared to control, no cisplatin treatment in siCtrl group (± SD). *$P < 0.05$ (Student's t-test). All experiments were done in at least triplicates

morphological switch. However, in vitro functional analysis demonstrated that EGFR expression levels can alter cell proliferation rates in TCCSUP BC cells. A dose dependent transfection of EGFR siRNAs (siEGFR_1, _2, or _3) revealed that EGFR deficiency evoked an approximately 50% decrease in cell proliferation (Fig. 3b). This data implicates that EGFR loss as an important mechanism through which BC cells keep proliferating.

We next assessed whether loss of EGFR expression can result in cell viability responses in relation to the effects of cisplatin and whether inhibition of EGFR can enhance the sensitivity of BC cells to cisplatin. We found that EGFR expression is associated with resistance to cisplatin-induced cytotoxicity. EGFR knockdown delayed cell recovery from 10 μM cisplatin treatment (Fig. 4).

Viability of control cells (siCtrl) in serum-free medium was compared with or without a challenge by 10 μM cisplatin. Cell viability assay revealed that silencing of EGFR sensitized TCCSUP BC cells to cisplatin treatment. Knockdown of EGFR was validated by western blot analysis (Fig. 4a). Cells transfected with EGFR siRNAs showed around 50% viability after cisplatin treatment compared to control TCCSUP cells (siEGFR). Removal of cisplatin from the culture medium of control cells resulted in 100% recovery of cell viabilitya (siCtrl) (Fig. 4b).

We next sought to determine whether gene silencing of EGFR might also increase drug sensitivity to cisplatin. TCCSUP BC cells were transfected with EGFR siRNAs or control siRNAs for 48 h. Immunoblotting confirmed that EGFR expression was significantly reduced in siEGFR-transfected cells (Fig. 5a). Interestingly, loss of EGFR made TCCSUP cells more sensitive to cisplatin-induced cell apoptosis, leading to reduced cell viability. TCCSUP cells were ~2x more sensitive to 5 or 10 μM cisplatin treatments (Fig. 5b). These results were further validated in T24 BC cells (Fig. 5c-d). These

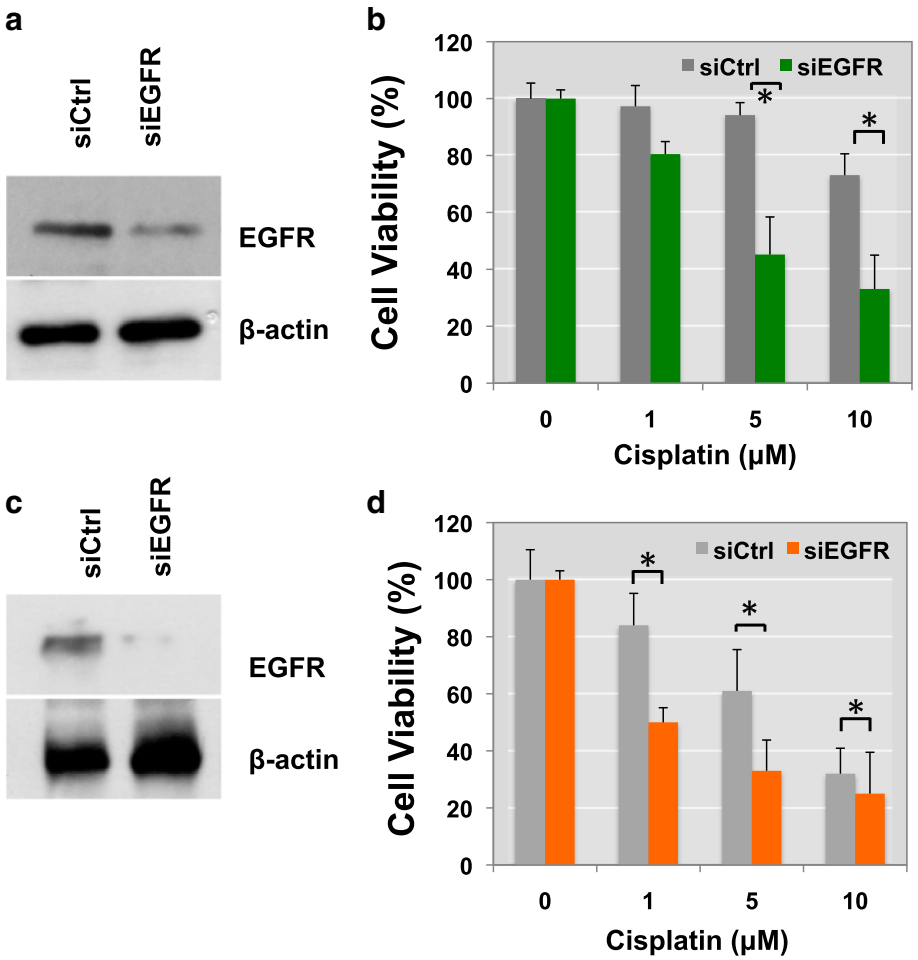

Fig. 5 Gene silencing of EGFR enhances drug sensitivity to cisplatin treatment. (**a** and **b**, TCCSUP; **c** and **d**; T24) Transiently transfected TCCSUP (**a**) or T24 (**c**) cells with siRNA of EGFR were treated with cisplatin (0, 1, 5 and 10 μM). Cisplatin was added together with siNRA for 48 h and then re-treated with cisplatin. Cell viability was measured by MTS assay after 2 days. Overexpression of siEGFR, but not a control siRNA, in TCCSUP (**c**) or T24 (**d**) cells reduced cell proliferation (Student's t-test, $*p < 0.05$)

findings suggest that EGFR knockdown not only suppresses the recovery of BC cells from cisplatin-reduced cell viability but also enhances the sensitivity of BC cells to cisplatin's cytotoxicity.

Discussion

Systemic chemotherapy is currently being used as the first line of treatment in advanced stages of BC. However, it is still unclear which group of patients will benefit and which patients will be more sensitive to cisplatin-based therapy. Our findings suggest that EGFR overexpression is associated with disease recurrence following adjuvant chemotherapy for advanced BC [17, 18]. Determining EGFR expression status may help predict prognoses and assist in deciding which patients would best benefit from adjuvant chemotherapy. Our findings also suggest that patients with higher EGFR expression may have a worse prognosis than those with little to no EGFR expression. An evaluation of intratumoral molecular marker(s) could be used to identify BC patients more likely to respond to cisplatin-based chemotherapy.

These findings align with previous studies showing that approximately 50% of BC tumor tissues overexpress EGFR and that EGFR positivity indicates more invasive cells and poor differentiation [13, 14]. However, the mechanisms through which BC tumors acquire cisplatin resistance are still elusive. Our results suggest that EGFR silencing may enhance cisplatin's capability to shrink tumors. This observation highlights the potential of EGFR targeting strategies (e.g., kinase inhibitors or EGFR neutralizing antibodies such as gefitini, erlotinib, trastuzumab, cetuximab, matuzumutab, panitumumab et al.) to improve the effects of cisplatin-based chemotherapy. Recent reports have demonstrated that a subgroup of muscle-invasive bladder carcinomas with a basal-like phenotype are sensitive to EGFR kinase blockers, such as erlotinib [19, 20]. Rebouissou et al. identified a subgroup of aggressive MIBC, which shows a basal-like phenotype using their 40-gene expression classifier. In this BC subgroup, the EGFR pathway was highly activated, suggesting that anti-EGFR therapy could be used as a powerful therapeutic strategy [21, 22]. EGFR-targeted agents have only shown modest success due to acquired resistance in current ongoing clinical trials. Therefore, comprehensive clinical studies using EGFR-targeting in combination with other therapies would be more attractive.

Conclusions

Many questions regarding EGFR silencing strategies remain unanswered. For example, what signaling cascades are modulated by high EGFR expression? How can these be regulated pharmacologically? Will BC cells obtain resistance to cisplatin? Can cells become resistant to EGFR silencing? In this study, our experimental results present EGFR as a marker of recurrence in Egyptian BC patients. Further studies are needed to better understand the regulatory mechanisms of EGFR overexpression and its downstream signaling pathways in BC, particularly in the context of squamous cell carcinoma (SCC) and transitional cell carcinoma (TCC). Our findings also suggest that elucidating some of these facets of EGFR and BC drug resistance might improve pharmacologic intervention.

Abbreviations

BC: Bladder cancer; EGFR: Epidermal growth factor receptor; MIBC: Muscle-invasive bladder cancer; siCtrl: Control cells; siRNAs: Small interfering RNAs

Acknowledgements

None

Funding

The authors acknowledge support from National Institutes of Health grants (1U01DK103260, 1R01DK100974, U24 DK097154, NIH NCATS UCLA CTSI UL1TR000124), Department of Defense grants (W81XWH-15-1-0415), Centers for Disease Controls and Prevention (1U01DP006079), IMAGINE NO IC Research Grant, the Steven Spielberg Discovery Fund in Prostate Cancer Research Career Development Award, and the U.S.-Egypt Science and Technology Joint Fund (to J.K.). J.K. is former recipient of Interstitial Cystitis Association Pilot Grant, a Fishbein Family IC Research Grant, New York Academy of Medicine, and Boston Children's Hospital Faculty Development. The funders had no role in the experimental design, data collection, analysis, preparation of the manuscript, or decision to publish. In addition, this article is derived from the Subject Data funded in whole or part by National Academies of Sciences, Engineering, and Medicine (NAS) and The United States Agency for International Development (USAID). Any opinions, findings, conclusions, or recommendations expressed in this article are those of the authors alone, and do not necessarily reflect the views of USAID or NAS.

Availability of data and materials

All of data were presented in the main paper. The data that support the findings of this study are available on request from the corresponding author [J.K.]. The data are not publicly available due to information that could compromise research participant privacy.

Authors' contributions

JK and AMM conceived of the study, designed experiments, evaluated data and wrote the paper. AMM, ML, EC, VS, TP, MS, AM, MA, AA, and ME performed experiments. MS, AS, and AM provided expertise and supervised data interpretation. JK, AMM, and HA-E have contributed conceptually and intellectually and to the writing of the manuscript. All authors have read and approved the final manuscript.

Ethics approval and consent to participate

The biospecimens used in the present retrospective study were available from Mansoura University. The Ethics Committee of Mansoura Urology and Nephrology Center approved the protocol used for this study. The Institutional Review Board of Mansoura Urology and Nephrology Center approved analysis of all samples and database reviewed retrospectively (Mansoura UNC IRB #RP-16-12-91). Consent from patients for use of the archived bladder specimens samples or their data was waived by the IRB because this study was retrospective study.

Consent for publication

Not applicable.

Competing interests

The authors declare that they have no competing interests.

Publisher's Note

Springer Nature remains neutral with regard to jurisdictional claims in published maps and institutional affiliations.

Author details
[1]Urology and Nephrology Center, Mansoura University, Mansoura, Egypt. [2]University of Texas Health Science Center, San Antonio, USA. [3]University of California Los Angeles, Los Angeles, CA, USA. [4]University of California, Berkerly, CA, USA. [5]Departments of Surgery and Biomedical Sciences, Samuel Oschin Comprehensive Cancer Institute, Cedars Sinai Medical Center, 8700 Beverly Blvd, Los Angeles, CA 90048, USA.

Received: 3 January 2017 Accepted: 19 October 2018
Published online: 09 November 2018

References

1. Antoni S, Ferlay J, Soerjomataram I, Znaor A, Jemal A, Bray F. Bladder Cancer incidence and mortality: a global overview and recent trends. Eur Urol. 2017;71(1):96–108.
2. Kamat AM, Hahn NM, Efstathiou JA, Lerner SP, Malmstrom PU, Choi W, Guo CC, Lotan Y, Kassouf W. Bladder cancer. Lancet. 2016;388(10061):2796–810.
3. Kaplan AL, Litwin MS, Chamie K. The future of bladder cancer care in the USA. Nature reviews Urology. 2014;11(1):59–62.
4. Mahdavifar N, Ghoncheh M, Pakzad R, Momenimovahed Z, Salehiniya H. Epidemiology, incidence and mortality of bladder cancer and their relationship with the development index in the world. Asian Pac J Cancer Prev. 2016;17(1):381–6.
5. Ibrahim AS, Khaled HM, Mikhail NN, Baraka H, Kamel H. Cancer incidence in Egypt: results of the national population-based cancer registry program. J Cancer Epidemiol. 2014;2014:437971.
6. Zaghloul MS, Nouh A, Moneer M, El-Baradie M, Nazmy M, Younis A. Time-trend in epidemiological and pathological features of schistosoma-associated bladder cancer. J Egyp Natl Cancer Inst. 2008;20(2):168–74.
7. Mostafa MH, Sheweita SA, O'Connor PJ. Relationship between schistosomiasis and bladder cancer. Clin Microbiol Rev. 1999;12(1):97–111.
8. Ghoneim MA, Abdel-Latif M, el-Mekresh M, Abol-Enein H, Mosbah A, Ashamallah A, el-Baz MA. Radical cystectomy for carcinoma of the bladder: 2,720 consecutive cases 5 years later. J Urol. 2008;180(1):121–7.
9. Grossman HB, Natale RB, Tangen CM, Speights VO, Vogelzang NJ, Trump DL, deVere White RW, Sarosdy MF, Wood DP Jr, Raghavan D, et al. Neoadjuvant chemotherapy plus cystectomy compared with cystectomy alone for locally advanced bladder cancer. N Engl J Med. 2003;349(9):859–66.
10. Mansour AM, Soloway MS, Eldefrawy A, Singal R, Joshi S, Manoharan M. Prognostic significance of cystoscopy findings following neoadjuvant chemotherapy for muscle-invasive bladder cancer. Can J Urol. 2015;22(2):7690–7.
11. Rosenblatt R, Sherif A, Rintala E, Wahlqvist R, Ullen A, Nilsson S, Malmstrom PU, Nordic Urothelial Cancer G. Pathologic downstaging is a surrogate marker for efficacy and increased survival following neoadjuvant chemotherapy and radical cystectomy for muscle-invasive urothelial bladder cancer. Eur Urol. 2012;61(6):1229–38.
12. Black PC, Dinney CP. Growth factors and receptors as prognostic markers in urothelial carcinoma. Curr Urol Rep. 2008;9(1):55–61.
13. Abbosh PH, McConkey DJ, Plimack ER. Targeting signaling transduction pathways in bladder Cancer. Curr Oncol Rep. 2015;17(12):58.
14. van Kessel KE, Zuiverloon TC, Alberts AR, Boormans JL, Zwarthoff EC. Targeted therapies in bladder cancer: an overview of in vivo research. Nature Rev Urol. 2015;12(12):681–94.
15. Lee HH, Wang YN, Hung MC. Non-canonical signaling mode of the epidermal growth factor receptor family. Am J Cancer Res. 2015;5(10):2944–58.
16. Tan X, Lambert PF, Rapraeger AC, Anderson RA. Stress-induced EGFR trafficking: mechanisms, functions, and therapeutic implications. Trends Cell Biol. 2016;26(5):352–66.
17. Kim WT, Kim J, Yan C, Jeong P, Choi SY, Lee OJ, Chae YB, Yun SJ, Lee SC, Kim WJ. S100A9 and EGFR gene signatures predict disease progression in muscle invasive bladder cancer patients after chemotherapy. Ann Oncol. 2014;25(5):974–9.
18. Symanowski JT, Kim ES. Gene expression and prognosis in bladder cancer--real progress? Editorial on 'S100A9 and EGFR gene signatures predict disease progression in muscle invasive bladder cancer patients after chemotherapy. Ann Oncol. 2014;25(5):919–20.
19. Choi W, Czerniak B, Ochoa A, Su X, Siefker-Radtke A, Dinney C, McConkey DJ. Intrinsic basal and luminal subtypes of muscle-invasive bladder cancer. Nature Rev Urol. 2014;11(7):400–10.
20. Shah JB, McConkey DJ, Dinney CP. New strategies in muscle-invasive bladder cancer: on the road to personalized medicine. Clin Cancer Res. 2011;17(9):2608–12.
21. Bladder cancers respond to EGFR inhibitors. Cancer discovery. 2014, 4(9):980–981.
22. Rebouissou S, Bernard-Pierrot I, de Reynies A, Lepage ML, Krucker C, Chapeaublanc E, Herault A, Kamoun A, Caillault A, Letouze E, et al. EGFR as a potential therapeutic target for a subset of muscle-invasive bladder cancers presenting a basal-like phenotype. Sci Transl Med. 2014;6(244):244ra291.

Ready to submit your research? Choose BMC and benefit from:

- fast, convenient online submission
- thorough peer review by experienced researchers in your field
- rapid publication on acceptance
- support for research data, including large and complex data types
- gold Open Access which fosters wider collaboration and increased citations
- maximum visibility for your research: over 100M website views per year

At BMC, research is always in progress.

Learn more biomedcentral.com/submissions

BMC

Cell Cycle

ISSN: 1538-4101 (Print) 1551-4005 (Online) Journal homepage: https://www.tandfonline.com/loi/kccy20

Centromere protein F (CENPF), a microtubule binding protein, modulates cancer metabolism by regulating pyruvate kinase M2 phosphorylation signaling

Muhammad Shahid, Min Young Lee, Honit Piplani, Allen M. Andres, Bo Zhou, Austin Yeon, Minjung Kim, Hyung L. Kim & Jayoung Kim

To cite this article: Muhammad Shahid, Min Young Lee, Honit Piplani, Allen M. Andres, Bo Zhou, Austin Yeon, Minjung Kim, Hyung L. Kim & Jayoung Kim (2018) Centromere protein F (CENPF), a microtubule binding protein, modulates cancer metabolism by regulating pyruvate kinase M2 phosphorylation signaling, Cell Cycle, 17:24, 2802-2818, DOI: 10.1080/15384101.2018.1557496

To link to this article: https://doi.org/10.1080/15384101.2018.1557496

View supplementary material

Accepted author version posted online: 09 Dec 2018.
Published online: 17 Dec 2018.

Submit your article to this journal

Article views: 269

View related articles

View Crossmark data

Citing articles: 2 View citing articles

Full Terms & Conditions of access and use can be found at
https://www.tandfonline.com/action/journalInformation?journalCode=kccy20

CELL CYCLE
2018, VOL. 17, NO. 24, 2802–2818
https://doi.org/10.1080/15384101.2018.1557496

Taylor & Francis
Taylor & Francis Group

RESEARCH PAPER

Check for updates

Centromere protein F (CENPF), a microtubule binding protein, modulates cancer metabolism by regulating pyruvate kinase M2 phosphorylation signaling

Muhammad Shahid[a], Min Young Lee[b], Honit Piplani[c,d], Allen M. Andres[c,d], Bo Zhou[a], Austin Yeon[a], Minjung Kim[e], Hyung L. Kim[a], and Jayoung Kim[a,f,g,h]

[a]Departments of Surgery and Biomedical Sciences, Cedars-Sinai Medical Center, Los Angeles, CA, USA; [b]Institute for Systems Biology, Seattle, WA, USA; [c]Department of Medicine, Cedars Sinai Medical Center, Los Angeles, CA, USA; [d]Cedars-Sinai Heart Institute, Los Angeles, CA, USA; [e]Department of Cell Biology, Microbiology and Molecular Biology, University of South Florida, Tampa, FL, USA; [f]Department of Medicine, University of California Los Angeles, CA, USA; [g]Samuel Oschin Comprehensive Cancer Institute, Cedars-Sinai Medical Center, Los Angeles, CA, USA; [h]Department of Urology, Ga Cheon University College of Medicine, Incheon, South Korea

ABSTRACT

Prostate cancer (PC) is the most commonly diagnosed cancer in men and is the second leading cause of male cancer-related death in North America. Metabolic adaptations in malignant PC cells play a key role in fueling the growth and progression of the disease. Unfortunately, little is known regarding these changes in cellular metabolism. Here, we demonstrate that centromere protein F (CENPF), a protein associated with the centromere-kinetochore complex and chromosomal segregation during mitosis, is mechanically linked to altered metabolism and progression in PC. Using the CRISPR-Cas9 system, we silenced the gene for CENPF in human PC3 cells. These cells were found to have reduced levels of epithelial-mesenchymal transition markers and inhibited cell proliferation, migration, and invasion. Silencing of CENPF also simultaneously improved sensitivity to anoikis-induced apoptosis. Mass spectrometry analysis of tyrosine phosphorylated proteins from CENPF knockout ($CENPF^{KO}$) and control cells revealed that CENPF silencing increased inactive forms of pyruvate kinase M2, a rate limiting enzyme needed for an irreversible reaction in glycolysis. Furthermore, $CENPF^{KO}$ cells had reduced global bio-energetic capacity, acetyl-CoA production, histone acetylation, and lipid metabolism, suggesting that CENPF is a critical regulator of cancer metabolism, potentially through its effects on mitochondrial functioning. Additional quantitative immunohistochemistry and imaging analyzes on a series of PC tumor microarrays demonstrated that CENPF expression is significantly increased in higher-risk PC patients. Based on these findings, we suggest the CENPF may be an important regulator of PC metabolism through its role in the mitochondria.

ARTICLE HISTORY
Received 20 August 2018
Revised 13 November 2018
Accepted 28 November 2018

KEYWORDS
CENP-F; prostate cancer; mitochondria

Introduction

Prostate cancer (PC) remains a major public health concern; it is the most common malignant neoplasia among men and is the 6th leading cause of cancer-related male mortality worldwide [1]. In the U.S., there are more than 200,000 newly diagnosed cases and nearly 40,000 deaths from PC annually. The current standard methods of diagnosing and monitoring PC involve testing the levels of prostate specific antigen (PSA) and digital rectal screening. However, recent studies have reported that these procedures contribute little to no reduction in overall PC mortality [2,3].

Proliferating PC cells generate the energy required to support accelerated cell division by modulating its metabolism. These cells exhibit increased glucose uptake and lactate production [4,5]. Rapidly dividing cells are able to convert glucose into lactate, regardless of oxygen availability, a phenomenon known as aerobic glycolysis or the Warburg effect [2]. The Warburg effect has been demonstrated to be a key contributor of tumorigenesis and can be a target for cancer therapy [6]. Many oncogenes and/or tumor suppressor genes have been reported to be involved in the metabolic switch towards aerobic glycolysis. For instance, oncogenes AKT [7], c-Myc [8], Ras [9], and HIF-1α [10] promote the Warburg effect; whereas tumor suppressors p53 and PTEN inhibit it [11,12]. Epithelial-mesenchymal transition (EMT) also plays a pivotal role in the development of metastatic castration-resistant prostate cancer (mCRPC)

CONTACT Jayoung Kim Jayoung.Kim@cshs.org
Supplemental data for this article can be accessed here.
© 2018 Informa UK Limited, trading as Taylor & Francis Group

[13] and chemoresistant PC [14]. However, current understandings of the dynamic metabolic changes underlying EMT are limited.

Centromere protein F (CENPF), which is located on chromosome 1q41, encodes for a protein that acts as part of the centromere-kinetochore complex and is a component of the nuclear matrix during G2 of interphase [15]. As a regulator of chromosome segregation, CENPF is expressed in a cell cycle-dependent manner; it gradually accumulates during the cell cycle, reaches peak levels in the G_2/M phase, and then degrades upon completion of mitosis [16]. CENPF is upregulated in PC and plays an important part in malignant progression [17,18]. Interestingly, CENPF also significantly enhances chemotherapeutic sensitivity [19]. It was recently observed that CENPF and forkhead box M1 (FOXM1) cooperate together, acting as synergistic master regulators of malignancy in PC [20]. Furthermore, COUP transcription factor 2 (COUP-TFII) may be promoting metastasis in PC through the CENPF signaling pathway [21].

In this study, we aimed to determine the functional role of CENPF and its underlying mechanism in PC progression. Our experimental results showed that silencing CENPF expression significantly inhibited EMT, cell proliferation, and colony formation, while also enhancing global phosphorylation and sensitivity to anoikis-induced apoptosis. Additional proteomics and computational analysis demonstrated that CENPF may regulate cancer cell metabolism through the phosphorylation of pyruvate kinase M2 (PKM2). Moreover, Seahorse Respirometry revealed that CENPF loss leads to a general decrease in metabolic activity in PC cells, which is characterized by reduced respiration and glycolysis. In summary, we propose CENPF as a novel target protein, providing a potential effective paradigm in curing PC.

Materials and methods

Cell culture and cell lines

Human prostate cancer cell lines PC3, DU145, and 22RV1 were purchased from American Type Culture Collection (ATCC, Manassas, VA, USA) and were cultured in 10% fetal bovine serum (FBS)/Dulbecco's Modified Eagle medium (DMEM) or RPM1640 medium. Cells were maintained in humidified incubators set at 37°C with 5% CO_2. A CENPF-knockout PC3 cell line ($CENPF^{KO}$) was constructed using the CRISPR/Cas9 system by ALSTEM, LLC (Richmond, CA). The combination of two gRNAs (GTTTCAGCTTGACAGTCTCG and CATTATTGACAGAGAAGTGC) targeted the deletion of an 85 bp fragment in the exon1-intron1 junction, with 32 bp of this deletion fragment in the exon1 and 54 bp deleted in intron. For transient transfection of cells with a CENPF-expressing construct or siRNA CENPF (ThermoScientific), we followed the previously established protocol using Lipofectamine 2000 (Invitrogen), according to the manufacturer's instructions [22]. All cell lines were confirmed and tested for mycoplasma every 6 months during the experimental period.

Antibodies and reagents

The following antibodies were used: β-Actin (A1978) from Sigma, E-Cadherin (610182), Phosphotyrosine (610000) from BD Transduction Laboratories, ACSS2 (PA5-52059) from ThermoFisher Scientific, ALDH7A1 (ab154218), CENPF (ab5), and OXPHOS (ab110413) from Abcam, and Tom40 (sc365467) from Santa Cruz Biotechnology, phospho-mTOR (2971), phospho-β-catenin (9564), phospho-p38 MAPK (9216), phospho-PAK1 (2601), phospho-NF-κB (3033), TCF8/ZEB1 (3396), phospho-PKM2 (3827), PKM2 (4053), Snail (3879), N-cadherin (13116), MMP2 (13132), MMP9 (13667), Slug (9585), phospho-p70 S6 Kinase (9206), phospho-Src Family (2101), Phospho-p44/42 MAPK (Erk1/2) (Thr202/Tyr204) (4370), β-Catenin (8480), Cleaved-PARP (9541), and Fatty acid and Lipid Metabolism Antibody Kit (8335), Acetyl-Histone Antibody Kit (9933), Tight Junction Antibody Kit (8683) and HRP-conjugated secondary antibodies (7074, 7076) from Cell Signaling Technology.

Proliferation assay

Cell proliferation was analyzed using trypan blue staining. Cells were seeded onto 6-well culture plates ($2x10^2$ cells/well) and cultured for 24 hrs. Each well culture was maintained and incubated for 2 d. The medium was replaced every day. The results are presented as the percentage of viable cells relative to that of the control.

Two-dimensional (2D) and three-dimensional (3D) colony formation assay

The growth capability of $CENPF^{KO}$ and control cells was examined using 2D colony formation assays. Approximately 500 controls and $CENPF^{KO}$ cells were seeded onto separate 15 cm culture plates. After incubation at 37°C for 14 d, the cells were washed with PBS twice, fixed with methanol and then stained with 0.1% crystal violet. The number of colonies containing >30 cells was counted under the microscope. Anchorage-independent growth was measured through a 3D colonization assay. Cells were seeded at 1×10^4 in 3 ml 0.35% agar in DMEM/FBS, overlaid on 2 ml of 0.7% agar in DMEM/FBS, in six-well plates. Plates were incubated for up to 14 d and cells were fed every 3–4 d. After two weeks, the plates were stained with MTT and the number of colonies that developed within each well was counted and visualized under a microscope. Colonies that were comprised of more than 10 cells were scored as positive. Experiments were run in triplicate for each cell line and data are representative of three independent trials.

Wound-healing assay

For the wound-healing migration assay, $CENPF^{KO}$ and control cells were seeded on 6-well plates at a density of 1×10^5 cells/well in culture medium. After 24 hrs post seeding, the confluent monolayer of the culture was scratched with a fine pipette tip and migration capacity was visualized under a microscope. The rate of wound closure was observed for an additional 24 hrs during incubation.

Anoikis assays

Cells (5×10^5) were plated onto poly-HEMA-coated six-well plates (Corning, Tewksbury, MA, USA) in growth medium to prohibit attachment. After 24, 48 and 72 hrs in suspension, cells were transferred onto regular cell culture plates in growth medium supplemented with FBS (1%) to aid attachment. Cells were incubated for 0, 1, 2, and 3 hrs prior to the MTT assay (no. G4100, Promega, Madison, WI, USA). Absorbance was read using a microplate reader (Tecan, Männedorf, Switzerland). Experiments were repeated three times.

Western blot analysis

Cells were lysed with RIPA buffer (20 mM Tris, 150 mM NaCl, 1% Nonidet, P-40, 0.1 mM EDTA) (Pierce, ThermoFisher) supplemented with a phosphatase inhibitor cocktail (ThermoFisher). The protein concentration of each sample was measured using the Bradford Protein Kit Assay, according to the manufacturer's instructions (Pierce, Thermofisher). Equal amounts of protein extract were separated via SDS-PAGE and transferred onto a PVDF membrane. The membranes were then blocked with 5% bovine serum albumin or 5% nonfat milk in TBST buffer [2.42 g/L Tris–HCl, 8 g/L NaCl, and 1 mL/L Tween 20 (pH 7.6)] and incubated overnight at 4°C with specific primary antibodies in TBST. The membranes were then incubated with secondary antibodies conjugated with horseradish peroxidase. β-actin was used as an internal control.

Immunohistochemistry (IHC) analysis

Two independent commercial PC tissue microarrays (TMAs) were purchased from US Biomax (Derwood, MD). Detailed information was not available except sex, TMN, grade, and stages. TMAs were immunestained with mAb CENPF, according to the manufacturer's recommended protocol. Immunostaining was considered positive when more than 10% of all tumor cells were immunoreactive. For quantification, the TMAs were scored for IHC intensity by two independent

investigators. Tumors that showed no positive staining were given a score of 0, those with weak staining were given a score of 1, and tumors with strong IHC staining were given a score of 2.

Acetate measurement assay

The acetate colorimetric assay kit (BioVision, Milpitas, CA) was used according to the instructions provided. The reaction was incubated at room temperature for 40 min. Acetate fluorescence (absorbance at 450nm) was measured using a POLARstar Galazy fluorometer in a 96-well plate.

Free fatty acid (FFA) and cholesterol quantification

Quantification of FFAs and cholesterol were determined using the Free Fatty Acid Quantification Kit and Cholesterol Quantification Kit (FFA: MAK044 and Cholesterol: MAK043, Sigma MO, USA). Briefly, cells were lysed in 1% Triton X-100 in chloroform (w/v). The samples were centrifuged at 13,000 × g for 10 min to remove insoluble debris. The organic phase was collected and air dried in a 50°C dry bath for 20 min. Samples were vacuum dried for 30 min to remove traces of chloroform. The dried lipids were resuspended via vortex in fatty acid assay buffer and further quantified, using the manufacturer's instructions.

Global proteomics

All chemicals used for preparation of liquid chromatography-tanden mass spectrometry (LC-MS/MS) samples were of at least sequencing grade and were purchased from Sigma-Aldrich, unless otherwise stated. Whole protein was extracted from CENPF^{KO} and control cells using 4% SDS-containing buffer. Protein concentration was measured with the Pierce 660nm Assay Kit. From each sample, 60 µg of protein was digested with trypsin, using FASP, and labeled with TMT6plex reagents in parallel. After TMT labeling, peptides were merged, desalted with C18, and fractionated by high-pH reverse phase liquid chromatography (RPLC). Peptides were sequenced and quantified by LC-MS/MS. Database searching and quantification were performed using Proteome Discoverer (v2.1). A standard false discovery rate of 1% was applied to filter peptide-spectrum matches, peptide identifications, and protein identifications. Next, data was normalized in the Proteome Discoverer environment, assuming that the total peptide amount in each different sample was the same. In addition, TMT126-labeled samples wereselected as a reference channel and ratios between samples were computed by Proteome Discoverer [23]. The fold-changes between CENPF^{KO} and parent PC3 cells were determined as the average ratios of the three TMT tags for each group. The significance of the differential abundances between the two groups was computed using Welch's t-test on the scaled abundances and Benjamini-Hochberg (BH) procedure for multiple testing corrections. Differentially expressed proteins (DEPs) were identified by applying a threshold of BH FDR ≤ 0.01 and ratio ≥ 1.5.

Phosphoproteomics

Proteins were eluted from p-Y conjugated beads and resolved by a quick separation (5–6mm height) in a 12% SDS-PAGE gel. Upon in-gel reduction, alkylation, and trypsin digestion, the tryptic peptides were extracted and reconstituted in 0.2% formic acid. The peptides were then separated in a 15 cm EASY-Spray C18 column and analyzed on a LTQ Orbitrp Elite Mass Spectrometer (Thermo Scientific). Up to 20 collision-induced dissociation (CID) spectra were acquired per survey scan in the rapid CID scan mode. The raw MS/MS spectra were searched against the Uniprot Human Database (released on 01/22/16, including 20,985 sequences) with MaxQuant (v 1.5.2.8) and Andromeda. A stringent 1% false discovery rate was set for peptide and protein identifications [24].

Network analysis

We identified gene ontology biological processes (GOBPs) and Kyoto Encyclopedia of Genes and Genomes (KEGG) pathways represented by the DEPs using DAVID [25]. The significance of terms was determined at a BH FDR ≤ 0.1. To delineate the associations of enriched biological functions and

DEGs, a network model was constructed using HitPredict, a database of experimentally determined protein-protein interactions [26]. The database update version, 04Jul2017, was downloaded and only high confidence interactions among genes involved in the selected terms were parsed for the network construction. Genes involved in the same biological functions were grouped into the same module, each of which was labeled by their corresponding GOBP and KEGG pathway terms. The network was visualized using Cytoscape (v. 3.2.1) [27].

Seahorse respirometry assay

CENPF^{KO} and control PC3 cells were seeded into a 24-well Seahorse culture plate at a density of 50,000 cells/well 24 hrs before the Seahorse assay. The media was then changed to a XF Base Medium (pH 7.4) supplemented with 10 mM glucose, 1mM sodium pyruvate and 1mM sodium glutamine. Cells equilibrated for 1 hour in a non-CO_2 incubator at 37°C before assay start. Chemical reagents (Sigma) were used at final concentrations as follows: 1 μM oligomycin – an ATP synthase inhibitor, 1 μM (FCCP) carbonyl cyanide 4-(trifluoromethoxy) phenylhydrazone – an uncoupling agent, and a mixture of 0.5 μM antimycin A – a cytochrome C reductase inhibitor and 0.5 μM rotenone – a complex I inhibitor. Oxygen consumption rate (OCR) and extracellular acidification rate was monitored during the duration of the assay run. Results were normalized to protein concentrations determined by a BCA assay (Thermo Scientific).

Statistical analysis

Statistical analyses were performed using a two-tailed Student's t-test. For all experiments with error bars, the standard deviation (SD) was calculated to indicate the variation within each experiment, and values represent mean ± SD. Differences were considered significant if $p < 0.05$.

Results

CENPF is associated with aggressive PC

To evaluate whether CENPF expression is associated with cancer progression, we performed two independent IHC imaging analyses using PC TMAs, as described in Methods section. Using commercial PC TMAs, we found that CENPF was overexpressed in approximately 70% of call cases, with an upward trend in tumors of higher grades (III-IV) (Figure 1(a)). IHC analyses using 2 different commercial TMAs revealed that CENPF was expressed in approximately 60% and 50% of all cases, respectively. We also found moderate staining in the normal prostate tissues and hyperplasia. CENPF expression was considerably higher in PC tissue compared to adjacent normal prostate tissue from the same patient. Levels of CENPF expression were also positively correlated to pathological stage and grade (Figure 2(b)). This observation was consistent with previous literature demonstrating CENPF as part of a signature that distinguishes biochemical recurrence and advanced cancer [28]. Collectively, the expression levels of CENPF in PC tissue were significantly higher than that of normal prostate tissue. These results point to the notion that CENPF expression may be potentially associated with PC progression.

CENPF loss reversed EMT in PC3 cells

To elucidate the role of CENPF in PC cells, CENPF was stably knocked-out in PC3 cells using the CRISPR/Cas9 system. These CENPF-knockout

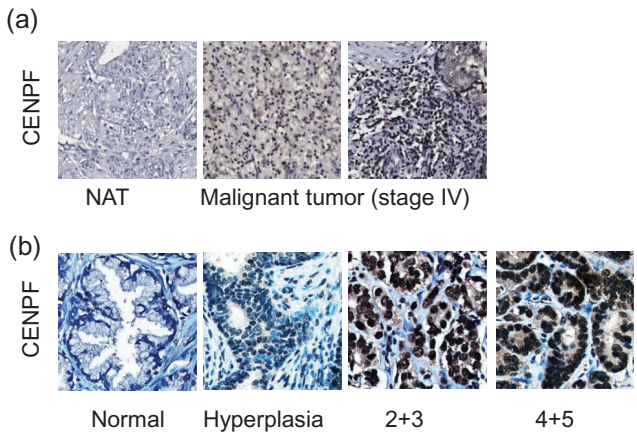

Figure 1. CENPF expression is correlated with PC progression. Two independent tissue microarrays (TMAs) were used. TMA slides were stained with CENPF specific antibody (brown) and counterstained with hematoxylin (blue). (a) The IHC images represent adjacent normal prostate tissues (NAT) or tumors from PC patients with different stages, as described in figures. (b) Representative IHC images show the differential CENPF protein levels.

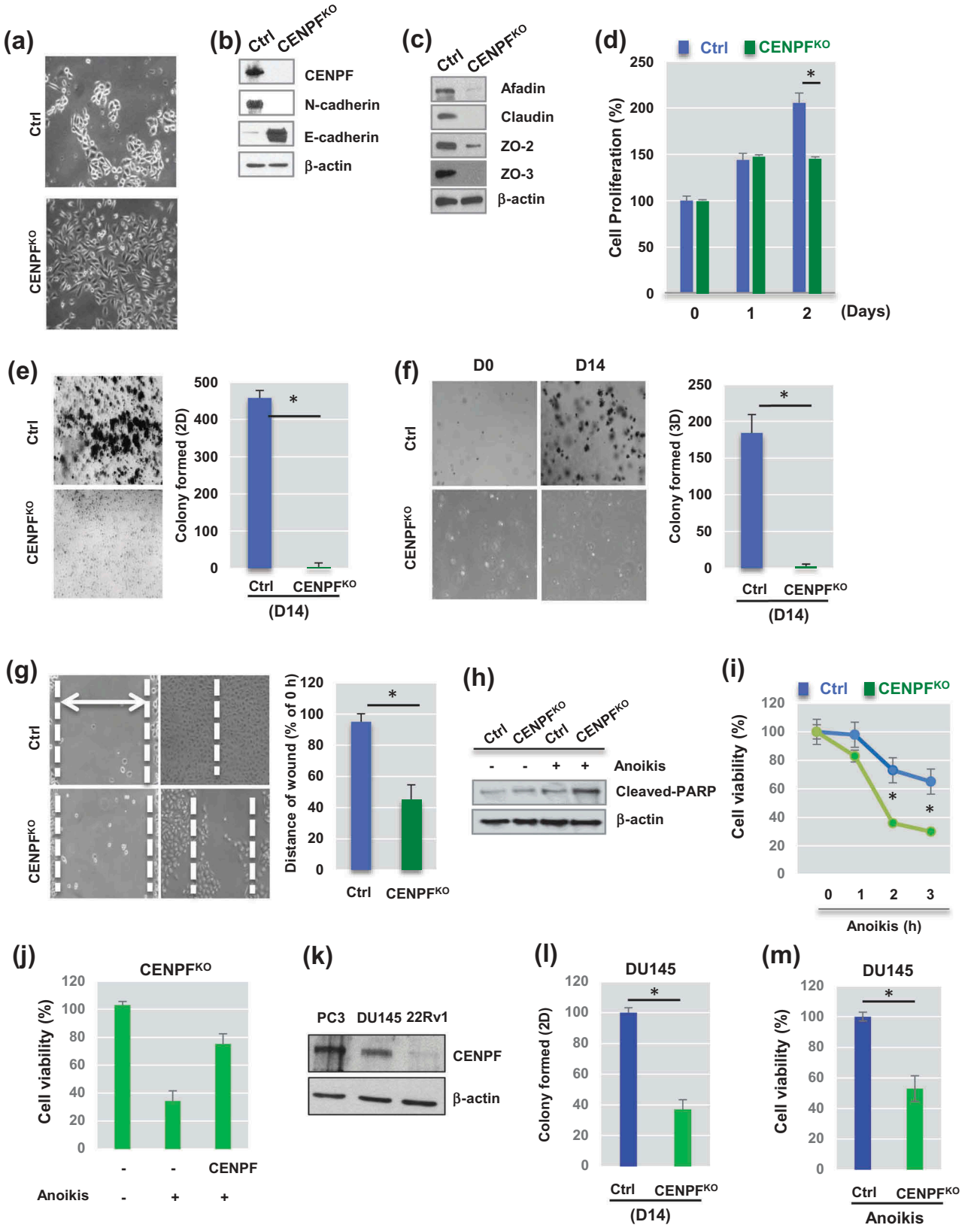

Figure 2. Knockout of CENPF reduces Epithelial-Mesenchymal transition (EMT) and slows proliferation of prostate cancer cells. (a) Morphological changes between parental PC3 cells (Ctrl) and CENPF – knockout PC3 cells (CENPF^{KO}) were observed. Representative images were shown. (b) Western blot analysis demonstrated well-known EMT markers in Ctrl and CENPF^{KO} cells. (c) Cell junction markers were assessed by Western blot analysis. (d) Cell proliferation was determined by trypan blue staining and compared in Ctrl and CENPF^{KO} cells at 0, 24 and 48hrs. (e-f) Gene knockout of CENPF reduced colony formation ability in 2D (e) or 3D (f) settings. (g)

(CENPF^{KO}) cells were then carefully characterized in the laboratory. There were some noted morphological alterations in the CENPF^{KO} cells, compared to the control PC3 cell line (Figure 2(a)). Western blot analysis demonstrated that CENPF expression was lost in the CENPF^{KO} cells (Figure 2(b)). Consistent with morphological changes, we found that protein expression of mesenchymal cell markers, including N-cadherin (Figure 2(b)), snail, slug, matrix metalloproteinase-2 (MMP2), MMP9, β-catenin (Supplementary Figure 1), was significantly reduced in CENPF^{KO} cells, compared to control cells [29,30]. E-cadherin, an epithelial marker, dramatically increased in CENPF^{KO} cells (Figure 2(b)). In addition, tight junction proteins (e.g. afadin, claudin, and zonula occludens (ZO), such as ZO-2 and ZO-3), which are involved in cell-cell contact regions [31], were also greatly reduced in CENPF^{KO} cells. This was consistent with the morphological changes observed (Figure 2(c)).

Effects of CENPF silencing on the biological outcomes of PC cells

We next sought to determine if CENPF plays any major roles in controlling cell proliferation, migration, invasion, and colony formation capability. *In-vitro* wound healing, migration, and Matrigel invasion assays were conducted on both PC3 CENPF^{KO} and control cells. Starting from day 2, the cell proliferation rate of CENPF^{KO} cells was significantly reduced compared to controls (Figure 2(d)).

We further assessed the ability of the cells to form colonies in the 2-dimensonal (2D) and 3-dimensional (3D) planes. These colony formation assays revealed that CENPF^{KO} cells formed very few colonies even after 2 wk of incubation (2D, $p < 0.0001$) (Figure 2(e)). Anchorage-independent cell proliferation was measured with the 3D colony formation assay, and, compared to control cells, CENPF^{KO} cells showed very low colony formation capacity (3D, $p < 0.003$) (Figure 2(f)).

For the cell wound healing assay, a scratch was inflicted on cell cultures once they reached 90% confluence. We found that the wound healing capability of CENPF^{KO} cells was significantly delayed than the control, suggesting that the migratory ability of CENPF^{KO} cells may be impaired (Figure 2(g)). Knockout of CENPF also increased PC3 cell death by anoikis, which is apoptosis that is induced when cells are unable to attach to the extracellular matrix (ECM) [32]. Expression levels of cleaved PARP (c-PARP), an apoptotic marker, were higher in CENPF^{KO} cells compared to controls (Figure 2(h)). This was consistent with the cell viability assay results (Figure 2(i)). Furthermore, a rescue experiment using a CENPF construct showed that the effects of CENPF knockout could be diminished by inducing overexpression of CENPF (Figure 2(j)). In addition, we found that CENPF plays the same roles in DU145 PC cells, whose CENPF expression levels were as redundant as PC3 cells (Figure 2(k)). Colony formation capability (Figure 2(l)) and viability (Figure 2(m)) were both significantly decreased when CENPF was knocked-down in DU145 cells. Collectively, these results indicate that CENPF inhibition reverses EMT and suppresses the proliferative characteristics of PC cells, while simultaneously enhancing anoikis-induced apoptosis.

CENPF silencing alters the whole proteome to promote signaling and glucose metabolism

Since there have been no previous proteomics studies showing the biological function of CENPF in the context of PC, we were prompted to understand the whole proteome alterations caused by CENPF silencing. In order to understand the mechanisms

Wound-healing assay showed the slower migration of CENPF^{KO} cells, compared to Ctrl. Knockout in prostate cancer cell line. (h-i) Anoikis-induced cell apoptosis was enhanced when CENPF was downregulated. (h) Western blot analysis showed that cleaved form of PARK, an apoptotic marker, was increased in CENPF KO. (i) Levels of cell viability were measured by MTT assay after anoikis for 0, 1, 2, or 3h. All experiments were carried out in triplicate. (j) CENPF overexpression reversed the effects of CENPF knockout on cell viability in response to anoikis. (k) The protein expression of CENPF was compared in PC3, DU145, and 22RV1 PC cells. (l-m) Downregulation of CENPF reduced colony formation (l) and decreased cell viability in response anoikis (m) in DU145 cells. For all Western blot analysis, β-actin was used as the loading control. Data are representative of at least three different experiments and are expressed as the means ± SD.

underlying CENPF function, we performed mass spectrometry-based proteomics analysis, as described in the Methods. Whole-cell lysates in biological triplicates were digested with trypsin. Using LC-MS/MS, we determined which proteins were differentially expressed following CENPF knockout. In total, 549 DEPs were identified (adjusted p-value based on BH procedure ≤ 0.01 and ratio ≥ 1.5) (Supplementary Table 1), of which 130 were upregulated and 419 were downregulated, as shown in the volcano plot (Figure 3(a)). We next conducted a functional gene enrichment analysis of DEPs using the DAVID software to understand the most perturbed pathways based on previously reported GOBPs or KEGGs. Significantly enriched GOBPs included "negative regulation of microtubule polymerization" and "canonical glycolysis" (Figure 3(b)). CENPF silencing significantly enriched KEGG terms for "glycolysis/gluconeogenesis" and various metabolic pathways (Figure 3(c)). To further understand the changes in relationships among biological networks, network analysis was performed. Phosphorylation signaling transduction pathways, various metabolisms (carbohydrate, lipid, amino acids), adhesion, actin cytoskeleton, and endocytosis pathways were clearly marked as being highly enriched for by DEPs in CENPF^{KO} cells (Figure 3(d)). DEPs linked to fatty acid degradation were enriched as well (Figure 3(d)). Figure 3(e) shows the top 10 enriched pathways and the DEPs that belong to each term.

Silencing of CENPF impeded epigenetic modulation of histone markers and lipid synthesis in PC3 cells

We further defined the biological roles of CENPF in PC3 cells. Fatty acid and lipid metabolism play critical roles in energy maintenance and cellular nutrition in cancer, particularly in PC [33,34]. Biosynthesis of fatty acids utilizes glucose and exploits a pathway that is mainly controlled by an enzyme, fatty acid synthase (FASN). Prior studies have presented evidence showing that FASN is also associated with cell growth, survival, and drug resistance in PC [33]. To test the hypothetical link between CENPF levels and metabolic shifts in PC, cholesterol and free fatty acid levels were quantified in CENPF^{KO} and control PC3 cells. We found significant reduction in both cholesterol and free fatty acid levels in the CENPF^{KO} cells (Figure 4(a,b)). We further measured the expression levels of genes related to fatty acid and lipid synthesis in both cell lines. Expression levels of long-chain fatty-acid-coenzyme A ligase (ACSL1) [35], FASN [36], acetyl-CoA carboxylase (ACC), and phosphorylation levels of ACC (p-ACC) [37] were significantly decreased in CENPF^{KO} cells (Figure 4(c)). This data demonstrated that knocking-out CENPF resulted in decreased expression of lipid metabolism-associated proteins, as well as intracellular concentrations of FFAs and cholesterol.

In addition, we found that expression levels of acyl-coenzyme A synthetase short-chain family members 1 and 2 (ACSS1 and ACSS2), which are key regulatory proteins for lipid synthesis and energy generation, were also downregulated when CENPF was silenced (Figure 4(d)). Western blot analysis of CENPF^{KO} cells showed that ACSS2 expression greatly decreased, while ACSS1 was modestly downregulated, compared to controls (Figure 4(d)). Interestingly, ACSS2 expression is positively correlated with PC progression [38–40]. ACSS2 has been reported to mediate acetyl modification of histone proteins (histone acetylation) and gene regulation through the generation of acetyl-CoA [41]. Thus, we speculated that CENPF is required for regulating acetate metabolism and contributes to epigenetic modification through its effects on histones via ACSS1 and/or ACSS2 (Figure 4(e)). Our acetate measurements, using a commercial kit, showed that acetate levels in CENPF^{KO} cells were almost completely diminished. We also evaluated for expression of acetylated histones in CENPF^{KO} and control cells. Western blot analysis found that expression levels of key acetylated histones, including H2A, H2B, H3 and H4, were significantly reduced in CENPF^{KO} cells (Figure 4(f)).

CENPF^{KO} cells have a distinct tyrosine phosphorylation profile

We next sought to profile the phosphorylation events that occur when CENPF is knocked-out. Just to get a general idea of the phosphorylation statuses of specific signaling pathways modulated by CENPF silencing, a series of western blot

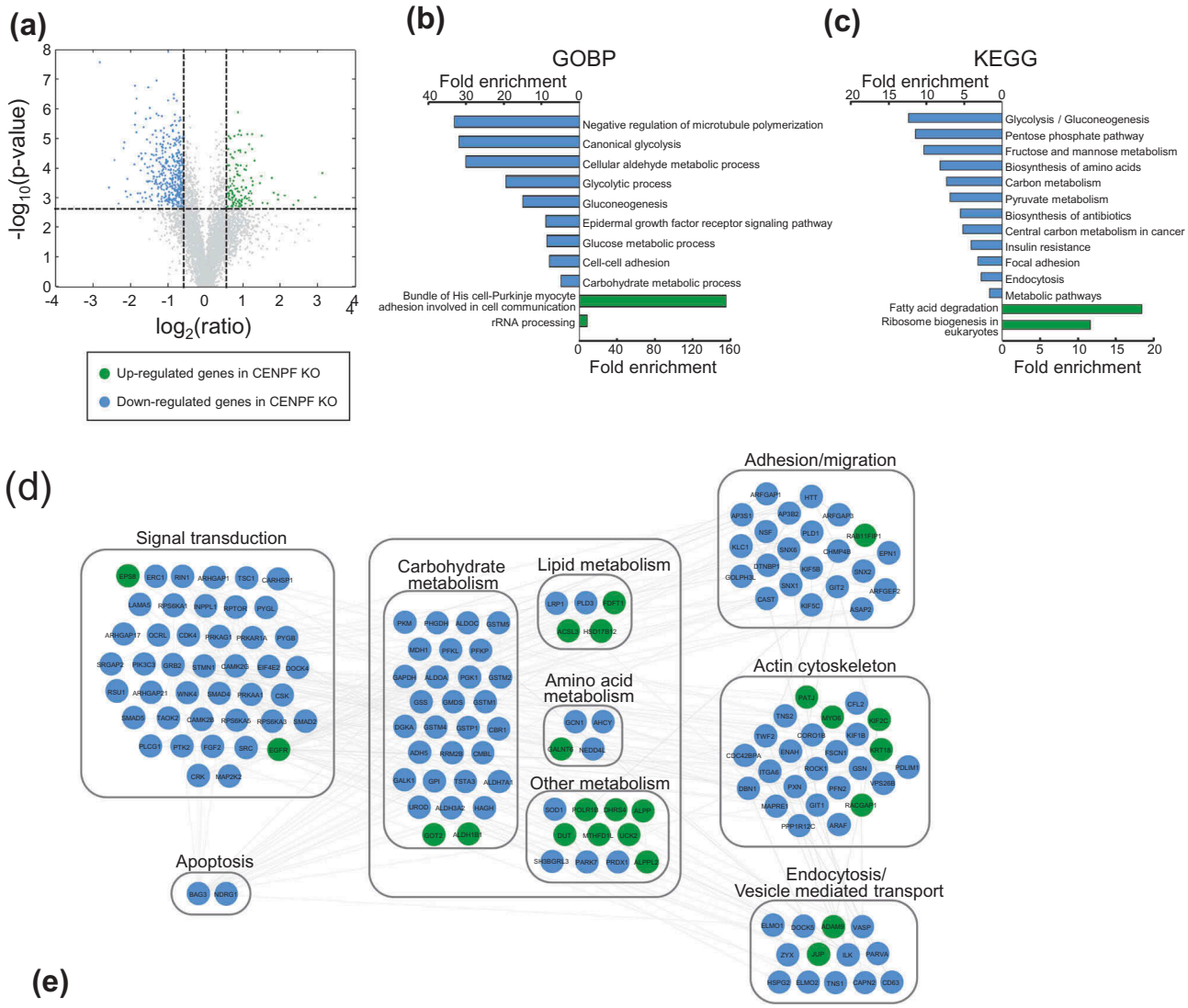

Term	Fold enrichment	Adjusted p-value	Genes
hsa00010:Glycolysis / Gluconeogenesis	12.38	1.38E-09	ALDOA, PFKL, ALDOC, PGAM1, ADH5, PFKP, ACSS2, ALDH3A2, PKM, GPI, ALDH7A1, AKR1A1, ENO2, PGK1, GAPDH
hsa00030:Pentose phosphate pathway	11.44	5.30E-03	ALDOA, GPI, PGLS, PFKL, ALDOC, PFKP
hsa00051:Fructose and mannose metabolism	10.37	7.16E-03	ALDOA, PFKL, GMDS, ALDOC, PFKP, TSTA3
hsa01230:Biosynthesis of amino acids	8.22	3.01E-05	ALDOA, PKM, ALDH7A1, PFKL, ALDOC, PHGDH, ENO2, PGAM1, PFKP, PGK1, GAPDH
hsa01200:Carbon metabolism	7.34	6.44E-07	ALDOA, PFKL, ALDOC, PGAM1, ADH5, PFKP, ACSS2, PKM, GPI, PGLS, PHGDH, ENO2, PGK1, GAPDH, MDH1
hsa00620:Pyruvate metabolism	6.91	8.78E-02	PKM, ALDH7A1, ACSS2, ALDH3A2, MDH1
hsa01130:Biosynthesis of antibiotics	5.48	7.43E-08	ALDOA, PFKL, ALDOC, PFKP, PGAM1, ADH5, AMPD2, ACSS2, ALDH3A2, CMBL, PKM, GPI, PGLS, ALDH7A1, AKR1A1, PHGDH, ENO2, PGK1, PAPSS2, GAPDH, MDH1
hsa05230:Central carbon metabolism in cancer	5.18	8.28E-02	SLC16A3, PKM, PFKL, MAP2K2, PGAM1, PFKP
hsa04931:Insulin resistance	4.09	5.64E-02	RPS6KA3, RPS6KA1, PYGL, PTPA, PRKAG1, MGEA5, PRKAA1, PYGB
hsa04510:Focal adhesion	3.22	2.91E-02	PTK2, ROCK1, ITGA6, LAMA5, GRB2, COL6A2, COL6A1, ZYX, CAPN2, SRC, VASP, PXN

Figure 3. Silencing of CENPF perturbed proteome. (a) Unbiased global proteomics analysis was performed using CENPF^{KO} cells and Ctrl. The volcano plot shows the differentially expressed proteins. Green, upregulated; Blue, downregulated proteins in CENPF^{KO} cells, compared to Ctrl (b-c) Functional enrichment analysis of DEPs was performed using DAVID. GOBP- (b) or KEGG-based analysis (c), (d) Network modeling suggested activation of phosphotyrosine signaling in PC cells. (e) The list of DEPs who belong to the 10 most-enriched pathways.

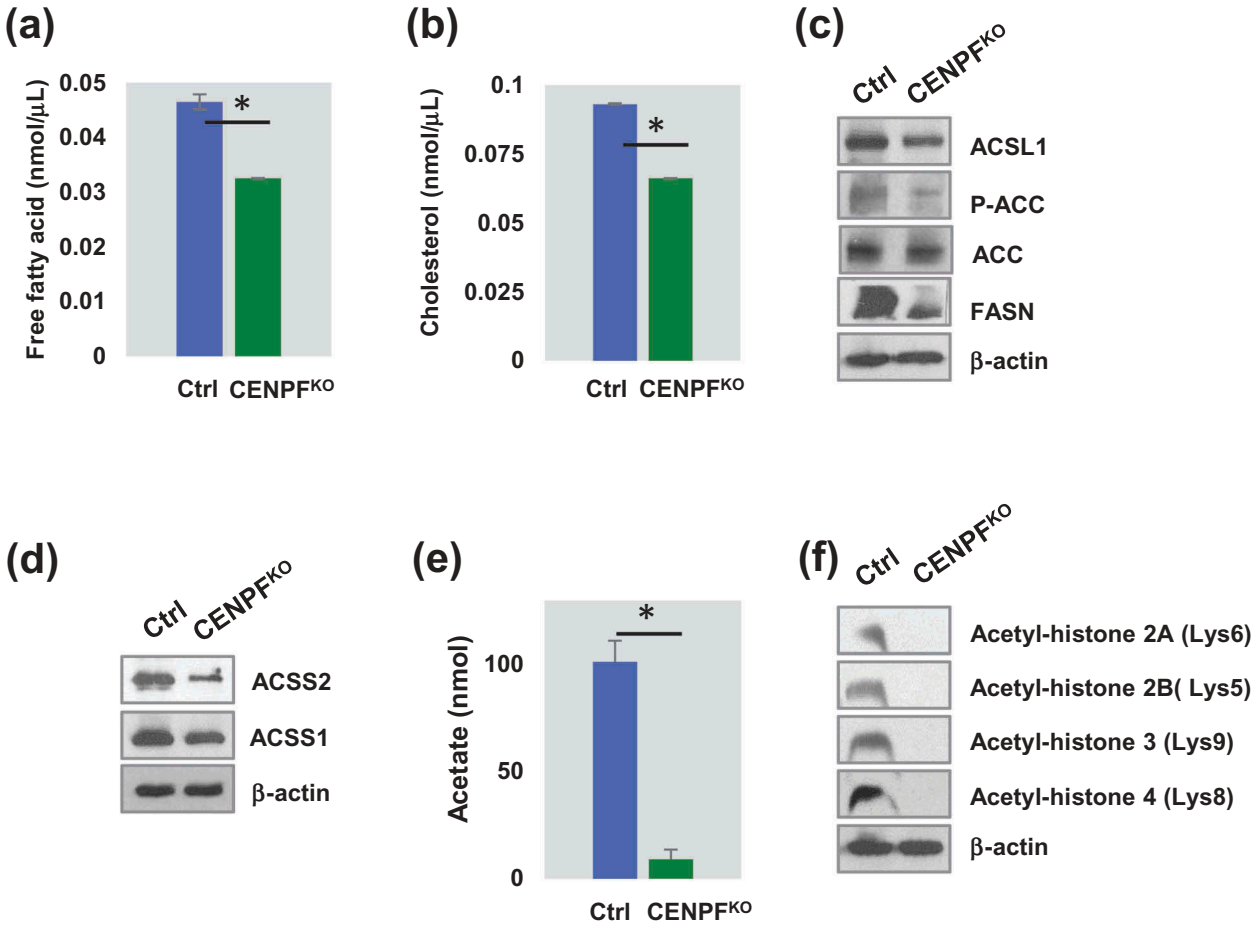

Figure 4. CENPF involved in epigenetic regulation of histone and lipid metabolism. (a) The histogram showed free fatty acid level. (b) Cholesterol level between CENPF^{KO} and Ctrl. (c) Western blot analysis showing long-chain fatty-acid-coenzyme A ligase (ACSL1), acetyl-CoA carboxylase (ACC), phosphorylation level of ACC (p-ACC) and fatty acid synthase (FASN). (d) Both ACSS1 and ACSS2 expression are reduced in CENPF^{KO}. (E) CENPF^{KO} decreased the synthesis of acetate to Ctrl. (f) Western blot analysis of key acetylated histone markers (H2A, H2B, H3, and H4) between CENPF^{KO} and Ctrl. The data represent the mean ± standard deviation. A two-tailed Student's t-test was used to calculate statistical significance. β-actin was used as the loading control.

analyses were carried out on both CENPF^{KO} PC3 cells and controls. We found that CENPF is required for maintaining various phosphorylation events that are important for PC progression. Compared to control cells, the phosphorylation levels of Src (Tyr416), β-catenin (Ser45), p21 activated kinase 1 (PAK1) (Thr423), and NF-κB (Ser536) were elevated in CENPF^{KO} cells (Figure 5(a)). In contrast, phosphorylation of Akt (Ser473), extracellular signal-regulated kinase 1/2 (ERK1/2) (Thr202/Tyr204), S6Kinase (Thr389), mTOR (Ser2448), and p38MAPK (Thr180/Tyr182) decreased in CENPF^{KO} cells compared to controls. However, the total protein expression levels remained unchanged (data were not shown) (Figure 5(a)). Interestingly, western blot analysis with anti-phospho-tyrosine antibodies revealed that CENPF^{KO} cells have stronger p-Tyr intensity with distinct phosphorylation patterns (Figure 5 (b)), signifying that subduing CENPF increased or changed patterns of tyrosine phosphorylation.

Tyrosine phosphorylation levels of pyruvate kinase M2 (PKM2) were decreased in CENPF^{KO} cells

Although phosphorylation of tyrosine sites constitutes less than a few percentage of all phosphorylation events, we next attempted to specifically focus on defining tyrosine phosphorylation events. This was because previous findings have indicated that phospho-tyrosine (pTyr) based phosphoproteomics can be utilized as a tool for measuring the critical events needed for activating key kinases. In

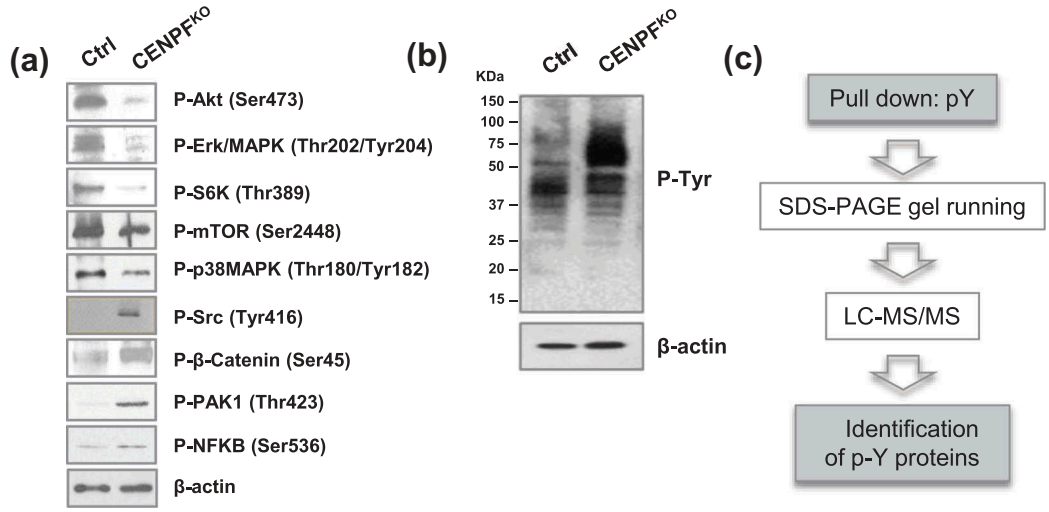

(d)

No.	Accession Number	Protein names	Gene names	Peptides	Unique Peptides	MS/MS count
1	P35579	Myosin-9	MYH9	182	157	509
2		unknown				
3	P60709	Actin, cytoplasmic 1;Actin, cytoplasmic 1, N-terminally processed	ACTB	30	1	166
4	P14618	Pyruvate kinase PKM	PKM	38	38	125
5	P06733	Alpha-enolase	ENO1	31	28	131
6	P35580	Myosin-10	MYH10	74	49	71
7	P08670	Vimentin	VIM	33	32	62
8		unknown				
9	P00558	Phosphoglycerate kinase 1	PGK1	24	24	77
10	P04406	Glyceraldehyde-3-phosphate dehydrogenase	GAPDH	21	21	90

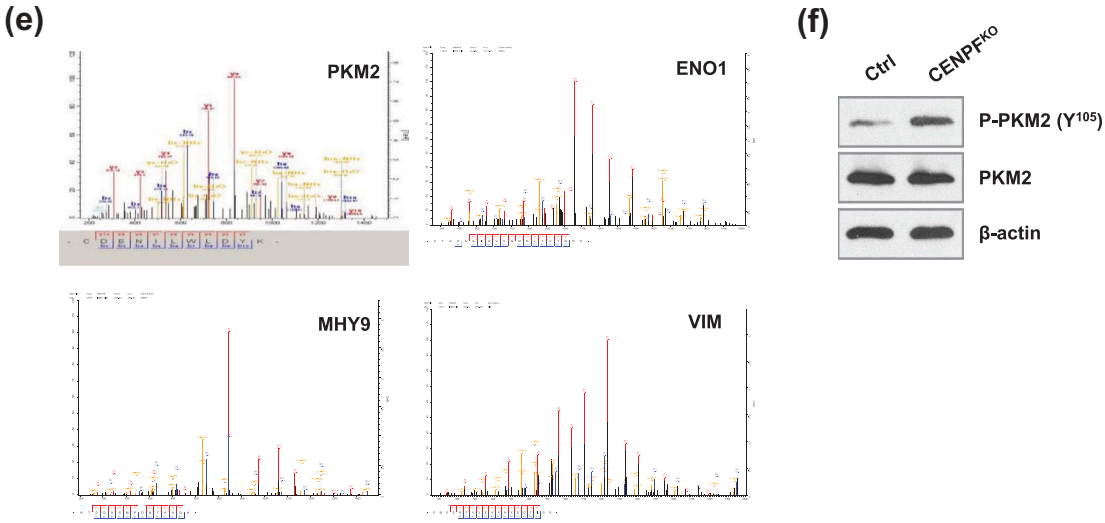

Figure 5. CENPF reduce metabolism in prostate cancer cells. (a) Western blot analysis of key signal transduction proteins. (b) Western blot analysis of phospho-tyrosine (pY) signaling was performed in CENPF^{KO} cells and Ctrl. (c) A workflow including phospho-tyrosine-enrichment by protein pull-down and LC–MS/MS illustrates the experimental design to identify the tyrosine phosphorylated proteins specifically enriched in CENPF^{KO} cells. (d) The 10 top proteins identified from B. (e) Representative MS spectrum of PKM2, ENO1, MHY9, and VIM, which were identified in this study. (f) Phosphorylation of PKM2 at Y^{105} and non-phosphorylated form of PKM2 were assessed by western blot analysis in CENPF^{KO} cells and Ctrl. β-actin was used as the loading control.

turn, this allows for better recognizing perturbation of downstream signaling pathways [42,43]. To further define tyrosine-phosphorylated proteins in CENPF^{KO} cells and controls, proteomics profiling and bioinformatics approaches were applied. Tyrosine-phosphorylated proteins were enriched for target protein identification via mass spectrometry. This enrichment was done using p-Tyr, an anti-phospho-tyrosine antibody coupled to agarose beads. The coupled proteomic identification was then carried out using LC-MS/MS (Figure 5(c)). This procedure resulted in a list of candidate proteins that may be biologically important for PC progression. Figure 5(d) shows the top 10 proteins, which included myosin-9, actin, PKM, alpha-enolase, myosin-10, vimentin, phosphoglycerate kinase 1, glyceraldehyde-3-phosphate dehydrogenase, and 2 additional proteins without annotations.

PKM2 is known as a tumor-specific isoform of pyruvate kinase (PK), the rate-limiting enzyme during glycolysis, which catalyzes the production of pyruvate and adenosine 5'-triphosphate (ATP) from phosphoenolpyruvate (PEP) and adenosine 5'-diphosphate (ADP) [44]. The detected tandem mass spectrum of PKM2 and other proteins (e.g. Enolase 1 (ENO1), myosin, heavy chain 9 (MHY9), Vimentin (VIM)) are shown in Figure 5(e). Additional western blot analysis confirmed that phosphorylation levels of PKM2 at site Y^{105} significantly increased in CENPF^{KO} cells, while expression of total PKM2 levels remained unchanged (Figure 5(f)). Given prior findings demonstrating that PKM2 activity is crucial for aerobic glycolysis and that phosphorylation of the Y^{105} site may inactivate PKM2 [45], our data suggests that knockout of CENPF may be inactivating PKM2 via Y^{105} site phosphorylation and this may be associated with the biological outcomes observed.

Both mitochondrial respiration and glycolysis are downregulated in CENPF^{KO} cells

Given that CENPF silencing leads to PKM2 inactivation, we hypothesized that CENPF can regulate cancer-associated metabolism, such as aerobic glycolysis and mitochondrial respiration. To determine the effect of CENPF knockout on PC energy shifts, we used the Seahorse XFe24 Analyzer [46]. Mitochondrial respiration was profiled by measuring the oxygen consumption rate (OCR), which can determine the changes in levels of oxidative phosphorylation (OXPHOS)-dependent ATP generation. Compared to the control PC3 cells, CENPF^{KO} cells had a considerable decrease in OCR (Figure 6(a)). Both the basal and maximum oxygen consumption rates were significantly reduced; approximately 35% and 50%, respectively, of the control rates were observed in CENPF^{KO} cells (Figure 6(b,c)). Extracellular acidification rate (ECAR), which is an indicator of glycolysis, also decreased in CENPF^{KO} cells (Figure 6(d)). Collectively, these experimental results suggest that biogenesis was significantly reduced in CENPF^{KO} cells and that these cells were metabolically quiescent, compared to controls.

We next examined whether CENPF regulates mitochondrial quantity. Mitochondrial metabolic respiration-associated proteins, including TOM40 (a central component of the translocase of outer membrane (TOM) receptor complex in mitochondria) and a series of mitochondrial oxidative phosphorylation (OXPHOS) proteins [47], were measured via western blot analysis. The expression levels of TOM 40, C I subunit (NDUFB8), C II subunit (SDHB), C III core protein 2 (UQCRC2), C IV subunit (I MTCO1), and C V alpha subunit (ATP5A) decreased in CENPF^{KO} cells (Figure 6(e)). These findings suggest that CENPF abrogation results in attenuated metabolism evidenced by impaired mitochondrial ATP production and glycolysis. Furthermore, we tested whether the increase in PKM2 phosphorylation can be reversed when mitochondrial biogenesis is boosted by pioglitazone, a medication that is widely used for diabetes [48,49]. Western blot analysis suggested that pioglitazone treatment significantly decreased CENPF knockout-induced tyrosine phosphorylation of PKM2 (Figure 6(f)).

Discussion

Since the discovery of evidence presenting that perturbed metabolic pathways, such as oxidative phosphorylation, glycolysis, and fatty acid biosynthesis, can suppress cancer cell growth,

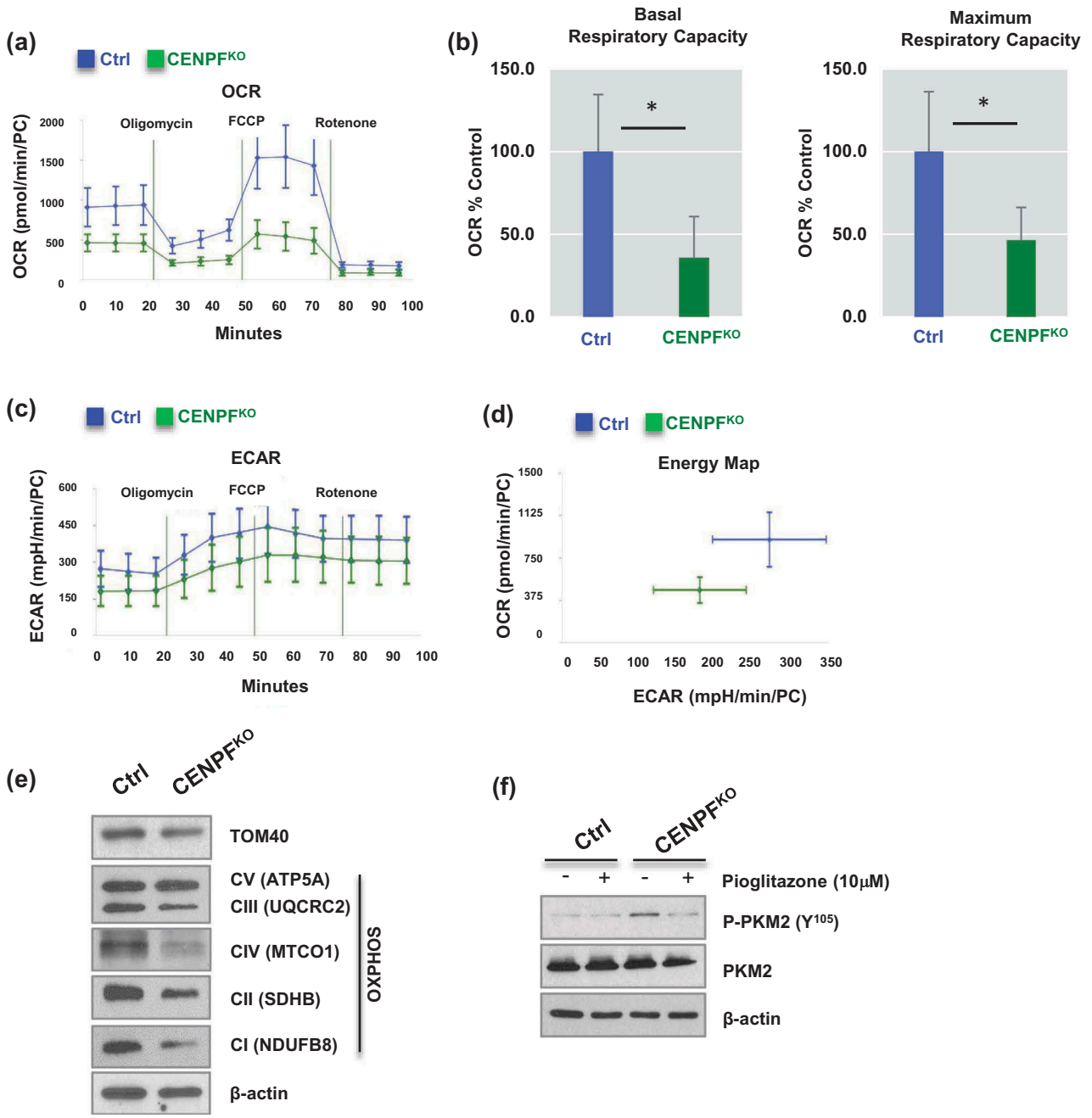

Figure 6. Silencing of CENPF decreased mitochondrial oxidative phosphorylation. The mitochondrial biogenetic activity was determined for CENPF^{KO} and Ctrl in real-time using the Seahorse extracellular flux analyzer. (a) The oxygen consumption rate (OCR) curves in CENPF^{KO} cells and Ctrl treated with oligomycin, FCCP and rotenone/antimycin A (n = 6 independent experiments). The OCR curves were determined by using a Seahorse XF24 Analyzer. (b) Basal and maximum respiratory capacity normalized to the cell numbers in CENPF^{KO} cells and Ctrl. (c) Extracellular acidification rate (ECAR) was determined. (d) An energy map showing difference between CENPF^{KO} cells and Ctrl. (e) Western blot analysis was performed to measure the levels of TAM20 and OXPHOS proteins. (f) Western blot data showing phospho-PKM2 (Y^{105}) and PKM2 expression in CENPF^{KO} cells and Ctrl in presence or absence of pioglitazone. Both cells were treated with 10μM pioglitazone for 24 h before sample preparation. The graphs shown here are representative examples of three independent experiments. The data represent the mean ± standard deviation. A two-tailed Student's t-test was used to calculate statistical significance.

cancer metabolism has become an emerging field [50–52]. In this study, a series of unbiased proteomics and consecutive functional experiments revealed that knocking-out CENPF impaired mitochondrial functioning and signaling activation that is required for PC growth and metastasis. We herein demonstrated that CENPF knock-out can reverse EMT and suppress

metabolic rates by reducing OXPHOS and glycolysis, possibly through its effects on PKM2.

High levels of PKM2 are expressed in a variety of human tumors, including lung, breast, and colon cancer [53], and are reported to promote the Warburg effect [44]. PKM2 exists as a low-activity dimeric or high-activity tetrameric form, and cancer cells predominantly express the low-activity dimeric form with a reduced ability to convert phosphoenolpyruvate to pyruvate [54]. Phosphorylation of PKM2 at Tyr105 is reported to disrupt its active tetrameric form [45,55] and reduce its catalytic activity. PKM2 phosphorylation at Tyr105 is known to impair PKM2's enzymatic activity and ability to catalyze the formation of ATP from ADP using a phosphate group from 2-phosphoenolpyruvate (PEP).

Our histone acetylation data suggested that metabolic reprogramming influences histone acetylation levels in PC (Figure 4(a)). Previous studies have demonstrated the correlation between histone acetylation levels and clinical outcomes, such as recurrence and patient survival, in various cancer types [56]. Other studies have shown that elevated nuclear levels of acetylated histone 2A.Z or decreased global histone acetylation in PC was correlated to poorer prognoses [52,57,58]. Although it is well-accepted that histone acetylation has important roles in gene regulation and DNA repair, the biological significance of global histone acetylation levels and its underlying effects on metabolic rewiring (e.g. how histone modification regulates PC progression and treatment response) remain elusive.

Since nuclear acetylation events are highly dependent on the availability of acetyl-CoA, we decided to survey acetate levels in our control and $CENPF^{KO}$ PC3 cell lines. An acetate assay showed decreased acetate levels in $CENPF^{KO}$ cells, which was consistent with their histone acetylation levels (Figure 4(b)). Lipogenic enzymes, such as ACCS, are the primary enzymatic sources of acetyl-CoA outside of the mitochondria. Several studies have demonstrated that ACLY may also be present in the nucleus and plays a crucial role in regulating histone acetylation. However, our study did not provide any evidence showing CENPF affecting ACLY's role in histone acetylation.

In summary, our study demonstrates that CENPF, a centromere protein, is required for PC progression through its effects on signaling, glucose metabolism, and epigenetic regulation. Improved understanding of whether a perturbed metabolism precedes changes in epigenetic regulation or vice versa could provide clues on the cross talk that occurs between oncogenic metabolic reprogramming and the epigenome. The finding that the PKM2–mediated glucose metabolism pathway is a key player in maintaining mitochondrial function represents potential therapeutic strategies against PC. Future functional studies assessing the causative role of histone acetylation with altered metabolism by CENPF silencing are needed to further grasp how CENPF regulates mitochondrial functioning during metabolic and epigenetic changes in PC progression.

Acknowledgments

We would like to thank Drs. Wei Yang at the Biomarker Discovery Platform Core (Cedars-Sinai Medical Center) for guidance with proteomics studies and assistance with liquid chromatography-mass spectrometry (LC-MS/MS). The authors acknowledge support from National Institutes of Health grants (1U01DK103260, 1R01DK100974, U24 DK097154, NIH NCATS UCLA CTSI UL1TR000124), Department of Defense grants (W81XWH-15-1-0415), Centers for Disease Controls and Prevention (1U01DP006079), IMAGINE NO IC Research Grant, the Steven Spielberg Discovery Fund in Prostate Cancer Research Career Development Award, the U.S.-Egypt Science and Technology Joint Fund (to J.K.), and Florida Department of Health, Bankhead-Coley Cancer Research Program (5BC03) (to M.K.). J.K. is former recipient of Interstitial Cystitis Association Pilot Grant, a Fishbein Family IC Research Grant, New York Academy of Medicine, and Boston Children's Hospital Faculty Development. The funders had no role in the design, data collection and analysis, decision to publish or preparation of the manuscript. In addition, this article is derived from the Subject Data funded in whole or part by National Academies of Sciences, Engineering, and Medicine (NAS) and The United States Agency for International Development (USAID). Any opinions, findings, conclusions, or recommendations expressed in this article are those of the authors alone, and do not necessarily reflect the views of USAID or NAS.

Author contributions

JK and HLK designed the study. MS, AY, PL, AA, BZ, and HP carried out all biochemical experiments and

mitochondrial metabolomics analysis. ML performed bioinformatics analysis. MS and MK participated in interpretation of data and writing of the manuscript. MK and AA provided valuable insights on study design and data interpretation. JK wrote the manuscript. All authors discussed the results and commented on the manuscript at all stages.

Disclosure statement

No potential conflict of interest was reported by the authors.

Funding

This work was supported by the Centers for Disease Control and Prevention [1U01DP006079]; Foundation for the National Institutes of Health [1U01DK103260];U.S. Department of Defense [W81XWH-15-1-0415]. The authors acknowledge support from National Institutes of Health grants (1U01DK103260, 1R01DK100974, U24 DK097154, NIH NCATS UCLA CTSI UL1TR000124), Department of Defense grants (W81XWH-15-1-0415), Centers for Disease Controls and Prevention (1U01DP006079), IMAGINE NO IC Research Grant, the Steven Spielberg Discovery Fund in Prostate Cancer Research Career Development Award, the U. S.- Egypt Science and Technology Joint Fund (to J.K.), and Florida Department of Health, Bankhead- Coley Cancer Research Program (5BC03) (to M.K.). J.K. is former recipient of Interstitial Cystitis Association Pilot Grant, a Fishbein Family IC Research Grant, New York Academy of Medicine,and Boston Children's Hospital Faculty Development. The funders had no role in the design, data-collection and analysis, decision to publish or preparation of the manuscript. In addition, this article is derived from the Subject Data funded in whole or part by National Academies of Sciences, Engineering, and Medicine (NAS) and The United States Agency for International Development (USAID). Any opinions, findings, conclusions, or recommendations expressed in this article are those of the authors alone, and do not necessarily reflect the views of USAID or NAS.

References

[1] Siegel RL, Miller KD, Jemal A. Cancer statistics, 2016. CA Cancer J Clin. 2016 Jan-Feb;66(1):7–30. PubMed PMID: 26742998.

[2] Schroder FH, Hugosson J, Roobol MJ, et al. Screening and prostate-cancer mortality in a randomized European study. N Engl J Med. 2009 Mar 26;360 (13):1320–1328. PubMed PMID: 19297566.

[3] Andriole GL, Crawford ED, Grubb RL 3rd, et al. Mortality results from a randomized prostate-cancer screening trial. N Engl J Med. 2009 Mar 26;360 (13):1310–1319. PubMed PMID: 19297565; PubMed Central PMCID: PMC2944770.

[4] Cutruzzola F, Giardina G, Marani M, et al. Glucose metabolism in the progression of prostate cancer. Front Physiol. 2017;8:97. PubMed PMID: 28270771; PubMed Central PMCID: PMC5318430.

[5] Mitsuzuka K, Arai Y. Metabolic changes in patients with prostate cancer during androgen deprivation therapy. Int J Urol. 2017 Oct 20. PubMed PMID: 29052905. DOI:10.1111/iju.13473

[6] Levine AJ, Puzio-Kuter AM. The control of the metabolic switch in cancers by oncogenes and tumor suppressor genes. Science. 2010 Dec 03;330 (6009):1340–1344. PubMed PMID: 21127244.

[7] Elstrom RL, Bauer DE, Buzzai M, et al. Akt stimulates aerobic glycolysis in cancer cells. Cancer Res. 2004 Jun 1;64(11):3892–3899. PubMed PMID: 15172999.

[8] Miller DM, Thomas SD, Islam A, et al. c-Myc and cancer metabolism. Clin Cancer Res. 2012 Oct 15;18 (20):5546–5553. PubMed PMID: 23071356; PubMed Central PMCID: PMCPMC3505847.

[9] Smith B, Schafer XL, Ambeskovic A, et al. Addiction to coupling of the Warburg effect with glutamine catabolism in cancer cells. Cell Rep. 2016 Oct 11;17 (3):821–836. PubMed PMID: 27732857; PubMed Central PMCID: PMCPMC5108179.

[10] Courtnay R, Ngo DC, Malik N, et al. Cancer metabolism and the Warburg effect: the role of HIF-1 and PI3K. Mol Biol Rep. 2015 Apr;42(4):841–851. PubMed PMID: 25689954.

[11] Dang CV, Kim JW, Gao P, et al. The interplay between MYC and HIF in cancer. Nat Rev Cancer. 2008 Jan;8 (1):51–56. PubMed PMID: 18046334.

[12] Vousden KH, Ryan KM. p53 and metabolism. Nat Rev Cancer. 2009 Oct;9(10):691–700. PubMed PMID: 19759539.

[13] Matuszak EA, Kyprianou N. Androgen regulation of epithelial-mesenchymal transition in prostate tumorigenesis. Expert Rev Endocrinol Metab. 2011 May;6(3):469–482. PubMed PMID: 23667383; PubMed Central PMCID: PMC3648215.

[14] Bitting RL, Schaeffer D, Somarelli JA, et al. The role of epithelial plasticity in prostate cancer dissemination and treatment resistance. Cancer Metastasis Rev. 2014 Sep;33(2–3):441–468. PubMed PMID: 24414193; PubMed Central PMCID: PMC4230790.

[15] Varis A, Salmela AL, Kallio MJ. Cenp-F (mitosin) is more than a mitotic marker. Chromosoma. 2006 Aug;115(4):288–295. PubMed PMID: 16565862.

[16] Liao H, Winkfein RJ, Mack G, et al. CENP-F is a protein of the nuclear matrix that assembles onto kinetochores at late G2 and is rapidly degraded after mitosis. J Cell Biol. 1995 Aug;130(3):507–518. PubMed PMID: 7542657; PubMed Central PMCID: PMC2120529.

[17] Testa JR, Zhou JY, Bell DW, et al. Chromosomal localization of the genes encoding the kinetochore proteins CENPE and CENPF to human chromosomes 4q24–>q25 and 1q32–>q41, respectively, by

fluorescence in situ hybridization. Genomics. 1994 Oct;23(3):691–693. PubMed PMID: 7851898.

[18] Li P, You S, Nguyen C, et al. Genes involved in prostate cancer progression determine MRI visibility. Theranostics. 2018;8(7):1752–1765. PubMed PMID: 29556354; PubMed Central PMCID: PMC5858498.

[19] Mitrofanova A, Aytes A, Zou M, et al. Predicting drug response in human prostate cancer from preclinical analysis of in vivo mouse models. Cell Rep. 2015 Sep 29;12(12):2060–2071. PubMed PMID: 26387954; PubMed Central PMCID: PMC4591242.

[20] Aytes A, Mitrofanova A, Lefebvre C, et al. Cross-species regulatory network analysis identifies a synergistic interaction between FOXM1 and CENPF that drives prostate cancer malignancy. Cancer Cell. 2014 May 12;25(5):638–651. PubMed PMID: 24823640; PubMed Central PMCID: PMC4051317.

[21] Lin SC, Kao CY, Lee HJ, et al. Dysregulation of miRNAs-COUP-TFII-FOXM1-CENPF axis contributes to the metastasis of prostate cancer. Nat Commun. 2016 Apr 25;7:11418. PubMed PMID: 27108958; PubMed Central PMCID: PMC4848536.

[22] Jung JH, You S, Oh JW, et al. Integrated proteomic and phosphoproteomic analyses of cisplatin-sensitive and resistant bladder cancer cells reveal CDK2 network as a key therapeutic target. Cancer Lett. 2018 Nov 28;437:1–12. PubMed PMID: 30145203; PubMed Central PMCID: PMCPMC6181132.

[23] Rinas A, Espino JA, Jones LM. An efficient quantitation strategy for hydroxyl radical-mediated protein footprinting using Proteome discoverer. Anal Bioanal Chem. 2016 Apr;408(11):3021–3031. PubMed PMID: 26873216.

[24] Morley S, You S, Pollan S, et al. Regulation of microtubule dynamics by DIAPH3 influences amoeboid tumor cell mechanics and sensitivity to taxanes. Sci Rep. 2015 Jul 16;5:12136. PubMed PMID: 26179371; PubMed Central PMCID: PMC4503992.

[25] Huang DW, Sherman BT, Lempicki RA. Systematic and integrative analysis of large gene lists using DAVID bioinformatics resources. Nat Protoc. 2009;4 (1):44–57. PubMed PMID: 19131956.

[26] Patil A, Nakai K, Nakamura H. HitPredict: a database of quality assessed protein-protein interactions in nine species. Nucleic Acids Res. 2011 Jan 39 (Database issue): D744–9. PubMed PMID: 20947562; PubMed Central PMCID: PMC3013773. DOI:10.1093/nar/gkq897

[27] Shannon P, Markiel A, Ozier O, et al. Cytoscape: a software environment for integrated models of biomolecular interaction networks. Genome Res. 2003 Nov;13(11):2498–2504. PubMed PMID: 14597658; PubMed Central PMCID: PMC403769.

[28] Horning AM, Wang Y, Lin CK, et al. Single-cell RNA-seq reveals a subpopulation of prostate cancer cells with enhanced cell-cycle-related transcription and attenuated androgen response. Cancer Res. 2018 Feb 15;78(4):853–864. PubMed PMID: 29233929; PubMed Central PMCID: PMCPMC5983359.

[29] Sun Y, Wang BE, Leong KG, et al. Androgen deprivation causes epithelial-mesenchymal transition in the prostate: implications for androgen-deprivation therapy. Cancer Res. 2012 Jan 15;72(2):527–536. PubMed PMID: 22108827.

[30] Gao F, Al-Azayzih A, Somanath PR. Discrete functions of GSK3alpha and GSK3beta isoforms in prostate tumor growth and micrometastasis. Oncotarget. 2015 Mar 20;6(8):5947–5962. PubMed PMID: 25714023; PubMed Central PMCID: PMCPMC4467413.

[31] Landers KA, Samaratunga H, Teng L, et al. Identification of claudin-4 as a marker highly overexpressed in both primary and metastatic prostate cancer. Br J Cancer. 2008 Aug 5;99(3):491–501. PubMed PMID: 18648369; PubMed Central PMCID: PMCPMC2527792.

[32] Sakamoto S, Kyprianou N. Targeting anoikis resistance in prostate cancer metastasis. Mol Aspects Med. 2010 Apr;31(2):205–214. PubMed PMID: 20153362; PubMed Central PMCID: PMCPMC2988681.

[33] Suburu J, Chen YQ. Lipids and prostate cancer. Prostaglandins Other Lipid Mediat. 2012 May;98(1–-2):1–10. PubMed PMID: 22503963; PubMed Central PMCID: PMC3348998.

[34] Itkonen HM, Brown M, Urbanucci A, et al. Lipid degradation promotes prostate cancer cell survival. Oncotarget. 2017 Jun 13;8(24):38264–38275. PubMed PMID: 28415728; PubMed Central PMCID: PMC5503531.

[35] Gao Y, Islam MS, Tian J, et al. Inactivation of ATP citrate lyase by Cucurbitacin B: A bioactive compound from cucumber, inhibits prostate cancer growth. Cancer Lett. 2014 Jul 10;349(1):15–25. PubMed PMID: 24690568.

[36] Huang M, Koizumi A, Narita S, et al. Diet-induced alteration of fatty acid synthase in prostate cancer progression. Oncogenesis. 2016 Feb 15;5:e195. PubMed PMID: 26878389; PubMed Central PMCID: PMC5154344.

[37] Park HU, Suy S, Danner M, et al. AMP-activated protein kinase promotes human prostate cancer cell growth and survival. Mol Cancer Ther. 2009 Apr;8 (4):733–741. PubMed PMID: 19372545; PubMed Central PMCID: PMCPMC2775041.

[38] Mews P, Donahue G, Drake AM, et al. Acetyl-CoA synthetase regulates histone acetylation and hippocampal memory. Nature. 2017 Jun 15;546(7658):381–386. PubMed PMID: 28562591; PubMed Central PMCID: PMC5505514.

[39] Shi L, Tu BP. Acetyl-CoA and the regulation of metabolism: mechanisms and consequences. Curr Opin Cell Biol. 2015 Apr;33:125–131. PubMed PMID: 25703630; PubMed Central PMCID: PMC4380630.

[40] Schug ZT, Vande Voorde J, Gottlieb E. The metabolic fate of acetate in cancer. Nat Rev Cancer. 2016 Nov;16 (11):708–717. PubMed PMID: 27562461.

[41] Gao X, Lin SH, Ren F, et al. Acetate functions as an epigenetic metabolite to promote lipid synthesis under

hypoxia. Nat Commun. 2016 Jun 30;7:11960. PubMed PMID: 27357947; PubMed Central PMCID: PMCPMC4931325.

[42] Drake JM, Graham NA, Stoyanova T, et al. Oncogene-specific activation of tyrosine kinase networks during prostate cancer progression. Proc Natl Acad Sci U S A. 2012 Jan 31;109(5):1643–1648. PubMed PMID: 22307624; PubMed Central PMCID: PMC3277127.

[43] Labots M, van der Mijn JC, Beekhof R, et al. Phosphotyrosine-based-phosphoproteomics scaled-down to biopsy level for analysis of individual tumor biology and treatment selection. J Proteomics. 2017 Jun 6;162:99–107. PubMed PMID: 28442448.

[44] Christofk HR, Vander Heiden MG, Harris MH, et al. The M2 splice isoform of pyruvate kinase is important for cancer metabolism and tumour growth. Nature. 2008 Mar 13;452(7184):230–233. PubMed PMID: 18337823.

[45] Hitosugi T, Kang S, Vander Heiden MG, et al. Tyrosine phosphorylation inhibits PKM2 to promote the Warburg effect and tumor growth. Sci Signal. 2009 Nov 17;2(97):ra73. PubMed PMID: 19920251; PubMed Central PMCID: PMC2812789.

[46] Wu M, Neilson A, Swift AL, et al. Multiparameter metabolic analysis reveals a close link between attenuated mitochondrial bioenergetic function and enhanced glycolysis dependency in human tumor cells. Am J Physiol Cell Physiol. 2007 Jan;292(1): C125–36. PubMed PMID: 16971499.

[47] Georgieva E, Ivanova D, Zhelev Z, et al. Mitochondrial dysfunction and redox imbalance as a diagnostic marker of "Free Radical Diseases". Anticancer Res. 2017 Oct;37(10):5373–5381. PubMed PMID: 28982845.

[48] Schernthaner G, Currie CJ, Schernthaner GH. Do we still need pioglitazone for the treatment of type 2 diabetes? A risk-benefit critique in 2013. Diabetes Care. 2013 Aug;36(Suppl 2):S155–S161. PubMed PMID: 23882041; PubMed Central PMCID: PMCPMC3920795.

[49] Boxall N, Bennett D, Hunger M, et al. Evaluation of exposure to pioglitazone and risk of prostate cancer: a nested case-control study. BMJ Open Diabetes Res Care. 2016;4(1):e000303. PubMed PMID: 28074141; PubMed Central PMCID: PMCPMC5174825.

[50] Kim WJ, Kim J. Looking to the metabolic landscapes for prostate health monitoring. Prostate Int. 2017 Sep;5 (3):85–88. PubMed PMID: 28828350; PubMed Central PMCID: PMC5551909.

[51] Lue HW, Podolak J, Kolahi K, et al. Metabolic reprogramming ensures cancer cell survival despite oncogenic signaling blockade. Genes Dev. 2017 Nov 14. PubMed PMID: 29138276. DOI:10.1101/gad.305292.117

[52] Webber LP, Wagner VP, Curra M, et al. Hypoacetylation of acetyl-histone H3 (H3K9ac) as marker of poor prognosis in oral cancer. Histopathology. 2017 Aug;71(2):278–286. PubMed PMID: 28326594.

[53] Luo W, Semenza GL. Emerging roles of PKM2 in cell metabolism and cancer progression. Trends Endocrinol Metab. 2012 Nov;23(11):560–566. PubMed PMID: 22824010; PubMed Central PMCID: PMCPMC3466350.

[54] Mazurek S. Pyruvate kinase type M2: a key regulator of the metabolic budget system in tumor cells. Int J Biochem Cell Biol. 2011 Jul;43(7):969–980. PubMed PMID: 20156581.

[55] Christofk HR, Vander Heiden MG, Wu N, et al. Pyruvate kinase M2 is a phosphotyrosine-binding protein. Nature. 2008 Mar 13;452(7184):181–186. PubMed PMID: 18337815.

[56] Chervona Y, Costa M. Histone modifications and cancer: biomarkers of prognosis? Am J Cancer Res. 2012;2 (5):589–597. PubMed PMID: 22957310; PubMed Central PMCID: PMC3433108.

[57] Ellinger J, Schneider AC, Bachmann A, et al. Evaluation of global histone acetylation levels in bladder cancer patients. Anticancer Res. 2016 Aug;36 (8):3961–3964. PubMed PMID: 27466500.

[58] Valdes-Mora F, Gould CM, Colino-Sanguino Y, et al. Acetylated histone variant H2A.Z is involved in the activation of neo-enhancers in prostate cancer. Nat Commun. 2017 Nov 07;8(1):1346. PubMed PMID: 29116202; PubMed Central PMCID: PMC5676741.

analytical chemistry

Article

Cite This: *Anal. Chem.* 2019, 91, 2155−2162

pubs.acs.org/ac

Structure Annotation of All Mass Spectra in Untargeted Metabolomics

Ivana Blaženović,[†] Tobias Kind,[†] Michael R. Sa,[†] Jian Ji,[‡] Arpana Vaniya,[†] Benjamin Wancewicz,[†] Bryan S. Roberts,[†] Hrvoje Torbašinović,[§] Tack Lee,[∥] Sajjan S. Mehta,[†] Megan R. Showalter,[†] Hosook Song,[∥] Jessica Kwok,[†] Dieter Jahn,[⊥,#] Jayoung Kim,[▽,○,◆,¶] and Oliver Fiehn*[,†]

[†]West Coast Metabolomics Center, University of California, Davis, Davis, California 95616, United States

[‡]School of Food Science, State Key Laboratory of Food Science and Technology, Jiangnan University, Wuxi, Jiangsu 330047, China

[§]Inovatus Ltd., Zagreb 10000, Croatia

[∥]Department of Urology, Inha University College of Medicine, Incheon 22212, South Korea

[⊥]Institute of Microbiology, Technische Universität Braunschweig, Braunschweig 38106, Germany

[#]Braunschweig Integrated Centre of Systems Biology (BRICS), Technische Universität Braunschweig, Braunschweig 38106, Germany

[▽]Departments of Surgery and Biomedical Sciences, Cedars-Sinai Medical Center, Los Angeles, California 90048, United States

[○]Department of Medicine, University of California Los Angeles, Los Angeles, California 90095, United States

[◆]Samuel Oschin Comprehensive Cancer Institute, Cedars-Sinai Medical Center, Los Angeles, California 90048, United States

[¶]Department of Urology, Ga Cheon University College of Medicine, Incheon 22212, South Korea

Supporting Information

ABSTRACT: Urine metabolites are used in many clinical and biomedical studies but usually only for a few classic compounds. Metabolomics detects vastly more metabolic signals that may be used to precisely define the health status of individuals. However, many compounds remain unidentified, hampering biochemical conclusions. Here, we annotate all metabolites detected by two untargeted metabolomic assays, hydrophilic interaction chromatography (HILIC)-Q Exactive HF mass spectrometry and charged surface hybrid (CSH)-Q Exactive HF mass spectrometry. Over 9,000 unique metabolite signals were detected, of which 42% triggered MS/MS fragmentations in data-dependent mode. On the highest Metabolomics Standards Initiative (MSI) confidence level 1, we identified 175 compounds using authentic standards with precursor mass, retention time, and MS/MS matching. An additional 578 compounds were annotated by precursor accurate mass and MS/MS matching alone, MSI level 2, including a novel library specifically geared at acylcarnitines (CarniBlast). The rest of the metabolome is usually left unannotated. To fill this gap, we used the *in silico* fragmentation tool CSI:FingerID and the new NIST hybrid search to annotate all further compounds (MSI level 3). Testing the top-ranked metabolites in CSI:Finger ID annotations yielded 40% accuracy when applied to the MSI level 1 identified compounds. We classified all MSI level 3 annotations by the NIST hybrid search using the ClassyFire ontology into 21 superclasses that were further distinguished into 184 chemical classes. ClassyFire annotations showed that the previously unannotated urine metabolome consists of 28% derivatives of organic acids, 16% heterocyclics, and 16% lipids as major classes.

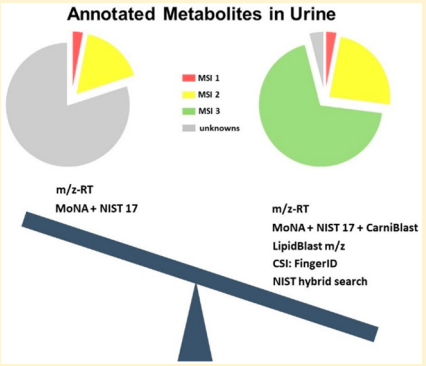

Metabolomics is used as one of the major -omics tools to tackle the complex area of personalized medicine and health.[1] Target analysis of metabolites is an integral part of clinical laboratories worldwide. Conversely, untargeted metabolomics provides comprehensive insights into complex metabolomes and allows for discovery of novel biomarkers and generating new metabolic hypothesis. Yet, untargeted metabolomics is challenged by very low identification rates.[2,3] Since there is no single platform capable of capturing the entire metabolome of urine, we have employed two chromatographic platforms that are highly suited for untargeted metabolome analysis: hydrophilic interaction chromatography (HILIC; for polar metabolite profiling) and charged-surface hybrid chromatography (CSH, for lipidomics profiling). While lipids are usually low abundant in (aqueous) urine samples, recent technological advancements of high-resolution mass spectrometry (MS) have largely improved the comprehensive lipid

Received: October 12, 2018
Accepted: January 2, 2019
Published: January 4, 2019

Downloaded via CEDARS-SINAI MEDICAL CTR on October 2, 2019 at 21:17:38 (UTC).
See https://pubs.acs.org/sharingguidelines for options on how to legitimately share published articles.

© 2019 American Chemical Society

DOI: 10.1021/acs.analchem.8b04698
Anal. Chem. 2019, 91, 2155−2162

profiling of cells, tissues, and biofluids, including urine. Lipids can serve as important biomarkers even in urine samples, for example for prostate cancer[4] or segmental glomerulosis.[5] Combined, metabolomics and lipidomics reveal biologically active metabolites in urine and provide a diagnostic chemical signature of human metabolic phenotypes. The urinary metabolome is associated with urological diseases, including bladder dysfunctions such as interstitial cystitis/bladder pain syndrome (IC).[6−8] IC is characterized by chronic bladder and/or pelvic pain, as well as nocturia and an increase in urinary frequency and urgency.[9−11] The work presented here investigated how many urine metabolites from IC patients could be identified, as defined by the Metabolomics Standards Initiative (MSI),[12] using freely available comprehensive metabolite annotation tools, novel databases, and libraries that were developed and used here for the first time.[13]

EXPERIMENTAL SECTION

Extraction. Subjects, urine specimen collection, and clinical and pathological features of subjects were described in a previous paper from our laboratory.[14] Deidentified urine samples were stored at −80 °C until further analysis. Urinary lipids were extracted with methanol and methyl *tert*-butyl ether both containing a cocktail of lipid standards.[15] Water was subsequently added for phase separation. This extraction protocol extracts all main lipid classes in urine with high recoveries, specifically phosphatidylcholines (PC), sphingomyelins (SM), phosphatidylethanolamines (PE), lysophosphatidylcholines (LPC), ceramides (Cer), cholesteryl esters (CholE), and triacylglycerols (TG).[16] Lipid standards were purchased from Avanti Polar lipids (Alabaster, USA). After concentrating extracts to complete dryness, samples were reconstituted prior to LC-MS analysis as published before.[17] Polar metabolites were retrieved by using the polar phase of the lipid extraction procedure. Samples were dried in a centrivap prior to a cleanup step of 50% acetonitrile and dried again. Samples were reconstituted for HILIC-MS analysis in an 80:20 acetonitrile:water solution containing internal standards from Sigma and CDN Isotopes.

Instrumentation. All measurements were carried out on a Thermo Q Exactive instrument. For lipidomics measurements, 1 μL of diluted samples was separated on a Waters Acquity UPLC CSH C18 column (100 × 2.1 mm; 1.7 μm) coupled to an Acquity UPLC CSH C18 VanGuard precolumn (5 × 2.1 mm; 1.7 μm). The column was maintained at 65 °C with a flow rate of 0.6 mL/min. The positive ionization mobile phases consisted of (A) acetonitrile:water (60:40, v/v) with ammonium formate (10 mM) and formic acid (0.1%) and (B) 2-propanol:acetonitrile (90:10, v/v) with ammonium formate (10 mM) and formic acid (0.1%). The negative ionization mobile phases consisted of (A) acetonitrile:water (60:40, v/v) with ammonium formate (10 mM) and (B) 2-propanol:acetonitrile (90:10, v/v) with ammonium formate (10 mM). The separation was conducted under the following gradient: 0 min 15% B; 0−2 min 30% B; 2−2.5 min 48% B; 2.5−11 min 82% B; 11−11.5 min 99% B; 11.5−12 min 99% B; 12−12.1 min 15% B; 12.1−15 min 15% B. The Q Exactive MS instrument was operated using positive mode electrospray ionization using the following parameters: Mass range, 120−1200 *m*/*z*; Sheath gas flow rate, 60; Aux gas flow rate, 25; Sweep gas flow rate, 2; Spray Voltage (kV) 3.6; Capillary temp, 300 °C; S-lens RF level, 50; Aux gas heater temp, 370 °C. Full MS parameters: Resolution, 60,000; AGC target, 1e6; Maximum IT, 100 ms; Spectrum data type, Centroid. Data dependent MS2 parameters: Resolution, 15,000; AGC target, 1e5; Maximum IT, 50 ms; Loop count, 4; TopN, 4; Isolation Window, 1.0 *m*/*z*; Fixed First Mass, 70.0 *m*/*z*; (N)CE/stepped (N)CE, 20, 30, 40; Spectrum data type, Centroid.

For profiling polar compounds and biogenic amines, HILIC-Q Exactive MS/MS data acquisition was performed. One μL of diluted samples was separated on a Waters Acquity UPLC BEH Amide column (150 × 2.1 mm; 1.7 μm) coupled to an Acquity UPLC BEH Amide VanGuard precolumn (5 × 2.1 mm; 1.7 μm). The column was maintained at 45 °C with a flow rate of 0.4 mL/min. The mobile phases consisted of (A) water with ammonium formate (10 mM) and formic acid (0.125%) and (B) acetonitrile:water (95:5, v/v) with ammonium formate (10 mM) and formic acid (0.125%). The separation was conducted under the following gradient: 0 min 100% B; 0−2 min 100% B; 2−7.7 min 70% B; 7.7−9.5 min 40% B; 9.5−10.25 min 30% B; 10.25−12.75 min 100% B; 12.75−17 min 100% B.

The Q Exactive MS instrument was operated using positive mode electrospray ionization (ESI HILIC) with the following parameters: Mass range, 60−900 *m*/*z*; Sheath gas flow rate, 60; Aux gas flow rate, 25; Sweep gas flow rate, 2; Spray Voltage (kV) 3.6; Capillary temp, 300 °C; S-lens RF level, 50; Aux gas heater temp, 370 °C. Full MS parameters: Microscans, 1; Resolution, 60,000; AGC target, 1e6; Maximum IT, 100 ms; Number of scans, 1; Spectrum data type, Centroid. Data dependent MS2 parameters: Microscans, 1; Resolution, 15,000; AGC target, 1e5; Maximum IT, 50 ms; Loop count, 4; MSX count, 1; TopN, 4; Isolation Window, 1.0 *m*/*z*; Isolation offset 0.0 *m*/*z*; (N)CE/stepped (N)CE, 20, 30, 40; Spectrum data type, Centroid.

Data Processing and Compound Identification. The LC-MS/MS data was analyzed by MS-DIAL software.[18] Detailed parameter settings are listed in Supplemental Table 1 (HILIC and lipidomics data processing settings). Data tables containing accurate masses, retention times, and peak heights were exported, and further analysis was performed in R and Metabox.[19] Automated annotation of metabolites was performed separately for polar metabolites and lipids. Table S1 lists libraries, methods, and software used for each platform.

Metabolite annotations were achieved using a combination of different tools. On MSI level 1, we developed and used a novel HILIC-MS/MS library of 1,102 authentic standards including retention time, precursor mass, and MS/MS spectra. All spectra, retention times, and chromatography conditions are freely available at MassBank of North America (http://massbank.us). Search windows were used as follows: 0.1 min RT tolerance (for the alignment of peaks), 0.0001 Da tolerance for the precursor masses, and 0.05 Da tolerance for the MS/MS spectral matching. Similarly, we used lipid retention times and MS/MS spectra for lipidomics identifications.[15] On MSI level 2, we annotated compounds that did not trigger MS/MS fragmentations in data dependent mode but that were still identified based on accurate mass and retention time using the HILIC-MS/MS library in addition to manually curated lipid retention times. Moreover, MSI level 2 annotations were also based on accurate mass and MS/MS annotations for spectra for which no authentic retention time library was available, such as the NIST17, HMDB,[20] GNPS,[21] the new CarniBlast library, and the LipidBlast libraries.[17,22,23] For MSI level 3 annotations, we used CSI:FingerID,[24] the NIST-Hybrid Search,[25] and LipidBlast accurate mass search services.

DOI: 10.1021/acs.analchem.8b04698
Anal. Chem. 2019, 91, 2155−2162

RESULTS AND DISCUSSION

MSI Level 1 Annotations. The number of precursors that triggered MS/MS fragmentations was sample dependent. Table S2 contains all 3,894 merged spectra for all samples that were aligned and processed by MS-DIAL software which were subsequently used for MSI level 1 and 2 annotations (Table 1). Compound identifications with the highest level of confidence (MSI level 1) were achieved using libraries of authentic standards. All library spectra and retention times were acquired under identical conditions as the experimental urine spectra. Specifically, a new HILIC-Q Exactive MS/MS library was established using 1,102 authentic compounds measured in positive mode. Data and metadata for this library can be downloaded from MassBank of North America (Fiehn HILIC). By matching experimental urine spectra against library retention times (RT), accurate precursor masses (m/z), and MS/MS spectra, overall 175 compounds were identified at MSI level 1. Specifically, we identified 72 lipids in CSH-Q Exactive MS/MS as members of 7 lipid classes and 103 hydrophilic compounds using HILIC-Q Exactive MS/MS as amino acids, biogenic amines, and other polar compound classes (Table S2). Detailed settings and cutoffs are listed in Table S1.

Table 1. Results of Comprehensive Annotation of Urinary Metabolomics and Lipidomics MS/MS Spectra

chromatography and databases	type of matching	MSI level of annotation	no. of annotations
HILIC	precursor m/z, RT experimental library MS/MS	MSI level 1	103
lipidomics	m/z, RT, experimental + *in silico* library MS/MS		72
HILIC: MoNA+NIST17	precursor m/z, experimental library MS/MS	MSI level 2	440
HILIC	precursor m/z and RT		13
lipidomics: CarniBlast	m/z, *in silico* library MS/MS		18
HILIC: CarniBlast	precursor m/z, *in silico* library MS/MS		107
lipidomics: mzRT lookup	precursor m/z with RT curation	MSI level 3	96
HILIC and lipidomics: NIST17 hybrid search	MS/MS (hybrid and experimental library)		6,447
HILIC: Sirius/CSI:FingerID	precursor m/z and *in silico* predicted MS/MS		728

MSI Level 2 Annotations. Retention-time based libraries of authentic standards are necessarily smaller than the complement of available MS/MS spectra in public or licensed mass spectral libraries. Therefore, it is a common practice in metabolomics research to perform mass spectral similarity searches of experimental to library MS/MS spectra to increase the annotation rate. While metabolite MS/MS fragmentations are independent of chromatography conditions, spectra often show differences due to slightly different fragmentation parameters or different mass spectrometers used. In addition, many metabolites show only a few characteristic fragment ions, rendering the use of classic spectral similarity searches unreliable. To retain high confidence, we combined accurate precursor mass and MS/MS searches for all over queries, using 750 dot-product score (HILIC-MS/MS) and 400 reverse dot-product (CSH-MS/MS) as lower threshold below which no further correct match hits were expected. Subsequently, each spectrum was manually inspected to verify spectral matches and retention time matches, where available.

MassBank of North America (MoNA; http://massbank.us) currently contains over 260,000 mass spectra from 15 individual mass spectral repositories such as MassBank, MassBank EU, GNPS, ReSpect, LipidBlast, MetaboBase, and HMDB, covering more than 80,000 compounds. We combined MoNA spectra with MS/MS data from the NIST17 library, the largest available licensed repository with over 550,000 experimental spectra from 13,808 chemical compounds. We merged all spectra from both resources into one.msp within MS-DIAL software for mass spectral similarity matching. In total, this approach yielded 480 identified compounds on MSI level 2.

While investigating and validating MS/MS spectra, we observed many spectra that appeared similar to 17 acylcarnitines annotated by using LipidBlast or MoNA spectra. Acylcarnitines in urine serve as biomarkers for bladder cancer,[26] diabetic nephropathy,[27] obesity,[28] and human kidney cancer.[29] The identification of acylcarnitines has to be performed either using authentic reference compounds or with reference library spectra.[30] However, only a few tandem mass spectra of acylcarnitines exist in commercial (NIST) and open mass spectral libraries (MassBank,[31] METLIN,[32] Respect DB[33]), covering less than 50 acylcarnitine structures. Conversely, when using a structure similarity search in the CAS SciFinder literature database, we found 453 acylcarnitine-like structures of which only 62 were commercially available. Such finding indicated a high chemical diversity of acylcarnitines that could not possibly be closed by purchasing more chemical compounds. To overcome this gap and identify all urinary acylcarnitines, we developed an *in silico* tandem mass spectral library of acylcarnitines using structure templates[23] similar to our previous LipidBlast[22] and FAHFA predicted MS/MS libraries.[34] Here, we constructed the CarniBlast library of 2,400 acylcarnitine species covering a wide range of saturated, unsaturated, -hydroxyl, -keto, -dicarboxylic, and oxidized acyl chain substituted acylcarnitines. We matched all experimental MS/MS spectra from both polar and lipidomics profiling against the new *in silico* database of acylcarnitines. After removing duplicates and manually validating each candidate spectrum, we identified 67 novel acylcarnitines through the CarniBlast library in addition to the 17 acylcarnitines obtained by LipidBlast and MoNA. Detailed settings and cutoffs are listed in Table S1.

All urinary metabolomic data were acquired by data-dependent MS/MS. Yet, we used retention-time based MS/MS libraries such as the new HILIC-Q Exactive MS/MS repository. For lipids, we have recently shown[35] that compound annotations can be based on accurate precursor mass and retention time alone with high confidence. Using these two orthogonal parameters (m/z and RT), six further acylcarnitines were annotated at MSI level 2. In the same manner, we assigned 201 further compounds that were too low abundant to trigger MS/MS fragmentations but that were covered in our m/z and RT libraries that were acquired under the same experimental conditions.

In combination, we identified 578 metabolites at MSI level 2 confidence (39 lipids, 85 acylcarnitines, and 454 hydrophilic compounds). Metadata such as dot product, reverse dot product scores, number of matching ions, and MS-DIAL calculated MS2 similarity have been taken into account. Detailed results are listed in Table S2.

DOI: 10.1021/acs.analchem.8b04698
Anal. Chem. 2019, 91, 2155−2162

MSI Level 3 Annotations. When combining compound annotations on MSI level 1 and 2, the 753 compound annotations only covered 19.3% of the acquired urinary MS/MS spectra (Figure 1). While this number of annotated compounds is already significantly higher than most other studies on urine metabolomics,[36,37] it is worrisome that more than 80% of all MS/MS spectra remain unannotated in metabolomics screens. Many biologists will focus their attention only on identified compounds and not even perform statistical assessments on complete metabolome data, including unknowns. Yet, it appears very likely that the fraction of more than 80% unknowns might include very important biomarkers or signatures of diseases, food patterns, exposome compounds, or other significant chemicals. We therefore used three tools to investigate this dark matter of metabolomics[38] closer: (a) accurate mass search, (b) structure elucidation tools, and (c) mass spectral library hybrid search. We used the most exhaustive MS/MS files for MSI level 3 annotations, using raw MS/MS spectra from individual IC patients for each stepped collision energy to enable best-possible annotations. Spectra were exported as either mgf or msp files and used in the different software programs. For HILIC-MS/MS analyses, we used between 5,192 and 6,447 MS/MS spectra; for CSH-MS/MS lipidomics analyses, the number of spectra ranged from 5,705 to 7,050 MS/MS spectra per sample (Table 1 and Table S2). The number of raw spectra is higher than in the MS-DIAL processed file because MS-DIAL merged the stepped collision energies during data acquisition.

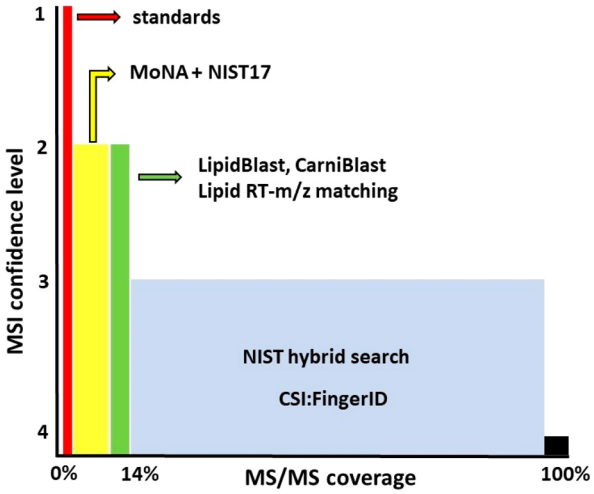

Figure 1. Categorized overview of the complete annotation of MS/MS spectra of human urine metabolomes based on MSI level 1, 2, and 3 confidence scores.

First, we used precursor mass lookups. In general, simple mass lookups yield many false discoveries due to a plethora of isomers and isobars at a given accurate mass level. This problem is especially pronounced in HILIC-MS for which hardly any constraint can be applied with respect to the number of possible chemicals. Yet, for lipidomics assays, lipids can already be assigned to specific lipid classes with some level of confidence based on m/z and retention time (in relation to MSI level 1 and 2 annotated lipids within the same study). Additional structure information on such lipid class annotations and their acyl chains cannot be made using accurate mass alone. We extracted m/z precursor information from the MS-

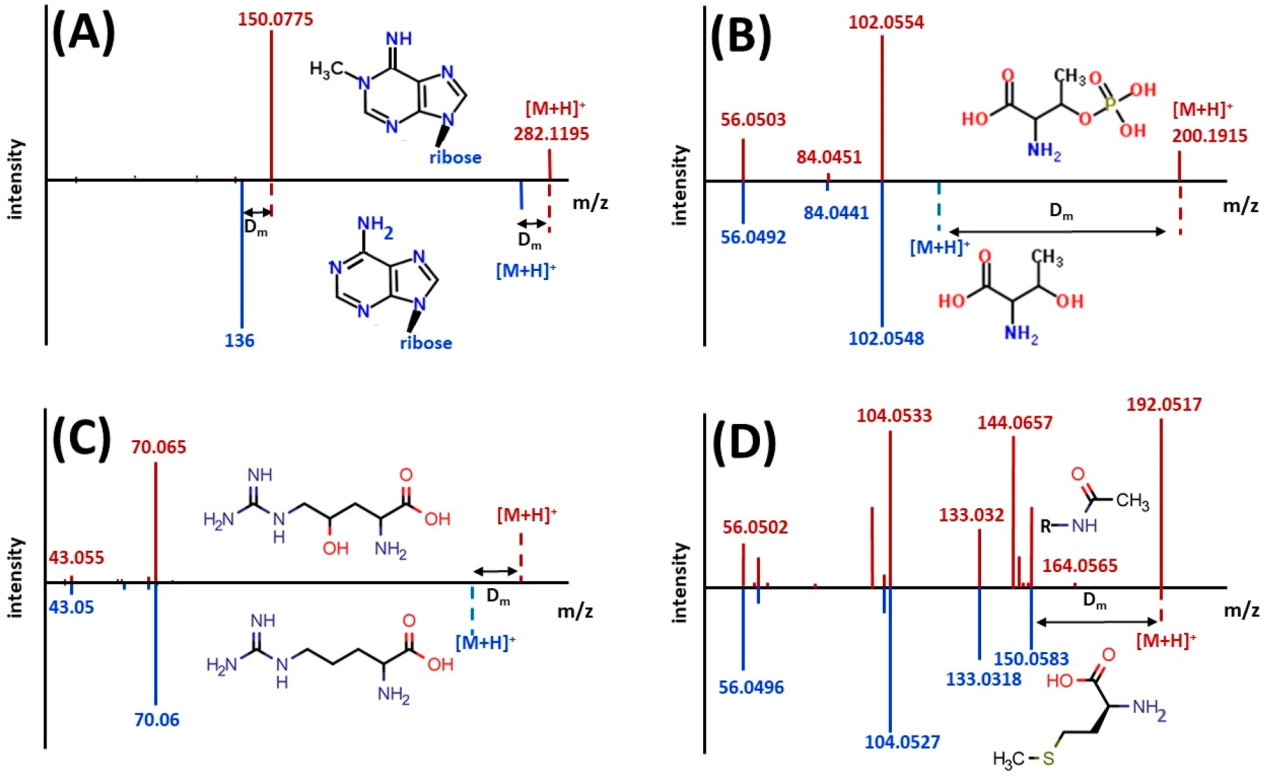

Figure 2. Head-to-tail comparison of MS/MS spectra of distinct shifts in spectra of modified versions of canonical metabolites. (A) methylation: 1-methyladenosine to adenosine, (B) phosphorylation: phosphothreonine to threonine, (C) hydroxylation: hydroxyarginine to arginine, (D): acetylation: *N*-acetylmethionine to methionine.

DOI: 10.1021/acs.analchem.8b04698
Anal. Chem. 2019, 91, 2155−2162

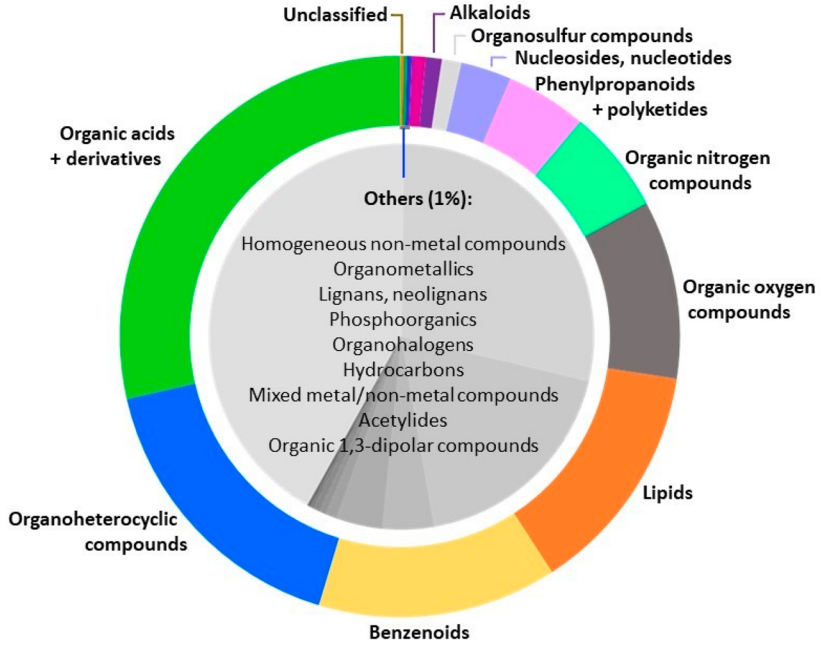

Figure 3. Structural categorization of compounds present in urine samples of 43 subjects diagnosed with interstitial cystitis. Chemicals are structured according to the "Superclass level" of the ClassyFire classification system.

DIAL output in positive ionization mode and used the *m/z* lookup macro within LipidBlast v49 to assign additional lipids. We used a 5 mDa mass tolerance for lipid assignments based on the mass accuracy of the Q Exactive instrument. This way, an additional 96 lipid annotations were obtained for the lipidomics data set in positive ionization mode.

Second, we used cheminformatics tools to annotate accurate mass HILIC-MS/MS spectra to likely chemical structures. A range of software tools has been published such as MS-FINDER,[39] Sirius, CFM-ID,[40] and others. Here, we used two programs, Sirius 4.0 with CSI:FingerID interface[24] and the new NIST17 hybrid-search.[25] Sirius/CSI:FingerID scored highly during the latest CASMI structure identification challenges[41,42] but has never been applied to urinary metabolomics. The NIST17 hybrid-search software was released after the CASMI challenges but offers advantages by greatly expanding the utility of existing mass spectral libraries. For Sirius/CSI:Finger ID, MS/MS spectra were exported as a MGF file from each raw file using the MSConvert program. The largest MGF file contained 6,447 MS/MS spectra. Formulas were assigned at 10 ppm search windows, retaining the 10 best formula candidates. Using Sirius, spectra were processed within 2 min on a 16 CPU machine, assigning formulas to a total of 6,184 features (96%). Subsequently, CSI:FingerID performed spectral fingerprint matching via a Web service to annotate isomer structures. Within 5 min processing time, 728 MS/MS spectra were assigned to chemical structures in the biodatabase, a filtered version of Pubchem containing over 270,000 structures of biological interest, and 1,557 MS/MS spectra were assigned to chemicals in the much larger PubChem database. Scored results of all isomeric structures were exported as CSV files. For structures returned by biodatabase searches, CSI:Finger ID yielded up to 130 results per MS/MS scan and up to 10,000 structure candidates per MS/MS spectrum in PubChem queries. Time-consuming manual investigations have to be performed to select the most likely structures. To test CSI:Finger ID accuracy, we selected 103 MS/MS spectra from the urinary HILIC-Q Exactive MS/MS data set that were unambiguously assigned by authentic standards and tested these spectra within 5 ppm mass accuracy and a biodatabase structure query. Using our publicly available HILIC library (see above), 41 compounds (40%) were correctly annotated by CSI:Finger ID as top hit, and 54 MS/MS spectra (52%) were correctly assigned within the top 3 isomer candidates. Detailed results are given in Table S3. CSI:FingerID is not optimized for use in lipidomics MS/MS spectra.

Third, we used the novel NIST17 hybrid search[25] that combines mass spectral library-based scoring with calculating fragment and precursor mass shifts for chemical modifications of library structures. Such a tool mimics the experience of well-trained chemists[43] because known biochemical modifications such as methylations or acetylations produce epimetabolites that are removed from their classic functions in canonical metabolic pathways.[44] Four examples of how the NIST17 hybrid search works are given in Figure 2 for head-to-tail MS/MS spectral comparisons of methyladenosine/adenosine, phosphothreonine/threonine, hydroxyarginine/arginine, and acetylmethionine/methionine. Spectra of modified metabolites show distinct shifts in precursor masses and fragments when comparing to nonmodified library spectra. Yet, the NIST17 hybrid search correctly associated the modified spectra with their best scoring related library spectra.

We exported all lipidomics and HILIC-MS/MS spectra from 43 interstitial cystitis patients from MS-DIAL to the NIST pepSearch software and used the NIST17 hybrid search function. The software supports batch processing, enables users to include or exclude specific MS/MS spectra, and yields quick overviews of the complement of chemical structures in mass spectral profiling studies. Results are given in Table S2. Within 10 min processing time, 95% of all spectra were assigned with structure annotations and compound names, including a set of confidence scores such as forward and reverse dot products and a probability score. Hybrid search annotations must be treated with caution as they do not

DOI: 10.1021/acs.analchem.8b04698
Anal. Chem. 2019, 91, 2155−2162

represent an identification but rather a nearest known neighbor to the unknown spectrum. While in many cases NIST17 hybrid searches give correct results (Figure 2), overall results highlight a high probability of chemical class annotations (MSI level 3) rather than exact structures. We therefore used these results for exactly this purpose, classifying the thousands of patient urinary MS/MS spectra to chemical classes. For this purpose, we implemented a batch search version of the automated chemical hierarchy classification system ClassyFire[45] (https://cfb.fiehnlab.ucdavis.edu). ClassyFire requires International Chemical Identifiers (InChI keys) as input.[46] Today, InChI keys are a standard tool in all chemical and biochemical databases to assign and compare chemical structures with machine-readable, unique keys. The ClassyFire Batch search utilizes the ClassyFire API to look up provided InChIKeys and, if no match is found, to query its nonstereo form. It yields a tabular CSV version of the results. We used the online tool Chemical Translation Services (CTS)[47] to convert chemical names from the NIST17 hybrid pepSearch results to InChI keys. This conversion reduced the compound list by ∼1% because some NIST17 hybrid search chemical names are not yet included in PubChem or the other 200 chemical databases that support the CTS tool. Hence, of the average number of 5,250 MS/MS spectra found per patient in lipidomics and HILIC-MS/MS, about 95% of all spectra were now annotated by exact chemical structures or by chemical classes (MSI level 3, Figure 1). Results of classifications are organized into Kingdom, Superclass, Class, Subclass, and two parent levels. Detailed results are given in Table S4, with varying chemical classes present in urines of different patients. An average MSI level 3 classification is given in Figure 3 using the superclass and subclass classifications as defined by ClassyFire. Roughly one-third of the urinary metabolome was classified as chemicals containing aromatic rings or heterocycles, one-third was classified as compounds containing ketones, alcohols, or acids, while the remaining one-third consisted of lipids, phenylpropanoids, and nitrogenous- or sulfur containing organics. As expected, organic phosphates, organometallic, or other compound classes comprised less than 1% of the urinary metabolome.

CONCLUSION

Unlike proteomic MS/MS spectra assignments, the field of metabolomics currently lacks generally accepted and validated automated calculations of compound identification confidence levels with false-discovery rate assessments. As remedy, structure annotation in untargeted MS/MS metabolomics reports must be annotated with MSI confidence levels to detail which metabolites can be trusted and used for metabolic pathway annotations (MSI level 1 and 2), especially if annotated spectra use accurate mass information and manual curation. While the majority of acquired MS/MS spectra cannot be annotated with certainty to specific chemicals, Sirius/CSI:Finger ID and NIST17 hybrid search results yield many structure assignments that are worthy to be validated by acquiring spectra from corresponding authentic chemicals. In addition, MSI level 3 chemical classes can be ordered by ClassyFire and used for chemical class enrichment statistics,[48] for example, in biomarker discovery studies. Moreover, MSI level 3 classifications may yield differences in urinary chemicals that detail differences in subjects due to diet and chemical exposure in epidemiology studies.

ASSOCIATED CONTENT

Supporting Information

The Supporting Information is available free of charge on the ACS Publications website at DOI: 10.1021/acs.analchem.8b04698.

Table S1, settings used for LC-MS/MS data processing of polar metabolites and biogenic amines (XLSX)

Table S2, multilevel compound annotations (XLSX)

Table S3, HILIC library annotations of all 43 IC patients (XLSX)

Table S4, structural classification of all spectra from 43 IC patients (XLSX)

AUTHOR INFORMATION

Corresponding Author

*Phone +1-530-754-8258 (office), +1-530-752-9922 (lab), +1-530-723-4450 (cell). Corresponding author address: NIH West Coast Metabolomics Center, UC Davis Genome Center, Room 1313, 451 Health Sci Drive, Davis, CA 95616.

ORCID

Tobias Kind: 0000-0002-1908-4916

Oliver Fiehn: 0000-0002-6261-8928

Author Contributions

I.B., T.K., J.J., K.J., D.J., and O.F. designed the study. Data processing and compound ID were performed by I.B. Data analysis, figures, and tables were produced by I.B. and O.F. T.K. processed data using CSI:FingerID, B.R. and B.W. assisted in sample preparation, data preprocessing, and validation, J.K. and O.F. edited the manuscript, H.T. assisted with Java support, A.V. performed IDs using *in silico* fragmentation tools, M.S. provided assistance with the HILIC library, and K.J., T.L., and H.S. selected the cohort and provided the IC urine samples. The manuscript was written through the support of all authors. All authors have given approval to the final version of the manuscript.

Notes

The authors declare no competing financial interest.

ACKNOWLEDGMENTS

The authors acknowledge support from National Institutes of Health grant U2C ES030158 (to O.F.) and the following grants to J.K.: NIH U01 DK103260, R01 DK100974, U01 DP006079, NIH NCATS UCLA CTSI UL1 TR000124, Department of Defense grant W81XWH-15-1-0415, IMAGINE NO IC research grant, the Steven Spielberg Discovery Fund in Prostate Cancer Research Career Development Award, and the U.S.-Egypt Science and Technology Joint Fund. The funders had no role in the design, data collection, and analysis, decision to publish, or preparation of the manuscript.

REFERENCES

(1) Jacob, M.; Lopata, A. L.; Dasouki, M.; Abdel Rahman, A. M. *Mass Spectrom. Rev.* **2017**, DOI: 10.1002/mas.21548.

(2) Bloszies, C. S.; Fiehn, O. *Current Opinion in Toxicology* **2018**, *8*, 87−92.

(3) Blazenovic, I.; Kind, T.; Ji, J.; Fiehn, O. *Metabolites* **2018**, *8*, 31.

(4) Yang, J. S.; Lee, J. C.; Byeon, S. K.; Rha, K. H.; Moon, M. H. *Anal. Chem.* **2017**, *89*, 2488−2496.

(5) Erkan, E.; Zhao, X.; Setchell, K.; Devarajan, P. *Pediatr. Nephrol.* **2016**, *31*, 581−588.

DOI: 10.1021/acs.analchem.8b04698
Anal. Chem. 2019, 91, 2155−2162

(6) Antunes-Lopes, T.; Cruz, C. D.; Cruz, F.; Sievert, K. D. *Current opinion in urology* **2014**, *24*, 352−357.
(7) Kuo, H. C. *Int. J. Urol.* **2014**, *21* (S1), 34−41.
(8) Pedroza-Diaz, J.; Rothlisberger, S. *Biochemia medica* **2015**, *25*, 22−35.
(9) Clemens, J. Q.; Clauw, D. J.; Kreder, K.; Krieger, J. N.; Kusek, J. W.; Lai, H. H.; Rodriguez, L.; Williams, D. A.; Hou, X.; Stephens, A.; Landis, J. R.; MAPP Research Network. *J. Urol.* **2015**, *193*, 1554−1558.
(10) Naliboff, B. D.; Stephens, A. J.; Afari, N.; Lai, H.; Krieger, J. N.; Hong, B.; Lutgendorf, S.; Strachan, E.; Williams, D.; MAPP Research Network. *Urology* **2015**, *85*, 1319−1327.
(11) Hanno, P. M.; Burks, D. A.; Clemens, J. Q.; Dmochowski, R. R.; Erickson, D.; Fitzgerald, M. P.; Forrest, J. B.; Gordon, B.; Gray, M.; Mayer, R. D.; Newman, D.; Nyberg, L., Jr.; Payne, C. K.; Wesselmann, U.; Faraday, M. M. *J. Urol.* **2011**, *185*, 2162−2170.
(12) Schymanski, E. L.; Jeon, J.; Gulde, R.; Fenner, K.; Ruff, M.; Singer, H. P.; Hollender, J. *Environ. Sci. Technol.* **2014**, *48*, 2097−2098.
(13) Kind, T.; Tsugawa, H.; Cajka, T.; Ma, Y.; Lai, Z.; Mehta, S. S.; Wohlgemuth, G.; Barupal, D. K.; Showalter, M. R.; Arita, M.; Fiehn, O. *Mass Spectrom. Rev.* **2018**, *37*, 513−532.
(14) Wen, H.; Lee, T.; You, S.; Park, S. H.; Song, H.; Eilber, K. S.; Anger, J. T.; Freeman, M. R.; Park, S.; Kim, J. *J. Proteome Res.* **2015**, *14*, 541−548.
(15) Cajka, T.; Fiehn, O.: LC−MS-Based Lipidomics and Automated Identification of Lipids Using the LipidBlast In-Silico MS/MS Library. In *Lipidomics: Methods and Protocols*; Bhattacharya, S. K., Ed.; Springer New York: New York, NY, 2017; pp 149−170, DOI: 10.1007/978-1-4939-6996-8_14.
(16) Matyash, V.; Liebisch, G.; Kurzchalia, T. V.; Shevchenko, A.; Schwudke, D. *J. Lipid Res.* **2008**, *49*, 1137−1146.
(17) Cajka, T.; Smilowitz, J. T.; Fiehn, O. *Anal. Chem.* **2017**, *89*, 12360−12368.
(18) Tsugawa, H.; Cajka, T.; Kind, T.; Ma, Y.; Higgins, B.; Ikeda, K.; Kanazawa, M.; VanderGheynst, J.; Fiehn, O.; Arita, M. *Nat. Methods* **2015**, *12*, 523−526.
(19) Wanichthanarak, K.; Fan, S.; Grapov, D.; Barupal, D. K.; Fiehn, O. *PLoS One* **2017**, *12*, No. e0171046.
(20) Wishart, D. S.; Feunang, Y. D.; Marcu, A.; Guo, A. C.; Liang, K.; Vazquez-Fresno, R.; Sajed, T.; Johnson, D.; Li, C.; Karu, N.; Sayeeda, Z.; Lo, E.; Assempour, N.; Berjanskii, M.; Singhal, S.; Arndt, D.; Liang, Y.; Badran, H.; Grant, J.; Serra-Cayuela, A.; Liu, Y.; Mandal, R.; Neveu, V.; Pon, A.; Knox, C.; Wilson, M.; Manach, C.; Scalbert, A. *Nucleic Acids Res.* **2018**, *46*, D608−D617.
(21) Wang, M.; Carver, J. J.; Phelan, V. V.; Sanchez, L. M.; Garg, N.; Peng, Y.; Nguyen, D. D.; Watrous, J.; Kapono, C. A.; Luzzatto-Knaan, T.; Porto, C.; Bouslimani, A.; Melnik, A. V.; Meehan, M. J.; Liu, W. T.; Crusemann, M.; Boudreau, P. D.; Esquenazi, E.; Sandoval-Calderon, M.; Kersten, R. D.; Pace, L. A.; Quinn, R. A.; Duncan, K. R.; Hsu, C. C.; Floros, D. J.; Gavilan, R. G.; Kleigrewe, K.; Northen, T.; Dutton, R. J.; Parrot, D.; Carlson, E. E.; Aigle, B.; Michelsen, C. F.; Jelsbak, L.; Sohlenkamp, C.; Pevzner, P.; Edlund, A.; McLean, J.; Piel, J.; Murphy, B. T.; Gerwick, L.; Liaw, C. C.; Yang, Y. L.; Humpf, H. U.; Maansson, M.; Keyzers, R. A.; Sims, A. C.; Johnson, A. R.; Sidebottom, A. M.; Sedio, B. E.; Klitgaard, A.; Larson, C. B.; Boya P, C. A.; Torres-Mendoza, D.; Gonzalez, D. J.; Silva, D. B.; Marques, L. M.; Demarque, D. P.; Pociute, E.; O'Neill, E. C.; Briand, E.; Helfrich, E. J. N.; Granatosky, E. A.; Glukhov, E.; Ryffel, F.; Houson, H.; Mohimani, H.; Kharbush, J. J.; Zeng, Y.; Vorholt, J. A.; Kurita, K. L.; Charusanti, P.; McPhail, K. L.; Nielsen, K. F.; Vuong, L.; Elfeki, M.; Traxler, M. F.; Engene, N.; Koyama, N.; Vining, O. B.; Baric, R.; Silva, R. R.; Mascuch, S. J.; Tomasi, S.; Jenkins, S.; Macherla, V.; Hoffman, T.; Agarwal, V.; Williams, P. G.; Dai, J.; Neupane, R.; Gurr, J.; Rodriguez, A. M. C.; Lamsa, A.; Zhang, C.; Dorrestein, K.; Duggan, B. M.; Almaliti, J.; Allard, P. M.; Phapale, P. *Nat. Biotechnol.* **2016**, *34*, 828−837.
(22) Kind, T.; Liu, K. H.; Lee, D. Y.; DeFelice, B.; Meissen, J. K.; Fiehn, O. *Nat. Methods* **2013**, *10*, 755−758.
(23) Kind, T.; Okazaki, Y.; Saito, K.; Fiehn, O. *Anal. Chem.* **2014**, *86*, 11024−11027.
(24) Duhrkop, K.; Shen, H.; Meusel, M.; Rousu, J.; Bocker, S. *Proc. Natl. Acad. Sci. U. S. A.* **2015**, *112*, 12580−12585.
(25) Burke, M. C.; Mirokhin, Y. A.; Tchekhovskoi, D. V.; Markey, S. P.; Heidbrink Thompson, J.; Larkin, C.; Stein, S. E. *J. Proteome Res.* **2017**, *16*, 1924−1935.
(26) Kim, W. T.; Yun, S. J.; Yan, C.; Jeong, P.; Kim, Y. H.; Lee, I. S.; Kang, H. W.; Park, S.; Moon, S. K.; Choi, Y. H.; Choi, Y. D.; Kim, I. Y.; Kim, J.; Kim, W. J. *Yonsei Med. J.* **2016**, *57*, 865−871.
(27) Mirzoyan, K.; Klavins, K.; Koal, T.; Gillet, M.; Marsal, D.; Denis, C.; Klein, J.; Bascands, J. L.; Schanstra, J. P.; Saulnier-Blache, J. S. *Biochem. Biophys. Res. Commun.* **2017**, *487*, 109−115.
(28) Rauschert, S.; Uhl, O.; Koletzko, B.; Hellmuth, C. *Ann. Nutr. Metab.* **2014**, *64*, 314−324.
(29) Ganti, S.; Taylor, S. L.; Kim, K.; Hoppel, C. L.; Guo, L.; Yang, J.; Evans, C.; Weiss, R. H. *Int. J. Cancer* **2012**, *130*, 2791−2800.
(30) Solberg, H. E.; Bremer, J. *Biochim. Biophys. Acta, Gen. Subj.* **1970**, *222*, 372−380.
(31) Horai, H.; Arita, M.; Kanaya, S.; Nihei, Y.; Ikeda, T.; Suwa, K.; Ojima, Y.; Tanaka, K.; Tanaka, S.; Aoshima, K.; Oda, Y.; Kakazu, Y.; Kusano, M.; Tohge, T.; Matsuda, F.; Sawada, Y.; Hirai, M. Y.; Nakanishi, H.; Ikeda, K.; Akimoto, N.; Maoka, T.; Takahashi, H.; Ara, T.; Sakurai, N.; Suzuki, H.; Shibata, D.; Neumann, S.; Iida, T.; Tanaka, K.; Funatsu, K.; Matsuura, F.; Soga, T.; Taguchi, R.; Saito, K.; Nishioka, T. *J. Mass Spectrom.* **2010**, *45*, 703−714.
(32) Zhu, Z.-J.; Schultz, A. W.; Wang, J.; Johnson, C. H.; Yannone, S. M.; Patti, G. J.; Siuzdak, G. *Nat. Protoc.* **2013**, *8*, 451−460.
(33) Sawada, Y.; Nakabayashi, R.; Yamada, Y.; Suzuki, M.; Sato, M.; Sakata, A.; Akiyama, K.; Sakurai, T.; Matsuda, F.; Aoki, T.; Hirai, M. Y.; Saito, K. *Phytochemistry* **2012**, *82*, 38−45.
(34) Ma, Y.; Kind, T.; Vaniya, A.; Gennity, I.; Fahrmann, J. F.; Fiehn, O. *J. Cheminf.* **2015**, *7*, 53.
(35) Blazenovic, I.; Shen, T.; Mehta, S. S.; Kind, T.; Ji, J.; Piparo, M.; Cacciola, F.; Mondello, L.; Fiehn, O. *Anal. Chem.* **2018**, *90*, 10758−10764.
(36) Bouatra, S.; Aziat, F.; Mandal, R.; Guo, A. C.; Wilson, M. R.; Knox, C.; Bjorndahl, T. C.; Krishnamurthy, R.; Saleem, F.; Liu, P.; Dame, Z. T.; Poelzer, J.; Huynh, J.; Yallou, F. S.; Psychogios, N.; Dong, E.; Bogumil, R.; Roehring, C.; Wishart, D. S. *PLoS One* **2013**, *8*, No. e73076.
(37) Zaghlool, S. B.; Mook-Kanamori, D. O.; Kader, S.; Stephan, N.; Halama, A.; Engelke, R.; Sarwath, H.; Al-Dous, E. K.; Mohamoud, Y. A.; Roemisch-Margl, W.; Adamski, J.; Kastenmuller, G.; Friedrich, N.; Visconti, A.; Tsai, P. C.; Spector, T.; Bell, J. T.; Falchi, M.; Wahl, A.; Waldenberger, M.; Peters, A.; Gieger, C.; Pezer, M.; Lauc, G.; Graumann, J.; Malek, J. A.; Suhre, K. *Hum. Mol. Genet.* **2018**, *27*, 1106−1121.
(38) da Silva, R. R.; Dorrestein, P. C.; Quinn, R. A. *Proc. Natl. Acad. Sci. U. S. A.* **2015**, *112*, 12549−12550.
(39) Tsugawa, H.; Kind, T.; Nakabayashi, R.; Yukihira, D.; Tanaka, W.; Cajka, T.; Saito, K.; Fiehn, O.; Arita, M. *Anal. Chem.* **2016**, *88*, 7946−7958.
(40) Allen, F.; Pon, A.; Wilson, M.; Greiner, R.; Wishart, D. *Nucleic Acids Res.* **2014**, *42*, W94−99.
(41) Schymanski, E. L.; Ruttkies, C.; Krauss, M.; Brouard, C.; Kind, T.; Duhrkop, K.; Allen, F.; Vaniya, A.; Verdegem, D.; Bocker, S.; Rousu, J.; Shen, H.; Tsugawa, H.; Sajed, T.; Fiehn, O.; Ghesquiere, B.; Neumann, S. *J. Cheminf.* **2017**, *9*, 22.
(42) Blazenovic, I.; Kind, T.; Torbasinovic, H.; Obrenovic, S.; Mehta, S. S.; Tsugawa, H.; Wermuth, T.; Schauer, N.; Jahn, M.; Biedendieck, R.; Jahn, D.; Fiehn, O. *J. Cheminf.* **2017**, *9*, 32.
(43) Nikolic, D.; Macias, C.; Lankin, D. C.; van Breemen, R. B. *Rapid Commun. Mass Spectrom.* **2017**, *31*, 1385−1395.
(44) Showalter, M. R.; Cajka, T.; Fiehn, O. *Curr. Opin. Chem. Biol.* **2017**, *36*, 70−76.
(45) Djoumbou Feunang, Y.; Eisner, R.; Knox, C.; Chepelev, L.; Hastings, J.; Owen, G.; Fahy, E.; Steinbeck, C.; Subramanian, S.; Bolton, E.; Greiner, R.; Wishart, D. S. *J. Cheminf.* **2016**, *8*, 61.

DOI: 10.1021/acs.analchem.8b04698
Anal. Chem. 2019, 91, 2155−2162

(46) Heller, S. R.; McNaught, A.; Pletnev, I.; Stein, S.; Tchekhovskoi, D. *J. Cheminf.* **2015**, *7*, 23.
(47) Wohlgemuth, G.; Haldiya, P. K.; Willighagen, E.; Kind, T.; Fiehn, O. *Bioinformatics* **2010**, *26*, 2647−2648.
(48) Barupal, D. K.; Fiehn, O. *Sci. Rep.* **2017**, *7*, 14567.

DOI: 10.1021/acs.analchem.8b04698
Anal. Chem. 2019, 91, 2155−2162

Editorial

Investig Clin Urol 2019;60:1-3.
https://doi.org/10.4111/icu.2019.60.1.1
pISSN 2466-0493 • eISSN 2466-054X

INVESTIGATIVE AND CLINICAL UROLOGY
IC UROLOGY

Innovative technologies for the smart E-Healthcare system

"Oh wow, a dolphin! It looks so real and it's swimming around me." Calming music in the background mingles with the faint sound of ocean water and aquatic animals. Several clown fish slowly move into view and swim in a circle. A cute dolphin beckons, as if to play, and a big whale is seen leisurely swimming in the distance.

Michael, a six-year old boy with burns on his two legs due to recent car accident, is enjoying his deep-sea adventure through smart phone virtual reality (VR), a three-dimensional (3D) computer-generated virtual environment. It was only a week ago when he was living in constant fear and pain from the daily dressing of his burn wounds at the hospital. His physicians needed to prescribe heavy doses of strong intravenous pain medication during these sessions. However, a VR kit was recently recommended as an alternative for Michael's pain management.

For severe, acute, and/or chronic pain, various painkillers, including opioids, are being used. Unfortunately, use of such powerful painkillers can often lead to financial burden and potential drug addiction. Misuse of addictive painkillers leads to the overdosing and death of about 47,000 people a year [1]. More and more physicians are starting to consider VR technologies as an alternative to painkillers. The basic idea behind using VR for pain management is that immersive environment and stimuli can distract patients from their pain and emotional states. In particular, hospitalized and/or bed-bound patients, such as women in labor and patients receiving chemotherapy, dialysis, radiation, or imaging procedures, may have biopsychosocial distress, such as depression, anxiety, and boredom due to their health condition and environment changes. Since 1996, the Harborview Burn Center in Seattle has used VR for burn patients, which has helped distract patients by providing relief and escape from painful treatments [2]. Recent studies from my institute at Cedars-Sinai Medical Center and others explored the use of VR in 100 hospitalized patients and found that those who participated in VR therapy showed a significant reduction in pain scores [3]. This suggests that VR may offer holistic inpatient care by effectively reducing anxiety and pain perception and helping patients relax before, during, or after procedures. Additionally, VR technology is now becoming more user-friendly, cost-effective, interactive, flexible, immersive, and portable. VR is now being considered an effective, safe, and feasible intervention for a variety of disease states, such as obesity, anxiety, eating disorders, post-traumatic stress disorder, cancer, Parkinson's, nicotine/alcohol addiction, cognitive/motor rehabilitation et al. However, the challenge remains on figuring out how to incorporate VR into standard of care procedures in the everyday clinical setting.

One interesting use of VR could be in urology. Medical training using VR and/or AR (augmented reality, an interactive experience of environments where objects in the real-world are "augmented" by computer-generated perceptual information) could improve education and surgical practice, thereby increasing the speed and accuracy of certain procedures. The traditional Halstedian method of "see one, do one, teach one" in medical training could be improved by applying VR/AR-based simulators before performing live surgery. Complicated anatomy can be visualized in a 3D hologram format, and AR navigation can then facilitate the recognition and localization of anatomic structures. Using a projector beam and a see-through device, such as a smart google, physicians can see the virtual model directly projected on the patient. Furthermore, individual medical records can be reviewed, and images can be portrayed on screens during camera-based AR procedures. VR stimulation training has also been shown to result in superior speed and significant reduction of procedure-related complications. VR/AR stimulators can provide a variety of surgical scenarios that can be used during medical training to improve the overall skills required for operations, such as transurethral

ⓒ The Korean Urological Association

resection of the prostate or prostatectomy. It can record the operative process of trainees in real-time, which can be used for evaluations. Considering how robotic surgical procedures continue to grow rapidly, a computer-derived virtual operative field with a tactile feedback system could be a new reliable standard method in robotic training programs.

A VR/AR simulator can not only be applied for surgeries, but also for personalized treatment of debilitating benign bladder dysfunctions, such as interstitial cystitis (IC)/painful bladder syndrome. IC is characterized by a need for frequent urination, typically urgent (and often uncontrollable), involuntary episodes, and flares of acute pain without any bacterial or yeast infections [4]. Along with no known etiology, IC has been challenging to urologists because there are no effective pharmacological, surgical, or behavioral treatments available. Current recommendations include exercising specific pelvic floor muscles to reduce severe urinary symptoms. To train unconscious physiological processes, a VR/AR-based biofeedback designed to visualize these exercising muscles could be applied. If patients can see the pelvic floor muscles through a head-mounted display, tablet, or hologram, they can easily understand exactly which muscles they are working and focus their efforts with more specificity; thereby, improving the overall efficacy of the therapy.

Including our own group, many scientific investigators have been developing biomarkers specific to each urological disease using biospecimens from tissues, blood, or other body fluids [5]. It is widely accepted that molecular biomarkers are useful since they can be used for prognoses and treatment response monitoring. Of note, accurate real-time monitoring can be immensely helpful for disease prevention, early diagnosis, and reduction of incidence rates. Biosensors are analytical devices designed to detect biological and physiochemical biomarkers and have been developed into smart health monitoring devices that can wirelessly sync with smartphones [6]. Data collection, storage, and analysis can be done in the connected cloud environment. The key components of potentially successful biosensors in the clinical setting include portability, rapidity, and cost-effectiveness. In particular, for efficient application in communication between urologists and patients, more effort should be placed on developing newer generations of highly sensitive molecular diagnostic biosensors with compact and user-friendly platforms.

While blood tests are currently the gold standard for noninvasive, painless, and continuous monitoring of biomarkers, urine is a particularly attractive resource in the urology field. Urine biosensors may provide real-time levels of the patients' urinary metabolite biomarkers, electrolytes, temperature, and pH. There have been studies on developing rapid diagnoses of urinary tract infections (UTIs) in the clinical setting, which would allow for the early identification of UTI and timely antibiotic treatment. UTI is one of the most common infections in women, elders, and infants. Recently, investigators developed a small and disposable UTI biosensor embedded in a diaper. When activated upon exposure to urine, the self-powered sensor can determine the presence of chemical compounds associated with UTI [7]. The data can then be collected via a wireless smartphone app and used for further analysis by urologists and patients, allowing them to discuss the patterns of UTI. For other bladder diseases, such as IC, urinary biosensors may be able to facilitate real-time identification of flares (acute pain) and fluctuation of biomarkers, such as specific metabolites [5]; thereby enabling personalized treatment regimens for patients. Wearable wireless urinary metabolic sensors enable remote tracking of disease biomarkers and bladder health 24/7. They can replace bladder diaries (voiding diaries) and help accelerate interventions regardless of location, time, or device.

Research related to smart health devices is already changing the paradigm of the healthcare industry. Smart healthcare is characterized by eHealth, which is supported by computer-based information and communication technology, and mHealth services, a medical practice supported by mobile devices. Our healthcare system is now rapidly evolving for better patient diagnoses and treatment by establishing the personal digital assistants for electronic record management and smart remote services through biosensor platforms that are wirelessly connected between urologists and patients.

CONFLICTS OF INTEREST

The authors have nothing to disclose.

ACKNOWLEDGMENTS

The authors acknowledge support from National Institutes of Health grants (1U01DK103260, 1R01DK100974, U24 DK097154, NIH NCATS UCLA CTSI UL1TR000124), Department of Defense grants (W81XWH-15-1-0415), Centers for Disease Controls and Prevention (1U01DP006079), the U.S.-Egypt Science and Technology Joint Fund by National Academies of Sciences, Engineering, and Medicine (NAS) and The United States Agency for International Development (USAID) (to J.K.). Any opinions, findings, conclusions, or

https://doi.org/10.4111/icu.2019.60.1.1

recommendations expressed in this article are those of the authors alone, and do not necessarily reflect the views of USAID or NAS. And this research was supported by the International Science and Business Belt Program through the Ministry of Science, ICT and Future Planning (to W.J.K.) (2015-DD-RD-0070).

Wun-Jae Kim[1], Jayoung Kim[2]
Corresponding Author: Wun-Jae Kim
ORCID: https://orcid.org/0000-0002-8060-8926
[1]Department of Urology, Chungbuk National University College of Medicine, Cheongju, Korea
[2]Departments of Surgery and Biomedical Sciences, Cedars-Sinai Medical Center, Los Angeles, CA, USA
E-mail: wjkim@chungbuk.ac.kr

REFERENCES

1. Rudman W Jr, Corcoran P, Elliott K. Prescription drug monitoring programs and opioid death rates. JAMA 2017 Nov 28 [Epub]. http://doi.org/10.1001/jama.2017.16300.
2. Escudero LA, Cerutti S, Olsina RA, Salonia JA, Gasquez JA. Factorial design optimization of experimental variables in the on-line separation/preconcentration of copper in water samples using solid phase extraction and ICP-OES determination. J Hazard Mater 2010;183:218-23.
3. Tashjian VC, Mosadeghi S, Howard AR, Lopez M, Dupuy T, Reid M, et al. Virtual reality for management of pain in hospitalized patients: results of a controlled trial. JMIR Ment Health 2017 Mar 29 [Epub]. http://doi.org/10.2196/mental.7387.
4. McLennan MT. Interstitial cystitis: epidemiology, pathophysiology, and clinical presentation. Obstet Gynecol Clin North Am 2014;41:385-95.
5. Wen H, Lee T, You S, Park SH, Song H, Eilber KS, et al. Urinary metabolite profiling combined with computational analysis predicts interstitial cystitis-associated candidate biomarkers. J Proteome Res 2015;14:541-8.
6. Jayanthi VSPKSA, Das AB, Saxena U. Recent advances in biosensor development for the detection of cancer biomarkers. Biosens Bioelectron 2017;91:15-23.
7. Yu W, Seo W, Tan T, Jung B, Ziaie B. A diaper-embedded disposable nitrite sensor with integrated on-board urine-activated battery for UTI screening. Conf Proc IEEE Eng Med Biol Soc 2016;2016:303-6.

Letter

Int Neurourol J 2019;23(1):86-87
https://doi.org/10.5213/inj.1938020.010
pISSN 2093-4777 · eISSN 2093-6931

INTERNATIONAL NEUROUROLOGY JOURNAL
INJ
OPEN ACCESS

Application of Low-Cost, Easy-to-Use, Portable Biosensor Systems for Diagnosing Bladder Dysfunctions

Nosang V. Myung[1], Sungyong Jung[2], Jayoung Kim[3,4,5,6]

[1]Department of Chemical and Environmental Engineering, University of California Riverside, Riverside, CA, USA
[2]Department of Electrical Engineering, University of Texas at Arlington, Arlington, TX, USA
[3]Departments of Surgery and Biomedical Sciences, Cedars-Sinai Medical Center, Los Angeles, CA, USA
[4]Samuel Oschin Comprehensive Cancer Institute, Cedars-Sinai Medical Center, Los Angeles, CA, USA
[5]University of California Los Angeles, Los Angeles, CA, USA
[6]Department of Urology, Gacheon University College of Medicine, Incheon, Korea

To the editor

A recently published series of articles in the *International Neurourology Journal* elegantly presented the current trends in Smart Health. In particular, 3 articles by Taeg-Keun Whangbo and colleagues [1,2] and Kang et al. [3] summarized how close we are to making personalized technology-based healthcare a reality in the clinical setting. Given that the authors provided an overview of the current applications of newly emerging technologies, we thought about how they could be utilized for diagnosing and monitoring nonfatal bladder diseases, such as interstitial cystitis (IC). Because of its unknown etiology and symptomatic manifestation as urinary discomfort in the absence of other causes, diagnosing IC is dependent on clinical parameters, such as pain, urinary urgency, and frequency. Additionally, due to the lack of proper conventional markers, diagnosis involves traditional urinalysis, urine culture, cystoscopy, bladder biopsy, and bladder hydro-distention. IC can cause a multitude of symptoms that have a negative impact on sexual activity and quality of life. The most significantly reported concern is chronic pelvic pain [4], which can also create sexual dysfunctions. Although the financial and personal burden of IC is extensive on the American public [5], there is still no clear diagnostic test for IC. Although our own group and several other laboratories have identified a series of IC urinary biomarkers, it is still unknown whether they would be clinically useful. Expanding use of this knowledge is costly and complexity of conventional analytic platforms, such as mass spectrometry, is hard to implement clinically.

Evaluating the impact duration, severity, pain localization, anxiety, and depression related to bladder dysfunctions may help identity risk factors. In addition to our own laboratory, many scientists have focused on developing biomarkers specific to each urological disease using biospecimens, such as tissue, blood, or other bodily fluids. Molecular biomarkers are widely accepted as a useful resource for prognoses and treatment response monitoring. Most importantly, accurate real-time monitoring of biomarkers may be immensely helpful for disease prevention, early diagnosing, and incidence rate reduction. Active oversight of biomarkers could be implemented using bio/chemical sensors, which are analytical devices designed to detect biological or physiochemical markers, that can also be integrated with other smart health monitoring devices that sync wirelessly with smartphones. This data can be collected, stored, and analyzed in a shared cloud environment between patients and physicians. In order for such internet of biosensors to be successful in the clinical setting, they need to be portable, rapid, and cost-effective. For particularly efficient application in urology, effort should be focused on developing next generations of highly sensitive diagnostic biosensors that are portable, user-friendly, and low cost.

Corresponding author: Jayoung Kim https://orcid.org/0000-0002-3683-4627
Departments of Surgery and Biomedical Sciences, Cedars-Sinai Medical Center, Davis 5071, 8700 Beverly Blvd., Los Angeles, CA 90048, USA
E-mail: Jayoung.Kim@cshs.org / Tel: +1-310-423-7168 / Fax: +1-310-967-3809
Submitted: January 21, 2019 / **Accepted after revision:** January 24, 2019

This is an Open Access article distributed under the terms of the Creative Commons Attribution Non-Commercial License (http://creativecommons.org/licenses/by-nc/4.0/) which permits unrestricted non-commercial use, distribution, and reproduction in any medium, provided the original work is properly cited.

Biosensors are analytical devices that can selectively detect and quantitatively measure analytes interacting with biological elements, such as tissues, microorganisms, antibodies, and nucleic acids. Biosensors consist of receptor-functionalized sensing materials that react to analytes and transducers that can convert biological responses into electrical signals. It is integrated with electronic circuits to readout and process signals, including amplifying, filtering, digitizing, analyzing, interfacing, transmitting, and displaying. The readout circuits are typically implemented with an operational amplifier, an analog-to-digital converter, a microcontroller, and a communication device. The types of biosensors can be categorized based on their detection mechanisms, such as electrochemical, thermal, electrical, magnetic, optical, and piezoelectric. Among these biosensors, electrochemical sensors are the most versatile, portable, and highly developed (approximately 58% of all chemical sensors) in the market. Prime examples of commercially available portable and easy-to-use electrochemical analyzers include glucose meters and portable blood analyzer (e.g., i-Stat Blood Chemistry Analyzer, Abbott, Princeton, NJ, USA), which have clearly demonstrated their ability to cost-effectively detect multiple analytes from small sample volumes. Like blood chemistry analyzers, high density electrochemical sensor arrays can be developed to accurately identify and quantify IC biomarkers from urine.

In addition to the development of portable analyzers for biological fluids, there has been rapid developments in gas sensor technology to mimic the human olfactory system to identify and quantify various gases (odors). This artificial olfactory system (e-nose) simulates the different stages of the human olfactory system, including sampling and filtering gaseous molecule. Using artificial gas sensors that odor molecules can react with, these sensors can then amplify and treat signal responses. Integrated artificial intelligence and web-based knowledge systems can evaluate key information to finally recognize the odor. Such devices could have a significant role in the early diagnosis and detection of IC by analyzing odors from urine samples.

Research and development related to mobile health devices will provide a game-changer in Smart Health and the future healthcare industry. Smart hospitals supported by computers, wireless network-based information, and communication technology are now rapidly evolving for more personalized care and electronic management of clinical records. As innovative thinkers, how can we apply biosensor technologies for medical diagnostics and health monitoring, particularly in urological care?

• **Conflict of Interest:** No potential conflict of interest relevant to this article was reported.

ACKNOWLEDGEMENTS

This was supported by the Future Materials Discovery Program from the National Research Foundation of Korea (NRF). Funding was received from the Ministry of Science, ICT & Future Planning (NRF-2016M3D1A1027836), and the NAVSEA METCAL program. The authors also acknowledge support from National Institutes of Health grants (1U01DK103260, 1R01DK100974, U24 DK097154, NIH NCATS UCLA CTSI UL1TR000124), Department of Defense grants (W81XWH-15-1-0415), Centers for Disease Controls and Prevention (1U01DP006079), the U.S.-Egypt Science and Technology Joint Fund by National Academies of Sciences, Engineering, and Medicine (NAS) and The United States Agency for International Development (USAID) (to J.K.). Any opinions, findings, conclusions, or recommendations expressed in this article are those of the authors alone, and do not necessarily reflect the views of USAID or NAS.

REFERENCES

1. Whangbo TK, Eun SJ, Jung EY, Park DK, Kim SJ, Kim CH, et al. Personalized urination activity recognition based on a recurrent neural network using smart band. Int Neurourol J 2018;22(Suppl 2):S91-100.
2. Eun SJ, Whangbo TK, Park DK, Kim KH. Development of personalized urination recognition technology using smart bands. Int Neurourol J 2017;21(Suppl 1):S76-83.
3. Kang M, Park E, Cho BH, Lee KS. Recent patient health monitoring platforms incorporating internet of things-enabled smart devices. Int Neurourol J 2018;22(Suppl 2):S76-82.
4. Katz L, Tripp DA, Carr LK, Mayer R, Moldwin RM, Nickel JC. Understanding pain and coping in women with interstitial cystitis/bladder pain syndrome. BJU Int 2017;120:286-292.
5. Tung A, Hepp Z, Bansal A, Devine EB. Characterizing health care utilization, direct costs, and comorbidities associated with interstitial cystitis: a retrospective claims analysis. J Manag Care Spec Pharm 2017;23:474-82.

Proteomics
www.proteomics-journal.com

Downregulation of CENPF Remodels Prostate Cancer Cells and Alters Cellular Metabolism

*Muhammad Shahid, Minhyung Kim, Min Young Lee, Austin Yeon, Sungyong You, Hyung L. Kim, and Jayoung Kim**

Metabolic alterations in prostate cancer (PC) are associated with progression and aggressiveness. However, the underlying mechanisms behind PC metabolic functions are unknown. The authors' group recently reported on the important role of centromere protein F (CENPF), a protein associated with the centromere–kinetochore complex and chromosomal segregation during mitosis, in PC MRI visibility. This study focuses on discerning the role of CENPF in metabolic perturbation in human PC3 cells. A series of bioinformatics analyses shows that CENPF is one gene that is strongly associated with aggressive PC and that its expression is positively correlated with metastasis. By identifying and reconstructing the CENPF network, additional associations with lipid regulation are found. Further untargeted metabolomics analysis using gas chromatography-time-of-flight-mass spectrometry reveals that silencing of CENPF alters the global metabolic profiles of PC cells and inhibits cell proliferation, which suggests that CENPF may be a critical regulator of PC metabolism. These findings provide useful scientific insights that can be applied in future studies investigating potential targets for PC treatment.

Dr. M. Shahid, Dr. M. Kim, A. Yeon, Prof. S. You, Prof. H. L. Kim, Prof. J. Kim
Department of Surgery
Cedars-Sinai Medical Center
Los Angeles, CA, USA
E-mail: Jayoung.Kim@cshs.org
Dr. M. Y. Lee
Institute for Systems Biology
98109, Seattle, WA, USA
Prof. S. You, Prof. H. L. Kim, Prof. J. Kim
Samuel Oschin Comprehensive Cancer Institute
Cedars-Sinai Medical Center
Los Angeles, CA, USA
Prof. S. You, Prof. J. Kim
Department of Biomedical Sciences
Cedars-Sinai Medical Center
Los Angeles, CA, USA
Prof. J. Kim
University of California Los Angeles
CA, USA
Prof. J. Kim
Department of Urology
Ga Cheon University College of Medicine
Incheon, South Korea

The ORCID identification number(s) for the author(s) of this article can be found under https://doi.org/10.1002/pmic.201900038

DOI: 10.1002/pmic.201900038

1. Introduction

Prostate cancer (PC) is the second most commonly diagnosed cancer and the fifth leading cause of male mortality worldwide, with an estimated 1.3 million new cases and 359 000 associated deaths in 2018.[1,2] It is now widely accepted that proliferating cancer cells alter their metabolic activities to satisfy increased needs for energy and biosynthetic precursors, such as glucose.[3] Rather than utilizing the normal process of oxidative phosphorylation, even with the presence of oxygen and fully functioning mitochondria, these proliferating cancer cells favor aerobic glycolysis, which dramatically increases the uptake of glucose and production of lactate; a process known as the Warburg Effect.[4] Glutamine metabolism also plays a vital role in cancer cell energy metabolism by providing Krebs cycle intermediates, which further corroborates the idea of altered cancer cell metabolism.[5] Most cancers depend on increased glutaminolysis to compensate for increased energy needs and fill their carbon and nitrogen pools for the biosynthesis of macromolecules.[6] Besides the higher utilization of the glycolytic pathway, cancer cells frequently exhibit a heightened ability to synthesize lipids, and this increased lipogenesis is tightly coupled to glucose metabolism.[7,8] Reprogrammed energy metabolism is an important hallmark of the upkeep of altered homeostasis in cancer.[9] For instance, increased glycolysis has been observed in many cancer types, including PC.[10,11] Several studies have shown that this dysregulated metabolism plays a crucial role in PC progression.[12–14] These alterations in metabolic features may represent potential prognostic biomarkers.[15] Therefore, investigating PC metabolism could be an opportunity to find new prognostic or therapeutic biological markers.

Metabolomics involves the study of metabolism and metabolite profiling and is an important analytical tool used in oncology for discovering novel biosignatures and therapeutic targets.[16] It is widely applied as an interdisciplinary omics approach, combining pattern recognition, bioinformatics, epidemiology, analytical biochemistry, and biology.[17] This comprehensive analysis provides a valuable opportunity to better understand the biochemical changes underlying cancer metabolism and improve early detection, progression, and therapeutic monitoring.[18] Metabolomics can also respond to clinical challenges by providing a method of

 © 2019 WILEY-VCH Verlag GmbH & Co. KGaA, Weinheim

detecting vital and promising novel biomarkers.[19,20] In terms of cancer, metabolomics can enable additional measurement of downstream activities, thereby allowing for the discovery of key oncometabolites.[21] These metabolites are markers of biochemical activity and are closely related to clinical phenotypes.[22] An increasing number of metabolomic studies have focused on improving the current understanding of PC. There have been several attempts at capturing metabolic PC biomarkers due to evidence suggesting that perturbed metabolism may play a crucial role in the development and progression of PC.[14] These metabolite profiles can be distinct and could provide important prognostic information. For example, a metabolomic study of PC and healthy controls found increased choline levels in malignant tissue.[23] PC can be a particularly attractive model for metabolic profiling; the healthy prostate has a unique metabolism that is needed for producing prostatic fluid and alterations can be feasibly tracked.[24]

Our group recently conducted a transcriptomic study on magnetic resonance imaging (MRI)-visible and -invisible prostate cancers to find differentially expressed genes (DEGs) between the two groups. We identified centromere protein F (CENPF) as one of four genes related to MRI visibility, progression-free survival, and metastatic deposits.[25] We further found that CENPF is a critical regulator of cancer metabolism, potentially through pyruvate kinase M2 (PKM2). Our findings align with previous reports suggesting that CENPF is a master regulator of malignancy in PC.[26,27] PKM2 is also well known to be a key player in PC metabolism[28]; however, its link between CENPF and the development of PC using untargeted metabolomics profiling has not been done before. By further defining the role of CENPF in PC, we can gain a deeper mechanistic understanding of its effects in downstream events and disease development.

This study aimed to determine the metabolic profile of CENPF-knockout ($CENPF^{KO}$) PC cells and identify differentially expressed metabolites (DEMs) that can be used as prognostic markers. Our experimental results showed that silencing of CENPF reduced global metabolism. Additional computational analysis demonstrated that CENPF regulates PC metabolism. Our results may allow us to derive new information that could be helpful in better targeting the underlying mechanisms driving PC.

Significance Statement

PC remains to be a worldwide public health concern. It has been accepted that proliferating PC cells satisfy elevated energy requirements needed to support accelerated cell division by modulating metabolism. However, the mechanisms behind these metabolic alterations are largely unknown. One key modulator that has been previously identified is CENPF, which is shown to be upregulated in PC cells. Despite this knowledge, there has been no detailed systematic analysis on how CENPF regulates PC cellular metabolism. In this study, we aimed to better understand the global metabolic changes mediated by CENPF in PC cells using a quantitative metabolomics approach, which includes GC-TOF-MS. The metabolites and metabolic enzymes that we identified may serve as potential biomarkers or therapeutic targets. These findings shed new light on the biochemical mechanisms and biological functions of CENPF in PC and may pave the way for novel treatment options.

2. Experimental Section

2.1. Cell Lines and Culturing

Human PC3 cells were obtained from American Type Culture Collection (ATCC) (Manassas, VA, USA). Cells were maintained in Dulbecco's modified Eagle medium (DMEM) supplemented with 10% heat-inactivated fetal bovine serum (FBS) and penicillin–streptomycin at 37 °C with 95% air and 5% CO2. DMEM and FBS were purchased from Life Technologies (Grand Island, NY, USA). The $CENPF^{KO}$ PC3 cell line was constructed using the CRISPR/Cas9 system by ALSTEM, LLC (Richmond, CA) and maintained as described previously.[29] If frozen, after thawing, cells were used under ten passages. Mycoplasma contamination was monitored for periodically.

2.2. Identification of DEGs

The transcriptome of 1,321 PC patient samples was obtained from the Prostate Cancer Transcriptome Atlas (PCTA; www.thepcta.org), which was then used to develop the prostate cancer subtype (PCS) classification system.[30] PC transcriptome data was then normalized and batch corrected by median-centering and quantile scaling (MCQ). Independent PC data describing gene expression changes in multiparametric (MP)-MRI-visible and invisible tumors based on ribonucleic acid (RNA) sequencing (GSE95369) was obtained from the Gene Expression Omnibus (GEO) database.[31] Read count data was normalized using the TMM normalization method.[32] The integrated hypothesis testing method was applied, as previously reported.[33] Briefly, three independent statistical tests were performed, including the T-test, median ratio test, and rank-sum test, on each gene. To compute the significance level (p-values) of the observed T-values, $\log_2$-median ratios, and rank-sum differences, the empirical null hypothesis distribution was used, which was estimated by random permutation of the samples. Finally, the adjusted p-values were computed using Stouffer's method.[34] DEGs between MRI visible and invisible patients in the MP-MRI data were selected for if they had adjusted p-values <0.05 and absolute fold-changes ≥ 2. DEGs between metastatic castration-resistant prostate cancer (mCRPC) and primary patients in the PCTA were selected for if they had adjusted p-values <0.01 and absolute fold-changes ≥ 1.5. Functional enrichment analyses were performed using gene set enrichment analysis (GSEA) for hallmark gene sets[35] and DAVID (Ver. 6.8).[36]

2.3. Selection of CENPF Network Genes

To identify genes that are differentially regulated by CENPF in PC, samples were selected from the PCTA data with high and low CENPF expression. High and low CENPF samples were defined as those with upper and lower terciles of expression, respectively. The adjusted p-values were then computed using the

© 2019 WILEY-VCH Verlag GmbH & Co. KGaA, Weinheim

same method, as described above. DEGs between the high- and low-CENPF groups were selected if they had adjusted *p*-values <0.05.

2.4. Identification of Hub Genes in the CENPF Network

To identify hub genes that could be potential regulator candidates of the CENPF network in PC, protein–protein interactions were collected from six different databases; the Biological General Repository for Interaction Datasets (BioGRID)[37], the Databased of Interacting Proteins (DIP[38]), High Confidence Protein–Protein Interactions (HitPredict)[39]), the IntAct Molecular Interaction Database (IntAct)[40]), the Molecular INTeraction Database (MINT),[12] and the Functional Protein Associations Network (STRING)[41]). The number of interactions in the up- and downregulated genes in the high and low-CENPF samples was then counted separately. Significance of the number of the interactions was computed as enrichment *p*-values using Fisher's exact test.

2.5. Reconstruction of a Network Model

To reconstruct a network model, we first selected for lipid metabolism and pathway-associated genes from the CENPF network genes using Gene Ontology Biological Process (GOBP). Then, protein–protein interaction and transcription factor (TF)-target interaction information of the differentially expressed lipid-related genes were collected from the six interactome databases that were used for our master regulator analysis. CENPF transcriptional target information from a prior study done by Aytes et al.[26] was also included. The network was visualized using Cytoscape (v. 3.2.1).[42]

2.6. GC-TOF-MS Analysis

Gas chromatography-time-of-flight-mass spectrometry (GC-TOF-MS) analysis was performed on $CENPF^{KO}$ and control PC3 cells.[43,44] Samples were dissolved in 1 ml of 20 °C mixture of acetonitrile, isopropanol, and water (3:3:2 v/v) at a pH of 7. The solution was then vortexed at 4 °C for 5 min. Samples were centrifuged for 2 min at 14 000 rcf and 500 μL were aliquoted. The aliquots were then evaporated in a Labconco Centrivap Cold Trap to complete dryness. The methoximation step was performed using a 10 μL solution of 40 mg mL^{-1} of O-methylhydroxylamine hydrochloride (CAS: [593-56-[6]]; formula: $CH_5NO.HCl$) and shaken for 90 min at 30 °C. Then, 90 μL of *N*-methyl-*N*-trimethylsilyltrifluoroacetamide (MSTFA) was added and the solution was shaken for 30 min at 37 °C. After that, a 1 μL mixture of fatty acid methyl ester (FAME) retention time markers was added. The mixture was transferred to amber crimp autosampler vials. Measurements were done on a Leco Pegasus IV Time of Flight Mass Spectrometer coupled to an Agilent 6890GC with an Agilent 6890 Split/Splitless Injector.

The column used was a Restek RTX-5Sil MS (95% dimethyl/5% diphenyl polysiloxane), which had 30 m length, 0.25 mm i.d., 0.25 μm film thickness, and an additional 10 m guard column. The injection volume used was 1 μL at 250 °C. The GC parameters were set to have a constant helium flow of 1 mL min^{-1} and an oven ramp temperature of 50 °C (1 min hold) that increased to 330 °C at a rate of 20 °C min^{-1} with a 5 min hold before cool down. The transfer line temperature was set to 280 °C, and spectra were recorded in the electron ionization mode at 70 eV with a filament temperature of 250 °C TOF and scan range of 85–500 Da.

2.7. Annotation and Identification of Compounds

Detection or deconvolution of peaks and compounds was performed using the Leco ChromaTOF software. Spectra were matched against the FiehnLib Mass Spectral and Retention Index Library.[23] Post-curation and peak replacements were done using the in-house developed BinBase software, which was set as follows: validity of chromatogram (<10 peaks with intensities $>10^7$ counts per second), unbiased retention index marker detection (MS similarity >800, validity of intensity range for high m/z marker ions), and retention index calculation by 5th order polynomial regression. Sample matrices with all known and unknown compounds were then exported to a Microsoft excel sheet. A total of 524 compounds were detected. Of these, 144 were annotated as known compounds with KEGG compound identifier.

2.8. Normalization and Identification of DEMs

The raw data was normalized based on mTIC, which is the sum of all peak heights for all identified metabolites for a sample.[45] The average mTIC was calculated and a normalization factor for a sample was defined by dividing the average mTIC by the mTIC of the individual sample. The normalized intensity was then calculated by multiplying the raw intensity by the normalization factor. DEMs were selected according to the criteria of a false discovery rate (FDR) adjusted *p*-value (*q*-value) ≤ 0.05 from a two-tailed Welch's *t*-test and a fold-change ≥ 1.5.[46]

The normalized intensities of the 524 metabolites were transformed into $\log_2$ scale and were standardized as *z*-score, and then principal component analysis (PCA) was applied to understand variations in the metabolite profiles of different cell lines. Hierarchical clustering of the DEMs was performed using Euclidean distance and ward linkage.

2.9. Metabolite Enrichment Analysis

Metabolites Biological Role (MBROLE) 2.0 was used to identify statistically significant metabolic pathways enriched by the DEMs.[47] MBROLE is a web-based tool containing functional annotations on chemical compounds compiled from various public databases, such as the Kyoto Encyclopedia of Genes and Genomes (KEGG) and PubChem. P-Values are computed based

© 2019 WILEY-VCH Verlag GmbH & Co. KGaA, Weinheim

on hypergeometric distribution by comparing the number of metabolites in the DEMs and background set, which is the annotated metabolites with KEGG compound identifiers. Pathways with P-values < 0.1 and at least 2 DEMs were selected for functional interpretation.

2.10. Proliferation Assay

Trypan blue assay was carried out to assess cell proliferation. Briefly, cells were seeded at a density of 2×10^2 cells per well onto six-well culture plates in complete medium. Following 24 h of cell growth, each well culture was maintained and incubated for 48 h. The medium was replaced every day. After 48 h, cells were trypsinized, washed, and resuspended in PBS containing 0.4% trypan blue. The number of viable cells was counted using a hemocytometer, as per standard protocol. Each experiment was done a minimum of three independent times. The results are presented as the percentage of viable cells relative to that of the control.

2.11. Branched-Chain Amino Acid/Aromatic Amino Acid Ratio

The branched-chain amino acid (BCAA)/aromatic amino acid (AAA) ratio was calculated as the ratio between the concentration of BCAAs (valine, leucine, and isoleucine) and AAAs (phenylalanine and tyrosine).[48]

$$\text{BCAA / AAA ratio} = \frac{[\text{valine}] + [\text{leucine}] + [\text{isoleucine}]}{[\text{phenylalanine}] + [\text{tyrosine}]}$$

The concentration of each amino acid was calculated by dividing the quantified intensity by the quantified m/z.

2.12. Acetate Measurement Assay

Acetate levels were measured using an Acetate Colorimetric Assay Kit (Biovision Inc.) according to the instructions provided. Briefly, cells (1×10^6) were rapidly homogenized with 100 μL of ice-cold acetate assay buffer for 10 min on ice. The mixture was then centrifuged at 12,000 rpm for 5 min, and the resulting supernatant was collected. After that, 1–50 μL of sample (50–200 μg) was added onto a 96-well plate. The final volumes were adjusted to 50 μL with acetate assay buffer. The reaction was incubated at room temperature for 40 min, and optical reading was taken at 450 nm using a spectrophotometer. The unknown sample concentration was calculated from the standard curve.

2.13. Statistical Analysis

Results were expressed as mean ± standard error (SE) from at least three independent experiments. To evaluate differences between two groups, statistical analysis was done using Student's *t*-test. Unless otherwise indicated, $p < 0.05$ was deemed significant. MATLAB (v.9.0; Mathworks, Natick, MA, USA) and R (v.3.5) were used for bioinformatic analyses.

3. Results

3.1. Transcriptome Analysis Reveals Genes Associated With Aggressive PC

To identify genes associated with aggressive PC, we utilized two independent transcriptome datasets. One was obtained from the PCTA database, which provided 1321 PC transcriptome profiles[30] (hereafter referred to as PCTA). The other was from a separate study that examined the gene expression differences between MP-MRI-visible and invisible tumors[25] (hereafter referred to as MRI). The transcriptome data was produced using RNA sequencing, and the count data was deposited in the GEO database under the accession number GSE95369. Of note, survival analysis of these independent study cohorts presented four gene signatures as being significantly correlated with metastatic progression and biochemical recurrence.

With this transcriptome data, we hypothesized that DEGs between mCRPC versus primary PC and MP-MRI-visible versus invisible tumors may be potential regulator candidates of PC progression. We then performed integrative hypothesis testing on the PCTA and MRI datasets to identify 182 (mCRPC vs PC) and 457 (MRI-visible vs invisible) DEGs (**Figure 1**A; see Section 2 for details). Between these two compared groups, ten shared DEGs were identified (Figure 1B). SPP1 (secreted phosphoprotein 1), CENPF, MEX3A (mex-3 RNA binding family member A), NUSAP1 (nucleolar and spindle associated protein 1), and TOP2A (DNA topoisomerase II alpha) were significantly upregulated in mCRPC and MRI-visible PC, while GAS1 (growth arrest specific 1), PGM5 (phosphoglucomutase 5), CHRDL1 (chordin-like 1), PCAT4 (prostate cancer associated transcript 4), and H19 (H19, imprinted maternally expressed transcript) were significantly downregulated. Interestingly, the clinical significance of CENPF in PC was previously reported[49] and identified as a potential master node of PC malignancy.[26]

3.2. CENPF Expression is Correlated with PC Progression

We examined CENPF expression in tissues with five distinct disease statuses (benign, Gleason score (GS) <6, GS = 7, GS >7, and mCRPC) to discern the association of CENPF with disease progression (**Figure 2**A). Consistent with previous studies,[27] CENPF gene expression levels increased significantly in higher GS and mCRPC tissue (one-way ANOVA P <0.001, rank-sum $p < 0.001$). A prior cross-species study[27] and MRI study[25] revealed a regulatory relationship between CENPF and FOXM1 in PC progression. We thus checked for a correlation between CENPF and FOXM1 expression in the PCTA data.[30] We found that expression of CENPF and FOXM1 exhibited a significant positive correlation in all PCTA samples and individual disease states (Figure 2B). This implies that gene expression and regulation of CENPF and FOXM1 are significantly associated with PC progression.

© 2019 WILEY-VCH Verlag GmbH & Co. KGaA, Weinheim

A

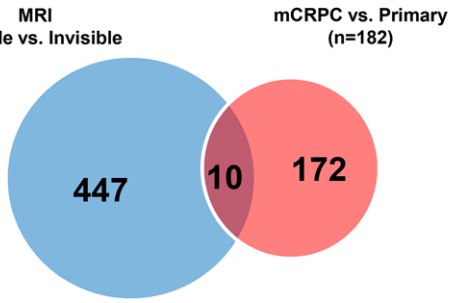

B

			Visible vs. Invisible		mCRPC vs. Primary	
	Symbol	Full name	FC	FDR	FC	FDR
Up	SPP1	secreted phosphoprotein 1	2.02998927	0.00248066	0.733542	3.4299E-05
	CENPF	**centromere protein F**	**1.65301529**	**0.00436199**	**0.705239**	**5.0738E-09**
	MEX3A	mex-3 RNA binding family member A	1.60233872	0.02067891	0.905354	1.7876E-11
	NUSAP1	nucleolar and spindle associated protein 1	1.08252272	0.0016237	0.60018	3.6683E-06
	TOP2A	DNA topoisomerase II alpha	1.0627985	0.00037213	0.583075	1.8778E-05
Down	GAS1	growth arrest specific 1	-1.1367365	0.02374247	-0.67864	2.2501E-05
	PGM5	phosphoglucomutase 5	-1.2673743	0.01346269	-1.18754	6.28E-08
	CHRDL1	chordin like 1	-1.4992521	0.00350331	-0.72711	3.8476E-08
	PCAT4	prostate cancer associated transcript 4 (non-protein coding)	-1.8653991	0.00268709	-0.62723	6.0481E-05
	H19	H19, imprinted maternally expressed transcript (non-protein coding)	-2.7404157	0.0049081	0.587755	0.0023771

Figure 1. Selection of genes associated with aggressive PC. A) Venn diagram depicts the number of DEGs in MP-MRI-visible versus invisible tumors and mCRPC versus primary PC. Transcriptome data of MP-MRI visibility was obtained from the GEO database (GSE95369), and mCRPC and PC gene expression profiles are from PCTA. DEGs for MRI visibility were selected if they had an adjusted p-value < 0.05 and fold-change ≥ 2. DEGs in the mCRPC and PC group were selected if they had an adjusted p-value < 0.01 and fold-change ≥ 1.5. B) List of overlapping genes associated with both MRI visibility and metastatic progression.

3.3. Genes Involved in the CENPF Network in PC

Given the significance of CENPF expression in PC progression, investigating the downstream CENPF transcriptional network may be relevant in discovering the molecular mechanisms of PC. For this, we defined high and low CENPF-expressing groups in the PCTA by selecting for upper and lower terciles. Secondly, we identified significantly up and downregulated CENPF-associated genes in the high and low groups (**Figure 3**A). To identify molecular pathways and cellular processes regulated by CENPF, we then performed GSEA and functional enrichment analysis using hallmark gene sets from MsigDB and GOBP. GSEA results showed that the E2F target, G2M checkpoint, MYC target, and mitotic spindle gene sets were significantly enriched for in the high-CENPF group. However, myogenesis, TGF-beta signaling, ultraviolet (UV) response, protein secretion, apical surface, apoptosis, epithelial-mesenchymal transition, apical junction, and hypoxia gene sets were significantly enriched in the low-CENPF group (Figure 3B).

Functional enrichment analysis results from DAVID also showed consistent results with GSEA. Cell cycle–related GOBPs, like mitosis, nuclear division, organelle fission, and chromosome segregation, were enriched in the high-CENPF group. This may be reflective of the known function of CENPF as a core member of the centromere–kinetochore complex. Development-related (cell development, muscle system processes, muscle structure development), motility-related (regulation of cell migration, locomotion, and motility), and response to stimuli–related GOBPs (response to wounding and chemical stimuli) were enriched in the low-CENPF group (Figure 3C). In addition to this, we searched for hub genes among the identified DEGs that could be key regulators of the CENPF downstream transcriptional network (see Section 2 for details).

When searching for both up- and downregulated genes among the DEGs, MYC, CCDC8 (coiled-coil domain-containing protein 8), BRCA1, CDK1 (cyclin-dependent kinase 1), and PLK1 (Polo-like kinase 1) were found to be the top five genes that act as key regulator candidates in the CENPF network (Figure 3D). When performing the same analysis with only upregulated genes, these five genes were selected with significant consistence (Figure 3E). When searching for only downregulated genes, SMAD3 (SMAD family member 3), GSK3B (glycogen synthase kinase 3 beta), CAV1 (caveolin 1), SMAD4 (SMAD family member 4), and PRKCA (protein kinase C alpha) were identified as the top five regulator candidates (Figure 3F).

3.4. CENPF and Lipid Regulation

Lipid-related GOBPs, including positive regulation of lipid biosynthetic process, regulation of lipid metabolic process, phospholipid scrambling, lipid modification, lipid metabolic process, cellular lipid metabolic process, lipid biosynthetic process, cellular response to lipid, and response to lipid, were highly enriched by the downregulated genes in high-CENPF samples (**Figure 4**A). To identify genes that both regulate lipid-related functions and are CENPF-dependent, we performed hub gene analysis on

© 2019 WILEY-VCH Verlag GmbH & Co. KGaA, Weinheim

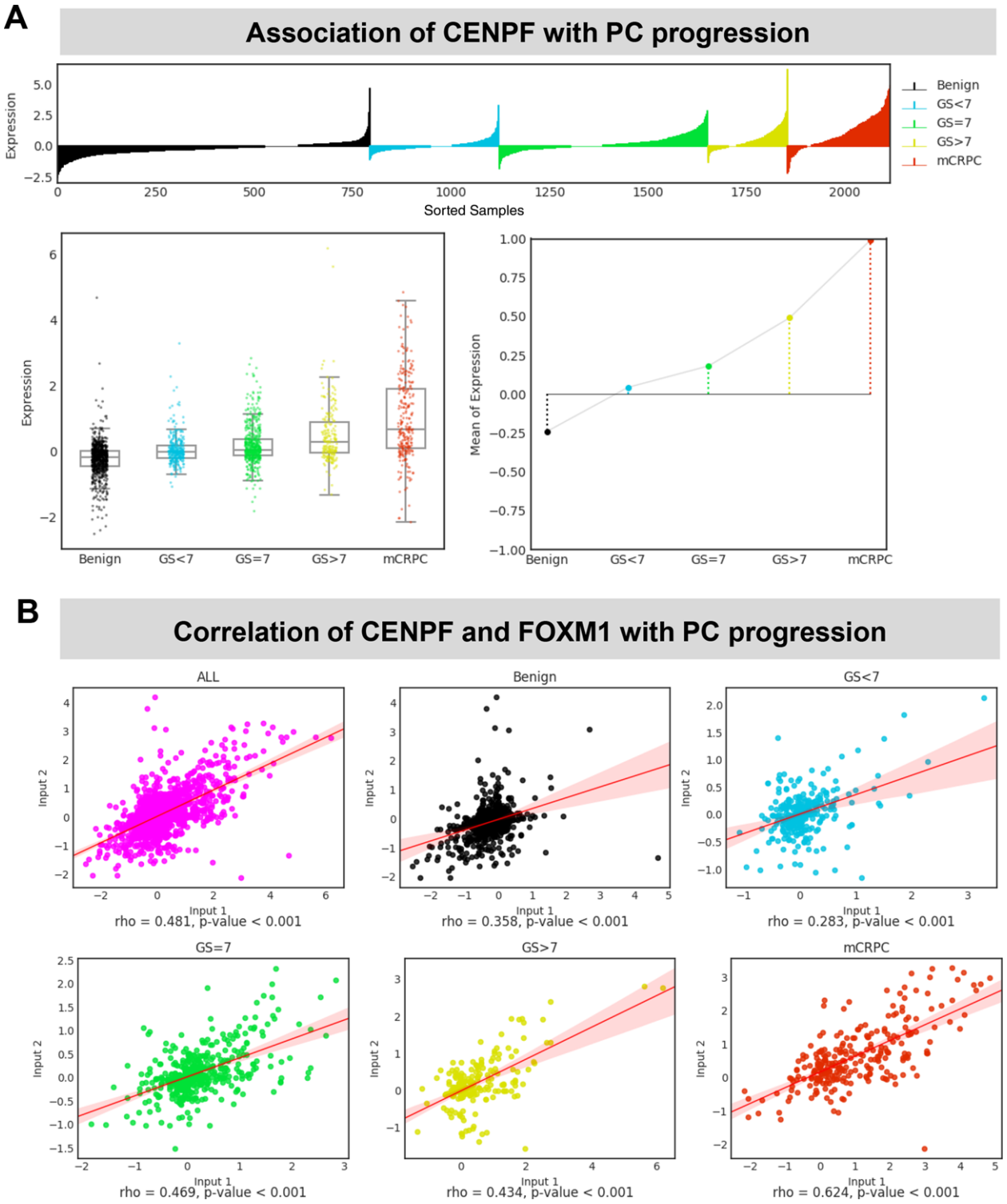

Figure 2. Gene expression of CENPF in PC progression. A) Lollipop plot (upper panel), box plot (lower left), and line plot (lower right) display CENPF gene expression patterns across disease progression from the PCTA data. Lollipop plot shows CENPF expression levels of individual samples. For each disease state, samples were sorted by CENPF expression. Whiskers on the box plot indicate interquartile range (IQR) and 1.5 times the IQR. Individual dots on the box plot represent individual samples. The line plot shows the average expression level of CENPF for each disease state. Dotted lines on the plot indicate the trend of gene expression between disease states. B) Scatter plot and regression lines were drawn to illustrate correlation between CENPF and FOXM1 in all the PCTA samples and each disease state. Input 1 and 2 represnt CENPF and FOXM1, respectively.

© 2019 WILEY-VCH Verlag GmbH & Co. KGaA, Weinheim

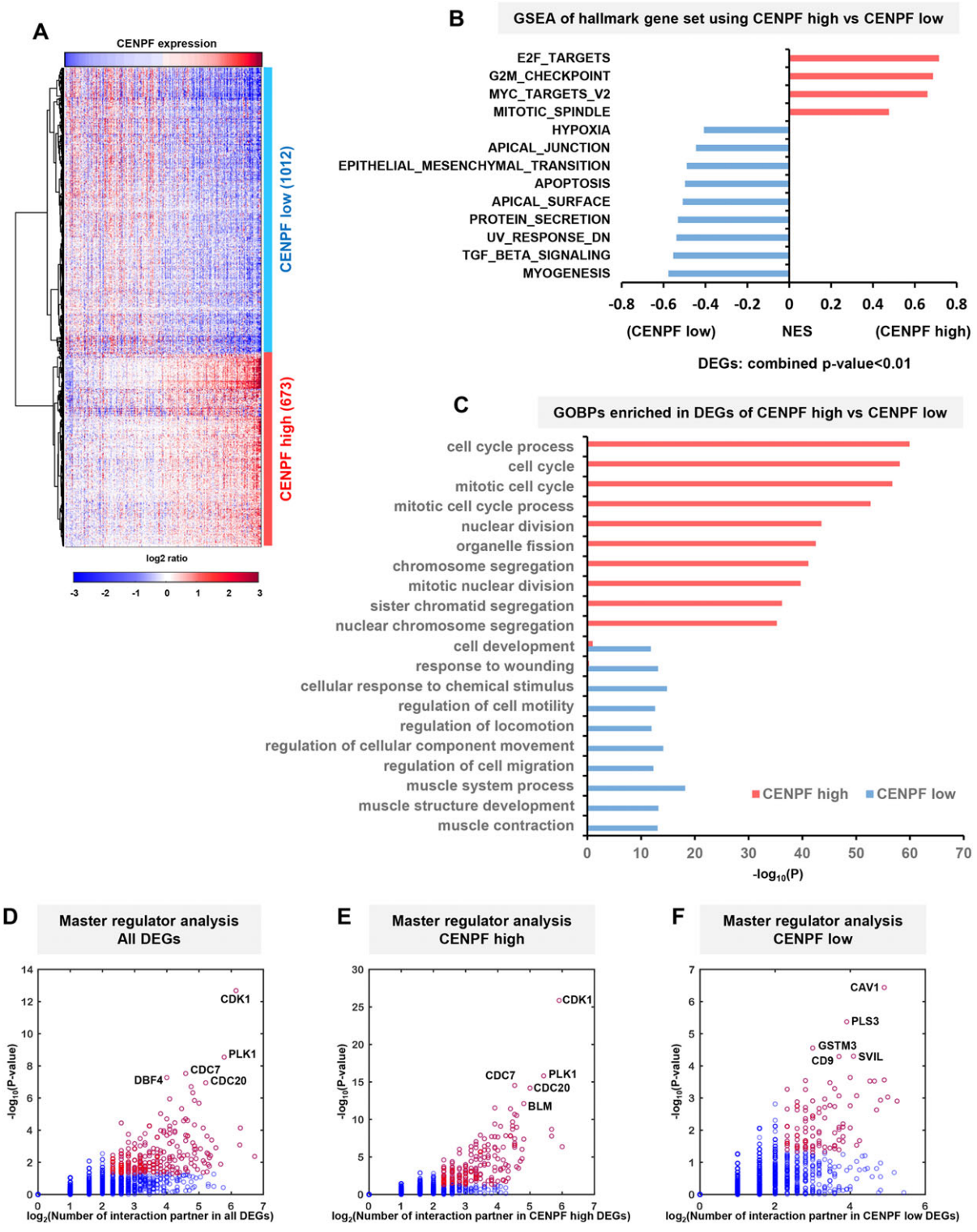

Figure 3. Identification of genes in the CENPF network. A) Heatmap depicts differential expression patterns of the genes between samples with high and low CENPF expression. Red and blue indicate up- and downregulated genes, respectively, in PC samples with high CENPF expression (CENPF high) compared with those with low expression (CENPF low). B) Bar plot displays enrichment scores of hallmark gene sets based on GSEA. All the gene sets on the plot were significantly enriched for in the CENPF-high or low groups with nominal p-value < 0.05. NES; normalized enrichment score. C) Gene Ontology Biological Processes (GOBPs) enriched by DEGs in CENPF-high versus CENPF-low with p-value < 0.05. D–F) Scatter plots illustrate up- and downregulated genes in the CENPF network (D), upregulated gene in the CENPF network (E), and downregulated genes in the CENPF network (F). Hub genes are indicated with red dots. These genes have more than three interactions in the CENPF network and p-values < 0.05.

© 2019 WILEY-VCH Verlag GmbH & Co. KGaA, Weinheim

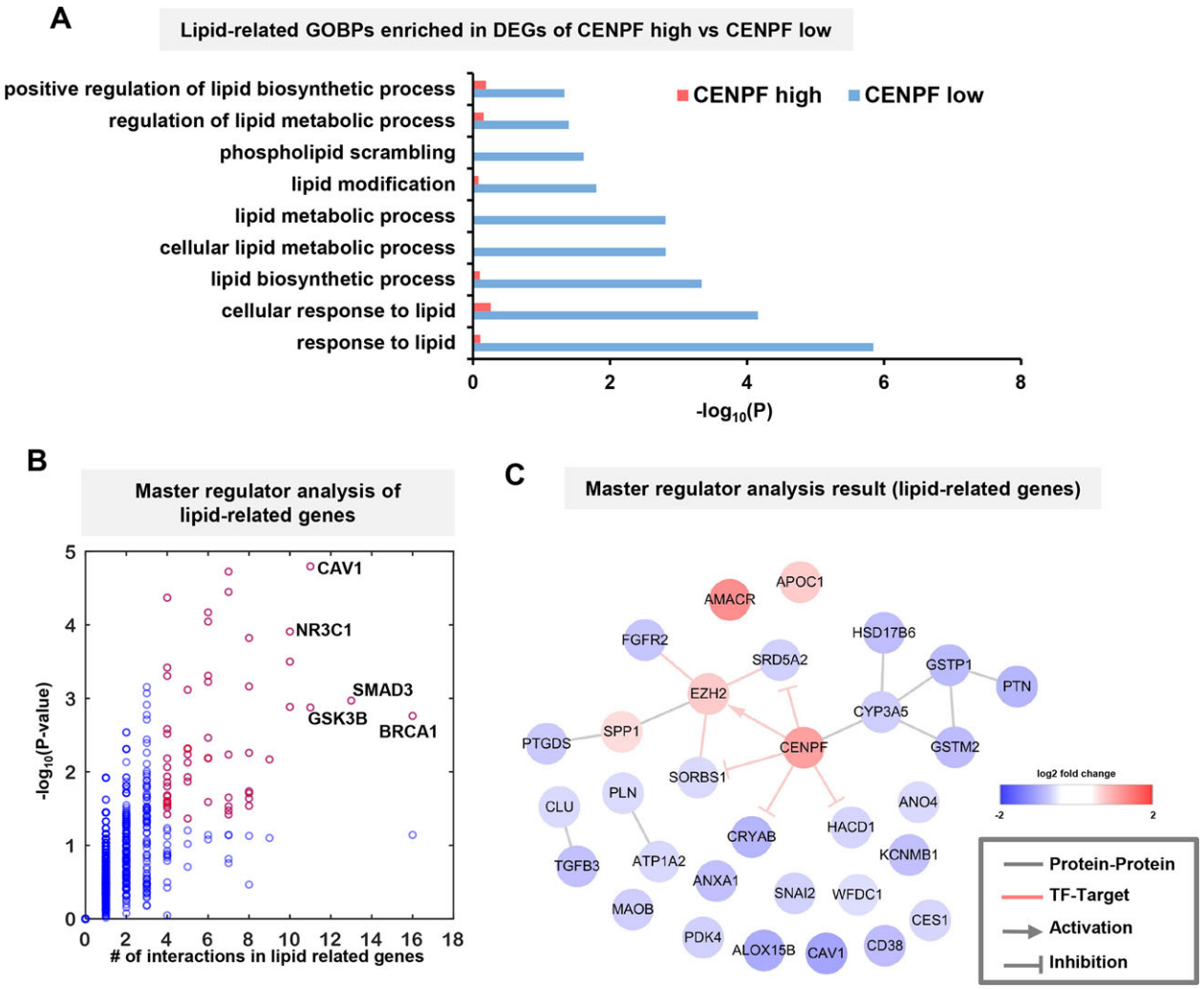

Figure 4. Association of the CENPF network with lipid regulation. A) Bar plot shows enrichment scores of the GOBPs associated with lipid metabolism and pathways in the DEGs of CENPF-high versus CENPF-low. B) Scatter plot illustrates the number of interactions among the lipid metabolism and pathway-associated genes in the CENPF network. Genes represented by red dots indicate hub genes with p-values < 0.05. C) A network model describing interactions among the lipid-associated genes in the CENPF network. Node color represents up- and downregulation in CENPF-high versus low PCs. Edges represent interactions.

those listed to be involved in lipid-related GOBPs in Figure 4A, which resulted in BRCA1, SMAD3, CAV1, GSK3B, and NR3C1 (nuclear receptor subfamily 3 group C member 1) ($p < 0.05$) (Figure 4B). We then reconstructed a network model describing the interactions between the presence of CENPF and lipid-related genes (Figure 4C).

3.5. CENPF^{KO} Cells Show Perturbed Cellular Metabolism and Metabolic Pathways

To elucidate on the metabolite enrichment analysis between control PC3 and CENPF^{KO} cells, the annotated DEPs were further explored for their corresponding biological meaning by gene ontology annotations retrieved from the Gene Ontology Consortium and mapped against their KEGG biological pathway information. A total of 524 metabolites were profiled and quantified from the GC-MS-based metabolomics experiment. The intensities of the 524 metabolites were normalized based on the peak sums, also called metabolite total ion chromatogram (mTIC). The normalized data was then sequentially $\log_2$ and z-score transformed before PCA, which revealed a difference in overall metabolite expression profiles between the control and CENPF^{KO} cells (**Figure 5**A). Further statistical significance analysis between the two cell lines identified a total of 92 DEMs. Of these 92 DEMs, 68 were upregulated and 24 were downregulated in CENPF^{KO} cells, compared to controls. These metabolites were determined based on a fold-change ≥1.5 and a FDR-adjusted p-value (q-value) ≤ 0.05 (Figure 5B). Among the 92 DEMs, 23 upregulated and 12 downregulated metabolites in CENPF^{KO} cells were annotated with a KEGG compound identifier (Figure 5C). The expression profiles of the 92 DEMs were illustrated in a heatmap (Figure 5D).

The annotated metabolites were labeled with the corresponding compound names. Functional enrichment analysis

© 2019 WILEY-VCH Verlag GmbH & Co. KGaA, Weinheim

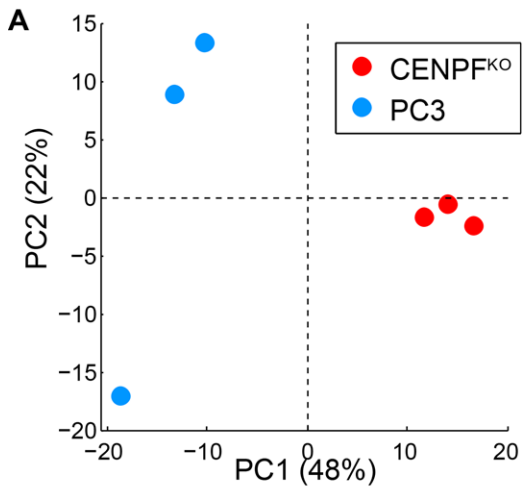

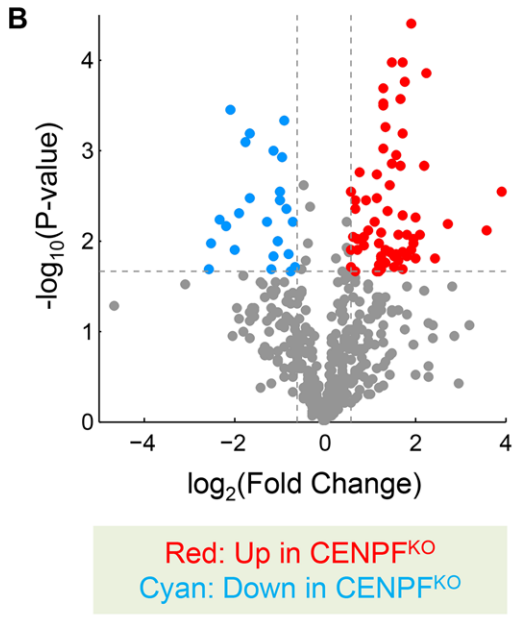

C

No. of metabolites	Up in CENPF^{KO}	Down in CENPF^{KO}
DEM	68	24
Annotated DEM with KEGG compound annotation	23	12

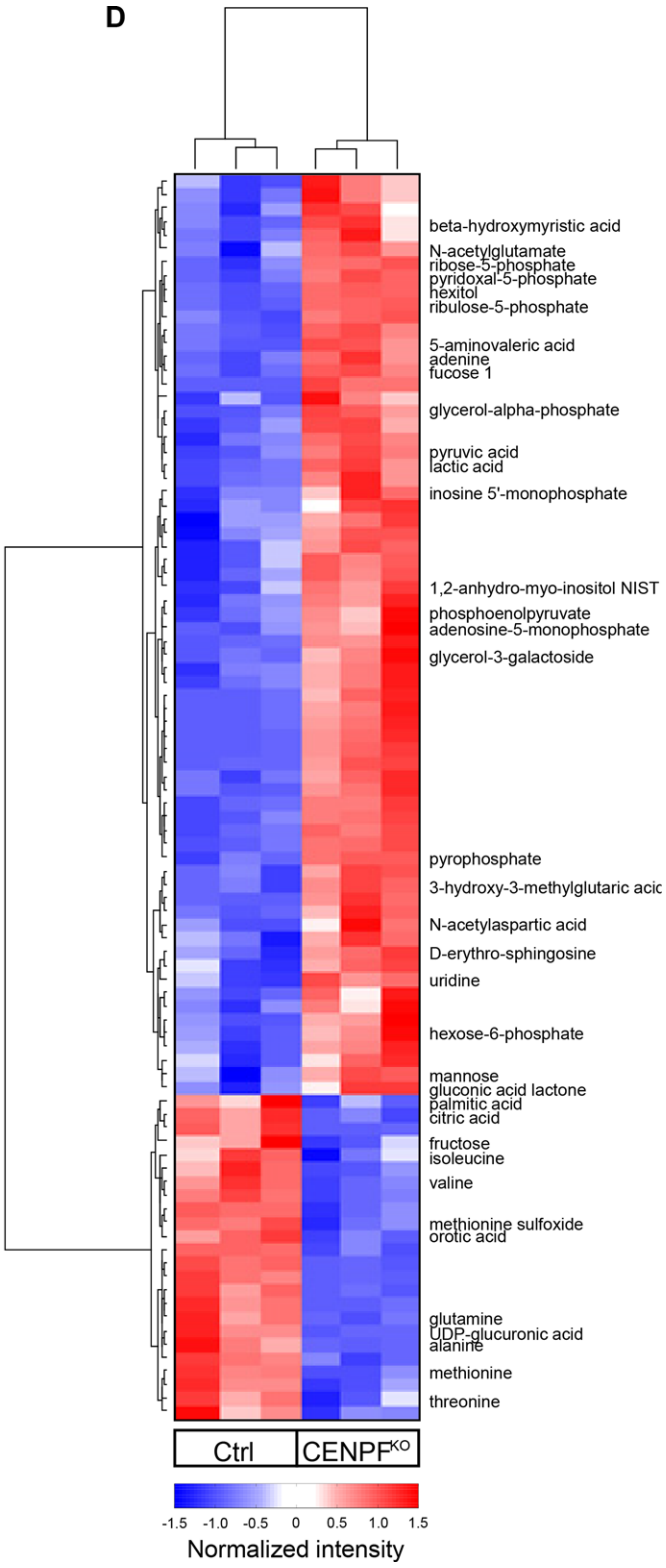

Figure 5. Metabolomic profiling of CENPF^{KO} PC3 cells. A) Principal component analysis (PCA) plot based on the 524 metabolites profiled as different between CENPF^{KO} and control PC3 cells. B) Volcano plot displaying the statistical significance ($\log_{10}$-based p-value) and magnitude of the changes ($\log_2$-based fold-change) of the metabolites. Red and cyan indicate statistically significant up- and downregulation in CENPF^{KO} cells, respectively (fold-change ≥ 1.5 and FDR-adjusted p-value (q-value) ≤ 0.05). C) The number of DEMs identified from the statistical analyses is summarized. D) The heatmap shows the expression profiles of the 92 DEMs. The 37 annotated DEMs with compound names were marked with the corresponding identifications.

© 2019 WILEY-VCH Verlag GmbH & Co. KGaA, Weinheim

Table 1. Pathways significantly enriched for by the DEMs.

	KEGG pathway	Count	*p*-Value	FDR	Metabolites
Up	Carbon fixation in photosynthetic organisms	4	0.0099	0.3510	Ribulose-5-phosphate, ribose-5-phosphate, pyruvic acid, phosphoenolpyruvate
	Vitamin B6 metabolism	3	0.0108	0.3510	Ribulose-5-phosphate, pyruvic acid, pyridoxal-5-phosphate
	Pyruvate metabolism	2	0.0218	0.3770	Pyruvic acid, phosphoenolpyruvate
	Pentose phosphate pathway	4	0.0290	0.3770	Ribulose-5-phosphate, ribose-5-phospahte, pyruvic acid, gluconic acid lactone
	Phosphotransferase system (PTS)	4	0.0290	0.3770	Pyruvic acid, phosphoenolpyruvate, mannose, hexitol
	Purine metabolism	4	0.0436	0.4720	Ribose-5-phosphate, inosine 5′-monophosphate, adenosine-5-monophosphate, adenine
	Zeatin biosynthesis	2	0.0594	0.5450	Adenosine-5-monophosphate, adenine
Down	Amino-tRNA biosynthesis	6	0.0038	0.1570	Valine, threonine, methionine, isoleucine, glutamine, alanine
	Valine, leucine, and isoleucine biosynthesis	3	0.0071	0.1570	Valine, threonine, isoleucine
	Glucosinolate biosynthesis	3	0.0221	0.2930	Valine, threonine, isoleucine
	Valine, leucine, and isoleucine degradation	2	0.0266	0.2930	Valine, isoleucine
	Cysteine and methionine metabolism	3	0.0470	0.4140	Methionine sulfoxide, methionine, alanine
	ABC transporter	5	0.0642	0.4710	Valine, threonine, isoleucine, glutamine, alanine

of the annotated DEMs based on KEGG pathways identified various dysregulated metabolic pathways in CENPF^{KO} cells (**Table 1**). Upregulated metabolites were enriched for pathways related to carbon fixation, vitamin B6 metabolism, pyruvate metabolism, pentose phosphate pathway, phosphotransferase, purine metabolism, and zeatin biosynthesis. Downregulated metabolites were primarily enriched for pathways related to amino acid biosynthesis and metabolism (Table 1).

3.6. CENPF-Stimulated PC Proliferation

To determine whether CENPF is also required for regular cell growth, our cell proliferation assay compared growth between CENPF^{KO} and control cells. The proliferation rate of CENPF^{KO} cells was significantly reduced after 48 h (**Figure 6**A). We speculated that CENPF is required for regulating acetate metabolism. As expected, our results showed that acetate levels in CENPF^{KO} cells were almost completely reduced (Figure 6B). Several studies have demonstrated that significant alterations are found in the utilization of BCAAs in cancers.[50] We then checked BCAA/AAA ratio from metabolomics data. In contrast to the control, BCAA/AAA ratio was significantly decreased (Figure 6C).

4. Discussion

The aim of this study was to determine the role of CENPF in tumor growth and aggression in both clinical PC tissue and human PC3 cells. Although CENPF is named after its association with the centromere–kinetochore protein complex, it has been reported to function in mitosis regulation and cellular proliferation as well.[51–53] Previous studies have also shown that CENPF can potentially predict PC clinical outcome and progression.[49] We decided to investigate if CENPF expression could stratify risk in PC patients, and if there are any resulting perturbed metabolite panels that can be used as a prognostic signature. Our study found that CENPF expression is necessary for cellular growth. Silencing of the gene resulted in significantly delayed proliferation. Furthermore, we found that increased CENPF expression may be correlated with PC aggressiveness. PC tissue with higher clinical grades showed increased expression of CENPF, which further validates the potential use of CENPF as a prognostic marker of PC progression.

Our current study also focused on the relationship of CENPF to other genes as well. Prior studies have suggested that CENPF and FOXM1 may have a synergistic interaction that drives PC malignancy and aggressiveness.[26],[54] In addition, our previous study found that ALDH2 may be negatively correlated to CENPF.[[25]] In order to validate these relationships in the context of predicting PC aggressiveness, we tested these genes in clinically graded PC samples. We found that PC samples with prediction analysis of microarray 50 (PAM50) scores >7 had higher CENPF expression and, consequently, increased FOXM1 and reduced ALDH2 levels (Figure S1, Supporting Information). This confirmed our initial speculation on the relationship of CENPF to these other genes.

To further examine the association of CENPF with various PC types, we tested for the expression of CENPF in PC tissue classified with our PCS signatures. Our prior analysis of subtype-specific gene expression patterns found that PCS1 and PCS2 tumors reflect luminal subtypes, while PCS3 tumors are basal.[30] We found that PCS1 and PCS2 tissues had significantly higher expression of CENPF, which suggests that CENPF is elevated in luminal subtypes (Figure S2, Supporting Information). Additionally, this could mean that testing for both CENPF expression and our PCS signature could potentially identity which PC tissues are luminal. Considering how luminal subtypes are transformation-competent and, thereby, more progressive and aggressive, it would be clinically helpful to be able to accurately identify tissue subtypes.

In this study, we found that CENPF and its network may be controlling PC aggression and progression by altering cellular metabolism. BCAA metabolism is one such pathway that is regulated by CENPF, and there have been several conflicting studies regarding the relationship between BCAA metabolism and cancer progression. Loss of BCAA catabolism has been shown to lead to BCAA accumulation and activation of mTORC1 in liver and ovarian cancers [55–57]. However, contrastingly, loss

© 2019 WILEY-VCH Verlag GmbH & Co. KGaA, Weinheim

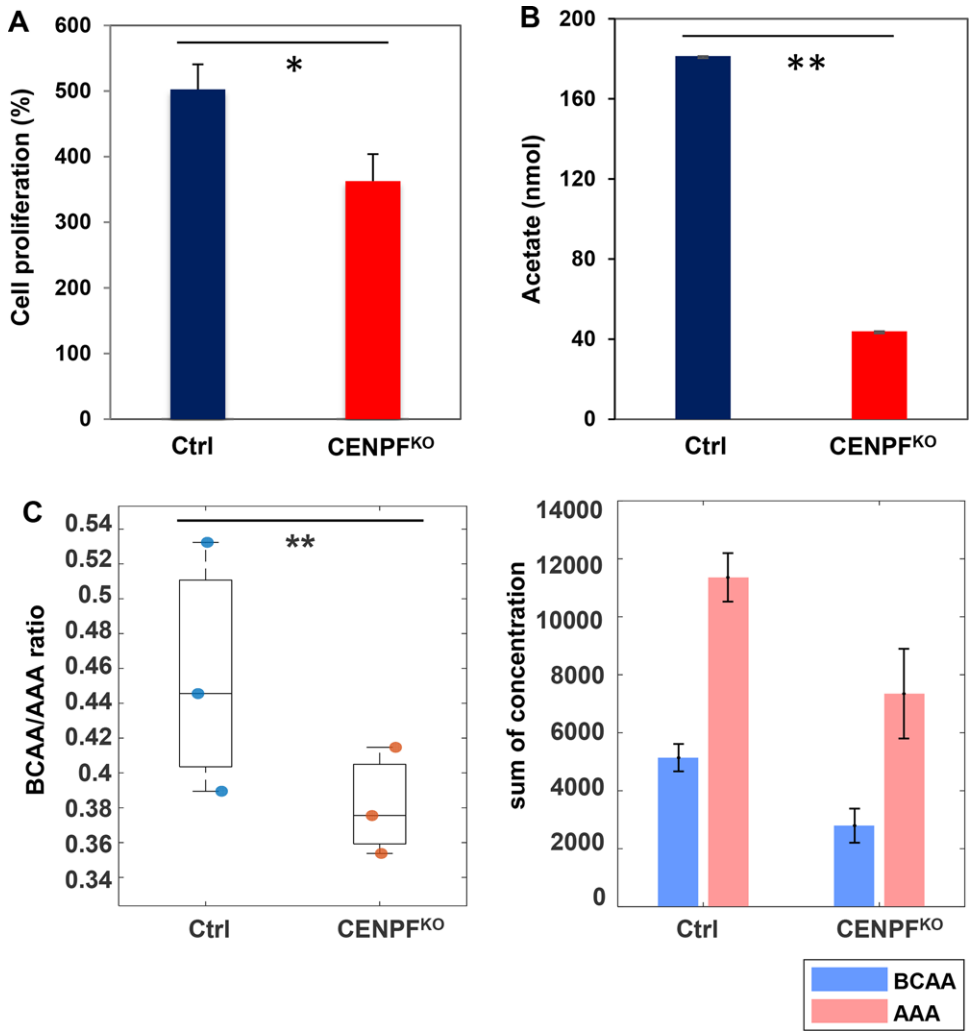

Figure 6. Perturbed metabolisms due to CENPF silencing. A) Cell growth analysis using trypan blue staining. Cell proliferation was suppressed in CENPF^{KO} cells compared to controls at 48 h. *$p < 0.05$ (two-sided Student's *t*-test). B) CENPF^{KO} cells showed decreased synthesis of acetate compared to control. C) Box plot showing BCAA/AAA ratio in Ctrl and CENPF^{KO} cells. CENPF^{KO} cells showed inhibited BCAA content compared to Ctrl. *$p < 0.05$ and **$p < 0.01$ (two-sided Student's *t*-test). Error bars represent standard deviation ($n = 3$).

of BCAA catabolism was found to limit proliferation in glioblastoma, NSCLC, and breast cancer [58–60]. As described recently by White et al.[61], BCAAs are also currently used as biomarker for disease pathogenesis. They have been shown to significantly involve in the development of different diseases, such as type 2 diabetes (T2D) and cardiovascular problems. Our own study found that elevated CENPF expression enhances BCAA catabolism, which leads to increased PC cell proliferation and tumor formation. Furthermore, we found that low-grade PC has limited BCAA catabolism, and this accumulation of BCAAs had no effect on mTORC1. The observed changes in CENPF-dependent acetate concentration also support the regulation of BCAA catabolism. Acetate is one of the major short-chain fatty acids and is a key substrate for cancer bioenergetics [62]. Fatty acid synthesis requires acetate and acyl-CoA synthetase short-chain family member 2 (ACSS2) [63]. Given acetate derived from glucose metabolism rewiring is elevated in cancer cells [64], it has now become apparent that acetate metabolism regulates many different types of cancer through its role in energy or lipid production. Additionally, acetate can also affect certain cancers through regulation of histone acetylation [65].

These findings provide a basis for further studies. Despite this exciting discovery, the main limitation of our study was the lack of a large prospective patient cohort to test on. Additionally, the functional mechanisms behind CENPF that are responsible for these effects in PC patients remain elusive. However, given our previous observations[25,29] and current human PC data bioinformatic analyses, future studies could be expanded to investigate the molecular mechanisms associated with CENPF and assess whether CENPF silencing can be a clinical biomarker for diagnosing PC or predicting aggressiveness.

The data obtained in this study will be accessible at the NIH Common Fund's Data Repository and Coordinating Center (supported by NIH grant, U01-DK097430) website, the Metabolomics Workbench, http://www.metabolomicsworkbench.org.

© 2019 WILEY-VCH Verlag GmbH & Co. KGaA, Weinheim

Supporting Information

Supporting Information is available from the Wiley Online Library or from the author.

Acknowledgements

M.S. and M.K. contributed equally to this work. J.K. designed the study, led the obtainment of funding, overviewed the analysis of literature, and oversaw drafting of the manuscript. M.S., A.Y., and M.L. were involved in performing metabolomics analysis and data interpretation. M.K. and M.L. performed computational analyses of metabolomics data. M.S. and A.Y. performed biochemical and functional experiments in the cell culture system. J.K. and H.L.K. carried out the analysis of references and drafted the manuscript. All authors read and approved the final manuscript. The authors thank their long-term collaborator, Dr. Oliver Fiehn, for providing guidance on this project, and the members of his lab for discussions. This work was supported by the National Institutes of Health grants (1U01DK103260, 1R01DK100974, NIH NCATS UCLA CTSI UL1TR000124), Department of Defense grants (W81XWH-15-1-0415), Centers for Disease Controls and Prevention (1U01DP006079), and the U.S.–Egypt Science and Technology Joint Fund (to J.K.). The funders had no role in the design, data collection and analysis, decision to publish, or preparation of the manuscript. In addition, this article is derived from the Subject Data funded in whole or part by National Academies of Sciences, Engineering, and Medicine (NAS) and The United States Agency for International Development (USAID). Any opinions, findings, conclusions, or recommendations expressed in this article are those of the authors alone and do not necessarily reflect the views of USAID or NAS.

Conflict of Interest

The authors declare no conflict of interest.

Keywords

CENPF, metabolomics, prostate cancer

Received: January 21, 2019
Revised: March 22, 2019
Published online: May 8, 2019

[1] a) R. L. Siegel, K. D. Miller, A. Jemal, *Ca-Cancer J. Clin.* **2016**, *66*, 7; b) F. Bray, J. Ferlay, I. Soerjomataram, R. L. Siegel, L. A. Torre, A. Jemal, *Ca-Cancer J. Clin.* **2018**, *68*, 394.
[2] M. G. Vander Heiden, *Drug Discovery* **2011**, *10*, 671.
[3] P. P. Hsu, D. M. Sabatini, *Cell* **2008**, *134*, 703.
[4] C. V. Dang, *Cancer Res.* **2010**, *70*, 859.
[5] B. J. Altman, Z. E. Stine, C. V. Dang, *Cancer* **2016**, *16*, 773.
[6] a) A. Baron, T. Migita, D. Tang, M. Loda, J Cell Biochem **2004**, *91*, 47; b) N. Zaidi, L. Lupien, N. B. Kuemmerle, W. B. Kinlaw, J. V. Swinnen, K. Smans, *Prog. Lipid Res.* **2013**, *52*, 585.
[7] P. S. Ward, C. B. Thompson, *Cancer Cell* **2012**, *21*, 297.
[8] a) F. Cutruzzola, G. Giardina, M. Marani, A. Macone, A. Paiardini, S. Rinaldo, A. Paone, *Front. Physiol.* **2017**, *8*, 97; b) D. Hanahan, R. A. Weinberg, *Cell* **2011**, *144*, 646.
[9] a) A. W. Hsing, L. C. Sakoda, S. Chua, Jr., *Am. J. Clin. Nutr.* **2007**, *86*, s843; b) J. E. McDunn, Z. Li, K. P. Adam, B. P. Neri, R. L. Wolfert, M. V. Milburn, Y. Lotan, T. M. Wheeler, *Prostate* **2013**, *73*, 1547.
[10] D. A. McGrowder, L. A. Jackson, T. V. Crawford, *Asian Pac. J. Cancer Prev.* **2012**, *13*, 1.
[11] M. G. Vander Heiden, L. C. Cantley, C. B. Thompson, *Science* **2009**, *324*, 1029.
[12] O. A. Aboud, R. H. Weiss, *Clin. Chem.* **2013**, *59*, 138.
[13] J. L. Spratlin, N. J. Serkova, S. G. Eckhardt, *Clin. Cancer Res.* **2009**, *15*, 431.
[14] N. J. Serkova, K. Glunde, *Methods Mol. Biol.* **2009**, *520*, 273.
[15] a) L. L. Cheng, M. A. Burns, J. L. Taylor, W. He, E. F. Halpern, W. S. McDougal, C. L. Wu, *Cancer Res.* **2005**, *65*, 3030; b) A. Sreekumar, L. M. Poisson, T. M. Rajendiran, A. P. Khan, Q. Cao, J. Yu, B. Laxman, R. Mehra, R. J. Lonigro, Y. Li, M. K. Nyati, A. Ahsan, S. Kalyana-Sundaram, B. Han, X. Cao, J. Byun, G. S. Omenn, D. Ghosh, S. Pennathur, D. C. Alexander, A. Berger, J. R. Shuster, J. T. Wei, S. Varambally, C. Beecher, A. M. Chinnaiyan, *Nature* **2009**, *457*, 910.
[16] E. Holmes, R. L. Loo, J. Stamler, M. Bictash, I. K. Yap, Q. Chan, T. Ebbels, M. De Iorio, I. J. Brown, K. A. Veselkov, M. L. Daviglus, H. Kesteloot, H. Ueshima, L. Zhao, J. K. Nicholson, P. Elliott, *Nature* **2008**, *453*, 396.
[17] G. J. Patti, O. Yanes, G. Siuzdak, *Mol. Cell Biol.* **2012**, *13*, 263.
[18] B. J. Trock, *Urol. Oncol.* **2011**, *29*, 572.
[19] R. S. Kelly, M. G. Vander Heiden, E. Giovannucci, L. A. Mucci, *Cancer Epidemiol. Biomarkers Prev.* **2016**, *25*, 887.
[20] P. Li, S. You, C. Nguyen, Y. Wang, J. Kim, D. Sirohi, A. Ziembiec, D. Luthringer, S. C. Lin, T. Daskivich, J. Wu, M. R. Freeman, R. Saouaf, D. Li, H. L. Kim, *Theranostics* **2018**, *8*, 1752.
[21] A. Aytes, A. Mitrofanova, C. Lefebvre, M. J. Alvarez, M. Castillo-Martin, T. Zheng, J. A. Eastham, A. Gopalan, K. J. Pienta, M. M. Shen, A. Califano, C. Abate-Shen, *Cancer Cell* **2014**, *25*, 638.
[22] S. C. Lin, C. Y. Kao, H. J. Lee, C. J. Creighton, M. M. Ittmann, S. J. Tsai, S. Y. Tsai, M. J. Tsai, *Nat. Commun.* **2016**, *7*, 11418.
[23] T. Hitosugi, S. Kang, M. G. Vander Heiden, T. W. Chung, S. Elf, K. Lythgoe, S. Dong, S. Lonial, X. Wang, G. Z. Chen, J. Xie, T. L. Gu, R. D. Polakiewicz, J. L. Roesel, T. J. Boggon, F. R. Khuri, D. G. Gilliland, L. C. Cantley, J. Kaufman, J. Chen, *Sci. Signaling* **2009**, *2*, ra73.
[24] M. Shahid, M. Lee, H. Piplani, A. M. Andres, B. Zhou, A. Yeon, M. Kim, H. L. Kim, J. Kim, Cell Cycle **2018**, *24*, 2802.
[25] S. You, B. S. Knudsen, N. Erho, M. Alshalalfa, M. Takhar, H. Al-Deen Ashab, E. Davicioni, R. J. Karnes, E. A. Klein, R. B. Den, A. E. Ross, E. M. Schaeffer, I. P. Garraway, J. Kim, M. R. Freeman, *Cancer Res.* **2016**, *76*, 4948.
[26] R. Edgar, M. Domrachev, A. E. Lash, Nucleic Acids Res **2002**, *30*, 207.
[27] M. D. Robinson, D. J. McCarthy, G. K. Smyth, *Bioinformatics* **2010**, *26*, 139.
[28] J. Shin, M. Kim, H. J. Jung, H. L. Cha, H. Suh-Kim, S. Ahn, J. Jung, Y. Kim, Y. Jun, S. Lee, D. Hwang, J. Kim, *Sci. Rep.* **2017**, *7*, 2826.
[29] D. Hwang, A. G. Rust, S. Ramsey, J. J. Smith, D. M. Leslie, A. D. Weston, P. de Atauri, J. D. Aitchison, L. Hood, A. F. Siegel, H. Bolouri, *Proc. Natl. Acad. Sci. U. S. A.* **2005**, *102*, 17296.
[30] A. Subramanian, P. Tamayo, V. K. Mootha, S. Mukherjee, B. L. Ebert, M. A. Gillette, A. Paulovich, S. L. Pomeroy, T. R. Golub, E. S. Lander, J. P. Mesirov, *Proc. Natl. Acad. Sci. U. S. A.* **2005**, *102*, 15545.
[31] W. Huang da, B. T. Sherman, R. A. Lempicki, Nat Protoc **2009**, *4*, 44.
[32] C. Stark, B. J. Breitkreutz, T. Reguly, L. Boucher, A. Breitkreutz, M. Tyers, *Nucleic Acids Res.* **2006**, *34*, D535.
[33] L. Salwinski, C. S. Miller, A. J. Smith, F. K. Pettit, J. U. Bowie, D. Eisenberg, *Nucleic Acids Res.* **2004**, *32*, D449.
[34] A. Patil, K. Nakai, H. Nakamura, *Nucleic Acids Res.* **2011**, *39*, D744.
[35] S. Orchard, M. Ammari, B. Aranda, L. Breuza, L. Briganti, F. Broackes-Carter, N. H. Campbell, G. Chavali, C. Chen, N. del-Toro, M. Duesbury, M. Dumousseau, E. Galeota, U. Hinz, M. Iannuccelli, S. Jagannathan, R. Jimenez, J. Khadake, A. Lagreid, L. Licata, R. C. Lovering, B. Meldal, A. N. Melidoni, M. Milagros, D. Peluso, L. Perfetto, P. Porras, A. Raghunath, S. Ricard-Blum, B. Roechert, et al., *Nucleic Acids Res.* **2014**, *42*, D358.

© 2019 WILEY-VCH Verlag GmbH & Co. KGaA, Weinheim

[36] D. Szklarczyk, A. Franceschini, S. Wyder, K. Forslund, D. Heller, J. Huerta-Cepas, M. Simonovic, A. Roth, A. Santos, K. P. Tsafou, M. Kuhn, P. Bork, L. J. Jensen, C. von Mering, *Nucleic Acids Res.* **2015**, *43*, D447.
[37] P. Shannon, A. Markiel, O. Ozier, N. S. Baliga, J. T. Wang, D. Ramage, N. Amin, B. Schwikowski, T. Ideker, *Genome Res.* **2003**, *13*, 2498.
[38] a) T. Kind, V. Tolstikov, O. Fiehn, R. H. Weiss, *Anal. Biochem.* **2007**, *363*, 185; b) T. Kind, G. Wohlgemuth, D. Y. Lee, Y. Lu, M. Palazoglu, S. Shahbaz, O. Fiehn, *Anal. Chem.* **2009**, *81*, 10038.
[39] M. Y. Lee, A. Yeon, M. Shahid, E. Cho, V. Sairam, R. Figlin, K. H. Kim, J. Kim, *Oncotarget* **2018**, *9*, 13231.
[40] J. D. Storey, *J. R. Stat. Soc.* **2002**, *64*, 479.
[41] J. Lopez-Ibanez, F. Pazos, M. Chagoyen, *Nucleic Acids Res.* **2016**, *44*, W201.
[42] J. E. Fischer, J. M. Funovics, A. Aguirre, J. H. James, J. M. Keane, R. I. Wesdorp, N. Yoshimura, T. Westman, *Surgery* **1975**, *78*, 276.
[43] Y. J. Zhuo, M. Xi, Y. P. Wan, W. Hua, Y. L. Liu, S. Wan, Y. L. Zhou, H. W. Luo, S. L. Wu, W. D. Zhong, C. L. Wu, *Int. J. Mol. Med.* **2015**, *35*, 966.
[44] V. E. Baracos, M. L. Mackenzie, *J. Nutr.* **2006**, *136*, 237S.
[45] a) P. Bomont, P. Maddox, J. V. Shah, A. B. Desai, D. W. Cleveland, *EMBO J.* **2005**, *24*, 3927; b) J. Feng, H. Huang, T. J. Yen, *Chromosoma* **2006**, *115*, 320; c) S. V. Holt, M. A. Vergnolle, D. Hussein, M. J. Wozniak, V. J. Allan, S. S. Taylor, *J. Cell Sci.* **2005**, *118*, 4889.
[46] I. Lokody, *Cancer* **2014**, *14*, 450.
[47] a) E. A. Ananieva, A. C. Wilkinson, *Curr. Opin. Clin. Nutr. Metab. Care* **2018**, *21*, 64; b) R. E. Ericksen, S. L. Lim, E. McDonnell, W. H. Shuen, M. Vadiveloo, P. J. White, Z. Ding, R. Kwok, P. Lee, G. K. Radda, H. C. Toh, M. D. Hirschey, W. Han, *Cell Metab.* **2019**; c) Z. Q. Wang, A. Faddaoui, M. Bachvarova, M. Plante, J. Gregoire, M. C. Renaud, A. Sebastianelli, C. Guillemette, S. Gobeil, E. Macdonald, B. Vanderhyden, D. Bachvarov, *Oncotarget* **2015**, *6*, 31522.
[48] a) M. Tonjes, S. Barbus, Y. J. Park, W. Wang, M. Schlotter, A. M. Lindroth, S. V. Pleier, A. H. C. Bai, D. Karra, R. M. Piro, J. Felsberg, A. Addington, D. Lemke, I. Weibrecht, V. Hovestadt, C. G. Rolli, B. Campos, S. Turcan, D. Sturm, H. Witt, T. A. Chan, C. Herold-Mende, R. Kemkemer, R. Konig, K. Schmidt, W. E. Hull, S. M. Pfister, M. Jugold, S. M. Hutson, C. Plass, et al., **2013**, *19*, 901; b) J. R. Mayers, M. E. Torrence, L. V. Danai, T. Papagiannakopoulos, S. M. Davidson, M. R. Bauer, A. N. Lau, B. W. Ji, P. D. Dixit, A. M. Hosios, A. Muir, C. R. Chin, E. Freinkman, T. Jacks, B. M. Wolpin, D. Vitkup, M. G. Vander Heiden, *Science* **2016**, *353*, 1161; c) L. Zhang, J. Han, *Biochem. Biophys. Res. Commun.* **2017**, *486*, 224.
[49] P. J. White, C. B. Newgard, *Science* **2019**, *363*, 582.
[50] T. Mashimo, K. Pichumani, V. Vemireddy, K. J. Hatanpaa, D. K. Singh, S. Sirasanagandla, S. Nannepaga, S. G. Piccirillo, Z. Kovacs, C. Foong, Z. Huang, S. Barnett, B. E. Mickey, R. J. DeBerardinis, B. P. Tu, E. A. Maher, R. M. Bachoo, *Cell* **2014**, *159*, 1603.
[51] S. A. Comerford, Z. Huang, X. Du, Y. Wang, L. Cai, A. K. Witkiewicz, H. Walters, M. N. Tantawy, A. Fu, H. C. Manning, J. D. Horton, R. E. Hammer, S. L. McKnight, B. P. Tu, *Cell* **2014**, *159*, 1591.
[52] H. Wen, S. Lee, W. G. Zhu, O. J. Lee, S. J. Yun, J. Kim, S. Park, *Biochim. Biophys. Acta Mol. Cell Biol. Lipids* **2019**, *1864*, 413.
[53] Z. T. Schug, J. Vande Voorde, E. Gottlieb, *Cancer* **2016**, *16*, 708.

© 2019 WILEY-VCH Verlag GmbH & Co. KGaA, Weinheim

Author Manuscript

Author Manuscript

Author Manuscript

Author Manuscript

HHS Public Access

Author manuscript

Divers Equal Health Care. Author manuscript; available in PMC 2019 April 22.

Published in final edited form as:

Divers Equal Health Care. 2019 ; 16(1): 1–8. doi:10.21767/2049-5471.1000185.

Effectiveness of a Tailored Colorectal Cancer Educational Seminar in Enhancing the Awareness, Knowledge, and Behavior of Korean Americans Living in the Los Angeles Koreatown Area

Sungjin Kim[1], **Austin Yeon**[2], **Eunho Cho**[2], **Muhammad Shahid**[2], and **Jayoung Kim**[1,2,3,4]

[1]Samuel Oschin Comprehensive Cancer Institute, Cedars-Sinai Medical Center, Los Angeles, CA, USA

[2]Departments of Surgery and Biomedical Sciences, Cedars-Sinai Medical Center, Los Angeles, CA, USA

[3]University of California, Los Angeles, CA, USA

[4]Department of Urology, Ga Cheon University College of Medicine, Incheon, South Korea

Abstract

Background: Improving rates of colorectal cancer (CRC) screening can reduce CRC-related mortality, which is estimated to cause about 50,630 deaths in the U.S. by the end of 2018. There is a noted increasing prevalence of CRC among Korean Americans. Although CRC screening has been widely implemented, Korean Americans over the age of 50 have the lowest rates of proper CRC screening, compared to those of other Asian ethnicities. Barriers, such as language and culture, may be making participation in screening procedures difficult for those with immigrant backgrounds. Thus, this study aimed to determine whether proper CRC education can enhance awareness, knowledge, and behavior in screening among Korean Americans living in the Los Angeles Koreatown area.

Design: This study was conducted among 100 self-identified Korean Americans between the ages of 45–75, who voluntarily participated in this study through local community outreach from January to June 2018. Educational brochures were provided for those in the control group, while those in the intervention group attended an additional short educational seminar. All participants were asked to complete a questionnaire after, and data were collected on site.

Results: We found that intervention had a significant effect on awareness regarding colorectal polyps (OR (odds ratio): 22.47; 95% CI: 6.42–78.62; p-value <0.001) and fecal occult blood tests (FOBTs)/stool blood test (OR, 245.37; 95% CI: 34.55–1742.75; p-value <0.001). Willingness for CRC screening in following 6 months significantly increased (OR: 87.17; 95% CI: 19.01–399.63; p-value <0.001). Knowledge on options for CRC screening (OR: 126.63; 95% CI: 23.61–679.07; p-value <0.001) and stool blood tests (OR: 157.17; 95% CI: 18.02–1370.41; p-value <0.001) were significantly enhanced. In additional univariate analysis, we found that Korean Americans with

ADDRESS OF CORRESPONDENCE: Jayoung Kim, Departments of Surgery and Biomedical Sciences, Cedars-Sinai Medical Center, Davis 5071, 8700 Beverly Blvd., Los Angeles, CA 90048, USA, Tel: +1-310-423-7168; Fax: +1-310-967-3809; Jayoung.Kim@cshs.org.

Author Manuscript Author Manuscript Author Manuscript Author Manuscript

higher level of education, birthplace in US or better general health showed better CRC awareness or knowledge.

Conclusion: There is a significant gap in our knowledge and understanding of the contributing factors that may be leading to low CRC screening rates in Korean Americans. This study suggests that well-tailored educational seminars can overcome certain barriers to screening and improve CRC knowledge and awareness, which is critical to achieving greater screening compliance. Our findings provide important references for designing effective strategies to increasing CRC screening rates among Korean Americans.

Keywords

Colorectal cancer screening; Korean Americans; Koreatown Los Angeles; Educational seminar; Inequality

Introduction

Colorectal cancer (CRC) is the third most common cancer and third leading cause of cancer-related deaths in both men and women in the United States (US) [1]. Changes in risk factors, improvements in treatment, and advancements in early detection have steadily lowered rates of CRC [2]. One of the most important factors that reduced CRC incidence and death is surveillance. A recent study found that, compared to no surveillance, one or two surveillance visits were associated with significantly lower CRC incidence [3]. While there are many options for CRC screening, including fecal occult blood testing, stool DNA analysis, and sigmoidoscopy, the gold standard remains to be colonoscopy [4]. According to statistics provided by the American Cancer Society (ACS), treatment options for CRC have greatly improved recently, resulting in more than 1 million CRC survivors in the US alone. Along with this development, early diagnosis through regular and timely screening can decrease CRC risk; however, there are certain populations that have shown a steady rise in CRC incidence. In particular, Asian communities have not only seen a higher rate of CRC, but an increasing trend as well [5].

Although there are no concrete explanations for this increase of CRC incidence among Asians, studies have shown some attribution to fatalistic attitudes, changes in diet, and education on screening [5–7]. This lapse in vigilant CRC monitoring is particularly evident in the Korean population [8]. CRC is ranked as one of the most common cancers in Korea and places an immense economic burden on patients and society at large [9]. This is not just limited to the Korean population overseas. Rates of colorectal cancer in immigrant patients have been found to be similar to those in their home countries, compared to Caucasians in the same area [10]. Additionally, studies on minority health have shown that the Korean American population has one of the lowest cancer screening rates [11]. Screening for CRC is further hindered by the socioeconomic and cultural barriers Korean Americans face [12]. A prior study found that less than 30% of Korean Americans in Los Angeles County had ever received screening for CRC [13]. Furthermore, a California Health Interview Survey found that, compared to other Asian American groups, Korean Americans had the lowest rates of CRC screening [14]. More than half of Japanese, Chinese, Filipino, and Vietnamese Americans between the ages of 50 to 64 years old received screening for CRC, while only

Author Manuscript Author Manuscript Author Manuscript Author Manuscript

37% of Korean Americans in the same age range have [15]. Therefore, there is an urgent need to solve this increasing discrepancy in the Korean population.

Southern California, particularly Los Angeles (LA) and Orange County (OC), has the highest concentration of Koreans and Korean Americans in the US, making up about 25% of all Koreans residing in America. A majority of Koreans are concentrated around the LA Koreatown area. Koreatown is the most densely populated district, by population, in LA county, with an average of 42,611 people per square mile. There is an increasing burden of CRC in Korean populations. CRC is the most commonly occurring cancer in males particularly [16]. Koreans over the age of 50 had the lowest rate of proper colorectal screening compared to those of other Asian and Asian American ethnicities [17]. In addition, there is a significant knowledge gap in the comprehensive understanding of the contributing factors that affect colorectal screening in Korean Americans. Being that LA is home to such a large number of Koreans, it provides the ideal environment to study and attempt to resolve this troubling issue.

To better understand how to improve current knowledge and awareness of CRC in the Korean American immigrant population, we conducted a survey of general questions regarding CRC on two different Korean audiences in LA Koreatown. This area was ideal because it is one of the most densely populated districts in LA and is home to the largest concentrations of Koreans outside of Korea. This study broadens our knowledge of the contributing factors of low CRC screening in Korean Americans living in LA county. The questionnaire inquired about whether primary healthcare providers recommended CRC screening (lack of awareness), which CRC screening methods were preferred (screening method), and if their health insurance covered the cost of screening (access to care). The findings from this study suggest that implementing cultural and language appropriate seminars significantly increase both knowledge and interest in CRC screening among Korean Americans.

Methods and Materials

Data collection procedures

Eligible participants included men and women between the ages of 45 to 75, who self-identified as of Korean ethnicity, were Korean or English speaking, and were living or had contacts in the LA Koreatown area. Individuals with a prior history of CRC or significant medical problems that affected attendance to the educational seminar or survey were excluded. The sample size for this study was limited to 100 participants, who were all recruited from Korean churches, senior recreation centers, senior community colleges, language schools, college cultural organizations, grocery stores, coffee shops, and nail/hair salons (Cedars-Sinai Medical Center Institutional Review Board Approval number Pro00048053).

Our structured research questionnaire, Korean Community Health Survey: Colorectal Cancer, was administered in either Korean or English. It involved inquiries about demographics, general health concerns and lifestyle factors, such as age, weight, height, and

Author Manuscript Author Manuscript Author Manuscript Author Manuscript

general health level (Table 1). The survey was designed to establish base information for future Korean community-based CRC epidemiologic research.

Those in the control group received an English-language brochure provided by Cedars-Sinai Medical Center. Participants in the intervention group received the brochure and an additional 30-min educational seminar with a slide presentation. American Cancer Society (ACS)-developed CRC educational materials and presentation slides were used after slight modifications and translation by a certified Korean translator. The presentation included information related to colon health and CRC (incidence rate, risk factors, diet and lifestyle recommendations, screening methods, etc.). During the seminar, participants were encouraged to ask their primary physicians about CRC and screening options.

Self-reported paper and pen-based surveys were distributed directly after intervention and confirmation of willingness to participate. Some demographic characteristics, such as sex, age range, marriage status, height, and weight (Q1-Q4) were asked. Participants' birth place, proportion of lifetime in the US, English proficiency, and education level were next questioned (Q5-Q8). Computer skills and usage of social network service were asked as well (Q10-Q11). To determine general information on healthcare utilization, participants gave responses to the three following questions; "How's your overall health?", "Do you frequently access a healthcare newsletter?", and "Where do you find health information from?" (Q9, Q12-Q13). The control group took the survey after only examining the brief brochure, while the intervention group took the survey after examining both the brochure and attending the seminar on CRC prevention, screening, and treatment.

Data analysis

Sociodemographic characteristics included age, sex, marital status, height, weight, birthplace, years lived in the US, English fluency, educational level, computer skill, and use of social networks. Health-related variables included self-perceived health status, family history of CRC, and reasons for reluctance to screen for CRC, if any. Self-reported CRC screening behavior was assessed as: 1) ever having had a fecal occult blood test (FOBT), colonoscopy, or any other test done, and 2) being up-to-date with CRC screening. Knowledge regarding CRC was assessed with 6 questions, which included knowing how many CRC screening tests exist, the age to begin screening, recommended frequency of tests, and awareness of gender differences in CRC risk. CRC awareness was measured by asking whether participants had ever heard of CRC, colon polyps, FOBT, and colonoscopy.

For statistical analysis, data are presented as frequency (percentage, %) for categorical variables and median (IQR, interquartile range) for continuous variables. Univariate associations were examined using Wilcoxon rank-sum tests for continuous variables, and chi-square test or Fisher's exact test for categorical variables, as appropriate. To avoid potential overfitting due to a large number of baseline characteristics and to balance potential confounding factors between the intervention and control groups, propensity score (PS) analysis was performed [18]. The propensity score of being in the intervention group (vs. control group) was estimated using a multivariable logistic regression model after adjusting for Q1 through Q11, Q13, and Q28-Q29 [18–20], and the estimated propensity scores were included as a covariate in the multivariable logistic regression model for each

Author Manuscript Author Manuscript Author Manuscript Author Manuscript

outcome [19]. Analyses were performed using SAS 9.4 (SAS Institute, Inc., Cary, North Carolina) with two-sided tests and a significance level of 0.05.

Results

Participant characteristics

A total of 100 Korean American participants voluntarily participated in this study. Table 1 presents baseline characteristics of the participants in this study. Most of the participants (96%) were over the age of 50. There were more female participants (63%) than males (37%), and most participants were married (74%). Almost all the participants were born in the Korea (98%), and 70% had lived in the US for more than 20 years. Many participants reported not speaking English fluently or well; they self-reported their English-speaking abilities to be at a beginner's level (96%). Only 32% of participants had a high school education or higher. A majority of participants reported that their overall health levels were fair/poor (77%). Most of them find health-related information from television (85%). Nearly all participants were not familiar with social network services (97%) and lacked computer skills (84%).

Comparison of intervention and control groups

Conventional educational materials on CRC and screening methods were provided for the control group (n=50). In addition to these materials, the intervention group received a 30-min health lecture designed for seniors. Both groups were asked to complete a 1-page questionnaire, which was translated by a certified English-Korean translator. Participants were allowed to choose from either an English or Korean version.

Awareness test included four "yes or no" screening questions –

""Q14. Have you heard about colorectal cancer?"

"Q15. Have you heard about colorectal polyp?

"Q16. Have you heard about the fecal occult blood test (FOBT) or stool blood test?", and

"Q19. Have you heard about colonoscopy?" Behavior domain contained five questions -

"Q17. Have your doctor told you that you should be tested for colon cancer (FOBT)?" "Q18. Have you ever had a FOBT?"

"Q20. Have your doctor recommend colonoscopy?" "Q21. Have you ever had a colonoscopy?", and

"Q30. Are you willing to undergo colon cancer testing within 6 months?" Knowledge domain consisted of six questions –

"Q22. I believe that there is only one screening test for colon cancer",

"Q23. There is a stool blood test using a "home" test",

Author Manuscript Author Manuscript Author Manuscript Author Manuscript

"Q24. I believe that people are supposed to start getting tested for colon cancer at age of 50",

"Q25. Once people start having stool blood test, they should have them every 3 years",

"Q26. In general, once people start having colonoscopy exams at age of 50, they should have them every 5 years", and

"Q27. I believe that colon cancer is mainly a problem for men" (Table 2).

Participants in the intervention group had significantly better awareness, behavior, and knowledge on compared to the control group. Both the control and intervention groups had awareness about CRC and colonoscopies; however, participants in the intervention group were significantly more aware on colorectal polyps (90% *vs.* 28%) and FOBT (94% *vs.* 8%) than the control group (Tables 2).

Willingness to undergo CRC screening within 6 months was significantly higher in the intervention group (88% *vs.* 8%). In addition, participant knowledge regarding CRC screening test options were higher in the intervention group. Most participants in the control group (90%) believed that there was only one screening test for CRC. The intervention group recognized other options for CRC screening, and only 8% thought there was only one form of screening. Only 2% of participants in the control group knew that the FOBT/stool blood test could be done at home, compared to 78% of intervention group.

There was no difference in knowledge on the recommended age for CRC screening and how often it should be conducted between the control and intervention groups (Tables 2).

Univariate and multivariable analyses of awareness, behavior, and knowledge

After propensity score (PS), we found that intervention remained a significant effect on awareness of colorectal polyps (OR (odds ratio): 22.47; 95% CI: 6.42–78.62; p-value <0.001) and FOBT or stool blood test (OR: 245.37; 95% CI: 34.55–1742.75; p-value <0.001). In the intervention group, willingness to screen for CRC in the following 6 months was significantly higher than the control group (OR: 87.17; 95% CI: 19.01–399.63; p-value <0.001). Knowledge on additional screening options (OR: 126.63; 95% CI: 23.61–679.07; p-value <0.001) and stool blood test (OR: 157.17; 95% CI: 18.02–1370.41; p-value <0.001) was also significantly enhanced (Table 3).

Further univariate analyses showed that, participants who reported overall health as "very good/good" were more likely to have heard about colorectal polyps than those who reported overall health as "fair/poor" (p-value=0.009, data not shown). Participants born in the US were more likely to have ever had a FOBT compared to those born in Korea (p-value=0.040, data not shown). Participants with higher education levels were more likely to answer yes regarding the possibility of using stool blood tests at home (p-value=0.006, data not shown). Overall health status was associated with increased knowledge regarding CRC and CRC screening (Q24. I believe that people are supposed to start getting tested for colon cancer at age of 50, p-value= 0.020; Q26. In general, once people start having colonoscopy exams at

Author Manuscript Author Manuscript Author Manuscript Author Manuscript

age of 50, they should have them every 5 years, p-value=0.018; Q27. I believe that colon cancer is mainly a problem for men, p-value=0.023, data not shown).

Discussion

The current study showed that a tailored CRC seminar can improve knowledge, behavior, and awareness among Korean American immigrants facing language barriers or those of lower socioeconomic status. This study examined the associations between groups (intervention vs. control), and outcomes/domains, such as knowledge, behavior and awareness in univariate and multivariable analyses. By conducting multivariable analysis of each outcome/domain, we calculated a PS. We further examined the associations between questionnaires and outcomes/domains in univariate analyses and found that better general health, higher education level, and birthplace in US were significantly associated with greater CRC awareness or knowledge.

Due to cultural and language barriers, Korean Americans in the LA Koreatown area have been a difficult population to reach when implementing cancer education and prevention programs. Our results were consistent with other studies suggesting that a lack of acculturation in the US seems to be a critical barrier in receiving preventive health services [21]. Providing culturally integrated and tailored cancer education to Korean Americans could significantly improve knowledge regarding CRC and screening; thereby, ultimately reducing CRC screening disparities in the Korean population. Our present study suggests several associated factors related to knowledge improvement of CRC after educational intervention. These results should be taken into consideration by local academic medical centers when creating culturally integrated educational programs.

Several previous reports have demonstrated that health education intervention can improve preventative cancer screening in the Asian American populations, including Vietnamese Americans, Chinese Americans, Hmong Americans, Korean Americans, Filipino Americans et al. [22–26]. Gu et al. suggested that small group-based education programs prepared by Chinese-speaking community health workers can enhance the implementation fidelity for breast cancer screening by mammography [27]. Aligned with these findings, our results strongly argue for the necessity and importance of raising self-awareness about CRC screening in Korean Americans. After health education, participants were more likely to be aware of and willing to try CRC screening options. Their own knowledge and inquiry influenced physicians who were also motivated by the specific request from their patients (action-reaction). We also found that detailed information could not be delivered efficiently or memorized by participants, particularly those were older. Considering the age range of our participants, we suggest that follow-up information via phone call, text, or voicemail regarding future CRC screenings should be considered by healthcare providers.

Findings from this pilot study indicate a strong need for education programs that are linguistically and culturally customized for the Korean American population. Although further studies should be conducted to determine the feasibility of such interventions and to ascertain their long-term impact on actual screening rates, tailored education will nevertheless be critically necessary for reducing CRC-related mortality and morbidity

Author Manuscript Author Manuscript Author Manuscript Author Manuscript

among Korean Americans. However, we are aware that there are several limitations in our study. First, considering that our study was based on self-reported responses and that the extent of reliability and validity of self-reporting is somewhat limited, we believe that an additional study assessing objective and quantitative results should be designed. Second, this study was restricted to concentrated populations living in the LA Koreatown area, and it may not be generalizable to Korean American populations based in other regions. Third, the study was not able to determine the long-term effects of intervention, such as actual CRC screening rates. Fourth, our voluntary participants may be more active and self-motivated about health issues in general, so the findings from this study cannot be expected to be the same in a less motivated population. Lastly, our sample size was relatively small, so conclusive statements cannot be made.

Despite our limitations, a major strength of our study was the finding that culturally and linguistically integrated seminars by trusted community leaders in the academic field can support the wellbeing of participants. Our educational seminar included a short slide presentation and provided a point-by-point lecture on layman's terminology, to particularly assist the older or less educated participants. This approach created a friendly and informal environment to help participants clearly understand the health messages in the educational materials. Participants were encouraged to ask questions in their own languages during and after the seminar.

Conclusion

In conclusion, our tailored intervention made a significant improvement in awareness, knowledge, and behavior related to CRC and screening in Korean Americans residing in Koreatown, many of whom could be considered underserved. Although further larger scale community-based studies are required to validate this finding, the results from our current study suggest that providing culturally and linguistically integrated educational community programs may greatly improve cancer prevention in high risk subgroups of Asian Americans and reduce disparities in CRC screening.

Acknowledgement

We sincerely thank all leaders and staff from participating community organizations. The authors acknowledge support from National Institutes of Health grants (1U01DK103260, 1R01DK100974, U24 DK097154, NIH NCATS UCLA CTSI UL1TR000124), Department of Defense grants (W81XWH-15-1-0415), Centers for Disease Controls and Prevention (1U01DP006079), IMAGINE NO IC Research Grant, the Steven Spielberg Discovery Fund in Prostate Cancer Research Career Development Award, and the U.S.-Egypt Science and Technology Joint Fund (to J.K.). J.K. is a former recipient of the Interstitial Cystitis Association Pilot Grant, a Fishbein Family IC Research Grant, New York Academy of Medicine, and Boston Children's Hospital Faculty Development. The funders had no role in the experimental design, data collection, analysis, preparation of the manuscript, or decision to publish. In addition, this article is derived from the Subject Data funded in whole or part by National Academies of Sciences, Engineering, and Medicine (NAS) and The United States Agency for International Development (USAID). Any opinions, findings, conclusions, or recommendations expressed in this article are those of the authors alone, and do not necessarily reflect the views of USAID or NAS.

Reference

1. Siegel R, Desantis C, Jemal A (2014) Colorectal cancer statistics. CA Cancer J Clin 64: 104–117. [PubMed: 24639052]

Author Manuscript Author Manuscript Author Manuscript Author Manuscript

2. Vogelaar I, van Ballegooijen M, Schrag D (2006) How much can current interventions reduce colorectal cancer mortality in the U.S? Mortality projections for scenarios of risk-factor modification, screening, and treatment. Cancer 107: 1624–1633. [PubMed: 16933324]

3. Atkin W, Wooldrage K, Brenner A (2017) Adenoma surveillance and colorectal cancer incidence: a retrospective, multicentre, cohort study. Lancet Oncol 18: 823–834. [PubMed: 28457708]

4. Schreuders EH, Ruco A, Rabeneck L (2015) Colorectal cancer screening: a global overview of existing programmes. Gut 64: 1637–1649. [PubMed: 26041752]

5. Deng Y (2017) Rectal Cancer in Asian vs. Western Countries: Why the Variation in Incidence? Curr Treat Options Oncol 18: 64. [PubMed: 28948490]

6. Jun J, Oh KM (2013) Asian and Hispanic Americans' cancer fatalism and colon cancer screening. Am J Health Behav 37: 145–154. [PubMed: 23026095]

7. Ng SC, Wong SH (2013) Colorectal cancer screening in Asia. Br Med Bull 105: 29–42. [PubMed: 23299409]

8. Lee HY, Lundquist M, Ju E (2011) Colorectal cancer screening disparities in Asian Americans and Pacific Islanders: which groups are most vulnerable? Ethn Health 16: 501–518. [PubMed: 22050536]

9. Jung KW, Park S, Won YJ (2012) Prediction of cancer incidence and mortality in Korea, 2012. Cancer Res Treat 44: 25–31. [PubMed: 22500157]

10. Lee J, Xiao YY, Sun YY (2017) Prevalence and characteristics of hereditary non-polyposis colorectal cancer (HNPCC) syndrome in immigrant Asian colorectal cancer patients. BMC Cancer 17: 843. [PubMed: 29237405]

11. Maxwell AE, Song H (2003) Cancer Screening of Korean Americans in Los Angeles County: Adding Pieces to the Puzzle. Korean Korean Am Stud Bull 13: 59–70. [PubMed: 17057820]

12. Jo AM, Maxwell AE, Rick AJ (2009) Why are Korean American physicians reluctant to recommend colorectal cancer screening to Korean American patients? Exploratory interview findings. J Immigr Minor Health Pp: 302–309. [PubMed: 18607728]

13. Jo AM, Maxwell AE, Wong WK (2008) Colorectal cancer screening among underserved Korean Americans in Los Angeles County. J Immigr Minor Health 10: 119–126. [PubMed: 17574545]

14. Hwang H (2013) Colorectal cancer screening among Asian Americans. Asian Pac J Cancer Prev 14: 4025–4032. [PubMed: 23991947]

15. Maxwell AE, Crespi CM, Antonio CM (2010) Explaining disparities in colorectal cancer screening among five Asian ethnic groups: a population-based study in California. BMC Cancer 10: 214. [PubMed: 20482868]

16. Liu L, Wang Y, Sherman RL (2016) Cancer in Los Angeles County: Trends by Race/Ethnicity 1976–2012 Los Angeles Cancer Surveillance Program, University of Southern California.

17. Maxwell AE, Crespi CM (2009) Trends in colorectal cancer screening utilization among ethnic groups in California: are we closing the gap?. Cancer Epidemiol Biomarkers Prev 18: 752–759. [PubMed: 19273482]

18. Rosenbaum PR (1983) The central role of the propensity score in observational studies for causal Effects. Biometrika 70: 41–55.

19. Rosenbaum PR (1984) Reducing bias in observational studies using subclassification on the propensity score. J Am Stat Assoc 79: 516–524.

20. D'Agostino RB, D'Agostino RB (2007) Sr. Estimating treatment effects using observational data. JAMA 297: 314–316. [PubMed: 17227985]

21. Society AC (2011) Colorectal cancer facts & figures 2011–2013

22. Carballeira NM, Shalabi F, Stefanov K (1995) Comparison of the fatty acids of the tunicate Botryllus schlosseri from the Black Sea with two associated bacterial strains. Lipids 30: 677–679. [PubMed: 7564924]

23. Cuaresma CF, Sy AU, Nguyen TT (2018) Results of a lay health education intervention to increase colorectal cancer screening among Filipino Americans: A cluster randomized controlled trial. Cancer 124: 1535–1542. [PubMed: 29578603]

Author Manuscript Author Manuscript Author Manuscript Author Manuscript

24. Jo AM, Nguyen TT, Stewart S (2017) Lay health educators and print materials for the promotion of colorectal cancer screening among Korean Americans: A randomized comparative effectiveness study. Cancer 123: 2705–2715. [PubMed: 28440872]

25. Lee S, Zhai S, Zhang GY (2015) Factors Associated with Hepatitis C Knowledge Before and After an Educational Intervention among Vietnamese Americans. Clin Med Insights Gastroenterol 8: 45–53. [PubMed: 26561280]

26. Nguyen TT, Tsoh JY, Woo K (2017) Colorectal Cancer Screening and Chinese Americans: Efficacy of Lay Health Worker Outreach and Print Materials. Am J Prev Med 52: e67–e76. [PubMed: 27986352]

27. Gu J, Maxwell AE, Ma GX (2018) Evaluating the Training of Chinese-Speaking Community Health Workers to Implement a Small-Group Intervention Promoting Mammography. J Cancer Educ

Author Manuscript Author Manuscript Author Manuscript Author Manuscript

Table 1:

Characteristics of Korean American Participants in Colorectal Cancer Screening Survey in Los Angeles, California: 2018

Variable	All participants (N=100)	Control (N=50)	Intervention (N=50)	P-value
Q1. Gender				
Female	63 (63)	30 (60)	33 (66)	0.534
Male	37 (37)	20 (40)	17 (34)	
Q2. Age (years)				
45	1 (1)	0 (0)	1 (2)	0.146
45–49	3 (3)	2 (4)	1 (2)	
50–64	45 (45)	27 (54)	18 (36)	
65 or over	51 (51)	21 (42)	30 (60)	
Q3. Marital status				
No	26 (26)	13 (26)	13 (26)	1.000
Yes	74 (74)	37 (74)	37 (74)	
Q4. Height (cm)				
Median (IQR)	153 (151 – 158)	153 (151 – 158)	154 (151 – 158)	0.206
Q4. Weight (kg)				
Median (IQR)	55 (45.5 – 61)	55 (45.5 – 61)	55 (45.5 – 61)	0.992
Q5. Where were you born?				
Korea	98 (98)	50 (100)	48 (96)	0.495
USA	2 (2)	0 (0)	2 (4)	
Q6. About how many years have you lived In the United States?				
< 11 years	12 (12)	4 (8)	8 (16)	0.184
11–20 years	18 (18)	12 (24)	6 (12)	
More than 20 years	70 (70)	34 (68)	36 (72)	
Q7. What is your level of English?				
Beginner	96 (96)	48 (96)	48 (96)	1.000
Low intermediate	2 (2)	1 (2)	1 (2)	
Intermediate	2 (2)	1 (2)	1 (2)	
Q8. What is the highest grade of education you have completed?				

Divers Equal Health Care. Author manuscript; available in PMC 2019 April 22.

Author Manuscript Author Manuscript Author Manuscript Author Manuscript

Variable	All participants (N=100)	Control (N=50)	Intervention (N=50)	P-value
First through 11th grade	68 (68)	36 (72)	32 (64)	0.293
High School graduate	25 (25)	13 (26)	12 (24)	
One to three years of college	4 (4)	1 (2)	3 (6)	
College graduate	3 (3)	0 (0)	3 (6)	
Q9. How's your overall health?				
Poor	2 (2)	0 (0)	2 (4)	0.022
Fair	75 (75)	41 (82)	34 (68)	
Good	11 (11)	7 (14)	4 (8)	
Very good	12 (12)	2 (4)	10 (20)	
Q9. How's your overall health? (combined)				
Fair/Poor	77 (77)	36 (72)	41 (82)	0.235
Very good/Good	23 (23)	14 (28)	9 (18)	
Q10. How would you rate your computer skills (your skill on the internet)?				
Great. I find most anything I search for	2 (2)	0 (0)	2 (4)	0.525
Ok, sometimes I have trouble finding information	14 (14)	6 (12)	8 (16)	
Not so great, I struggle with how to use it	69 (69)	37 (74)	32 (64)	
I have little to no experience	15 (15)	7 (14)	8 (16)	
Q11. Do you frequently use Social Network Service?				
No	97 (97)	48 (96)	49 (98)	1.000
Yes	3 (3)	2 (4)	1 (2)	
Q13. Where do you find health information from?				
Television	85 (85)	43 (86)	42 (84)	1.000
Internet	10 (10)	5 (10)	5 (10)	
Newspaper	5 (5)	2 (4)	3 (6)	
Q28. Have any of your relatives ever had colon cancer?				
No	94 (94)	47 (94)	47 (94)	1.000
Yes	6 (6)	3 (6)	3 (6)	
Q29. If you may be reluctant to have test for colon cancer, what is the reason for that?				
It Is because of the cost	78 (78)	39 (78)	39 (78)	

Divers Equal Health Care. Author manuscript; available in PMC 2019 April 22.

Author Manuscript Author Manuscript Author Manuscript Author Manuscript

Variable	All participants (N=100)	Control (N=50)	Intervention (N=50)	P-value
Having the tests done would be embarrassing	10 (10)	4 (8)	6 (12)	
I am worried that testing will show that I have colon cancer	12 (12)	7 (14)	5 (10)	

Data are presented as number of patients (column %) or median (IQR, interquartile range).

P-value is calculated by Wilcoxon rank-sum test for numerical variables, and chi-square or Fisher's exact test for categorical variables.

Note: All subjects answered 'Yes' to 'Q12: Do you frequently access health care newsletter?'

Author Manuscript Author Manuscript Author Manuscript Author Manuscript

Table 2:

Domains stratified by group.

Domain	All participants (N=100)	Control (N=50)	Intervention (N=50)
Awareness			
Q14. Have you heard about colorectal cancer?			
No	5 (5)	2 (4)	3 (6)
Yes	95 (95)	48 (96)	47 (94)
Q15. Have you heard about colorectal polyp?			
No	41 (41)	36 (72)	5 (10)
Yes	59 (59)	14 (28)	45 (90)
Q16. Have you heard about the fecal occult blood test (FOBT) or stool blood test?			
No	49 (49)	46 (92)	3 (6)
Yes	51 (51)	4 (8)	47 (94)
Q19. Have you heard about colonoscopy?			
No	9 (9)	3 (6)	6 (12)
Yes	91 (91)	47 (94)	44 (88)
Behavior			
Q17. Have your doctor told you that you should be tested for colon cancer (FOBT)?			
No	50 (50)	47 (94)	3 (6)
Yes	50 (50)	3 (6)	47 (94)
Q18. Have you ever had a FOBT?			
No	98 (98)	49 (98)	49 (98)
Yes	2 (2)	1 (2)	1 (2)
Q20. Have your doctor recommend colonoscopy?			
No	39 (39)	37 (74)	2 (4)
Yes	61 (61)	13 (26)	48 (96)
Q21. Have you ever had a colonoscopy?			
No	87 (87)	46 (92)	41 (82)
Yes	13 (13)	4 (8)	9 (18)

Divers Equal Health Care. Author manuscript; available in PMC 2019 April 22.

Author Manuscript Author Manuscript Author Manuscript Author Manuscript

Domain	All participants (N=100)	Control (N=50)	Intervention (N=50)
Q30. Are you willing to undergo colon cancer testing within 6 months?			
No	52 (52)	46 (92)	6 (12)
Yes	48 (48)	4 (8)	44 (88)
Knowledge			
Q22. I believe that there is only one screening test for colon cancer.			
No	51 (51)	5 (10)	46 (92)
Yes	49 (49)	45 (90)	4 (8)
Q23. There is a stool blood test using a "home" test			
No	60 (60)	49 (98)	11 (22)
Yes	40 (40)	1 (2)	39 (78)
Q24. I believe that people are supposed to start getting tested for colon cancer at age of 50.			
No	64 (64)	32 (64)	32 (64)
Yes	36 (36)	18 (36)	18 (36)
Q25. Once people start having stool blood test, they should have them every 3 years.			
No	68 (68)	29 (58)	39 (78)
Yes	32 (32)	21 (42)	11 (22)
Q26. In general, once people start having colonoscopy exams at age of 50, they should have them every 5 years.			
No	52 (52)	28 (56)	24 (48)
Yes	48 (48)	22 (44)	26 (52)
Q27. I believe that colon cancer is mainly a problem for men.			
No	50 (50)	43 (86)	7 (14)
Yes	50 (50)	7 (14)	43 (86)

Data are presented as number of patients (column %).

Author Manuscript Author Manuscript Author Manuscript Author Manuscript

Table 3:

Comparison in awareness, behavior, and knowledge between Korean American participants in the post-intervention and control groups. Univariate and multivariable analyses of each domain for post-intervention vs. control are shown.

Domain	Univariate		Multivariable *	
	Odds Ratio (95% CI)	P-value	Odds Ratio (95% CI)	P-value
Awareness				
Q14. Heard about colorectal cancer	0.65 (0.10–4.08)	0.649	0.97 (0.11–8.30)	0.980
Q15. Heard about colorectal polyp	23.14 (7.62–70.31)	<0.001	22.47 (6.42–78.62)	<0.001
Q16. Heard about the FOBT or stool blood test	180.17 (38.20–849.83)	<0.001	245.37 (34.55–1742.75)	<0.001
Q19. Heard about colonoscopy	0.47 (0.11–1.99)	0.303	0.64 (0.12–3.32)	0.593
Behavior				
Q17. Ever been recommended for colon cancer (FOBT) test	245.44 (47.11–1278.77)	<0.001	1473.56 (68.58–31660.02)	<0.001
Q18. Ever had a FOBT	1.00 (0.06–16.44)	1.000	0.23 (0.01–9.56)	0.437
Q20. Ever been recommended for colonoscopy	68.31 (14.51–321.58)	<0.001	91.90 (15.06–560.96)	<0.001
Q21. Ever had a colonoscopy	2.52 (0.72–8.82)	0.147	2.08 (0.51–8.50)	0.309
Q30. Are you willing to undergo colon cancer testing within 6 months?	84.33 (22.28–319.14)	<0.001	87.17 (19.01–399.63)	<0.001
Knowledge				
Q22. I do not believe that there is only one screening test for colon cancer. **	158.39 (32.45–773.18)	<0.001	126.63 (23.61–679.07)	<0.001
Q23. There is a stool blood test using a “home” test.	173.73 (21.49–1404.51)	<0.001	157.17 (18.02–1370.41)	<0.001
Q24. I believe that people are supposed to start getting tested for colon cancer at age of 50.	1.00 (0.44–2.26)	1.000	0.75 (0.29–1.95)	0.561
Q25. Once people start having stool blood test, they should have them every 3 years **.	2.57 (1.07–6.15)	0.034	2.64 (0.97–7.21)	0.057
Q26. In general, once people start having colonoscopy exams at age of 50, they should have them every 5 years **.	0.73 (0.33–1.59)	0.424	0.87 (0.35–2.14)	0.761

Abbreviations: FOBT, fecal occult blood test.

Odds ratio is for the intervention group relative to the control group. 100 observations were used in the multivariable models.

* The propensity score (PS) of being in the intervention group was estimated using a multivariable logistic regression model including Q1 through Q11, Q13, and Q28-Q29. Then, the multivariable model was adjusted for the PS.

** Models were fitted with a response ‘No’ vs. ‘Yes’ as ‘No’ is the correct answer.

Kim et al. BMC Urology (2019) 19:47
https://doi.org/10.1186/s12894-019-0478-0

BMC Urology

REVIEW Open Access

Sexual pain and IC/BPS in women

Su Jin Kim[1,5], Jayoung Kim[2,3*] and Hana Yoon[4*]

Abstract

Interstitial cystitis/bladder pain syndrome (IC/BPS) and female sexual dysfunction (FSD) are common conditions that substantially reduce women's health. In particular, women with IC/BPS show vulvodynia, a kind of FDS that originates from consistent pain around the vulvar area. There have been many studies attempting to find the underlying mechanisms that induce the chronic pain associated with IC/BPS and vulvodynia and explain why these two conditions often coexist. Proposed theories suggest that pain hypersensitivity is being mediated by peripheral and central sensitization. However, there are still many unknown factors, such as etiologies, that can evoke pain hypersensitivity and may be linking the casual relationship between IC/BPS and vulvodynia. At present, knowledge regarding IC/BPS and vulvodynia are insufficient when considering their clinical importance. Therefore, efforts are necessary to elucidate the issues surrounding IC/BPS and vulvodynia.

Keywords: Cystitis, interstitial, Sexual dysfunction, Chronic pain, Vulvodynia, Lower urinary tract symptoms, Quality of life

Background

Female sexual dysfunction (FSD) and interstitial cystitis/bladder pain syndrome (IC/BPS) are two conditions affecting women's health. A study on the association between sexual and general well-being found that women reported better quality of life (QoL) with higher sexual satisfaction, regardless of age and/or menopausal status [1]. Both FSD and IC/BPS significantly impairs a woman's abilities to pursue and enjoy sexual relations. Approximately 40–50% of women experience FSD and 0.5–12% experience IC/BPS. Considering these incidence rates, both FSD and IC/BPS present serious challenges for patients and clinicians [2–6].

Chronic pain deteriorates not only personal health and wellness, but also QoL. Chronic pain can induce sexual dysfunction, such as arousal disorder, and relationship problems [7]. Furthermore, studies have shown that significantly more women with chronic pelvic pain (CPP) show FSD compared to those without CPP. Women with CPP and FSD reported various types of sexual dysfunctions, including hypoactive sexual desire disorder, sexual arousal disorder, orgasmic disorder, and sexual pain disorder [8].

The symptoms of IC/BPS, such as urinary frequency, urgency, and pelvic pain, can have a negative impact on sexual activity and QoL [9]. Women with overactive bladder (OAB) frequently have a risk for sexual dysfunction [10]. In the postmenopausal group, women with scores indicating severe OAB reported worse sexual function, particularly in the arousal, lubrication, orgasm, pain, and total domains [11]. Despite the known association between FSD and bladder diseases, contributing risk factors have yet to be explored. Evaluating the impact of duration, severity, pain localization, sexual trauma history, anxiety, and depression associated with sexual dysfunction may help elucidate risk factors. Increasing our knowledge about sexual dysfunction as it relates to bladder diseases may aid in clinical diagnoses, treatment strategies, and overall symptom improvement. This review will provide an overview of studies that address FSD in women with IC/BPS.

Pain in FSD

According to consensus from the 4th Internaional Consultation on Sexual Medicine (ICSM), FSD is classified as hypoactive sexual desire dysfunction, female sexual arousal dysfunction, female orgasmic dysfunction, female-genital-pelvic pain dysfunction, persistent genital arousal disorder, postcoital syndrome, hypohedonic orgasm, or painful orgasm [2, 12]. Guidelines from the 4th ICSM also define pain-associated FSD as female-genital-pelvic pain dysfunction and include all conditions that inhibit sexual

* Correspondence: Jayoung.Kim@csmc.edu; wowhana@ewha.ac.kr
[2]Departments of Surgery and Biomedical Sciences, Cedars-Sinai Medical Center, Los Angeles, CA 90048, USA
[4]Department of Urology, Medical Research Center, Ewha Womans University School of Medicine, Seoul, Republic of Korea
Full list of author information is available at the end of the article

© The Author(s). 2019 **Open Access** This article is distributed under the terms of the Creative Commons Attribution 4.0 International License (http://creativecommons.org/licenses/by/4.0/), which permits unrestricted use, distribution, and reproduction in any medium, provided you give appropriate credit to the original author(s) and the source, provide a link to the Creative Commons license, and indicate if changes were made. The Creative Commons Public Domain Dedication waiver (http://creativecommons.org/publicdomain/zero/1.0/) applies to the data made available in this article, unless otherwise stated.

intercourse or induce negative effects on sexual functions. Female-genital-pelvic pain dysfunction is different from the previous classification characterized as pain associated with FSD, which includes sexual pain disorder including dyspareunia and vaginismus [13]. According to the ICSM, female-genital-pelvic pain dysfunction includes persistent or recurrent difficulties with at least one of the following: (1) vaginal penetration during intercourse, (2) marked vulvovaginal or pelvic pain during genital contact, (3) marked fear or anxiety about vulvovaginal or pelvic pain in anticipation of, during, or as a result of genital contact, or (4) marked hypertonicity or overactivity of pelvic floor muscles with or without genital contact [14]. Painful orgasm also falls under this category and is defined as genital and/or pelvic pain during or shortly after orgasm [2]. These recent new definitions reflect the evolving concept behind pain-associated FSD as it also now includes pain in the vulvovaginal and pelvic area and pelvic floor hypertonicity. The new categorization of female-genital-pelvic pain dysfunction has broadened the view on pain-associated FSD and has differentiated it from its previous classification, which confined symptoms to each organ or single disease. This recent change in classification by the ICSM considers pain-associated FDS as a complex condition influenced by psychological and physical factors and supports the general thought that FSD is multifactorial.

Previously, vulvodynia had been generalized under chronic vulvar pain with no precise discrimination for it. However, recent consensus has redefined chronic vulvar pain as vulvar pain associated with specific diseases, such as inflammation, neoplasm, and/or injury. This was conducted at a conference with the International Society for the Study of Vulvovaginal Disease, the International Society for the Study of Women's Sexual Health, and the International Pelvic Pain Society [15]. Vulvodynia can have diverse pain characteristics; therefore, pain-based classification helps in identification, diagnosis, and treatment. Vulvodynia can be characterized as either general (entire vulva) or localized (parts of the vulva). Additionally, based on the situation of the pain, vulvodynia can be classified as either provoked (triggered by physical contact) or unprovoked (spontaneous occurrence without specific triggers) [16]. Women of all ages can experience vulvodynia, and provoked vulvodynia is the most commonly diagnosed [17, 18]. Provoked vulvodynia is thought to be more widely diagnosed than unprovoked because its symptoms can be better recognized by doctors. Therefore, there is an great need to better identify unprovoked vulvodynia patients.

Sexual pain and IC/bps

IC/BPS is a disorder that induces chronic pain or discomfort in the bladder and surrounding pelvic organs [19, 20]. At present, IC/BPS is not a disease confined to just the bladder and pelvic area; it is a complex disease that includes the outside of the genitourinary tract. Tripp et al. [21] investigated the pain characteristics of IC/BPS using whole-body diagram pain locators. They found that women with IC/BPS reported significantly more pain all over their body, compared to healthy women without. Only 52 of the 193 IC/BPS diagnosed women (27%) presented pain restricted to the bladder and pelvic area. Moreover, IC/BPS patients had various co-morbidities. Diseases, such as irritable bowel syndrome, fibromyalgia, vulvodynia, chronic pelvic pain, endometriosis, OAB, allergies and chronic fatigue syndrome, were found to coexist in IC/BPS patients [22–28].

In addition, there are several reports that IC/BPS can increase the risk for or worsen other diseases, including FSD. A population-based study found higher prevalence of FSD in women with IC/BPS [29]. FSD incidence also increased depending on the severity of IC/BPS symptoms, suggesting that FSD is a factor may be worsening IC/BPS. In regards to the pain associated with FSD, vulvodynia may be contributing to flare-ups of IC/BPS symptoms and could be the reason why IC/BPS patients avoid sexual activity [9, 30].

Can FSD and IC/bps be generalized as one disease?

Diseases characterized with lower urinary tract symptoms (LUTS) in females, such as incontinence and OAB, are known to have a negative impact on all domains in female sexual function. Symptoms of IC/BPS can also deteriorate patient's sexual activities and QoL. A significant number of IC/BPS patients avoid sexual activity because of pain. In addition, FSD and IC/BPS share similar clinical characteristics and comorbidities, making it difficult to discriminate between the two [31–33]. As mentioned previously, there are many clinical reports presenting an association between IC/BPS and vulvodynia, mainly due to shared FSD conditions.

Although the mechanisms of the association between IC/BPS and vulvodynia are unclear, visceral nerve cross-talking and the anatomic relationship between genital organs and the bladder offer a simple proximity explanation. Another possible mechanism behind the relationship is abnormal pain hypersensitivity induced by peripheral and central sensitization. The abnormal pain response frequently observed in vulvodynia patients is caused by central or peripheral maladaptive pain processing from local insult, injury, or trauma (Fig. 1).

Role of peripheral sensitization in the pain hypersensitivity of vulvodynia and IC/BPS

Exposure of nociceptors to repetitive pain stimulation reduces the pain threshold and amplifies the responsiveness of nociceptors. Therefore, this can abnormally increase peripheral transduction of sensitivity and lead to the

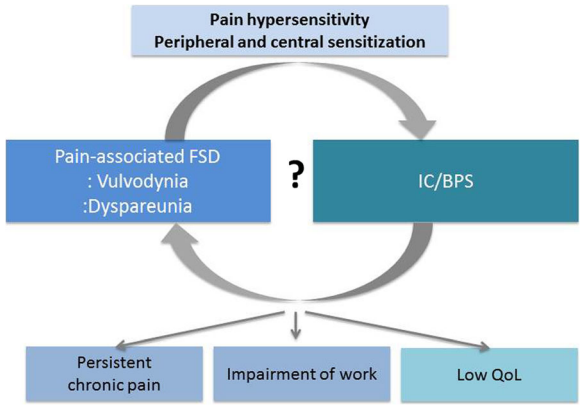

Fig. 1 FSD and IC/BPS: FSD; Female sexual dysfunction, *IC/BPS* Interstitial cystitis/bladder pain syndrome, *QoL* Quality of life

development of peripheral pain hypersensitivity [34–36]. The potential underlying mechanism of peripheral pain hypersensitivity noted in both vulvodynia and IC/BPS could be due to sensory nerve upregulation. Previous studies have shown that sensory nerve density is significantly increased in the vulva vestibule and bladder. Compared to the normal controls, patients with vulvodynia were found to have increased nociceptors in their vulvar vestibule [37–40]. Consequentially, this increased density of peripheral nociceptors results in increased sensitivity. It was also found that transient receptor potential V1 (TRPV1) exists in these nociceptive nerve endings and enhances pain signaling [37, 41, 42]. Pukall CF et al. [43] and Giesecke J et al. [44] reported increased peripheral tactile, pressure, and pain sensitivity in the patients with vulvodynia and confirmed histologic and molecular changes of peripheral nociceptors is associated with clinical manifestations. Similarly with vulvodynia, it has been reported that IC/BPS patient bladders have upregulated sensory innervation and TRPV1 expression [45–47].

Role of central sensitization in the pain hypersensitivity of vulvodynia and IC/BPS

Central sensitization is an important mechanism underlying various conditions associated with chronic pain and induces pain hypersensitivity through pathologically enhanced pathways that are not normally associated with nociception. For example, the low-threshold Aδ fiber, that is mostly used for temperature and pressure signaling, can be sensitized to pain. Chronic pain induced by central sensitization is persistent even after initiation of the signal and disappearance of the peripheral cause [48]. Studies have shown that the pain characteristics of central sensitization can be found in vulvodynia patients. Foster DC et al. [49] observed that vulvar vestibulitis syndrome patients experienced hyperalgesia and allodynia more often than normal controls after intradermal foot and forearm capsaicin injections. In addition, pelvic organ crosstalk has an important role in central sensitization because pelvic organs, such as the bladder, colon and vulva, are controlled by the same neural pathway [50]. Thus, afferent signals from other pelvic organs can provoke pain through neural crosstalk even though the initiation and peripheral causes of vulvodynia and IC/BPS have gone. Therefore, central sensitization plays an important role in the chronic pain observed in vulvodynia and IC/BPS. Clinically, similar manifestations of vulvodynia and IC/BPS have also existed. Moreover, recently, there has been an attempt to categorize various pain-associated conditions due to central sensitization as central sensitivity syndrome (CSS). Vulvodynia and IC/BPS are considered subgroups of CSS [51]. Previous studies on clinical findings support the notion that the same mechanisms associated with central sensitization are involved in the pain behind vulvodynia and IC/BPS [52–54].

Recently, evidence supporting central sensitization using functional and structural brain imaging were reported in vulvodynia and IC/BPS. Previously, Pukall et al. [55] showed that increased perception and activation of pain-related brain regions were observed in women with vulvar vestivulitis syndrome, compared to normal women, after tacticle stimulation of the vulvar vestibule. Other studies have reported that vulvodynia patients show increased grey matter density in pain-modulating and stress-related regions of the brain as well as alterations in the intrinsic connectivity of regions comprising the sensorimotor, salience, and default mode resting state networks [56, 57]. Similarly, women with IC/BPS showed alterations of oscillation frequency and functional connectivity of brain regions previously reported in other chronic pain conditions [58] and various white matter (right anterior thalamic radiation, left forceps major, and right longitudinal fasciculus, right superior and bilateral inferior longitudinal fasciculi) abnormalities that correlated with severity of pain, urinary symptoms, and impaired QoL [59]. Fig. 2 shows common therapeutic approaches and points of divergence among IC/BPS, IC/BPS + vulvodynia, and vulvodynia patient groups.

Approach and management of vulvodynia and IC/bps patients

Clinically, vulvodynia and IC/BPS often coexists and differentiation between the two is not easy, especially when the patient reports LUTS combined with pain. A majority of patients also seek medical care after relatively longer periods of initially feeling pain, leading to central sensitization that has been firmly established. Furthermore, clinical manifestations of chronic pain found in various other comorbidities can mask vulvodynia and IC/BPS, making it confusing and difficult to officially diagnose.

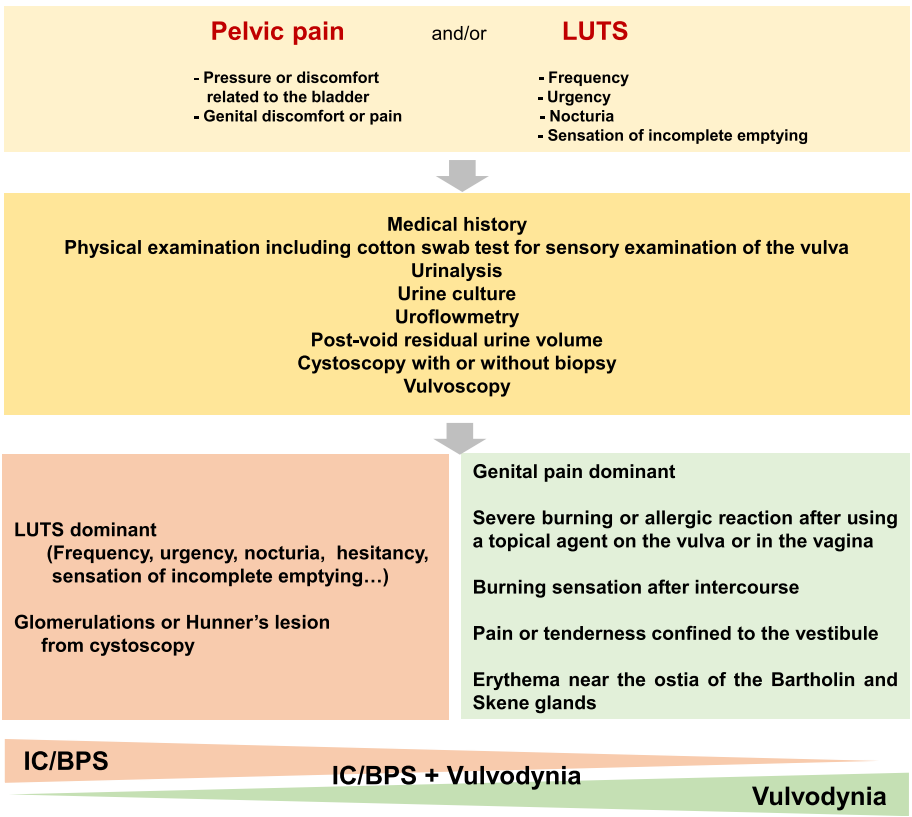

Fig. 2 Approach for differential diagnosis of IC/BPS, vulvodynia, and IC/BPS + vulvodynia (*LUTS* lower urinary tract symptoms, *IC/BPS* interstitial cystitis/bladder pain syndrome)

Table 1 Characteristics of FSD observed in women with IC/BPS

	Age	Types of FSD	Prevalence (%)	Other associated conditions
Verit et al. [8][a]	34.73 ± 8.07 years	NA	67.8 (78 of 112)	NA
Gardella et al. [28]	38.7 ± 12 years	Vulvodynia Dyspareunia	Vulvodynis: 85.1 (40 of 47)	LUTS (frequency, urgency)
			Vaginal burning: 65.9 (31 of 47)	
			Dyspareunia: 31.9 (15 of 47)	
Carrico et al. [24]	52 years (range, 19–90)	Vulvodynia	Vulvar pain: 48.1 (91/189)	Sexually transmitted infections (genital warts, positive HPV, gonorrhea, chlamydia)
			Pain with intercourse: 66.9 (117/175)	
Yoon et al. [9]	51.0 ± 14.7 years	Vulvodynia Dyspareunia	NA	LUTS (frequency, urgency)
Bogart et al. [27]	43.6 ± 16.7 years	NA	Women experienced with sexual dysfunction symptoms: 88 (866/985)	NA
Gardella et al. [23]	38.2 ± 11.3 years	Vulvodynia Dyspareunia	Spontaneous vulvodynia: 23.4 (11 of 47)	NA
			Provoked vulvodynia: 74.5 (35/47)	
			Localized vulvodynia: 80.9 (38/47)	
			Generalized vulvodynia: 17 (8/47)	
			Dyspareunia: 87.2 (41/47)	

[a]This study was done in the women diagnosed of chronic pelvic pain. *FSD* female sexual dysfunction, *IC/BPS* interstitial cystitis/bladder pain syndrome, *LUTS* lower urinary tract symptom, *NA* Not applicable

Many previous studies have revealed a close correlation between LUTS and impaired sexual function; IC/BPS is not an exception. Besides, it is not uncommon to have trouble differentiating sexual pain and IC/BPS-related genital pain in women. Unfortunately, despite the growing population of affected individuals, there is a lack of comprehensive studies regarding sexual dysfunction and IC/BPS (Table 1). Clinicians should take more concern regarding sexual dysfunction and pain in IC/BPS patients, and more randomized controlled studies should be conducted to better understand correlations and diagnostic differentiations.

Conclusions

Both vulvodynia and IC/BPS are common and irritable conditions that disrupt normal life and reduce QoL in women. Vulvodynia also manifests itself along with IC/BPS and there are several reports supporting an association between the two diseases. Unfortunately, knowledge concerning vulvodynia and IC/BPS is inadequate when considering the clinical impact and importance of these two conditions. Therefore, there is an essential need for further studies that delve into discovering the features of vulvodynia and IC/BPS.

Abbreviations

CPP: Chronic pelvic pain; CSS: Central sensitivity syndrome; FSD: Female sexual dysfunction; IC/BPS: Interstitial cystitis/bladder pain syndrome; ICSM: International consultation on sexual medicine; LUTS: Lower urinary tract symptoms; OAB: Overactive bladder; QoL: Quality of life; TRPV1: Transient receptor potential V1

Acknowledgements

The authors would like to thank Mr. Taeeun Daniel Park and Mr. Austin Yeon for careful review and editing the manuscript.

Authors' contributions

HY and JK made substantial contributions to conception and design and involved in critically for important intellectual content. SK was involved in acquisition of data, interpretation of data, and drafting the manuscript. All authors gave final approval of the version to be published.

Funding

The authors acknowledge support from National Institutes of Health grants (1U01DK103260), Department of Defense grants (W81XWH-15-1-0415 and W81XWH-19-1-0109), Centers for Disease Control and Prevention (1U01DP006079), the Steven Spielberg Discovery Fund in Prostate Cancer Research Career Development Award, the U.S.-Egypt Science and Technology Development Fund by the National Academies of Sciences, Engineering, and Medicine, Burroughs Wellcome Fund (BWF) 2017 Collaborative Research Travel Grant (CRTG), and Southeast Center for Integrated Metabolomics (SECIM) Pilot and Feasibility Grant (to J.K.). This funding source had no role in the design of this study and will not have any role during its execution, analyses, interpretation of the data, or decision to submit results.

Availability of data and materials

Not applicable.

Ethics approval and consent to participate

Not applicable.

Consent for publication

Not Applicable.

Competing interests

The author(s) declare(s) that they have no competing interests.

Author details

[1]Department of Urology, Seoul St. Mary's Hospital, The Catholic University of Korea College of Medicine, Seoul, Republic of Korea. [2]Departments of Surgery and Biomedical Sciences, Cedars-Sinai Medical Center, Los Angeles, CA 90048, USA. [3]Department of Medicine, University of California Los Angeles, Los Angeles, CA 90095, USA. [4]Department of Urology, Medical Research Center, Ewha Womans University School of Medicine, Seoul, Republic of Korea. [5]Current address: Department of Urology, Yonsei University Wonju College of Medicine, Wonju, Republic of Korea.

Received: 16 February 2018 Accepted: 22 May 2019
Published online: 06 June 2019

References

1. Davison SL, Bell RJ, LaChina M, Holden SL, Davis SR. The relationship between self-reported sexual satisfaction and general well-being in women. J Sex Med. 2009;6:2690–7.
2. McCabe MP, Sharlip ID, Lewis R, Atalla E, Balon R, Fisher AD, Laumann E, Lee SW, Segraves RT. Incidence and prevalence of sexual dysfunction in women and men: a consensus statement from the fourth international consultation on sexual medicine 2015. J Sex Med. 2016;13:144–52.
3. Leppilahti M, Tammela TL, Huhtala H, Auvinen A. Prevalence of symptoms related to interstitial cystitis in women: a population based study in Finland. J Urol. 2002;168:139–43.
4. Clemens JQ, Meenan RT, O'Keeffe Rosetti MC, Brown SO, Gao SY, Calhoun EA. Prevalence of interstitial cystitis s Urology 2009 Mar;73(3):494–498. https://doi.org/10.1016/j.urology.2008.01.053. Epub 2009 Jan.
5. Lifford KL, Curhan GC. Prevalence of painful bladder syndrome in older women. Urology. 2009;73:494–8.
6. Clemens JQ, Link CL, Eggers PW, Kusek JW, Nyberg LM Jr, McKinlay JB; BACH Survey Investigators. Prevalence of painful bladder symptoms and effect on quality of life in black, Hispanic and white men and women. J Urol 2007;177:1390–1394.
7. Ambler N, Williams AC, Hill P, Gunary R, Cratchley G. Sexual difficulties of chronic pain patients. Clin J Pain. 2001;17:138–45.
8. Verit FF, Verit A, Yeni E. The prevalence of sexual dysfunction and associated risk factors in women with chronic pelvic pain: a cross-sectional study. Arch Gynecol Obstet. 2006;274:297–302.
9. Yoon HS, Yoon H. Correlations of interstitial cystitis/painful bladder syndrome with female sexual activity. Korean J Urol. 2010;51:45–9.
10. Juliato CRT, Melotti IGR, Junior LCS, Britto LGO, Riccetto CLZ. Does the severity of overactive bladder symptoms correlate with risk for female sexual dysfunction? J Sex Med. 2017;14:904–9.
11. Cohen BL, Barboglio P, Gousse A. The impact of lower urinary tract symptoms and urinary incontinence on female sexual dysfunction using a validated instrument. J Sex Med. 2008;5:1418–23.
12. Jayasena CN, Alkaabi FM, Liebers CS, Handley T, Franks S, Dhillo WS. A systematic review of randomized controlled trials investigating the efficacy and safetyof testosterone therapy for female sexual dysfunction in postmenopausal women. Clin Endocrinol. 2019;90:391–414.
13. Leiblum SR. Classification and diagnosis of female sexual disorders. In: Goldstein I, Meston CM, Davis S, Traish AM, editors. Women's sexual function and dysfunction: study, diagnosis and treatment. London: Taylor and Francis; 2005. p. 323–31.
14. McCabe MP, Sharlip ID, Atalla E, Balon R, Fisher AD, Laumann E, Lee SW, Lewis R, Segraves RT. Definitions of sexual dysfunctions in women and men: a consensus statement from the fourth international consultation on sexual medicine 2015. J Sex Med. 2016;13:135e143.
15. 2015 Consensus terminology and classification of persistent vulvar pain. http://www.isswsh.org/images/PDF/Consensus_Terminology_of_Vulvar_Pain.pdf
16. Haefner HK. Report of the International Society for the Study of vulvovaginal disease terminology and classification of vulvodynia. J Low Genit Tract Dis. 2007;11:48–9.
17. Clare CA, Yeh J. Vulvodynia in adolescence: childhood vulvar pain syndromes. J Pediatr Adolesc Gynecol. 2011;24:110–5.
18. Reed BD, Harlow SD, Sen A, Legocki LJ, Edwards RM, Arato N, Haefner HK. Prevalence and demographic characteristics of vulvodynia in a population-based sample. Am J Obstet Gynecol. 2012;206:170.e1–9.

19. Barr S. Diagnosis and management of interstitial cystitis. Obstet Gynecol Clin N Am. 2014;41:397–407.
20. Hanno P, Nordling J, van Ophoven A. What is new in bladder pain syndrome/interstitial cystitis? Curr Opin Urol. 2008;18:353–8.
21. Tripp DA, Nickel JC, Wong J, Pontari M, Moldwin R, Mayer R, Carr LK, Doggweiler R, Yang CC, Mishra N, Nordling J. Mapping of pain phenotypes in female patients with bladder pain syndrome/interstitial cystitis and controls. Eur Urol. 2012;62:1188–94.
22. Nickel JC, Tripp DA, Pontari M, Moldwin R, Mayer R, Carr LK, Doggweiler R, Yang CC, Mishra N, Nordling J. Interstitial cystitis/painful bladder syndrome and associated medical conditions with an emphasis on irritable bowel syndrome, fibromyalgia and chronic fatigue syndrome. J Urol. 2010;184: 1358–63.
23. Chelimsky G, Heller E, Buffington CA, Rackley R, Zhang D, Chelimsky T. Co-morbidities of interstitial cystitis. Front Neurosci. 2012;6:114.
24. Alagiri M, Chottiner S, Ratner V, Slade D, Hanno PM. Interstitial cystitis: unexplained associations with other chronic disease and pain syndromes. Urology. 1997;49:52–7.
25. Gardella B, Porru D, Nappi RE, Dacco MD, Chiesa A, Spinillo A. Interstitial cystitis is associated with vulvodynia and sexual dysfunction—a case-control study. J Sex Med. 2011;8:1726–34.
26. Carrico DJ, Sherer KL, Peters KM. The relationship of interstitial cystitis/painful bladder syndrome to vulvodynia. Urol Nurs. 2009;29:233–8.
27. Pontari MA. Chronic prostatitis/chronic pelvic pain syndrome and interstitial cystitis: are they related? Curr Urol Rep. 2006;7:329–34.
28. Elliott CS, Payne CK. Interstitial cystitis and the overlap with overactive bladder. Curr Urol Rep. 2012;13:319–26.
29. Bogart LM, Suttorp MJ, Elliott MN, Clemens JQ, Berry SH. Prevalence and correlates of sexual dysfunction among women with bladder pain syndrome/interstitial cystitis. Urology. 2011;77:576–80.
30. Gardella B, Porru D, Ferdeghini F, Martinotti Gabellotti E, Nappi RE, Rovereto B, Spinillo A. Insight into urogynecologic features of women with interstitial cystitis/painful bladder syndrome. Eur Urol. 2008;54:1145–51.
31. Groysman V. Vulvodynia: new concepts and review of the literature. Dermatol Clin. 2010;28:681–96.
32. Shah M, Hoffstetter S. Vulvodynia. Obstet Gynecol Clin N Am. 2014;41:453–64.
33. Dasgupta J, Tincello DG. Interstitial cystitis/bladder pain syndrome: an update. Maturitas. 2009;64:212–7.
34. Hucho T, Levine JD. Signaling pathways in sensitization: toward a nociceptor cell biology. Neuron. 2007;55:365–76.
35. Chen X, Tanner K, Levine JD. Mechanical sensitization of cutaneous C-fiber nociceptors by prostaglandin E2 in the rat. Neurosci Lett. 1999;267:105–8.
36. Petho G, Derow A, Reeh PW. Bradykinin-induced nociceptor sensitization to heat is mediated by cyclooxygenase products in isolated rat skin. Eur J Neurosci. 2001;14:210–8.
37. Bohm-Starke N, Hilliges M, Falconer C, Rylander E. Increased intraepithelial innervation in women with vulvar vestibulitis syndrome. Gynecol Obstet Investig. 1998;46:256–60.
38. Bohm-Starke N, Hilliges M, Falconer C, Rylander E. Neurochemical characterization of the vestibular nerves in women with vulvar vestibulitis syndrome. Gynecol Obstet Investig. 1999;48:270–5.
39. Tympanidis P, Terenghi G, Dowd P. Increased innervation of the vulval vestibule in patients with vulvodynia. Br J Dermatol. 2003;148:1021–7.
40. Goetsch MF, Morgan TK, Korcheva VB, Li H, Peters D, Leclair CM. Histologic and receptor analysis of primary and secondary vestibulodynia and controls: a prospective study. Am J Obstet Gynecol. 2010;202:614.e1–8.
41. Halperin R, Zehavi S, Vaknin Z, Ben-Ami I, Pansky M, Schneider D. The major histopathologic characteristics in the vulvar vestibulitis syndrome. Gynecol Obstet Investig. 2005;59:75–9.
42. Tympanidis P, Casula MA, Yiangou Y, Terenghi G, Dowd P, Anand P. Increased vanilloid receptor VR1 innervation in vulvodynia. Eur J Pain 2004; 8129–33.
43. Pukall CF, Binik YM, Khalifé S, Amsel R, Abbott FV. Vestibular tactile and pain thresholds in women with vulvar vestibulitis syndrome. Pain. 2002;96:163–75.
44. Giesecke J, Reed BD, Haefner HK, Giesecke T, Clauw DJ, Gracely RH. Quantitative sensory testing in vulvodynia patients and increased peripheral pressure pain sensitivity. Obstet Gynecol. 2004;104:126–33.
45. Hanno P, Andersson KE, Birder L, Elneil S, Kanai A, Pontari M. Chronic pelvic pain syndrome/bladder pain syndrome:taking stock, looking ahead: ICI-RS 2011. Neurourol Urodyn. 2012;31:375–83.
46. Amaya F, Oh-hashi K, Naruse Y, Iijima N, Ueda M, Shimosato G, Tominaga M, Tanaka Y, Tanaka M. Local inflammation increases vanilloid receptor 1 expression within distinct subgroups of DRG neurons. Brain Res. 2003;963:190–6.
47. Liu BL, Yang F, Zhan HL, Feng ZY, Zhang ZG, Li WB, Zhou XF. Increased severity of inflammation correlates with elevated expression of TRPV1 nerve fibers and nerve growth factor on interstitial cystitis/bladder pain syndrome. Urol Int. 2014;92:202–8.
48. Latremoliere A, Woolf CJ. Central sensitization: a generator of pain hypersensitivity by central neural plasticity. J Pain. 2009;10:895–926.
49. Foster DC, Dworkin RH, Wood RW. Effects of intradermal foot and forearm capsaicin injections in normal and vulvodynia-afflicted women. Pain. 2005; 117:128–36.
50. Klumpp DJ, Rudick CN. Summation model of pelvic pain in interstitial cystitis. Nat Clin Pract Urol. 2008;5:494–500.
51. Yunus MB. Editorial review: an update on central sensitivity syndromes and the issues of nosology and psychobiology. Curr Rheumatol Rev. 2015;11:70–85.
52. Kayhan F, Küçük A, Satan Y, İlgün E, Arslan Ş, İlik F. Sexual dysfunction, mood, anxiety, and personality disorders in female patients with fibromyalgia. Neuropsychiatr Dis Treat. 2016;12:349–55.
53. Bel LG, Vollebregt AM. Van der Meulen-de Jong AE, Fidder HH, ten Hove WR, Vliet-Vlieland CW, Ter Kuile MM, de Groot HE, both S. sexual dysfunctions in men and women with inflammatory bowel disease: the influence of IBD-related clinical factors and depression on sexual function. J Sex Med. 2015;12:1557–67.
54. Clemens JQ, Elliott MN, Suttorp M, Berry SH. Temporal ordering of interstitial cystitis/bladder pain syndrome and non-bladder conditions. Urology. 2012; 80:1227–31.
55. Pukall CF, Strigo IA, Binik YM, Amsel R, Khalifé S, Bushnell MC. Neural correlates of painful genital touch in women with vulvar vestibulitis syndrome. Pain. 2005;115:118–27.
56. Schweinhardt P, Kuchinad A, Pukall CF, Bushnell MC. Increased gray matter density in young women with chronic vulvar pain. Pain. 2008;140:411–9.
57. Gupta A, Rapkin AJ, Gill Z, Kilpatrick L, Fling C, Stains J, Masghati S, Tillisch K, Mayer EA, Labus JS. Disease-related differences in resting-state networks: a comparison between localized provoked vulvodynia, irritable bowel syndrome, and healthy control subjects. Pain. 2015;156:809–19.
58. Kilpatrick LA, Kutch JJ, Tillisch K, Naliboff BD, Labus JS, Jiang Z, Farmer MA, Apkarian AV, Mackey S, Martucci KT, Clauw DJ, Harris RE, Deutsch G, Ness TJ, Yang CC, Maravilla K, Mullins C, Mayer EA. Alterations in resting state oscillations and connectivity in sensory and motor networks in women with interstitial cystitis/painful bladder syndrome. J Urol. 2014;192:947–55.
59. Farmer MA, Huang L, Martucci K, Yang CC, Maravilla KR, Harris RE, Clauw DJ, Mackey S, Ellingson BM, Mayer EA, Schaeffer AJ, Apkarian AV, Research Network MAPP. Brain white matter abnormalities in female interstitial cystitis/bladder pain syndrome: a MAPP Network neuroimaging study. J Urol. 2015;194:118–26.

Publisher's Note

Springer Nature remains neutral with regard to jurisdictional claims in published maps and institutional affiliations.

Ready to submit your research? Choose BMC and benefit from:

- fast, convenient online submission
- thorough peer review by experienced researchers in your field
- rapid publication on acceptance
- support for research data, including large and complex data types
- gold Open Access which fosters wider collaboration and increased citations
- maximum visibility for your research: over 100M website views per year

At BMC, research is always in progress.

Learn more biomedcentral.com/submissions

Editorial Commentary

Looking into the clinical application of CD47-targeted near-infrared photoimmunotherapy for human bladder cancer treatment

Jayoung Kim[1,2,3]

[1]Department of Surgery and Biomedical Sciences, Cedars-Sinai Medical Center, Los Angeles, CA, USA; [2]Department of Medicine, University of California Los Angeles, CA, USA; [3]Department of Urology, Ga Cheon University College of Medicine, Incheon, Republic of Korea

Correspondence to: Jayoung Kim, PhD. Department of Surgery and Biomedical Sciences, Cedars-Sinai Medical Center, 8700 Beverly Blvd., Los Angeles, CA 90048, USA. Email: Jayoung.Kim@cshs.org.

Provenance: This is an invited article commissioned by Section Editor Xiao Li (Department of Urology, Jiangsu Cancer Hospital & Jiangsu Institute of Cancer Research & Nanjing Medical University Affiliated Cancer Hospital, Nanjing, China).

Comment on: Kiss B, van den Berg NS, Ertsey R, *et al*. CD47-Targeted Near-infrared Photoimmunotherapy for Human Bladder Cancer. Clin Cancer Res 2019;25:3561-71.

Submitted May 20, 2019. Accepted for publication May 28, 2019.
doi: 10.21037/tau.2019.05.13
View this article at: http://dx.doi.org/10.21037/tau.2019.05.13

A recently published paper by a Stanford research team led by Dr. Joseph C. Liao in *Clinical Cancer Research* (1) reported on their well-designed study demonstrating the potential application of CD47-targeted near-infrared photoimmunotherapy (NIR-PIT) for human bladder cancer (BC) (*Figure 1*).

CD47, also known as an integrin-associated protein, is a cell surface transmembrane protein that plays a role in neutrophil migration and T-cell co-stimulation. In the context of BC, high expression levels of CD47 have been observed in BC tumor cells (in both non-muscle invasive and muscle invasive BC). However, expression was found to be absent in terminally differentiated luminal umbrella cells of the normal bladder epithelium. Thus, blocking CD47 may enable our immune system to selectively recognize BC cells, leading to the hypothesis that targeting CD47 may be the potential strategy for specifically killing cancer cells while avoiding unnecessary harm to normal bladder cells. In this paper, the authors elegantly performed a series of *in vitro* experiments using well-characterized BC cell lines. Their *in vivo* experiments used human specimens, which successfully showed that anti-CD47-IR700 may play as a molecular photosensitizer for NIR-PIT of BC. Further experimental results using a xenograft mouse model suggested that CD47-targeted NIR-PIT may effectively block BC growth.

Phototherapy, also known as light therapy, utilizes specific wavelengths of light to treat medical conditions. The inception of this idea began in the late 19th century by Ryberg Finsen, who developed phototherapy for the treatment of lupus vulgaris, a type of skin condition (2). Since then, phototherapy has been adapted and modified into various forms, such as photoimmunological, photochemical, and photodynamic therapies (3). These different phototherapies have become incredibly advantageous when it comes to treating cancer. They have diversified treatment options and are versatile enough to be combined with other therapies. For instance, photoimmunotherapy (PIT) has been shown to increase nano-drug uptake 24-fold in tumor tissues compared to normal (4). Photodynamic therapy (PDT) has been demonstrated to successfully destroy tumor cells, which leads to stimulation of anti-tumor immunity and generation of an innate immune response (5). Because treatment options for BC are mainly limited to surgery and chemotherapy, utilization of these phototherapies are of particular interest.

Unfortunately, when it comes to BC, PDT has largely been abandoned. Clinical trials of PDT lead to several noted adverse events that ultimately demonstrated toxicity and bystander effects on normal bladder cells (6). Another potential challenge of using PDT in BC is the hypoxic microenvironment in BC tissues, which limits

© Translational Andrology and Urology. All rights reserved.

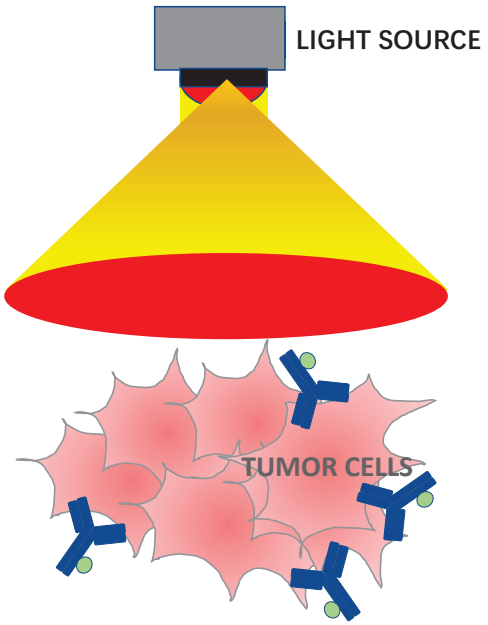

Figure 1 CD47-targeted near-infrared photoimmunotherapy.

the needed O_2 supply for creating reactive oxygen species and eventual cell death (7,8). There have been some studies that have addressed the issue of hypoxia and demonstrated potential reintroduction of PDT in BC, but clinical application remains far ahead (9). On the other hand, PIT has had promising results and is being further explored as a viable treatment option. Studies have demonstrated highly-selective targeting of BC cells by conjugating a photoabsorber dye with panitumumab, an anti-EGFR antibody (10). This strategy takes advantage of the fact that EGFR is overexpressed in BC tissue, with relatively low expression in normal bladder urothelial cells (11,12). A recent study took this a step further by targeting HER2 along with EGFR, which would allow for more effective apoptosis of BC cells across different tumor phenotypes (13).

Collectively, these promising findings by this research team was able to provide persuasive evidence that CD47-targeted NIR-PIT can be deployed endoscopically and holds the potential to augment treatment of localized BC. NIR-PIT, a localized molecular cancer therapy combining a photosensitizer-conjugated monoclonal antibody and light energy, is a particularly attractive tool to use in the urinary tract due to ease of access. One major and important concern is related to safety and therapeutic efficacy. Since it is currently being investigated in other clinical trials for hematopoietic and solid cancers (ClinicalTrials.gov NCT02216409), I believe that we will have better idea how CD47-targeted NIR-PIT therapy can be used as a potential standard option of treatment against BC in the real clinical setting soon.

Acknowledgments

The author would like to thank Mr. Austin Yeon for careful review and editing the manuscript.

Funding: The author acknowledges support from National Institutes of Health grants (1U01DK103260), Department of Defense grants (W81XWH-15-1-0415 and W81XWH-19-1-0109), Centers for Disease Control and Prevention (1U01DP006079), the Steven Spielberg Discovery Fund in Prostate Cancer Research Career Development Award, the U.S.-Egypt Science and Technology Development Fund by the National Academies of Sciences, Engineering, and Medicine, Burroughs Wellcome Fund (BWF) 2017 Collaborative Research Travel Grant (CRTG), and Southeast Center for Integrated Metabolomics (SECIM) Pilot and Feasibility Grant (to J Kim).

Footnote

Conflicts of Interest: The author has no conflicts of interest to declare.

References

1. Kiss B, van den Berg NS, Ertsey R, et al. CD47-Targeted Near-infrared Photoimmunotherapy for Human Bladder Cancer. Clin Clin Cancer Res 2019;25:3561-71.
2. Grzybowski A, Pietrzak K. From patient to discoverer--Niels Ryberg Finsen (1860-1904) --the founder of phototherapy in dermatology. Clin Dermatol 2012;30:451-5.
3. Li Y, Li X, Zhou F, et al. Nanotechnology-based photoimmunological therapies for cancer. Cancer Lett 2019;442:429-38.
4. Kobayashi H, Choyke PL. Super enhanced permeability and retention (SUPR) effects in tumors following near infrared photoimmunotherapy. Nanoscale 2016;8:12504-9.
5. Mroz P, Hashmi JT, Huang YY, et al. Stimulation of anti-tumor immunity by photodynamic therapy. Expert Rev Clin Immunol 2011;7:75-91.
6. Railkar R, Agarwal PK. Photodynamic Therapy in the Treatment of Bladder Cancer: Past Challenges and

© Translational Andrology and Urology. All rights reserved.

Current Innovations. Eur Urol Focus 2018;4:509-11.
7. Blick C, Ramachandran A, Wigfield S, et al. Hypoxia regulates FGFR3 expression via HIF-1alpha and miR-100 and contributes to cell survival in non-muscle invasive bladder cancer. Br J Cancer 2013;109:50-9.
8. Hunter BA, Eustace A, Irlam JJ, et al. Expression of hypoxia-inducible factor-1alpha predicts benefit from hypoxia modification in invasive bladder cancer. Br J Cancer 2014;111:437-43.
9. Lin T, Zhao X, Zhao S, et al. O2-generating MnO2 nanoparticles for enhanced photodynamic therapy of bladder cancer by ameliorating hypoxia. Theranostics 2018;8:990-1004.
10. Railkar R, Krane LS, Li QQ, et al. Epidermal Growth Factor Receptor (EGFR)-targeted Photoimmunotherapy (PIT) for the Treatment of EGFR-expressing Bladder Cancer. Mol Cancer Ther 2017;16:2201-14.
11. Chaux A, Cohen JS, Schultz L, et al. High epidermal growth factor receptor immunohistochemical expression in urothelial carcinoma of the bladder is not associated with EGFR mutations in exons 19 and 21: a study using formalin-fixed, paraffin-embedded archival tissues. Hum Pathol 2012;43:1590-5.
12. Rotterud R, Nesland JM, Berner A, et al. Expression of the epidermal growth factor receptor family in normal and malignant urothelium. BJU Int 2005;95:1344-50.
13. Siddiqui MR, Railkar R, Sanford T, et al. Targeting Epidermal Growth Factor Receptor (EGFR) and Human Epidermal Growth Factor Receptor 2 (HER2) Expressing Bladder Cancer Using Combination Photoimmunotherapy (PIT). Sci Rep 2019;9:2084.

Cite this article as: Kim J. Looking into the clinical application of CD47-targeted near-infrared photoimmunotherapy for human bladder cancer treatment. Transl Androl Urol 2019;8(Suppl 3):S322-S324. doi: 10.21037/tau.2019.05.13

© Translational Andrology and Urology. All rights reserved.